MC 0241

BOX 7 FOLDER 46

Publications, 1964 - 1956

W B Nottingham 1956

REPRINT FROM

HANDBUCH DER PHYSIK

ENCYCLOPEDIA OF PHYSICS

EDITED BY

S. FLÜGGE / MARBURG

VOLUME XXI

SPRINGER-VERLAG / BERLIN · GÖTTINGEN · HEIDELBERG

THERMIONIC EMISSION

BY

PROFESSOR DR. WAYNE B. NOTTINGHAM
INSTITUTE OF TECHNOLOGY, CAMBRIDGE/MASS. (USA)

WITH 62 FIGURES

Thermionic Emission.

By

WAYNE B. NOTTINGHAM[1].

With 62 Figures.

Glossary of symbols.

a	Thermionic constant, Eq. (9.1).
a	Ratio of radii as defined by Eq. (60.6).
a_A, a_B	Empirical constants of Eqs. (77.1) and (77.2).
A	Universal thermionic constant, Eqs. (5.2) and (18.6).
A	Area of conduction specimen, Eq. (65.28).
A	Area of electron emitter as used in Eq. (82.5).
A_F	FOWLER's thermionic constant defined by Eq. (64.24).
A_R	RICHARDSON constant, Eq. (50.2).
A_v	Constant in general equation as in Eq. (50.8).
B	Symbol introduced into Eq. (26.1) to represent barrier properties.
C_g	Grid to emitter capacitance (Sect. 82).
C_p	Correction factor to pore-conduction equation to include porosity of specimens, Eq. (65.28).
C_s	Correction factor in Eq. (65.9).
C_x	Capacitance calculated as in Sect. 82.
D	Distance between emitter and collector, Eq. (27.4).
$D(p, B)$	Transmission over emission barrier, Eq. (26.1).
$\overline{D(p, B)}$	Average transmission of electrons from the interior of a solid across a barrier to the outside, Eq. (64.22).
$\overline{D}$	An abbreviation $\overline{D(p, B)}$ (Sect. 64).
e	Electron charge, Eq. (5.1).
E	Used as abbreviation of E_D in Eq. (64.6).
E	Electric intensity, Eq. (27.3).
E_c	Electric intensity at critical distance x_c, Eq. (27.7).
E_x	Component of electric intensity, Eq. (23.3).
E_a	Activation energy defined by Eq. (65.13).
E_D	Energy level of donors relative to bottom of conduction band (Sect. 64).
f	Fraction of a MAXWELLian distribution, Eqs. (33.2) and (34.1).
f_M	Maximum fractional distance from an emitter of very high capability to space-charge minimum, Eq. (61.3).
FL	FERMI level (Fig. 2).
$F_c(p, V, T)$	Probability of electron absorption by collector depends on momentum, potential and temperature of emitter, Eq. (26.1).
$F(S, a)$	Function given in Eq. (60.4) and computed for Table 10, plotted in Fig. 19.
$F_c(S, kT/\omega)$	Tabulated function applied to theory of electron emission from a cylinder in a retarding field, Eq. (26.9).
$F(V_s, V_T, n)$	Defined by Eq. (62.6)
$F(x)$	Force function, Eq. (27.6).
$f(\psi_c)$	Function of collector region potential difference given by Eq. (46.14) and Table 6.
$F(\psi_c)$	A function applied to the collector space defined by Eqs. (38.4) and (39.5).
g	Conduction per unit area, Eq. (65.28).
g_m	Transconductance (or mutual-conductance) defined by Eq. (82.5).
G	Abbreviated form of $G(x)$ as in Eq. (27.11).
$G(S)$	Electron flow in a retarding field between cylinders, Eq. (26.11), and Tables 2 and 10.

[1] This work was supported in part by the Signal Corps; the Office of Scientific Research, Air Research and Development Command; the Office of Naval Research; the Research Laboratory of Electronics and the Department of Physics of the Massachusetts Institute of Technology.

$G(x)$ Geometrical function relating E to V_c, Eq. (27.3).
G' Empirical value of constant of Eq. (79.1).
GE-218 Special form of General Electric tungsten wire (Sect. 70).
h PLANCK's constant, Eq. (15.1).
h^3 Extention in phase space per quantum state (Sect. 15).
i Emission current as in Eq. (82.8).
I Electron current density, Eqs. (5.1) and (5.2).
I_c "Random" electron current density in a cavity, Eqs. (18.2) and (18.4).
I_s Current density at the surface of a cavity. Same as I_{00}, Eq. (18.1).
I_0 Constant of the SCHOTTKY Equation, Eq. (27.11).
I_0 Current density at zero field as in Eqs. (27.14) and (40.1).
I_{00} Current density defined by Eqs. (18.5) and (26.10).
I_L Minimum current density with zero field at emitter computed by Eq. (46.12).
I_m Maximum possible current density flowing across a diode with zero field at the collector, Eq. (43.2).
I_M Maximum current density given by Eqs. (46.11) or (58.2).
I'_r Current density computed by Eq. (52.4).
I_R Current density under critical condition of zero field at the collector, Eq. (43.1).
I_Θ Current density with zero field at the emitter and the critical temperature Θ, Eq. (47.1).
k BOLTZMANN's constant, Eq. (5.1).
K^2 A number defined by Eq. (64.14).
K_L The LANGMUIR-CHILD constant, Eq. (38.3).
l_p Average free flight distance in a pore, Eq. (65.17).
l_s Free flight distance in a semiconductor, Eq. (65.6).
l_{s0} Free flight distance at some low temperature T_0, Eq. (65.6).
L Thickness of a test specimen for pore conduction in a high field, Eq. (66.3).
L_M Designation of straight lines in Figs. 11 and 12.
m Electron mass, Eq. (5.1).
$\overline{m}$ Average dipole moment per atom, Eq. (73.2).
$\overline{m}_0$ Dipole moment per atom at very low surface concentration.
m_g Proportionality constant defined by Eq. (82.3).
M_p Electron mobility in a pore, Eq. (65.4).
$M_{p\,\mathrm{II}}$ Mobility of electrons in a pore over temperature range II, Eq. (65.18).
M_s Electron mobility in a semiconducting solid, Eq. (65.3).
n Concentration of free electrons, Eqs. (5.1) and (22.1).
n Term index in summation of Eqs. (62.3) and (62.5).
n_a Number of atoms per unit area, Eq. (73.2).
n_c Concentration of electrons in cavity space, Eq. (18.3).
n_D Donor concentration used in Sect. 64.
n_1 Adsorbed atoms per unit area in a monolayer, Eq. (75.1).
n_0 Electron concentration at cavity center of Fig. 3.
n_{0m} Maximum possible electron density at the center of a cavity, Eq. (24.4).
n_s Concentration of electrons at emitting surface of cavity, Eq. (24.8).
N A numerical constant defined by Eqs. (38.8) or (46.4).
N_{xc} Number of electrons that can cross a solid boundary out of a cavity per second per unit area per unit range in energy, Eq. (17.2).
N_{xs} Number of electrons that can cross a solid boundary into a cavity per second per unit area per unit range in energy, Eq. (17.1).
$N(\varepsilon_x)$ Number of electrons crossing unit area per second per unit range in ε_x, Eq. (16.1).
p Momentum of an electron, Eq. (26.2).
p_x, p_y, p_z Momentum component along x, y, z direction.
$\overline{p}_x$ Average momentum component, Eq. (33.3).
p'_x Momentum component in the x direction of an electron at the limiting part of the barrier, Eq. (26.4).
$\overline{\Delta p_x}$ Average gain in momentum as in Eq. (65.1).
p_r Radial component of momentum, Eq. (60.1).
p_{rs} Same as p_r at the surface of the emitter, Eq. (60.1).
p_{rl} Limiting value of initial radial momentum at the emitter for arrival at a potential point V_s negative, Eq. (60.3).
$p_{\Theta l}$ Limiting value of tangential momentum at the emitter for arrival at a potential point V_s negative, Eq. (60.3).
p_Θ Tangential component of momentum, Eq. (60.1).
$p_{\Theta s}$ Same as p_Θ but at the surface of the emitter, Eq. (60.1).

P Abbreviation for contact difference in potential, Eq. (38.10).

P_0 Contact difference in potential at 0° K by extrapolation according to Eq. (38.10) (usually not the true value).

P_T Contact difference in potential (a function of temperature), Eq. (27.1).

$P(\psi^{\frac{1}{2}})$ Probability integral, Eq. (34.6).

r Radius of emitter, Eqs. (26.5) and (27.5).

r Radius between that of the emitter and the collector, Eq. (60.2).

r_s Radius of emitter in Eq. (60.20).

R Radius of collector, Eqs. (26.5) and (27.5), or radius at potential minimum as in Eq. (60.3).

R_c Collector radius as used in Sect. 67.

s A dimensionless measure of applied voltage defined by Eq. (56.1).

s_R Dimensionless measure of applied voltage for zero field at collector, Eq. (57.1).

S Retarding potential in dimensionless units, Eqs. (26.8) and (56.5).

S_a Slope of line in Fig. 11.

S_b Slope of line in Fig. 12.

S' Dimensionless change in potential with zero field at collector as reference, Eq. (57.1).

S'_0 Maximum value of collector potential change in dimensionless units (Fig. 14).

S'_u Value of S' when current ratio is expressed as u^2, Eq. (58.13).

$S_{z'}$ Slope given by Eq. (52.8) and illustrated in Fig. 13.

T Temperature on Kelvin scale (see also V_T).

T_a Activation temperature (Sect. 75).

T_0 Matching temperature for relating thermionic constants, Eq. (50.5).

T_0 A low temperature at which a free flight distance l_{s0} is known, Eq. (65.6).

ΔT Increase in temperature above the critical value Θ, Eq. (40.2).

u^2 Current ratio as in Eq. (57.3).

u_0^2 Maximum current ratio between space-charge limits, Eq. (57.4).

U^2 Current ratio defined by Eq. (58.3).

$\bar{v}$ Average speed of electrons of low concentration, Eq. (65.6).

v Applied potential, Eq. (27.1).

v'' Applied voltage for current density I_M (Sect. 47).

v' Applied voltage for current density I_L (Sect. 47).

v^{**} Voltage computed from observables as in Eq. (47.5).

v_1 Applied voltage for a calculated current, Eq. (52.1).

v_1^* Defined by Eq. (52.2).

v_i Defined by Eq. (52.3).

v'_r Observable applied voltage, Eq. (52.5).

v_R Applied voltage for zero gradient at the collector (Sect. 57).

v_Θ Applied voltage at critical condition of zero field at the emitter, Eq. (49.7).

Δv Observable potential difference over temperature difference of ΔV_T with zero net current (Sect. 86).

$\Delta v'$ Internal potential due to surface charges as in Sect. 86.

V Magnitude of true retarding potential in the space between the emitter and collector in Eqs. (26.5) and (26.6).

V Potential with respect to the space-charge minimum of Fig. 3, see Eq. (22.1).

V_l A constant depending on tube geometry and temperature. See Sect. 9 and Eq. (27.11).

V_c Potential difference between emitter and collector as in Eq. (27.11) or potential across the collector space as in Eq. (32.1).

V_m Lowest temperature of range expressed in electron-volts, Eq. (49.1) and (11.3).

V_n Highest temperature of range expressed in electron-volts, Eq. (49.1) and (11.3).

V_p Voltage drop over an average pore distance of l_p, Eq. (66.2).

V_r Retarding potential difference between surface of emitter and surface of collector, Eq. (42.1).

V_s Potential difference in emitter space as in Eq. (32.1) in Fig. 7.

V_s Difference in potential between center of cavity and its boundary just outside the conducting surface as in Sect. 24.

V_T The electron volt equivalent of the energy kT, Eq. (46.9).

V'_T Electron-volt equivalent of minimum temperature for space-charge minimum of V_T as in Eq. (82.7).

V_{T0} Electron volt equivalent of T_0 in Eq. (65.6).

V_w Characteristic temperature expressed in electron volts defined by Eq. (47.12).

V_{z1}, V_{z2} Critical temperatures expressed in electron volt equivalent, Eq. (53.1).

V_Θ Electron-volt equivalent of the critical temperature Θ and given by $\Theta/11600$ (Sect. 47).

w Distance between plane conducting surfaces (Sect. 21, Figs. 1, 2, 3, and 7).

w	Separation of surface charges, Eq. (73.1) (Fig. 34).
W_a	Potential energy difference shown in Fig. 2—Electron affinity of a solid, Eq. (17.4).
W_v	Electron affinity modified by an externally applied potential, Eq. (27.10).
x	Integration variable, Eqs. (26.11) and (60.4).
x	Distance variable as in Sect. 27.
x_1	Characteristic unit distance of space-charge theory, Eqs. (35.1), (35.2) and (38.9).
x_c	Escape distance as in Fig. 5 and Eq. (27.6).
x_c	Distance from potential minimum to collector Fig. 7 and Eq. (38.2).
x_g	Distance from emitter to control grid of idealized triode.
x_0	Location of mirror-image surface with respect to an arbitrary reference as in Eq. (27.8).
X_s	Maximum value of distance from emitter to space-charge minimum, Eq. (46.10).
y	Integration variable, Eqs. (26.12) and (34.3).
z	Ratio of distances as in Eqs. (24.2) and (43.4).
z^2	Ratio of electron concentrations as in Eq. (24.11) or currents as in Eqs. (43.4) and (51.2).
z'^2	Arbitrary ratio of currents as in Eq. (52.4).
z'_1, z'_2	Arbitrary choices of z, Eq. (53.1).
z^2_R	Current ratio defined by Eq. (58.7).
α	$(d\varphi/dV_T)$ or the temperature coefficient of work-function with temperature expressed in its electron-volt equivalent, Eq. (65.21).
γ	Proportionality constant of Eq. (80.2).
δ	Distance from potential minimum to surface at which ψ_s is infinite, Eqs. (24.1) and (43.1).
ε	Kinetic energy when potential energy is zero.
ε	Energy, Eq. (15.1).
ε_0	Permitivity of free space, Eq. (22.1).
ε_x	Kinetic energy associated with motion in the positive x direction, Eq. (16.2).
ε_x	$p_x^2/2m$ or kinetic energy over an image barrier as in Eq. (63.2).
ε'_x	Kinetic energy associated with the x direction of motion in the cavity of Fig. 2.
ε_{x2}	Kinetic energy associated with electron motion in the semiconductor illustrated in Fig. 27.
$\bar{\varepsilon}_x$	Average kinetic energy of an electron, Eqs. (63.1) and (63.2).
$\Delta\varepsilon_x$	Difference in energy between bottom of conduction band in the semiconductor and that of the metal in Fig. 27.
Θ	Temperature critical for zero field at either the collector or emitter with space charge (Sect. 31).
ϑ	Fraction of surface covered by adsorbed atoms.
ϑ_p	Coefficient of thermal emf (thermoelectric power) defined by Eq. (86.5) for a pore in a semiconducting structure.
ϑ_s	Coefficient of thermal emf (thermoelectric power) defined by Eq. (86.3) for semiconducting solid.
λ	Approximately half of the characteristic pore length l_p, Eq. (66.1).
μ	FERMI level measured relative to bottom of conduction band as in Eqs. (16.1) and (64.1).
μ'	A measure of donor concentration and temperature as in Eq. (64.9).
μ_1	FERMI level in the metal illustrated in Fig. 27.
μ_2	FERMI level in a semiconductor illustrated in Fig. 27.
μ_c	FERMI level in cavity (see Fig. 2).
μ_s	FERMI level in solid (see Fig. 2).
$\Delta\mu$	Change in the FERMI level with temperature relative to its value at $T = 0°$ K as used in Eq. (81.4).
$\Delta\mu$	Change in FERMI level with a temperature change of ΔV_T as in Eq. (86.2).
ν	Number of electrons per unit volume.
ν_0	Electron concentration at space-charge minimum, Eq. (35.3).
ν	Temperature exponent in Eq. (50.8).
σ	Integration variable representing energy in dimensionless units as in Figs. 23 and 24 and Eqs. (62.3) and (62.7).
σ	Conductivity as in Eq. (65.2).
σ	Surface charge per unit area, Eq. (73.1).
σ_A	Conductivity over range I of Fig. 37.
σ_B	Conductivity over temperature range II, Eq. (65.19).
$\sigma_{p\,\mathrm{II}}$	Pore conductivity over temperature range II, Eq. (65.19).
Σ	Change in applied potential in dimensionless units, Eq. (58.5).

$\bar{\tau}$ Average time between inelastic collisions as in Eq. (65.1).
τ_E Average time of flight across a pore in a strong field, Eq. (66.2).
$\bar{\tau}_p$ Average time for electrons in pores, Eq. (65.4).
$\bar{\tau}_{p\,\mathrm{II}}$ Average time of flight across a pore in temperature range II, Eq. (65.17).
$\bar{\tau}_s$ Average time for electrons in solids, Eq. (65.3).
φ True work-function and specifically defined by Eq. (19.1).
$\Delta\varphi$ Reduction of true work-function by accelerating field (Sect. 27).
φ_c True work-function of collector, Eq. (27.2).
φ_F FOWLER work-function or true work-function at 0° K for an N type semiconductor.
φ_R RICHARDSON work-function, Eq. (50.2).
φ_s True work-function of emitter, Eq. (27.2).
φ_v Constant in general equation as in Eq. (50.8).
Φ Work-factor, Eq. (9.1), related to work-function in Sect. 50.
Φ_σ Activation energy for pore conductivity, Eq. (65.27).
Φ_A Activation energy of Eq. (77.1).
Φ_B Activation energy of Eq. (77.1).
χ Dimensionless measure of distance from the space-charge potential minimum, Eqs. (22.4), (35.2) and (35.4).
χ_a, χ_b Values associated with the arbitrary choices of ψ_a and ψ_b (Sect. 47).
χ_c Collector region distance in dimensionless units, Eq. (37.8).
χ_m Maximum value of χ_s which is 1.806 as in Eq. (37.6).
χ_s Emitter region distance in dimensionless units, Eqs. (37.5) and (37.6).
χ_{cu}, χ_{su} Values corresponding to the potentials ψ_{cu} and ψ_{su}, Eq. (58.11).
χ_{sR} Value corresponding to ψ_{sR} of Eq. (58.9).
ψ Dimensionless representation of potential differences in units of kT.
ψ_a Arbitrary choice of ψ_c (Sect. 47).
ψ_b Arbitrary choice of ψ_c (Sect. 47).
ψ_c Collector region potential difference in dimensionless units, Eq. (37.7), Fig. 14.
ψ_s Dimensionless potential difference in the emitter space, Eq. (37.1), Fig. 14.
$\Delta\psi_s$ Change in ψ_s as in Eq. (57.2) and Fig. 14.
ψ_{c0} Maximum value of collector region potential in dimensionless units, Fig. 14 and Eq. (57.9).
ψ_{cu} Potential at the collector with reference to the potential minimum when current ratio is u^2, Eq. (58.11).
ψ_{sR} Maximum value of emitter region potential in dimensionless units (Fig. 14).
ψ_{su} Potential at the emitter with reference to the potential minimum when current ratio is u^2, Eq. (58.10).
ω Empirical constant, Eq. (46.4).

A. Scope and objectives.

1. Definitions. The emission of electrons across the boundary surface that separates a heated electronic conductor from an otherwise nonconducting space has become synonomous with the term "thermionic emission". The broadest application of the word thermionic might include the emission of charged atomic or molecular particles that may carry with them either a net positive or a net negative charge. Since these phenomena are so very different basically, this article will be devoted exclusively to the more fundamental aspects of the experimental and the theoretical investigations of the phenomenon of *electron* emission from heated conductors.

Thousands of experiments have been reported in the literature and serve as the basic work material from which an explanation of the phenomenon in terms of the fundamental principles of physics emerges. The studies relate to four surface classifications which are:

1. clean homogeneous surfaces;
2. clean heterogeneous surfaces;
3. simple composite surfaces;
4. complex surfaces.

To clarify these classifications an illustration of each will be given. Single crystal wires of circular cross section have been used as sources of thermionic electrons and provide the nearest approach to the realization of experimental conditions appropriate to theoretical interpretation[1,2,3].

Emission can be observed and investigated in detail from the more important crystallographically homogeneous surfaces. These surfaces must be maintained under such perfect vacuum conditions that an absolutely negligible fraction of a monomolecular layer of impurity is present. Since fundamental studies show that the thermionic emission is dependent not only on the atomic composition of the emitting conductor but also on the crystallographic structure of the exposed surfaces, it is evident that practically all investigations that describe the electron emission from polycrystalline substances yield data characteristic only of the particular specimen. In general such observations measure the electron emission summed over an assembly of *heterogeneous surfaces*, which can never be accurately described. Most of the work reported in the literature of the subject applies to these surfaces.

At a given temperature, the efficiency of electron emission from a given conductor may be altered through many orders of magnitude by the adsorption of polarizable atoms or molecules on an otherwise clean homogeneous or heterogeneous underlying conductor. The presence of a surface-layer coverage having a density even smaller than $^1/_{100}$ part of a monolayer can be observed to alter the emission properties[4–7]. Such surfaces are classified as *simple composite surfaces* if the extent of the coverage is of the order of a monolayer or less.

The last of the above four classifications, the *complex surface*, is by far the most important in terms of its usefulness as a source of electrons and includes as its most important member the *oxide cathode*. The structure represents an emitter which depends on the conduction of a heated metallic support such as nickel or platinum upon which has been placed, after due processing, a layer of alkaline earth oxide crystals. The surfaces of these crystals serve as the emitting areas. These crystals are generally solid solutions of barium oxide and strontium oxide of comparable proportions and sometimes have traces of other substances added. It is not unexpected that such a complex emitter will have properties very difficult to explain.

It is considered within the scope of this chapter to review critically some of the important investigations that yield information relevant to all four of these classifications of thermionic emitters. It is not the purpose of this chapter to give an exhaustive bibliography; only such references as apply specifically to the information given here will be cited. The reader may refer to a recently published bibliography[8] on physical electronics which contains several hundred references to contributions on thermionic emission.

2. Theory and experiment. It is an illusion to believe that the main features of thermionic emission have been worked out theoretically and are in agreement with experiment. In spite of the generality often associated with the thermo-

[1] M. H. NICHOLS: Phys. Rev. **57**, 297 (1950).
[2] G. F. SMITH: Phys. Rev. **94**, 295 (1954).
[3] A. R. HUTSON: Phys. Rev. **98**, 889 (1955).
[4] J. B. TAYLOR and I. LANGMUIR: Phys. Rev. **44**, 423 (1933).
[5] J. A. BECKER: Phys. Rev. **28**, 341 (1926); **33**, 1082 (1929).
[6] J. A. BECKER and G. E. MOORE: Phil. Mag. **29**, 129 (1940).
[7] W. B. NOTTINGHAM: Phys. Rev. **49**, 78 (1936).
[8] W. B. NOTTINGHAM: Bibliography in Physical Electronics. Cambridge, Massachusetts: Addison-Wesley Press 1954.

dynamic interpretation of thermionic emission, emphasis must be given to the fact that this branch of theory cannot be relied upon to give accurate information concerning the current flow across a boundary under experimental conditions that violate the basic assumptions of the theory. The most important assumption made is that the system under consideration can be bounded in a manner that will still permit the actual measurement of an electron emission across a boundary. Thermodynamic considerations can be applied to the electron gas in the interior of a single crystal of conducting substance so cut out as to bound the interior cavity by surfaces of perfect homogeneity as regards their crystal structure. With the combined help of the equations of thermodynamics and electrostatics the time average of the density of electrons can be specified as a function of the coordinates within the cavity. The pressure that these electrons would exert on the surface of the cavity can be computed with confidence and from these quantities one might presume to calculate a current of electrons which would flow from the interior of the conducting specimen across a surface boundary to the region just outside the conductor. To assume that such a calculation of the current would be directly related to an observable emission current is wrong. No theory as general as this can predict the fraction of the electrons which are reflected at the boundary.

Even though usually considered to be less general, the statistical theory of an assembly of free electrons is more capable of giving valid information concerning the thermionic emission process. It will therfore be appropriate to base practically all of the theoretical analysis brought forward in this chapter on the application of the statistics of free electrons to thermionic emission phenomena.

B. Historical highlights.

I. General background.

3. Introduction. It will be the purpose of this section to review briefly some of the main events that have marked both the development of the theory and the understanding of thermionic emission as well as the technological advances which have been made during the past 70 years. Following this qualitative review of events a detailed analysis will be given to review the present state of our understanding with respect both to theory and experiment.

4. Discovery and identification of thermionic emission. That negative electricity escapes from hot filaments was probably first established by THOMAS A. EDISON and later identified by WILLIAM H. PREECE[1] as the "EDISON Effect". The account by PREECE of his own experiments on the EDISON effect does not separate the phenomenon now recognized as thermionic emission from the "blue effect" which was evidently the ionization of the residual gas produced by the electrons as they were accelerated from the negative hot filament to the plate of the diode. The identification of the charge carrier emitted from the hot carbon filament as a particle with a very small mass compared with that of a hydrogen ion and with a charge equal in magnitude but opposite in sign to that of the hydrogen ion was made by J. J. THOMSON[2]. In spite of the important experiments of J. J. THOMSON, general agreement that electron flow through conductors and electron emission from hot surfaces are truly different phenomena

[1] W. H. PREECE: Proc. Roy. Soc. Lond. **38**, 219 (1885).
[2] J. J. THOMSON: Phil. Mag. **48**, 547 (1899).

from ionic flow through substances and ionic conduction through gases did not come until about 1914[1].

5. RICHARDSON equations. Thermionic emission is so intimately associated with the phenomenon of electronic conduction in solids that advances in these two fields of scientific investigation are associated. The DRUDE[2] development of the theory of free electrons in metallic conductors paved the way for the better understanding of thermionic emission which marked the contributions of O. W. RICHARDSON. The basic idea of work-function as being a measure of the energy per electron required to transfer charges from the interior of the conductor to the field-free space outside of it is largely due to RICHARDSON[3]. Founded on a very literal classical interpretation of the free electron theory of electronic conduction in metals, RICHARDSON[4] derived his first thermionic emission equation which took the following form:

$$I = n\,e\left(\frac{k}{2\pi m}\right)^{\frac{1}{2}} T^{\frac{1}{2}} \mathrm{e}^{-\frac{e\varphi}{kT}}. \tag{5.1}$$

The recognition of difficulties encountered by the classical free electron theory of conduction and its relation to the specific heat of metals led RICHARDSON[5] and VON LAUE[6] to the "T^2" equation given as follows:

$$I = A\,T^2 \mathrm{e}^{-\frac{e\varphi}{kT}}. \tag{5.2}$$

In its original form this equation depended upon thermodynamic arguments and at the present time it is accepted as the correct expression for electron current flow at a boundary which is in a system maintained under conditions of thermodynamic equilibrium. The mistake generally made in the application of this equation is that the current I is identified as the thermionic emission current one should expect to observe in a laboratory experiment. The current density of Eq. (5.2) is independent of reflection and of other phenomena that may alter the distribution in energy of the electrons which do cross the boundary in an actual emission experiment. A second common error in the application of Eq. (5.2) to thermionic emission is the assumption that the true work-function φ is a constant.

DUSHMAN[7] was one of the first to apply quantum theory to the analysis upon which Eq. (5.2) is based and he deduced that the constant A is a universal constant. His numerical value for this constant was in error by a factor of 2 because it was not known at the time that the "statistical weight" for a free electron should be 2 in order to take into account electron spin.

6. SCHOTTKY mirror-image effect. Of the many important contributions made by SCHOTTKY to the better understanding of thermionic emission, one of the

[1] I. LANGMUIR: Proc. Inst. Radio. Engrs. **3**, 261 (1915). — Gen. Electr. Rev. **18**, 327 (1915). — Trans. Amer. Electrochem. Soc. **29**, 125 (1916), (see p. 134). — The FREDERICK GUTHRIE [Phil. Mag. **46**, 257 (1873)] report "On a Relation Between Heat and Static Electricity" has been interpreted by some readers to indicate thermionic emission. The low temperatures involved in his experiments and the general phenomena reported can more easily be interpreted in terms of ionic production, both positive and negative, than as a clear indication of electron emission.

[2] P. DRUDE: Ann. Phys., Lpz. **1**, 566 (1900); **3**, 369 (1900). — H. A. LORENTZ: Theory of Electrons. New York: G. E. Stechert & Co. 1909.

[3] O. W. RICHARDSON: Phil. Mag. **23**, 263 (1912).

[4] O. W. RICHARDSON: Proc. Cambridge Phil. Soc. **11**, 286 (1902).

[5] O. W. RICHARDSON: Phil. Mag. **23**, 594 (1912).

[6] M. v. LAUE: Jb. Radioakt. u. Elektr. **15**, 205, 257, 301 (1918).

[7] S. DUSHMAN: Phys. Rev. **21**, 623 (1923).

most important was his recognition that the mirror-image force acting on an electron as it escapes from the surface of a good conductor accounts for the major part of the total work which must be supplied for an electron to escape[1]. Since this mirror-image force extends over such a great distance compared with interatomic distances, it is possible to counteract it by the application of an externally applied accelerating electric field. This neutralization of forces results in a reduction in the work required for an electron to escape and as a consequence there is an increase in the thermionic emission observed from a constant temperature emitter as the accelerating field is increased. The correctness of this theory and the supporting experimental data leave the "SCHOTTKY Effect" unchallenged. Details of this theory are given in Sect. 27.

7. CHILD-LANGMUIR space charge. A second effect produced by accelerating fields—an important one in the understanding of thermionic emission—was recognized by LANGMUIR[2] and CHILD[3] and others as being accounted for by the phenomenon of space charge.

As the temperature of an emitting conductor increases, the observed current does not increase indefinitely, even though a fixed strongly accelerating positive potential is maintained on the electron collector. If the number of electrons in transit between the emitter and the collector exactly equals the total surface charge maintained on the collector by the external circuit, then the electric field at the emitter becomes zero. Further increases in temperature are followed by very little increase in observed current because of the development of a retarding field at the surface of the emitter produced by space-charge. Even though space-charge effects are strongly dependent on electrode geometry and act in the space well outside of the thermionic emitter itself, it is necessary to have a full understanding of their influence. Thermionic emission is an electron flow observed as a current between suitably placed electrodes and the phenomenon of space charge seldom should be neglected in the interpretation of the observations.

8. SOMMERFELD'S free electron theory. SOMMERFELD[4] applied the statistical theories of FERMI and DIRAC to reconstruct the DRUDE free-electron theory of conduction in metals to include the concept of quantization of phase space and the introduction of PAULI's exclusion principle. This SOMMERFELD theory of conduction by free electrons was applied by FOWLER[5] and NORDHEIM[6] to form the basis of the quantum theory derivation of Eq. (5.2). It is from this beginning that we have the means for the better understanding of the mechanism of thermionic emission even though some phases of the theory are incomplete at the present time.

II. Experiments with clean surfaces.

9. Empirical equations and work-factor. As knowledge of the thermionic emission process has developed, it has become more and more evident that little or no theoretical significance can be attributed to the application of the RICHARDSON form of thermionic equation as given by Eq. (5.2) for heterogeneous

---

[1] W. SCHOTTKY: Phys. Z. **15**, 872 (1914). — Z. Physik **14**, 63 (1923).
[2] I. LANGMUIR: Phys. Rev. **2**, 450 (1913); **21**, 419 (1923).
[3] C. D. CHILD: Phys. Rev. **32**, 498 (1911).
[4] A. SOMMERFELD: Z. Physik **47**, 1 (1928).
[5] R. H. FOWLER: Proc. Roy. Soc. Lond., Ser. A **117**, 549 (1928); **118**, 229 (1928).
[6] L. NORDHEIM: Z. Physik **30**, 177 (1929).

surfaces whether clean or not. The experiments of NICHOLS[1], SMITH[2] and HUTSON[3] have given data on homogeneous clean surfaces which will be shown later in this chapter to yield the only data appropriate for analysis by the RICHARDSON form of equation. This statement is not a denial of the engineering usefulness of some equation by which experimental data on the thermionic emission properties of clean metals can be expressed. The nearly universal application of the RICHARDSON equation for the correlation of the observed data is in some respects unfortunate, since the equation is in fact used purely as an empirical one containing two empirically determined constants. An equation of the following form is a far more useful empirical equation:

$$I = a\, e^{-\frac{e\Phi}{kT}}. \tag{9.1}$$

In this equation a is a thermionic constant determined by experiment to fit the observed data. This constant depends on the substance from which the electrons are emitted and also on the details of its crystallographic configuration. In general the experimenter describes his specimen as one of some specified composition and as "polycrystalline". The use by others of empirical constants so determined to predict the emission properties of other samples of the same material implies that, averaged over the entire emitting surface, the heterogeneous distribution of crystal surfaces is reproducible. The constant Φ of Eq. (9.1) is referred to as the "work-factor" and again it is dependent on the detailed surface configuration of the specimen.

It is self-evident that Eq. (9.1) is easier to use as an empirical equation than is Eq. (5.2). The computation required to determine the emission current for a particular temperature is easy to make with either equation but the reverse process of determining the temperature at which specified current density may be expected is difficult with Eq. (5.2) but is straightforward with Eq. (9.1). A number[4,5] of tabulations have been made of the empirical constants suitable for use in the RICHARDSON form of empirical equation but no complete tabulation has been made of the constants suitable for use in Eq. (9.1). For this reason, tabulations of both sets of empirical constants are given in Appendix 1 to this article. The equations for conversion from one representation to the other are given in Sect. 50.

The "SCHOTTKY effect"[6], which is the reduction in work-function at constant temperature under the influence of an applied electron-accelerating field at the surface of the emitter, accounts for an increase in emission current density proportional to the factor $\exp(V_c^{\frac{1}{2}}/V_1^{\frac{1}{2}})$. For this expression to hold, the geometric relations between the emitter and the electron collector must be such that the surface field at the emitter is everywhere constant and proportional to the potential difference (V_c) between the emitter and the collector. In this relation the constant (V_1) depends upon the geometry and the temperature of the emitter and can be computed with accuracy [see Eq. (27.11)]. Experimental results seldom show an increase in current with applied potential as predicted by this factor, for two reasons. The "SCHOTTKY effect" refers exclusively to the reduction in that part of the work-function that depends on mirror-image forces. Electrons which escape from heterogeneous polycrystalline surfaces are acted

[1] M. H. NICHOLS: Phys. Rev. **57**, 297 (1940).
[2] G. F. SMITH: Phys. Rev. **94**, 295 (1954).
[3] A. R. HUTSON: Phys. Rev. **98**, 889 (1955).
[4] C. HERRING and M. H. NICHOLS: Rev. Mod. Phys. **21**, 185 (1949).
[5] H. B. MICHAELSON: J. Appl. Phys. **21**, 536 (1950).
[6] W. SCHOTTKY: Phys. Z. **15**, 872 (1914). — Z. Physik **14**, 63 (1923).

upon by additional electrical forces arising from the work-function differences that occur between different crystallographic faces of an otherwise pure surface of the material being investigated. It follows, therefore, that the SCHOTTKY effect experiment may be used to yield information concerning these other forces.

10. Periodic deviations from the "SCHOTTKY effect". A second and more basic cause of the difference between experimental results and the "SCHOTTKY effect" theory relates to the fact that the accelerating field not only lowers the work-function precisely as computed by SCHOTTKY but it alters the *transmission* of the barrier for the impinging electron stream[1-5]. This escape probability and its variation with the electric field is a matter not well understood in all of its detail. Experiments[6,7,8] show that this field-dependent effect results in a very small "periodic" alteration in the integrated transmission probability that is indicated by a periodic deviation with respect to the SCHOTTKY law of emission current. The existence of this periodic deviation effect is the latest of the series of discoveries relevant to the thermionic emission properties of clean surfaces. More details concerning this effect will be presented in Sect. 70.

III. Experiments with composite surfaces (mainly the discoveries).

11. Oxide cathodes. WEHNELT[9] discovered in 1903 that barium oxide and other alkaline earth oxides could be applied to poorly emitting surfaces such as platinum with the result that such a thermionic emitter would yield an emission current many million-fold greater than that characteristic of the base metal in the absence of the oxide. Resulting from extensive research, the oxide cathode has become economically the most important thermionic emitter ever discovered and is the most indispensable member of the group of inventions and discoveries upon which our "Electronic Age" depends. In spite of a half century of research, many of the most fundamental problems related to the phenomenon of thermionic emission from oxide cathodes are understood only in a qualitative manner. Much disagreement exists among workers in this field.

12. Thoriated filaments. LANGMUIR and ROGERS[10] discovered in 1913 that tungsten wire into which a small amount of thoria had been inserted could, by suitable heat treatment, be made to emit a current density of electrons at a given temperature 10^5 times greater than that observed from pure tungsten. Later analysis by LANGMUIR and others showed that this enhanced emission, produced as a result of the creation of a simple composite surface could be related quantitatively to the average dipole moment per unit area created at the surface by the polarizable atoms adsorbed on it. This discovery and the related experiments, including the adsorption of the alkalies and specifically of cesium[11], led to a far better understanding of the properties of thermionic emitters than would have been available to us otherwise.

---

[1] R. L. E. SEIFERT and T. E. PHIPPS: Part I, Phys. Rev. **56**, 652 (1939).
[2] E. GUTH and C. J. MULLIN: Phys. Rev. **59**, 575 (1941); **59**, 867 (1941); **51**, 339 (1942).
[3] C. HERRING and M. NICHOLS: Rev. Mod. Phys. **21**, 185 (1948).
[4] D. W. JUENKER, G. S. COLLADAY and E. A. COOMES: Phys. Rev. **90**, 772 (1953).
[5] S. C. MILLER jr. and R. H. GOOD jr.: Phys. Rev. **92**, 1367 (1953).
[6] W. B. NOTTINGHAM: Phys. Rev. **57**, 935 (1940) (L).
[7] E. G. BROCK, A. L. HOUDE and E. A. COOMES: Phys. Rev. **89**, 851 (1953).
[8] D. W. JUENKER, G. S. COLLADAY and E. A. COOMES: Phys. Rev. **90**, 772 (1953).
[9] A. WEHNELT: Verh. dtsch. phys. Ges. **5**. 255, 423 (1903). — Ann. Phys. **14**, 425 (1904).
[10] I. LANGMUIR and W. ROGERS: Phys. Rev. **4**, 544 (1914).
[11] J. B. TAYLOR and I. LANGMUIR: Phys. Rev. **44**, 423 (1933).

13. Dispenser cathodes. The application of efficient thermionic emitters to new contemporary cathode structures has stimulated the development of an emitter which in many respects is a combination of the oxide cathode and the simple composite surface type[1]. The various embodiments of this type fall under a general classification of dispenser cathodes. A base metal of tungsten or molybdenum, usually sintered, can be prepared with a high degree of porosity so that active material, such as barium, can be diffused through it at a rate suitable for maintaining on the porous structure of the exposed surface an activating layer of polarizable molecules or atoms. Another form of the dispenser cathode has the activating material formed right into the sintered structure. Although these cathodes are of commercial importance and go far to satisfy certain specialized needs for high-current density as electron emitters, this development is of such recent origin that important details concerning the basic emission mechanism still remain to be established by experiment.

The first of these dispenser cathodes to become popular was that proposed by LEMMENS. It is referred to in present-day literature as the "*L*" cathode. This simple designation has been well received but is no longer quite appropriate because there are new forms of dispenser cathodes that have superseded the "*L*" cathode. It is therefore considered desirable to use the expression "*D*" cathode for all of the more recent forms of dispenser cathodes.

C. Theory.

I. Statistical mechanics as a basis for emission equations.

14. Free electrons. The basic concepts needed for the derivation of thermionic emission equations are very elementary and yet they are sufficient for the purpose. One pictures the interior of a conducting crystal as an organized arrangement of atoms characterized by specific interatomic distances which are specifically dependent on the atomic composition and the phase taken on by the crystal, depending upon the temperature and the previous temperature history of the specimen. Each crystal as a whole should be thought of as being electrically neutral within any extended region in the interior. Any excess of charge either positive or negative will be found at the surface only. Quantum theory indicates that most of the electrons that neutralize the positive charge on the atomic nuclei are localized near them and in general contribute nothing to the electrical conductivity of the specimen. The valence electrons associated with these atoms, however, occupy quantum states that extend throughout the entire interior of each isolated crystal and it is to these electrons that the statistical theory of the free electron gas may be applied. The free electron theory as applied to these valence electrons describes their behavior in practically classical terms and finally depends upon experiment to justify the applicability of the simplifying assumptions. It is the purpose of this article to indicate as clearly as possible that the most recent experiments serve to support strongly the concepts of the mechanism of thermionic emission which can be derived from the theory even though they are based on a semiclassical analysis of behavior of valence electrons in a conductor.

15. Three basic assumptions. The first assumption made for the development of this theory is that the inter-electronic forces can be neglected and therefore

[1] A. W. HULL: Phys. Rev. **56**, 86 (1939). — H. J. LEMMENS, M. J. JANSEN and R. LOOSJES: Philips techn. Rev. **11**, 341 (1950). — R. C. HUGHES and P. P. COPPOLA: Phys. Rev. **85**, 388 (1952). — J. Appl. Phys. **23**, 1261 (1952).

the electrons behave as though they were particles of three degrees of freedom. The phase space suitable for representing the behavior of an assembly of electrons can therefore be taken to be a six-dimensional phase space in which a representative point exists for each electron in the assembly. The six bits of information needed to localize this representative point are three coordinates and three components of momentum. The second assumption is that for each quantum state an extension in phase space of size h^3 is needed and that a representative point cannot be localized (nor need it be) more specifically than to indicate that one representative point lies within the quantum-state region. Actually this is not quite the whole story because quantum principles permit two electrons to occupy a single quantum state if their spin vectors are always antiparallel. A factor 2 that appears repeatedly in the equations derived on these assumptions is therefore this weight factor which is thus incorporated into the theory. Already the third postulate has been mentioned, namely, the PAULI Exclusion Principle, which limits the number of electrons in a given quantum state to two with antiparallel spin vectors.

It is the purpose of a statistical theory to find an expression for the distribution of representative points in phase space which is consistent with basic principles of thermodynamics and has associated with it the greatest likelihood of occurrence. The function thus obtained, without the need for introducing any additional assumptions, is the following:

$$f(\varepsilon)\, dx\, dy\, dz\, dp_x\, dp_y\, dp_z = 2\,\frac{dx\, dy\, dz\, dp_x\, dp_y\, dp_z}{h^3}\left[\frac{1}{e^{\frac{\varepsilon-\mu}{kT}}+1}\right]. \qquad (15.1)$$

Some explanation of this equation may make its use and meaning easier to grasp. The energy ε is generally separable into two terms, one of which expresses the kinetic energy of a particle whose representative point lies in a specified region in phase space, and the other term is the potential energy expressible in terms of the coordinates of a particle whose representative point is in that region in phase space. The quantity μ is a constant for a given problem which contains implicitly the concentration of electrons and is a function of the temperature. The fundamental concept that determines the value of this parameter is that the integration of Eq. (15.1) over the entire phase space shall exactly equal the number of electrons in the assembly, that is, the number of free electrons within a crystal, for example. Although this statement defines the manner in which the constant μ is determined, there is a second meaning to the constant which is interesting to note, if it applies to a concentration of electrons of the order of 10^{20} per cm.^{3}. The energy value μ is that to be associated with that quantum state for which the probability of occupancy is exactly one-half.

For electron concentrations less than approximately 10^{19} per cm.^{3} the appropriate value of μ is generally a *negative* number. This statement demands a word of explanation. The simplest application of Eq. (15.1) is made to regions in coordinate space over which there is no change in potential energy. It is therefore sufficient for the present purpose to apply Eq. (15.1) to problems in which the potential energy may be taken to be zero. In that case the energy ε will be the kinetic energy of the electron whose representative point lies in a particular region of phase space. In problems of this kind which occur in connection with the theory of the oxide cathode, the algebraic sign of the quantity μ can be defined as negative, and therefore, it lies below the conduction band in the energy, band system. All of the available quantum states associated with the particular problem for low-density distributions of the electrons are less than half filled if μ is negative.

Note that the extension in phase space $(dx\,dy\,dz\,dp_x\,dp_y\,dp_z)/h^3$ represents the number of quantum states in this extension, since the extension per quantum state is h^3, as mentioned previously. The factor 2 is the double occupancy of a quantum state by the two electrons with antiparallel spin vectors.

Finally, the factor in the square brackets of Eq. (15.1) can be identified by its name the "FERMI factor" which gives a direct means of computing the probability that a given quantum state identified by its energy ε will be occupied. The energy is given explicitly in terms of the momenta and the coordinate values associated with the representative point in phase space. The name given to the quantity μ is the "FERMI level". It is evident at once that if the numerical value of μ is positive, then there can be an energy level ε exactly equal to μ and, as mentioned above, the FERMI factor takes on the value $^1/_2$.

16. The electron flow equation. Although Eq. (15.1) is the basic starting point for all equations relevant to thermionic emission, the following equation which is derived directly from Eq. (15.1) without the introduction of any approximations is the most important equation applicable to thermionic emission.

$$N(\varepsilon_x)\,d\varepsilon_x = 2\,\frac{(2\pi m kT)}{h^3}\ln\left(1+e^{-\frac{\varepsilon_x-\mu}{kT}}\right)d\varepsilon_x. \tag{16.1}$$

The independent variable in this equation ε_x is defined by

$$\varepsilon_x = \frac{p_x^2}{2m}. \tag{16.2}$$

By the use of Eq. (16.1), the number of electrons $N(\varepsilon_x)\,d\varepsilon_x$ that cross a unit area in unit time with kinetic energy associated with the positive x direction of motion can be computed for the energy range, $d\varepsilon_x$. This equation holds for all values of μ, either positive or negative, and therefore applies to all densities of electrons provided μ is expressed relative to the energy level for which the kinetic energy is zero or, in other words, with respect to the potential energy at the region in space for which the number of electrons crossing a boundary perpendicular to the x direction is being computed. The first application of this formula will be to compute the "random" currents which impinge on various boundaries of a pillbox-like cavity within the interior of a homogeneous crystal.

17. Electrons in a cavity. The pillbox problem is of interest because it is the only example of the application of theory to an experimentally realizable structure for which all of the essential details are easy to describe. The structure visualized is shown in Fig. 1. The cross-hatched solid structure S represents a section through the interior of a single crystal and the cavity within this crystal is represented by C.

The perpendicular distance across that cavity, ab, should be visualized as being not less than 10^{-4} cm. and can very well be any amount larger than this. The requirement that the cavity be esentially pillbox form is necessary because of the need to have the entire interior of the cavity of a single surface structure type. The pillbox has the further advantage that the problem can be handled exactly, even though sufficient electrons exist in the cavity to give an appreciable space-charge field there. The first steps of the discussion can be carried through without the introduction of space charge as a factor of any importance. The space-charge solution of the problem will be introduced later (Sect. 21).

In the energy diagram of Fig. 2 the potential[1] energy of an electron is shown as a function of distance as one progresses in the x direction from A to B. The

[1] See Sect. 27.

region A to a, is the potential in the interior of the solid taken here to be uniform. It will be shown later that the periodicity of the true potential is of no consequence in the thermionic emission theory. The potential of the electron in the space between a and b is shown to be higher than that in the interior of the metal by an amount W_a. This energy difference is the integration of all of the actual forces that act on an electron as it escapes from the metal into the cavity. In the absence of space charge the cavity potential will be constant at distances greater than approximately 10^{-5} cm. from either surface, since the dominant long-range force acting on an electron is the mirror-image force which at this distance has fallen to a negligible amount. Eq. (16.1) may be used to calculate the number of electrons which approach the boundary from the left at a, with energy between ε_x and $\varepsilon_x + d\varepsilon_x$ associated with the x component of the momentum. In the space between a and b the corresponding energy state lies at ε'_x.

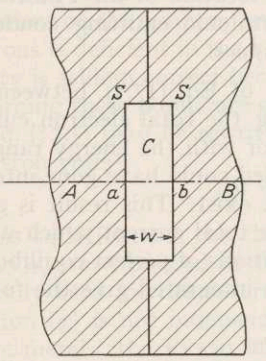

Fig. 1. Cross section of pillbox cavity.

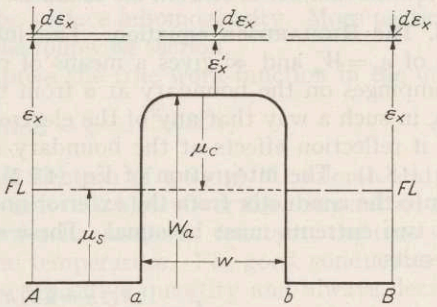

Fig. 2. Potential energy diagram for an electron in the pillbox cavity problem.

For the net current to be zero it is necessary that the current in this band from the left be equal and opposite to the current in the band which approaches surface a from the right. This statement would in general not be true if it were applied to a geometrical configuration in which currents were being observed as electron emission currents in the usual way. An essential part of this analysis is that the entire region surrounding the cavity be at a constant temperature and of course this includes the cavity itself.

In the interior of the crystal the FERMI level, FL, is located at an energy μ_s positive with respect to the potential energy line Aa relative to which the kinetic energy ε_x is referred. The application of Eq. (16.1) shows that there is a simple and yet a necessary condition which must be satisfied if the cavity currents are in statistical equilibrium with the currents flowing in the solid. This condition is that the FERMI level be continuous right through the cavity space. Relative to the potential energy of an electron in the cavity, the FERMI level is *negative*, the amount shown as μ_c. The formal writing of the two equations for the two electron streams serves to illustrate this point and will be used for further development. These equations are the following:

$$N_{xs}\, d\varepsilon_x = \frac{2(2\pi m kT)}{h^3} \ln\left(1 + e^{-\frac{\varepsilon'_x - \mu_s}{kT}}\right) d\varepsilon_x, \tag{17.1}$$

$$N_{xc}\, d\varepsilon_x = \frac{2(2\pi m kT)}{h^3} \ln\left(1 + e^{-\frac{\varepsilon'_x - \mu_c}{kT}}\right) d\varepsilon_x. \tag{17.2}$$

It is clear from an inspection of these two equations that the necessary condition for the equality of these two flows of electrons is that the exponents be equal and the following equation may therefore be written:

$$\varepsilon_x - \mu_s = \varepsilon'_x - \mu_c. \tag{17.3}$$

Eq. (17.4) gives additional relations as a result of the reorganization of Eq. (17.3) which are self-evident:

$$\varepsilon_x - \varepsilon'_x = \mu_s - \mu_c = W_a. \tag{17.4}$$

The final rearrangement of this equation is written as follows:

$$-\mu_c = W_a - \mu_s = (\text{true work-function}) \times e = \varphi e. \tag{17.5}$$

This equation stated in words demonstrates the fact that the true work-function expressed in energy units is a direct measure of the location of the FERMI level appropriate to the cavity space outside of a thermionic emitting conductor *when equilibrium exists between the conductor and the space.*

18. The RICHARDSON equation. The integration of Eq. (17.1) between the limits of $\varepsilon_x = W_a$ and ∞ gives a means of calculating the total electron current that impinges on the boundary at a from the interior with the energy range limited, in such a way that any of the electrons included could have gone into the space if reflection effects at the boundary a did not exist. This result is given as Eq. (18.1). The integration of Eq. (17.2) gives the total current which would flow into the conductor from the exterior under conditions of perfect equilibrium. These two currents must be equal. These equations integrated give the following results:

$$I_s = \frac{2e(2\pi m kT)kT}{h^3} e^{-\frac{W_a - \mu_s}{kT}}, \tag{18.1}$$

$$I_c = \frac{2e(2\pi m kT)kT}{h^3} e^{\frac{\mu_c}{kT}}. \tag{18.2}$$

The validity of Eq. (18.2) depends on the assumption that the numerical value of μ_c is not less than $5\,kT$ for an accuracy of better than 1%. For smaller values of μ_c other terms in the power series expansion must be used.

The fact that μ_c is clearly a negative number implies that the electron density in the cavity space is smaller than approximately 10^{19} per cm.^{3}. Under these conditions the statistical theory gives a suitable expression for μ_c which is the following:

$$\mu_c = -kT \ln \left[\frac{2(2\pi m kT)^{\frac{3}{2}}}{n_c h^3} \right]. \tag{18.3}$$

The substitution of this value for μ_c into Eq. (18.2) yields the following:

$$I_c = n_c e \left(\frac{kT}{2\pi m} \right)^{\frac{1}{2}} \tag{18.4}$$

in which n_c is the concentration of electrons in the cavity space near enough to the surface so that space-charge fields can be neglected and yet far enough from the surface so that the mirror-image fields are negligible. This equation is the familiar one from classical mechanics and may be explained in the following terms: $(n_c/2)$ represents the concentration of electrons moving with a component of velocity in any specified direction; $2(kT/2\pi m)^{\frac{1}{2}}$ represents the average of the velocity component of these electrons in a classical distribution; and e is the charge on an electron.

The rewriting of Eq. (18.1) yields at once the RICHARDSON form of the equation so often misused when it is identified with observable thermionic emission.

$$I_s = \frac{4\pi m k^2 e}{h^3} T^2 e^{-\frac{W_a - \mu_s}{kT}} . \tag{18.5}$$

The first factor of this equation may be recognized as the familiar universal thermionic constant A.

$$A = \frac{4\pi m k^2 e}{h^3} = 120 \text{ amp/cm.}^2 \, T^2. \tag{18.6}$$

19. The true work-function and its temperature coefficient. An explanation of the reason why Eq. (18.5) cannot be taken as a theoretical prediction of the true functional relation between the observed thermionic current emission density and temperature is in order. Three features of thermionic measurements stand in the way of the direct use of this equation. First, the true work-function is dependent on the temperature; second, the observed energy distribution of emitted electrons is deficient in the low-energy range and, third, the evaluation of current density is seldom correct because of the surface inhomogeneity. More particulars concerning these points are given in the following section.

Eq. (17.5) may be rewritten to express the true work-function in the unit of "electron volts"

$$\text{true work-function} = \varphi = \frac{W_a - \mu_s}{e} . \tag{19.1}$$

In this equation, e is the charge on an electron of 1.6×10^{-19} coulomb and both W_a and μ_s are expressed in the energy unit of joules. Over the temperature range generally used for the determination of a RICHARDSON constant, the true work-function (φ) is not independent of the temperature. For good conductors such as the metals, the FERMI level (μ_s) is a positive quantity and always decreases with an increase in temperature. It is not possible to make a completely generalized statement concerning μ_s if the specimen is a semiconductor except when it applies to the most important of the semiconductor emitters, namely, the oxide cathode. In that case μ_s is generally negative and *increases* in *absolute* value as the temperature is raised (see Sect. 64). At the surface of good conductors the potential energy difference (W_a), (as measured between the "bottom" of the conduction band and an electron at rest at infinity) is of the order of 10 electron volts, whereas for semiconductors the value is close to one electron volt. This quantity is given the name "electron affinity" and depends not only upon the crystal structure of the surface but also on the average dipole moment of any adsorbed atoms. The temperature coefficient of the electron affinity for clean metallic surfaces is in all probability negative. That is, W_a decreases with a temperature increase. Notice, however, that φ may nevertheless increase or decrease with the temperature depending on the relative rates of change of the two terms of Eq. (19.1).

If electropositive adsorbed layers exist on the surface of a good conductor, it is generally true that their dipole moment per unit area will decrease more rapidly than μ_s with increasing temperature. If follows, therefore, since the dipole moment operates to reduce the electron affinity of the composite surface, that with these electropositive layers, W_a will actually *increase* with the temperature. The opposite effect is to be expected for the adsorption of electronegative impurity atoms or molecules.

20. The RICHARDSON equation and its relation to experiment. Eq. (18.5) can be accepted with a great deal of confidence since its validity is derived both from a generalized thermodynamical argument and from the theory of quantum

statistics. It is not this equation that is tested in any of the direct experiments usually associated with the measurement of the thermionic emission of electrons from practical specimens.

Since Eq. (18.1) and its equivalent Eq. (18.5) were derived directly from Eq. (17.1) it is equally evident that the validity of Eq. (17.1) in its possible application to the actual thermionic emission problem should be established independently. The uncertainty with regard to the temperature coefficient of the true work-function, which has just been discussed, does not in any way interfere with the experimental determination of the energy distribution of the electrons that are emitted. The prediction made by Eq. (17.1) on the distribution that must be observed to make Eq. (18.5) valid, has been found by direct experiment to be in error. Later in this chapter the detailed experiments by which Eq. (17.1) has been evaluated as a true representation of the energy distribution will be discussed. It is sufficient for the present purposes to state without qualification that the energy distribution predicted by this equation is not found experimentally. The observed distributions found in all experiments capable of yielding direct information in answer to this question show that there is a marked deficiency of low energy electrons. It cannot be stated at present, that the true explanation for this deficiency is a "reflection effect" at the boundary of the surface. The internal consistency in the experimental interpretation that comes very easily from this hypothesis tends to support the view that the deficiency is caused by reflection. An alternative explanation which qualitatively seems less able to correlate the experimental results depends on the assumption that the extraction of the electrons observed as electron emission current disturbs the population of the quantum states near the immediate surface of the conductor. When those electrons capable of escape are taken away, the quantum states will not be refilled continuously, as they would in the pillbox, and a deficiency in slow electrons may be the result.

Finally, a third effect, which is seldom taken into account in the application of the RICHARDSON form of the equation to experimental data, is the lack of uniformity of emission over the surface of the specimen, since in most calculations of current density the total area of the surface is used. If the emission current is observed in the presence of a moderately strong electric field designed specifically to sweep the emitted electrons over to the collector, then the emission is largely dominated by the low work-function areas.

This discussion should serve to justify the statement made above that the current density predicted by Eq. (18.5) should not be identified with thermionic emission as measured by the usual laboratory methods.

II. The density of an electron atmosphere in an enclosed space[1].

21. Introduction. In spite of the uncertainty with regard to the true energy distribution of the electrons emitted from a surface, a solution can be given for the distribution in electron density within a cavity bounded by parallel planes. Even though this problem in itself is somewhat artificial and relates only indirectly to practical needs, the solution can be worked out exactly and is of interest. In its qualitative aspects it bears most directly on the emission properties of hollow cathodes, but, in addition, it may be of importance in connection with the flow of electrons across the cavities within the body of oxide cathodes.

The solution to the "pillbox" problem depends on the assumptions that a cavity is created within the interior of a uniform substance and that two plane

[1] R. H. FOWLER: Statistical Mechanics, 2nd edit., p. 366. Cambridge Univ. Press 1936.

conducting surfaces are separated as shown in Fig. 1 by a distance w. It is assumed that this separation between the surfaces is small compared with the linear surface dimensions in order to eliminate the effects of the boundaries that form the periphery of the pillbox. Because of the relatively high ionization potential of atoms making up the emitting surface bounding the cavity, the presence of positive ions can be neglected and at once, it becomes evident that the distribution of electron density within the cavity will be a function only of the distance variable, x, and that the electron density at the midpoint across the cavity will be a minimum. To make the statement that the density of electrons will depend upon the potential according to the BOLTZMANN relation is the equivalent of stating that the FERMI level is continuous from the interior of one conducting surface right through the evacuated space to the interior of the other conductor. Fig. 2 illustrates in a qualitative manner the variation in the motive with distance from the metallic interior at A through the surface boundary at a and across the cavity to the surface at b and then to the interior at B if space charge is neglected. The true potential distribution in the cavity is to be found by the analysis which follows.

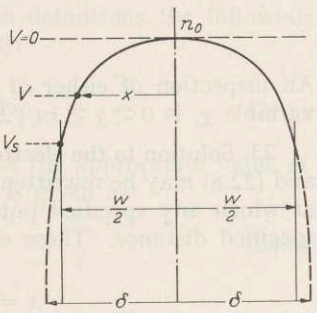

Fig. 3. Electrostatic potential in a cavity with space-charge present.

22. Mathematical formulation of the electron density problem. It is mathematically convenient to measure distances from the motive maximum (see Sect. 27) which lies half-way between the two emitting surfaces. Since the motive is the measure of the potential energy of an electron in this example a motive maximum is a potential minimum in the electrostatic sense. The potential will be expressed as a function of x with reference to its value at this minimum point. This potential, V, at any point x will be positive, since the diagrams of Figs. 2 and 3 represent the variation in the potential energy of an electron which in itself carries a negative charge. Fig. 3 shows the corresponding distribution in electrostatic potential with space charge present. The two basic equations are the following:

$$\frac{d^2 V}{dx^2} = -\frac{n e}{\varepsilon_0}, \tag{22.1}$$

$$n = n_0 \mathrm{e}^{\frac{eV}{kT}}. \tag{22.2}$$

In POISSON's relation given as Eq. (22.1), n is the concentration of electrons, e is the electron charge and ε_0 is the permitivity of free space. Eq. (22.2) is the BOLTZMANN relation which expresses the concentration in terms of the potential, V, with respect to the midpoint and the electron density, n_0, at the midpoint. Qualitatively the variation in potential with distance is illustrated in Fig. 3.

It is the purpose of this section not only to outline as briefly as possible the results that one obtains from the simultaneous solution of these two equations, but also to show how those results can be fitted to specific boundary conditions for their application.

These two equations can be brought together and simplified by the introduction of dimensionless variables defined as follows:

$$\psi = \frac{eV}{kT}, \tag{22.3}$$

$$\chi = \frac{x}{x_1} \text{ with } x_1^2 = \left[\frac{kT\varepsilon_0}{e^2 n_0}\right]. \tag{22.4}$$

By direct substitution of these equations into Eqs. (22.1) and (22.2) the following relation may be written:

$$\frac{d^2\psi}{d\chi^2} = -e^{\psi}. \tag{22.5}$$

The first step in the solution of this equation yields a relation from which the electric field in the cavity can be calculated and is given as follows:

$$\frac{d\psi}{d\chi} = \sqrt{2}\,(e^{\psi} - 1)^{\frac{1}{2}}. \tag{22.6}$$

The second step in the solution results in the final answers expressed in either of the forms that follow:

$$\chi = \sqrt{2}\,\arctan\sqrt{e^{\psi} - 1}, \tag{22.7}$$

$$\psi = \ln\left(\sec^2\frac{\chi}{\sqrt{2}}\right). \tag{22.8}$$

An inspection of either of these equations shows that the total range for the variable χ, is $0 \leqq \chi \leqq (\pi/\sqrt{2})$.

23. Solution to the electron density problem. The solutions given as Eqs. (22.7) and (22.8) may be rewritten in terms of the original variables to give the distance at which any specified potential occurs or to give the potential found at any specified distance. These equations are as follows:

$$x = \left[\frac{2kT\varepsilon_0}{e^2 n_0}\right]^{\frac{1}{2}} \arctan\left(e^{\frac{eV}{kT}} - 1\right)^{\frac{1}{2}}, \tag{23.1}$$

$$V = \frac{kT}{e}\ln\sec^2\left[x\left(\frac{e^2 n_0}{2kT\varepsilon_0}\right)^{\frac{1}{2}}\right]. \tag{23.2}$$

The equation for the electric intensity E_x or the field at any point is written as follows:

$$E_x = -\frac{dV}{dx} = \left[\frac{2kTn_0}{\varepsilon_0}\right]^{\frac{1}{2}} \tan\left[x\left(\frac{e^2 n_0}{2kT\varepsilon_0}\right)^{\frac{1}{2}}\right], \tag{23.3}$$

$$E_x = -\frac{dV}{dx} = \left[\frac{2kTn_0}{\varepsilon_0}\right]^{\frac{1}{2}} \left(e^{\frac{eV}{kT}} - 1\right)^{\frac{1}{2}}. \tag{23.4}$$

24. The fit to boundary conditions. The difficulty with these equations as they now stand is that the concentration at the center of the cavity, that is, n_0, must be known before quantitative calculations can be made. This concentration depends not only on the properties of the emitting surfaces, a and b, but also on the dimensions of the cavity (see Fig. 3). The following steps will serve as a guide to one of the more satisfactory methods of applying these results.

An inspection of the diagram of Fig. 3 indicates that there is a distance, δ, always greater than $w/2$ at which the potential approaches infinity for any given value of the electron concentration, n_0. Eq. (24.1) serves to define this value of δ and the relation may be written as follows:

$$\delta^2 = \frac{kT\varepsilon_0}{e^2 n_0}\cdot\frac{\pi^2}{2}. \tag{24.1}$$

It is convenient for the purpose of calculation to define the ratio of the actual half width $w/2$ of the cavity to this quantity δ as follows:

$$z = \frac{w}{2\delta}. \tag{24.2}$$

It is to be noted that if the concentration, n_0, is very small then δ would be very large and it is therefore clear that the range in the quantity z is from zero to one.

A rewriting of Eq. (24.1) gives an expression for the electron concentration at the center of a cavity.

$$n_0 = z^2 \left[\left(\frac{2}{w} \right)^2 \frac{\pi^2 k \varepsilon_0}{2e^2} T \right]. \tag{24.3}$$

Notice that the maximum possible value of the concentration occurs if z is unity. Define this quantity as n_{0m} and it may be computed in terms of the temperature and the cavity width by the following equation:

$$n_{0m} = 9.4 \times 10^4 \frac{T}{w^2} \text{ electrons per m}^3. \tag{24.4}$$

Let the concentration of electrons at the emitting surface of the cavity be n_s and let the difference in potential between the center of the cavity and the region just outside of the surface be V_s. With these definitions the following relations may be written from Eqs. (22.2) and (22.8):

$$n_0 = n_s e^{-\frac{eV_s}{kT}} = n_s \cos^2 \left(\frac{\pi}{2} z \right). \tag{24.5}$$

The final equation which permits the determination of the appropriate value of z in terms of the known parameters of the problem is given as:

$$\frac{n_s}{n_{0m}} = \frac{z^2}{\cos^2 \left(\frac{\pi}{2} z \right)}. \tag{24.6}$$

The equation which will serve for the computation of n_s comes directly from the fact that I_s of Eq. (18.1) is $n_s e (kT/2\pi m)^{\frac{1}{2}}$ and may be written as follows:

$$n_s = \frac{2 (2\pi m k T)^{\frac{3}{2}}}{h^3} e^{-\frac{e\varphi}{kT}}. \tag{24.7}$$

For this equation to be exact, the true work-function φ is needed and it is to be identified as $(W_a - \mu_s)/e$. To simplify the calculation, the assembly of fundamental constants may be evaluated and the equation written as follows:

$$n_s = 4.83 \times 10^{21} T^{\frac{3}{2}} e^{-\frac{e\varphi}{kT}} \text{ (electrons per m}^3\text{)}. \tag{24.8}$$

For any given problem, a numerical value can be established for the ratio (n_s/n_{0m}) from Eqs. (24.4) and (24.8) and it is only necessary, therefore, to determine the correct value of z to satisfy Eq. (24.6). To make this procedure easy, values of this function have been computed for the range of z from 0.05 to 0.99 and are given in Table 1. Eq. (24.9) and (24.10) serve as the most convenient means of calculating z in the extreme low range and in the extreme high range:

$$z = \left(\frac{n_s}{n_{0m}} \right)^{\frac{1}{2}} \quad \text{for} \quad 0 < z < 0.1, \tag{24.9}$$

$$z = 1 - \frac{2}{\pi} \left(\frac{n_{0m}}{n_s} \right)^{\frac{1}{2}} \quad \text{for} \quad 0.98 < z < 1. \tag{24.10}$$

In terms of the density ratio, Eq. (24.9) applies when the surface density is less than one percent of the maximum possible density at the center of the cavity n_{0m} and Eq. (24.10) applies when the surface density is more than a thousand times greater than the maximum density at the center.

Since the maximum density will have been calculated already from Eq. (24.4), the true density at the center of the cavity is given at once by the following:

$$n_0 = z^2 n_{0m}. \tag{24.11}$$

As an aid to computation, the solutions to this problem may be written in terms of the parameter z and the controllable variables w and T.

The distance x from the midpoint of the cavity at which a specified V is found may be computed as

$$x = \frac{w}{\pi z} \arctan \left(e^{\frac{eV}{kT}} - 1\right)^{\frac{1}{2}}. \tag{24.12}$$

The potential at any distance is given by

$$V = \frac{kT}{e} \ln \left(\sec^2 \pi z \frac{x}{w}\right). \tag{24.13}$$

The field may be computed at any distance point or potential by the following equations:

$$E_x = -\frac{dV}{dx} = \left(\frac{2\pi k}{e}\right) \frac{zT}{w} \tan \left(\pi z \frac{x}{w}\right), \tag{24.14}$$

$$E_x = -\frac{dV}{dx} = \left(\frac{2\pi k}{e}\right) \frac{zT}{w} \left(e^{\frac{eV}{kT}} - 1\right)^{\frac{1}{2}}. \tag{24.15}$$

The results of this analysis may be summarized by the following statements:

1. The maximum electron density that can be obtained at the center of a cavity is proportional to the temperature and inversely proportional to the square of the smallest dimension.

2. To attain approximately 90% of this maximum density at the center, the concentration of electrons at the surface of the cavity must be greater by a factor of approximately 200.

3. Further increase in the density of electrons at the surface of the cavity, even though it be many orders of magnitude, cannot increase the density at the center by more than 10%.

4. By the proper control of the porosity of the surface of a cathode, the effective emission current density of the cathode can be made higher than the actual average net current density that crosses the surface boundary which separates the solid from the evacuated space within the pore. This property may have an important bearing on the performance characteristics of suitably constructed oxide cathodes.

III. Field effects with current flow.

25. Three field effects. The three most important field effects that relate to thermionic emission are: 1. the influence of retarding potentials, externally applied; 2. the influence of accelerating fields, externally applied; and 3. the influence of the combined effect of a space charge and external fields. The theoretical aspects of these three field effects will be discussed in this order.

26. The influence of retarding fields. The earliest experiments on thermionic emission established that the observed currents that flow across the space in a diode structure are very dependent upon the applied voltage difference between the electron emitter and the collector. If the emission current density is sufficiently low, so that space-charge effects can be neglected, the two principal regions associated with the applied voltage are: 1. the accelerating field range, and 2. the retarding field range. These ranges are separated quite sharply because of the fact that the current change in the first region is almost negligible, while in the

second region the current change goes through many orders of magnitude for each additional volt of applied retarding potential. Superficially, this phenomenon is accounted for as a measure of the energy distribution of the emitted electrons. It is so difficult to satisfy the necessary experimental conditions which will permit the direct interpretation of the results in terms of the electron energy distribution that very few authentic data are available.

The starting point of any theory covering this phase of the subject is Eq. (15.1) From this equation, it is possible to write a general expression for the current received as a function of the applied voltage between the emitter and the collector. This equation is the following:

$$I = e \int_{p_z=-\infty}^{p_z=\infty} \int_{p_y=-\infty}^{p_y=\infty} \int_{p_x=0}^{p_x=\infty} D(p, B)\, F_c(p, V, T)\, n(p)\, dp_x\, dp_y\, dp_z \tag{26.1}$$

$D(p, B)$ = transmission over emission barrier; $F(p, V, T)$ = transmission to and over collector barrier.

$$n(p) = \frac{2p_x}{h^3 m} \frac{1}{e^{\frac{(p_x^2+p_y^2+p_z^2)/2m-\mu_s}{kT}} + 1}. \tag{26.2}$$

Even though Eq. (26.1) gives the current observed at the collector per unit area of the emitter, the two transmission functions $D(p, B)$ and $F(p, V, T)$ must be known to make the calculation. Therefore to apply Eq. (26.1) to experimental results, it is necessary to design the experiment in such a manner that simplifying assumptions with regard to the transmission coefficients are legitimate. Since the crucial part of this theory is dependent on these assumptions, the following paragraphs will deal with the more important aspects of the restrictions needed.

The symbol $D(p, B)$ used for the transmission of electrons over the emission barrier has been chosen to call attention to the dependence of this factor upon the components of momentum (p) with which the electron approaches the barrier and the symbol B includes the properties of the emission surface barrier itself. The simplest known surface barrier is that for a clean, atomically smooth single face of a single crystal of a good conductor. The only experiment reported in the literature which is designed to evaluate this transmission function specifically is that of HUTSON[1].

Although the experimental result obtained by HUTSON does not lend itself to a representation by a simple analytic expression for the transmission coefficient, the results are in such excellent quantitative agreement with an analytic function found empirically by NOTTINGHAM[2] that this expression will best serve the present purpose. These results may be summarized by the following relations:

Clean single crystal surface

I. Range in $(p_x^2/2m) < W_a$

$$D(p, B) = 0. \tag{26.3}$$

II. Range $(p_x^2/2m) \geq W_a$

$$D(p, B) = \left(1 - e^{-\frac{p_x'^2/2m}{\omega}}\right) \tag{26.4}$$

where $(p_x'^2/2m) = p_x^2/2m - W_a$.

The interpretation placed on these conditions is that no electron can escape unless it approaches a barrier perpendicular to the x direction with a kinetic

[1] A. R. HUTSON: Phys. Rev. **98**, 889 (1955).
[2] W. B. NOTTINGHAM: Phys. Rev. **49**, 78 (1936).

energy associated with that component of the momentum which is greater than the electron affinity W_a. The usual assumption is that, if this kinetic energy exceeds W_a then its probability of escape is unity. The expression given in Eq. (26.4) indicates that the probability of escape approaches unity only after the *excess* kinetic energy expressed as $(p'^2_x/2m)$ exceeds the empirical constant ω by a considerable factor. The empirical value of ω is 3.05×10^{-20} joules or 0.191 electron volt.

Even though this transmission coefficient given by Eq. (26.4) is in excellent agreement with the experiments of both HUTSON[1] and NOTTINGHAM[2], it yet remains to be proven conclusively that the phenomenon is correctly interpreted as a deficiency of slow electrons because of the "reflection effect" at the boundary. Reflection can be established unambiguously only by the experimental observation of it for very slow electrons which impinge on the external surface of a clean, single crystal face. This direct evaluation is being undertaken by LANGE[3].

If the surface is not uniform, the transmission over it may be far more complex and may even be field-sensitive when the retarding field is small. Polycrystalline surfaces, even though they are clean, generally exhibit different crystal facets for the individual crystals that make up the surface. Since these facets are likely to have different work-functions, local contact-difference in potential fields will make the specification of a suitable choice for the electron affinity W_a difficult, if not impossible. The expression "patch effect" is used to describe this difficulty qualitatively. It will become clear after a discussion of the collection coefficient $F_c(p, V, T)$ that all cathode inhomogeneities become more and more unimportant as the retarding potential increases.

The transmission coefficient through and over the collector barrier is also very difficult to evaluate. Factors that are important may be enumerated: 1. geometrical arrangement of the collector with respect to the emitter and all other elements in the experimental diode such as glass walls, insulators, etc. 2. the surface structure of the collector including non-uniformities in work-function that are derived either from a polycrystalline structure or a non-uniform distribution of polarizable adsorbed atoms, 3. the energy distribution of the electrons that impinge on the collector barrier since there may be a reflection effect at this barrier which is energy-dependent, 4. changes in the surface properties of the collector (specifically, its work-function) which often accompany changes in the current density being received as well as the previous history of the electron bombardment of that surface[4].

If the purpose of the experiment is to determine the energy distribution of the electrons emitted from the cathode, then every means must be adopted to eliminate as many of the complexities enumerated above as possible. Hence, the reader is therefore warned in his future studies that results obtained from experiments in which due consideration has not been given to these factors should be viewed with scepticism.

A superficial examination of the problem suggests immediately that the ideal geometrical arrangement for the determination of an electron energy distribution

---

[1] A. R. HUTSON: Phys. Rev. **98**, 889 (1955).
[2] W. B. NOTTINGHAM: Phys. Rev. **49**, 78 (1936).
[3] W. J. LANGE: Research in progress, Department of Physics, Massachusetts Institute of Technology, Cambridge, Massachusetts.
[4] W. B. NOTTINGHAM: Phys. Rev. **39**, 183 (1932); **44**, 311 (1933); P. L. COPELAND: Phys. Rev. **57**, 625 (1940).

would be that of a closely-spaced diode formed with parallel planes. It is safe to say that such a diode is practically impossible to achieve since for it to be successful the collector would have to be a single crystal capable of being heated sufficiently to drive off all adsorbed films. Collectors such as these have not been made[1]. The next best solution involves the construction of a diode with coaxial cylinders. This structure, also, is subject to the difficulty of reflection from the collector, unless the collector radius is large compared with the emitter radius. The coaxial diode has the distinct advantage that electron reflections from the collector are minimized because any electron which leaves the filamentary cathode with sufficient energy to have been collected will, in general, find itself repeatedly coming to the collector even though it may have been reflected one time or more. Since the collecting cylinder can be constructed from a refractory metal such as tantalum, the purity of the surface can be insured under proper vacuum conditions. A structural form like this eliminates practically all the objectionable features that might interfere with the correct interpretation of the emission properties of the emitter in the presence of a retarding field. For a cylindrical structure, Eq. (26.1) has been put into usable form by NOTTINGHAM[2].

The emitter transmission function $D(p, B)$ is taken to be that given as Eqs. (26.3) and (26.4). The factor $F_c(p, V, T)$ which represents the probability of electron collection at the collector, has two ranges that can be explained most concisely by the following equations if the z direction is along the axis, the x direction along the radius and the y direction tangent to the emitting filament at the surface point of electron emission.

I. Range:

$$\left.\begin{aligned} p_x'^2 + p_y^2\left(1 - \frac{r^2}{R^2}\right) &< 2meV, \\ F_c(p, V, T) &= 0. \end{aligned}\right\} \tag{26.5}$$

II. Range:

$$\left.\begin{aligned} p_x'^2 + p_y^2\left(1 - \frac{r^2}{R^2}\right) &\geqq 2meV, \\ F_c(p, V, T) &= 1. \end{aligned}\right\} \tag{26.6}$$

In these expressions the potential (V) is defined as the *retarding* potential in the space and is the work required to carry an electron from a point just outside the emitter surface to a point just outside the collector surface. Since it is a necessary condition that the radius of the emitter (r) be small compared with the radius of the collector (R) in order to minimize the effect of reflection at the collector, the condition equation given above (which was derived from an analysis of the electron trajectory between coaxial electrodes) can be approximated by one's neglecting (r^2/R^2) in comparison with unity. It is this condition on the probability of transmission to the collector that establishes the limits of integration not specified explicitly in Eq. (26.7). This equation gives the electron emission current density expected as a function of the temperature and the retarding potential.

$$I = \frac{2e}{h^3} e^{-\frac{W_a - \mu_s}{kT}} \int_{p_z=-\infty}^{+\infty} \int^{+\infty} \int^{+\infty} \left(1 - e^{-\frac{p_x'^2}{2m\omega}}\right) \frac{p_x'}{m} e^{-\frac{p_x'^2 + p_y^2 + p_z^2}{2mkT}} dp_x' dp_y dp_z. \tag{26.7}$$

---

[1] H. SHELTON: Research Laboratory of Electronics, Massachusetts Institute of Technology, Cambridge, Massachusetts, is experimenting with a single crystal tantalum collector to receive an electron beam collimated by a magnetic field.

[2] W. B. NOTTINGHAM: Phys. Rev. **49**, 78 (1936).

In spite of the apparent complexity of this equation, it can be integrated and put into the usable form indicated by the following equations:

$$S = \frac{eV}{kT} = \frac{11\,600}{T} V, \tag{26.8}$$

$$I = I_{00}\left[G(S) - F(S, kT/\omega)\right], \tag{26.9}$$

$$I_{00} = \frac{4\pi m k^2 e}{h^3} T^2 \mathrm{e}^{-\frac{W_a - \mu_s}{kT}}, \tag{26.10}$$

$$G(S) = \frac{2}{\sqrt{\pi}} S^{\frac{1}{2}} \mathrm{e}^{-S} + 1 - \frac{2}{\sqrt{\pi}} \int_0^{S^{\frac{1}{2}}} \mathrm{e}^{-x^2} dx, \tag{26.11}$$

$$F(S, kT/\omega) = \frac{1}{1 + \frac{kT}{\omega}} \left[\left(\frac{\omega}{kT}\right)^{\frac{1}{2}} \frac{2}{\sqrt{\pi}} \mathrm{e}^{-S\left(1+\frac{kT}{\omega}\right)} \int_0^{\left(\frac{SkT}{\omega}\right)^{\frac{1}{2}}} \mathrm{e}^{y^2} dy + 1 - \frac{2}{\sqrt{\pi}} \int_0^{S^{\frac{1}{2}}} \mathrm{e}^{-x^2} dx \right]. \tag{26.12}$$

Since the controllable variables are the retarding potential V and the temperature T, the function expressed in Eq. (26.12) must be worked out in tabular form with sufficient detail so that smooth curves can be drawn for the purpose of interpolation. An inspection of Eqs. (26.11) and (26.12) shows that Eq. (26.12) reduces exactly to Eq. (26.11) as (kT/ω) approaches zero. It is, therefore, not necessary to tabulate the function $G(S)$[1], of since the values of this function for the range S from 0 to 10 will be found in the first row of the Table 2. A graphical representation of Eq. (26.9) is shown in Fig. 4. Three of the curves show the computed result for the three temperatures, 813, 1160, and 1852° K. The value of ω used is the one found experimentally: 3.05×10^{-20} joules (0.191 ev). The fourth curve in the diagram is the universal curve expected for a transmission coefficient $D(p, B)$ of unity for all positive values of p'_x.

Even though retarding potential measurements often have questionable validity for the determination of the true energy distribution of the electrons emitted from a thermionic source, an analysis of these measurements may yield other useful information. The temperature of the emitter may be determined sufficiently accurately to be useful information if the rate of change of emission is determined as a function of the applied voltage for the largest retarding potentials. Observations in this range demand the measurement of the smallest currents possible consistent with the insulation properties of the diode structure. At high retarding fields, cathode inhomogeneity in structure and reflection effects become less and less important. The accuracy of the agreement found by FAN[2] and HUNG[3] also supports the view that cathode temperatures may be determined in this manner under specialized geometrical conditions.

An analysis of this problem by IKEHARRA[4] has supplied a method of determining the temperature of oxide cathodes by evaluation of higher order harmonics observed in the output of a diode (or its equivalent) while a small range in the retarding potential characteristic is swept by a sinusoidal voltage variation. (For additional discussion see Sects. 60 and 62.)

---

[1] W. SCHOTTKY: Ann. Phys., Lpz. **44**, 1011 (1914). Tabulated by L. H. GERMER: Phys. Rev. **25**, 795 (1925).
[2] H. Y. FAN: J. Appl. Phys. **14**, 552 (1943).
[3] C. S. HUNG: J. Appl. Phys. **21**, 37 (1955).
[4] S. IKEHARRA: J. Appl. Phys. **25**, 725 (1954).

A second use for thermionic measurements in retarding fields is in the quantitative determination of changes in the work-function of the collector. The work of I. LANGMUIR and KINGDON[1] and also of D. B. LANGMUIR[2] may be cited as examples of the use of a retarding potential method for the determination of the variation in the work-function of the collector.

Although the current received by a particular collector operated at a high retarding potential is practically independent of the emission properties of the cathode for a given *applied* potential, the current observed is a very sensitive function of the anode itself. The reason for this sensitivity is that the applied potential measures the difference in energy of the FERMI level of the collector with respect to the FERMI level of the emitter. The motive[3-6] maximum over which the electrons must flow in order to register as a current at the collector is higher than the FERMI level of the collector by its own work-function. Therefore, even though the applied potential be maintained constant, the change in the work-function of the collector can alter the current that flows to it in a very significant manner; while a corresponding change in the emitter is generally of no measurable significance under these conditions. To use this method as a quantitative measure of any change in the work-function of the collector, it is necessary that other fields that might possibly alter the electron trajectories remain unchanged or else some method must be used for normalizing them. This method, which is adaptable for the study of surface conditions and alterations in these surface conditions, should find a wider application than it seems to have at present.

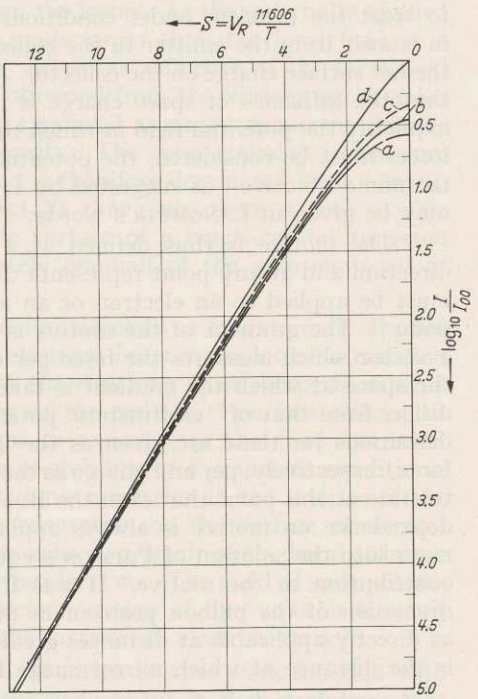

Fig. 4. Computed energy distributions. *a* 813° K with reflection. *b* 1160° K with reflection. *c* 1852° K with reflection. *d* No reflection.

Two additional precautions need to be mentioned in association with the analysis of retarding potential measurements. Gross inhomogeneities on the emitter surface, such as are found on partially coated oxide surfaces, must be considered. Care must be exercised to confine the range of emission current density to that for which space-charge effects are negligible (see Sect. 83). Development of a space-charge limitation first occurs at the collector as the retarding potential is reduced, and then the maximum in the motive for an escaping electron progresses across the diode as the applied potential to the collector is made more positive. This motive maximum is produced by the

[1] I. LANGMUIR and K. H. KINGDON: Phys. Rev. **34**, 129 (1929).
[2] D. B. LANGMUIR: Phys. Rev. **49**, 428 (1936).
[3] See Sect. 27.
[4] I. LANGMUIR and K. H. KINGDON: Proc. Roy. Soc. Lond., Ser. A **107**, 61 (1925).
[5] P. W. BRIDGEMAN: The Thermodynamics of Electrical Phenomena in Metals. New York: Macmillan Co. 1934.
[6] C. HERRING and M. H. NICHOLS: Rev. Mod. Phys. **21**, 185 (1949).

space charge and limits the emission. In simple geometrical cases, a theoretical analysis can be applied to determine the space-charge distribution and, therefore, the emission properties in the presence of space charge. In most practical tubes, it is not profitable to try to work out a detailed theory to be applied to a particular structure.

27. The influence of accelerating fields. In order to discuss the influence of electron accelerating fields on thermionic emission phenomena, it is desirable to treat the problem under conditions such that the total charge of electrons in transit from the emitter to the collector will be negligible in comparison with the net surface charge on the collector. This limitation is the equivalent of stating that the influence of space charge is negligible. It is also necessary to define explicitly the potential field in which the electron is moving. Since mirror-image forces must be considered, the potential is defined in a special way and is given the name "motive" as suggested by I. LANGMUIR[1]. The definition of "motive" may be given in LANGMUIR'S words:

"The motive is thus defined as a scalar quantity whose gradient in any direction and at any point represents the force component per unit charge which must be applied to an electron or an ion to hold it in equilibrium at the given point." The gradient of the motive is the "motive intensity" and is therefore a vector which measures the force per unit charge *on an electron* at the point in the space at which the gradient is taken. It is to be noted that this definition differs from that of "electrostatic potential" and of "electric intensity" in that definitions for these are given as the limit of the time average of the work or force, respectively, per unit charge as the charge approaches zero. It is appropriate to state at this point that even the BOLTZMANN equation for the electron density dependence on motive is always applicable. The potential and the fields that enter into the solution of POISSON'S equation deal only with the "electrostatic" contribution to the motive. It was for this reason that the formulation and discussion of the pillbox problem in Sect. 22 defined the potentials used there as directly applicable at distances greater than 10^{-5} cm. from the surface. This is the distance at which mirror-image forces are usually negligible.

As an electron leaves a conducting surface, it is acted upon by short-range and by long-range forces. The short-range forces dominate for a distance of the order of 1 or 2 interatomic distances (10^{-7} cm. or less) and depend on the surface composition, that is, the orientation of the actual surface with respect to atomic or crystallographic arrangement of the interior and with respect to the adsorbed atoms in the immediate neighborhood of the emission point. Even though there can be no doubt about the existence of these forces, no experiments have been formulated which yield quantitive information other than the knowledge that the integral of all of the forces with respect to distance determines the true work-function. It is this variation in the short-range forces from substance to substance and from surface to surface that accounts for the observed differences in their true work-functions. The most important of the long-range forces was identified by SCHOTTKY[2] as the "mirror-image" force.

The second kind of long-range force arises from cathode inhomogeneity. No practical electron emitter has ever been constructed which is truly free from inhomogeneity. For example, a single crystal of tungsten formed as part of a wire and used in a coaxial diode always exhibits in its surface a variation in the crystal structure which depends on the orientation of the crystal axes with respect

[1] I. LANGMUIR and K. H. KINGDON: Proc. Roy. Soc. Lond., Ser. A **107**, 61 (1925).
[2] W. SCHOTTKY: Phys. Z. **15**, 872 (1914).

to the axis of the wire. For the present purposes it is sufficient to say that the greater the linear dimensions of the areas of inhomogeneity, the greater the distance into space near the cathode that these local field effects will extend. Since extreme differences in work-function are unlikely to exceed one or two electron volts, these very extended fields will be correspondingly weaker the larger the area of each patch of high or low work-function. Neighboring high work-function areas cause local fields to exist over the low work-function areas which inhibit the emission of electrons from the latter. As the externally applied accelerating field is increased, it can be made larger than the local field at a relatively low value of applied potential. After the influence of the local field has been largely wiped out, the emission obtained from the various patch areas is that which would have been available, expressed as emission current density independent of the presence of inhomogeneity. The total emission is the sum of the emissions from the various areas and is therefore dominated by low work-function regions. It will be shown in Sect. 71 that since there is such a wide variation in the current density over the surface of a single-crystal tungsten wire of circular cross section, approximately one-half of the wire emits all of the observed electrons.

Basically, the reason that electron emission increases as an externally applied accelerating field is increased is that more electrons become available for emission as the maximum in the barrier over which the electrons must escape is reduced relative to the FERMI level in the interior of the emitter. Spurious effects can occur which conceivably cause a decrease in emission as the field increases. These spurious effects always reflect lack of stability of the surface conditions, which can be brought about either by the ionic migration in the interior of the solid near its emission surface or by the adsorption on the surface of electronegative gases (cathode poisons) that often arise as a result of the bombardment of the anode or an associated insulator by the electrons. The yield of such poisonous products is often negligible for an electron energy of five volts or less but it continues to increase after onset with the increase in electron energy[1].

There are two ways of evaluating the reduction in true work-function with accelerating field, if one carries through the experiment in such a manner that the emitter surface remains unchanged. These ways are: 1. direct measurement of the actual energy distribution of the electrons, 2. the measurement of the variation in the integrated thermionic emission as a function of the field. The thermionic emission method depends on the validity of certain assumptions which can be explained most easily by a quick review of the detailed theory applicable to this experiment.

The motive function for an electron as it leaves a conducting surface is represented qualitatively by the solid line of Fig. 5 a. Corresponding to this motive function, there is a force function per unit charge which is represented by the line in Fig. 5 b. This motive intensity is obtained, at least in principle, from the gradient of the motive as defined above. In the presence of an accelerating field, the modified motive function is everywhere lower than the zero field curve and the computation which must be made in order to determine the extent of the lowering is most easily seen in the force-function diagram of Fig. 5 b. Over the range in distance from x_0 to x_c the force function in the absence of space charge is diminished by an amount directly proportional to the accelerating potential V_c multiplied by a geometric factor $G(x)$. The accelerating potential

[1] J. D. HOBBS: Energy Dependence of Electron Produced Poisoning of Oxide Cathodes. Master's Thesis, M. I. T., 1954.

is defined as the applied potential v corrected for by the contact difference in potential P_T as shown in Eq. (27.1).

$$V_c = v - P_T. \tag{27.1}$$

The contact difference in potential is defined as the difference between the true work-function of the collector and that of the emitter when these work-functions are expressed in electron-volts. This relation is given as Eq. (27.2).

$$P_T = \varphi_c - \varphi_s. \tag{27.2}$$

The electric intensity (E), shown in Fig. 5 b, may be a function of the distance from the emitter surface depending on the geometrical arrangement of the emitter and the collector. The general expression for the intensity is the following:

$$E = V_c G(x). \tag{27.3}$$

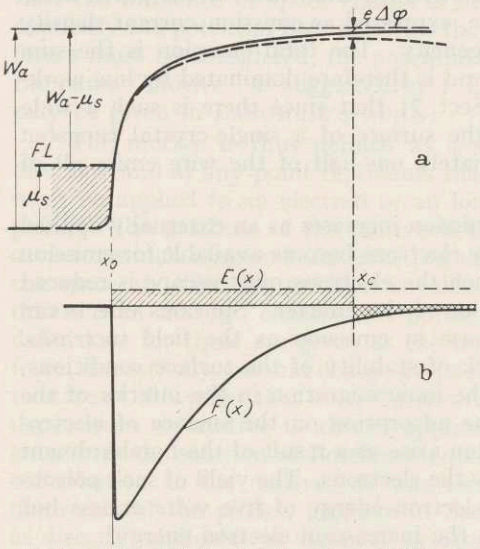

Fig. 5 a and b. a) Motive function for an electron as it leaves a conducting surface. b) Motive intensity for an electron.

The specific expression for parallel planes separated by distance D gives the field as independent of x as follows:

$$E = V_c/D. \tag{27.4}$$

For coaxial cylinders of radii r and R, the field depends on x and is

$$E = V_c \left[\frac{1}{\left(1 + \frac{x}{r}\right) r \ln \frac{R}{r}} \right]. \tag{27.5}$$

Notice that the field in the neighborhood of an emitting cylinder of radius r is constant for distances from the surfaces which are small compared with the emitter radius.

An inspection of Fig. 5 b permits one to write the expression for the reduction in true work-function as a function of the accelerating potential. This result is written as follows:

$$\Delta\varphi = V_c \int_{x=x_0}^{x=x_c} G(x)\, dx + \int_{x=x_c}^{x=\infty} F(x)\, dx. \tag{27.6}$$

It is evident from this equation that if the force function $F(x)$ is known, the reduction in work-function can be computed, since at the critical distance (x_c) the force function and the accelerating field are also related by Eq. (27.7):

$$V_c G(x_c) + F(x_c) = E_c + F(x_c) = 0. \tag{27.7}$$

The converse of the above statement is also true: that is, if there is an experimental way of making a direct determination of the change in work-function $\Delta\varphi$ with field, then the force function $F(x)$ can be determined. Both of these procedures have been used and will be illustrated below.

The method followed by SCHOTTKY was to assume the force function per unit charge (motive intensity at zero external field) to be dominated by the mirror image. This function is the following:

$$F(x) = -\frac{e}{16\pi (x - x_0)^2 \varepsilon_0} \text{ newtons per coulomb (or volts per meter)}. \tag{27.8}$$

This function serves as a means of difining the location (x_0) which can be taken as the "perfect" image boundary of the conductor. The original distances used in the above equations were presumably measured from some arbitrary point $x=0$ considered to be at the surface of the emitter. If the long-range forces at some distance from the surface are given in terms of Eq. (27.8), it is as though the actual force were matched to this equation in such a manner that, if the mirror-image function continued in exactly this form down to x_0 it would become infinite. The finiteness of the actual integral (i.e., the electron affinity) establishes that the true forces against which the electron works as it escapes are weaker than the mirror-image force at short range. It has been pointed out by DE BOER[1], LANGMUIR, and others that, in a qualitative manner, the difference between the true motive-intensity function and the mirror-image function should be related to the interatomic spacing of the surface atoms or to the roughness of the surface through which the electron is escaping. For a smooth and closely packed surface, such as the 110 surface of tungsten, the short-range forces are the strongest and the integral of these forces gives a very high electron affinity. It follows directly from Eqs. (27.7) and (27.8) that the escape distance (x_c) is given by Eq. (27.9):

$$x_c = x_0 + \left(\frac{e}{16\pi\,\varepsilon_0\,G\,(x_c)\,V_c}\right)^{\frac{1}{2}}. \tag{27.9}$$

If the structure of the diode is such that the geometrical function $G(x)$ is dependent on the distance, full knowledge of that function is needed in order to carry through the evaluation indicated by Eq. (27.6). If over the range of distance from the surface to x_c, the value of $G(x)$ is a constant (as is the case for parallel planes and cylinders if the distance is small compared with the radius of curvature of the emitter), it is possible to carry through the integration. The result is the well-known SCHOTTKY equation which shows that the decrease in work-function is directly proportional to the square root of the surface electric intensity. This equation checks with experiment only if the dominating long-range force, that acts upon an electron as it escapes, is the mirror-image force.

The only direct observation of this "SCHOTTKY effect" was made by HUTSON[2] even though *indirect* observations have been made both in association with thermionic emission and with photoelectric emission.

One needs only to refer to Eq. (26.1) to realize that the introduction of this accelerating field effect can best be made by incorporating it into the definition of $D(p, B)$ which expresses the probability that an electron can escape from the emitter. If it is possible to substitute for the electron affinity, W_a, its modified value as given in Eq. (27.10), then the analysis can be carried through very simply:

$$W_v = W_a - (\Delta\varphi)\,e. \tag{27.10}$$

A necessary condition for the application of SCHOTTKY's results to an experiment in thermionic emission is that the energy distribution of the electrons as they pass over the limiting barrier at the distance x_c from the surface remains independent of the externally imposed electric field.

It could be assumed from the NOTTINGHAM[3] experiment that the energy distribution of the electrons observed at zero field was one deficient in low-energy electrons, but there was no evidence prior to the HUTSON experiments

[1] J. H. DE BOER: Electron Emission and Adsorption Phenomena, p. 18. Cambridge Univ. Press. 1935.

[2] A. R. HUTSON: Phys. Rev. **98**, 889 (1955).

[3] W. B. NOTTINGHAM: Phys. Rev. **49**, 78 (1936).

that the same energy distribution was applicable to the electrons emitted in the presence of a strong accelerating field. He showed that the distribution was invariant with the applied field. It is this result which could not possibly have been predicted that warrants the use of Eqs. (26.3) and (26.4) for the transmission probability. There is one minor difference, however, and that is that W_v as defined by Eq. (27.10) must be used to establish the ranges for the use of Eqs. (26.3) and (26.4) and that the momentum component (p'_x) used in Eq. (26.4) is defined as the momentum of the particular electron as it passes over the limiting barrier at the distance x_c. With these limitations in mind it is possible to write the SCHOTTKY equation immediately, both in the direct form and in its logarithmic form. These equations are the following:

$$I = I_0 \exp\left\{\frac{e}{k}\left[\frac{e}{4\pi\varepsilon_0}\right]^{\frac{1}{2}}\frac{(G V_c)^{\frac{1}{2}}}{T}\right\}, \tag{27.11}$$

$$\ln I = \ln I_0 + 0.4402\,\frac{(G V_c)^{\frac{1}{2}}}{T}, \tag{27.12}$$

$$\log_{10} I = \log_{10} I_0 + 0.1912\,\frac{(G V_c)^{\frac{1}{2}}}{T}. \tag{27.13}$$

In these equations the current I_0 is a constant of the equation which superficially represents the "observed" emission current at zero field, that is, when the accelerating potential V_c is zero. Experiment shows, as discussed in detail in Sect. 70 that the observed current at zero field is always less than the value predicted by these equations when it is compared with the empirical value of the constant I_0 that best fits the data observed at high field strength.

Undoubtedly, one of the most important influences in this disagreement is the inhomogeneity of all laboratory specimens. The high field data apply more directly to the emission from the low work-function areas, uninhibited by the local fields brought about in these areas by the neighboring high work-function regions.

It was pointed out above that if the change in work-function were known as a function of the accelerating potential, the force-function could be deduced by the proper application of Eq. (27.6). To obtain this change in work-function from thermionic emission directly, it is necessary to make the assumption that the actual energy distribution of the electrons is independent of the applied voltage, but it is not necessary to assume that the emission is a true MAXWELLian distribution. A reflection deficiency of the type described in connection with the derivation of the SCHOTTKY equation and illustrated originally by Eq. (26.4) will not alter the result. The current is related to the decrease of the work-function by an amount $\Delta\varphi$ by Eq. (27.14)

$$I = I_0\, e^{-\frac{e\Delta\varphi}{kT}}. \tag{27.14}$$

In this equation the current I_0 is that found at a given temperature before any modification has occurred in the work-function. The actual choice of I_0 is not so very important in the analysis since it is the change in emission that is used.

Eq. (27.14), in its logarithmic form, can be differentiated with respect to V_c to obtain the following result:

$$\frac{d(\Delta\varphi)}{dV_c} = \frac{kT}{e}\,\frac{d(\ln I)}{dV_c}. \tag{27.15}$$

This equation shows that if $\ln I$ is known as a function of the accelerating voltage, then the slope of that curve, multiplied by (kT/e) will give the rate with which

the change of work-function shifts with voltage. One needs only to differentiate Eq. (27.6) with respect to the accelerating voltage to obtain the result given in Eq. (27.16)

$$\frac{d(\Delta\varphi)}{dV_c} = \int_{x_0}^{x_c} G\,dx. \tag{27.16}$$

In order to obtain this equation, it was necessary to make use of the equality of the force-function and field as given in Eq. (27.7). Since in most applications the geometrical function $G(x)$ is constant over the important range from x_0 to x_c, the integration can be carried forward and one obtains, by combination with Eq. (27.15), the following value for the critical distance:

$$x_c - x_0 = \frac{kT}{eG}\frac{d(\ln I)}{dV_c}. \tag{27.17}$$

Having determined the critical distance x_c from the observed data, one then makes use of Eq. (27.7) to determine the value of the force-function which is effective at that distance.

Although it is possible to deduce the fact that the force-function is of the mirror-image type at applied potentials great enough to overcome the patch fields, it is clearly more practical to use the SCHOTTKY equation first and plot, as is indicated in Eq. (27.13), the logarithm of the current as a function of $(V_c)^{\frac{1}{2}}/T$. If the plot gives a straight line of slope $0.1912\,G^{\frac{1}{2}}$, the experiment shows that SCHOTTKY's mirror-image force dominates. In general, experiments carried out under suitable conditions yield results that agree well with this equation over a considerable range in surface field. A small systematic variation has been observed which will be discussed in the next section.

28. Periodic deviations from the SCHOTTKY theory prediction. A very detailed study of the increase in thermionic emission with accelerating field by SEIFERT and PHIPPS[1] showed that the so-called "SCHOTTKY Plot" is not a straight line but deviates in a regular manner as a function of the surface electron accelerating field. Since the average slope of the plotted data is that predicted by the SCHOTTKY mirror-image theory, there is a temptation to describe the observed deviation as a "periodic" deviation with reference to this line. Although the effect is extremely small, it has been verified by a number of researchers[2].

The nonlinearity of the SCHOTTKY plot acquires significance mainly because it can be explained only on the basis of a complete wave-mechanics understanding of the behavior of electrons as they escape over a mirror-image barrier in the presence of a strong field. The theories of GUTH and MULLIN[3] have been presented and also discussed in considerable detail by HERRING and NICHOLS[4].

The theoretical explanation of the periodic deviations brings the conclusion that a small reflection effect exists, and that the integrated influence of this reflection is dependent on the location and shape of the mirror-image barrier modified by the external field. Since the extent of reflection effects at the surface of an electron emitter is clearly an open question, the details of the theoretical analysis will be omitted from this presentation. A brief review of the experimental evidence will be given later in Sect. 70.

---

[1] R. L. B. SEIFERT and T. E. PHIPPS: Phys. Rev. **56**, 652 (1939).

[2] W. B. NOTTINGHAM: Phys. Rev. **57**, 935 (1940) (L). — E. G. BROCK, A. L. HOUDE and E. A. COOMES: Phys. Rev. **89**, 851 (1953). — D. W. JUENKER: G. S. COLLADAY and E. A. COOMES: Phys. Rev. **90**, 772 (1953).

[3] E. GUTH and C. J. MULLIN: Phys. Rev. **59**, 575 (1941); **59**, 867 (1941); **51**, 339 (1942).

[4] C. HERRING and M. H. NICHOLS: Rev. Mod. Phys. **21**, 185 (1949).

IV. LANGMUIR'S space-charge theory.

29. Statement of the problem. Early observations showed that for a given diode structure and a particular applied accelerating potential on the collector, the thermionic emission current increased exponentially with the temperature up to a fairly sharp limited current and showed very little further increase as the temperature exceeded this critical value. The limiting current was found to increase approximately as the $\frac{3}{2}$ power of the applied voltage and, of course, the critical temperature at which current limitation took place was voltage-dependent. The first step toward the theoretical understanding of this problem came when CHILD[1] and also LANGMUIR[2] applied the POISSON equation and the equation for current continuity as a pair of simultaneous relations.

Further study indicated that the current limitation was really due to the motive[3] maximum (for electrons) between the emitter and the electron collector because under the conditions of the experiment there were more electrons carrying negative charges in transit between the emitter and the collector than the total of positive charge on the surface of the collector. This motive maximum acts directly as a retarding potential and, therefore, limits the emission. It will be shown in this analysis that the magnitude of this retarding potential is directly proportional to the temperature in excess of the critical temperature at which the surface field at the emitter shifts from an electron accelerating field to zero field. The theory to be presented also may be applied in the retarding potential region near zero field. The correct analysis to this problem therefore involves the solution of three basic equations which are: 1. POISSON's equation. 2. The BOLTZMANN density relation by which the energy dependence on temperature enters. 3. The equation of continuity of current. LANGMUIR[4] gave one of the first analyses of this problem which will be summarized here[5, 6, 7].

In the discussion of an electron atmosphere in a cavity (given in Sect. 21) mathematical simplification resulted from the choice of a "pillbox" which permitted the exact computation on the basis of an electron density variation with respect to distance which was a function of a single coordinate. For the same reason this analysis will be applied to a "plain parallel diode" structure. One surface of this diode is assumed to be capable of electron emission and its motive at all points over the surface at a distance of about 10^{-5} cm. differs in energy from the FERMI level in the interior of the emitter by the true work-function of the surface. This work-function must be assumed to be uniform all over the surface.

In the analysis which follows, the potentials and the potential gradients will apply only in the space between the two elements of the diode and will not include the distance over which mirror-image forces are appreciable. The electron collector must be assumed to be a perfect receiver of electrons. Any reflections or secondary emission that might occur at the surface of the electron collector must be assumed to be negligible. With these restrictions, it is obvious that no practical diode can satisfy the detailed requirements necessary for an exact application of the theory to experiment. In spite of this limitation, the theory certainly aids in the interpretation of experimental results.

[1] C. D. CHILD: Phys. Rev. **32**, 492 (1911).
[2] I. LANGMUIR: Phys. Rev. **2**, 450 (1913).
[3] See Sect. 27.
[4] I. LANGMUIR: Phys. Rev. **21**, 419 (1923).
[5] P. H. J. A. KLEYNEN: Philips Res. Rep. **1**, 81 (1946).
[6] A. VAN DER ZIEL: Philips Res. Rep. **1**, 97 (1946).
[7] H. F. IVEY: Advances in Electronics, Vol. VI, p. 137 . New York: Academic Press 1954.

Even though experiment has established that the distribution in energy of the electrons emitted from smooth surfaces constituting a measurable emission current is deficient in the low-energy group, it would complicate the analysis to attempt to bring this fact into the theory. The strict application of the theory as it will be developed here can be made only after qualitative consideration has been given to all of these special limitations in terms of emitter and collector properties.

30. Uses of space-charge theory. The qualitative aspects of space-charge theory are well known and often used, but application in a truly quantitative manner is not widespread. The coverage of this subject in most text books is incomplete because the incorporation into the theory of the energy distribution of the electrons is usually treated superficially. As the properties of oxide cathodes have become better understood within recent years, more and more research effort has been directed toward the solution of the cathode evaluation problem. It has not been easy to devise generally acceptable methods for cathode evaluation because the usual tests carried out at the normal operating temperature of the emitter border on being destructive of the cathode under test. Even though the tube structure under investigation can withstand the high voltage required to evaluate cathode emission properties by sweeping out the space-charge for a very short period of time, the validity of the results is definitely open to question. The practical use of the emitter is generally under a condition of strong space-charge limitation. An alternate method of cathode evaluation involves an analysis of the emission as a function of the temperature and with relatively small applied voltages over the temperature range below and up to the critical temperature at which space-charge limitation sets in. This method also has its drawbacks, since it does not evaluate the emitter at or even near the normal operating temperature. Indirect methods of cathode evaluation based largely on empirical procedures have been developed and are widely used (see Sects. 80 and 82).

It will be the purpose of the following sections to develop the theory of space charge in a plane parallel diode with the ultimate objective of applying it in a practical manner to the quantitative evaluation of emitter properties in the useful range in temperature and in a completely nondestructive manner.

The development of methods for the application of the theory depends on the combination of three factors not hitherto applied to this problem. The basic formulation of the problem is that of LANGMUIR. His final results were made available in tabular form. Although these tables are a necessary step toward the final application of the theory, the derivation of empirical equations adapted to represent the tabular data with the required accuracy has made it possible to carry LANGMUIR'S results nearer to experimental applicability. Another factor that simplifies the analysis is the introduction of the emission equation given as Eq. (9.1).

The tangibly observable quantities are emission currents, applied voltages, emitter temperature, and the geometrical configuration. The emitter and collector properties are the intangible factors that actually determine the relations between the four observables. One must, therefore, use the space-charge theory to discover the emitter and collector properties that are most consistent with the laboratory observations.

31. Potential curves and the critical temperature. Figs. 6a and 6b apply, respectively, to the application of accelerating fields in the space between the electrodes and that of retarding fields. The straight line (I) in each example represents the distribution in electrostatic potential in the absence of space

charge from a point just outside the emitter to the corresponding point in space just outside of the collector. The second line (II) shows qualitatively the potential distribution after the temperature of the emitter has been raised to exactly that critical value designated as Θ at which the gradient of the potential at either of the electrodes is exactly zero. In Fig. 6a the surface charge on the collector is measured directly by the gradient of the potential at that surface and the total of this surface charge is exactly equal to the total volume charge of all of

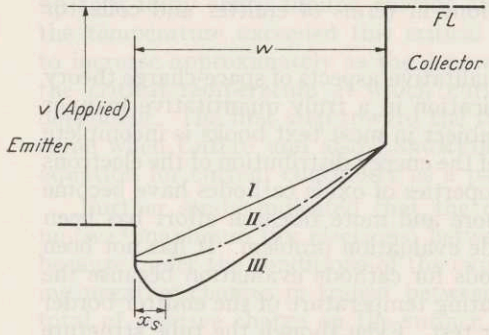

Fig. 6a. Potential distributions for three different cathode temperatures. Constant applied potential; positive temperature coefficient of work-function. I) No space charge. II) Zero field at emitter. III) With space-charge minimum at x_s.

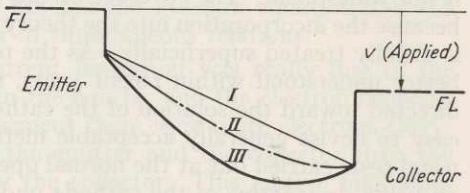

Fig. 6b. Potential distributions for three temperatures. I) No space charge. II) Zero field at the collector. III) With space-charge minimum.

the electrons in transit between the emitter and the collector. Under these conditions no lines of electric intensity extend all the way from the one electrode to the other. In Fig. 6b Curve (I) shows the surface charge on the emitter positive and the number of electrons in the space is negligible. The surface charge on the collector is negative. As the temperature of the emitter increases, its surface charge becomes still more positive and finally is exactly equal to the total charge in the space. At this temperature, Θ, the potential distribution of Curve (II), has a zero gradient at the collector. In both examples (accelerating and retarding), temperatures in excess of Θ produce a potential minimum (motive maximum for electrons) which is located between the two electrodes. Under these circumstances the mathematical theory which is applicable is the same for both figures, since positive charge will be found on both electrode surfaces. The sum of all of these positive charges will exactly equal the total charge of the electrons in the interelectrode space.

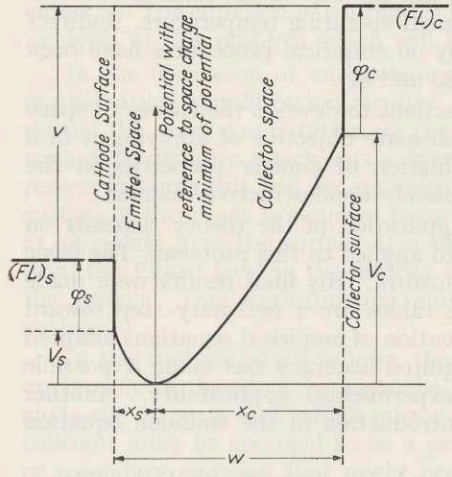

Fig. 7. Electrostatic potential with a space-charge minimum between the emitter and collector with applied accelerating potential.

32. Boundary conditions with positive applied potential. In general, there is more interest in the analysis as it applies to Curve (III) of Fig. 6a. The curve in Fig. 7 represents the electrostatic potential as a function of the distance either way from the potential minimum, which will always be found between the electrodes if the temperature is greater than Θ and the current is limited by space charge. The problem to be solved is that of determining the actual value of the potential as a function of distance which will satisfy the experimentally describable boundary conditions. The requirements are: 1. emitter to collector separation

is w; 2. the true work-function of the emitter is φ_s; 3. the true work-function of the collector is φ_c; 4. the applied difference in potential v establishes the FERMI level of the collector with respect to the FERMI level of the emitter; 5. the difference in potential between points just outside the collector and the emitter is related to the applied difference in potential by the following equation:

$$V_c - V_s = v - (\varphi_c - \varphi_s); \tag{32.1}$$

6. the temperature of the emitter is T, which is greater than the critical temperature Θ.

33. Formulation of the general space-charge problem. With the above parameters specified, the density of charge in the immediate neighborhood of the cathode will be given by Eq. (24.7). Notice, however, that this equation applied only to the *ideal cathode* and that no real cathode ever satisfies the necessary ideal conditions.

Subject to the conditions specified above, a potential minimum will be found at a distance x_s away from the cathode and with reference to the potential at this minimum; the point in space just outside of the emitter will be positive V_s. The corresponding point just outside of the collector will be V_c positive with respect to the potential minimum. The plane surface at the distance x_s from the cathode surface divides the interelectrode region into two parts which may be designated as the "emitter space" and the "collector space". The potential function is not symmetrical about this dividing line, because in the emitter space electrons are streaming in both directions from the emitter to the potential minimum and back to the emitter. A small *net* current of electrons, which left the emitter with high energy, stream over the potential minimum and result in a current which flows in one direction only in the collector space.

It is the purpose of this theory to formulate the solution to the problem of satisfying POISSON's equation, the BOLTZMANN relation, and the continuity of current requirement. These three relations expressed in equation form are written as follows:

POISSON's equation:

$$\frac{d^2V}{dx^2} = \frac{\nu e}{\varepsilon_0}. \tag{33.1}$$

BOLTZMANN relation:

$$\nu = \left(n_0 e^{\frac{eV}{kT}}\right) f. \tag{33.2}$$

Continuity of current:

$$I = \nu \frac{\overline{p}_x}{m} e. \tag{33.3}$$

The new symbols used in these equations may be defined as follows:

ν = number of electrons per unit volume near any plane located at a distance x from the potential minimum.

n_0 = number of electrons per unit volume that would be found in a complete MAXWELLian distribution at the potential minimum.

f = the fraction of a complete MAXWELLian distribution found at any plane between the two electrodes. For further explanation note that for a high-emission cathode, this fraction may approach unity very close to the cathode. The fraction will be exactly one-half at the potential minimum and may approach zero in the immediate neighborhood of the collector, when it is operated at a high positive potential.

I = electron current density in the direction from emitter to collector which is a constant at any plane between the emitter and the collector.

$\bar{p}_x/m$ = average velocity of the electrons that cross any plane in the direction emitter to collector. Notice that this average velocity depends on the temperature of the cathode and the potential, since it involves the actual energy distribution of the electrons. The potential value at the point in question determines the gain in kinetic energy which the electrons have received from the electric field.

Clearly, any theory dependent on the above conditions applies only if any change in external potential occurs very slowly in comparison with the average transit time of an electron as it crosses from the emitter to the collector.

34. Equation from statistical mechanics. In order that there be no misunderstanding with regard to the method by which f is calculated, the basic equation which comes directly from the statistical theory of free particles is the following:

$$f = \frac{\int_{p_z=-\infty}^{p_z=+\infty}\int_{p_y=-\infty}^{p_y=+\infty}\int_{p_x=\pm\sqrt{2meV}}^{p_x=+\infty} e^{-\frac{p_x^2+p_y^2+p_z^2}{2mkT}}\, dp_x\, dp_y\, dp_z}{(2\pi mkT)^{\frac{3}{2}}}. \tag{34.1}$$

The writing of this equation comes directly from an inspection of the distribution of representative points in momentum space. The proper incorporation of the potential at the space point at which the fraction f is determined, comes in the setting of the limits of integration with respect to p_x. If the region in space for which f is being calculated lies in the emitter space as shown in Fig. 7, then the minus sign is used, whereas if the space location is in the collector space, the plus sign is used. Eq. (34.1) can be simplified and made appropriate for calculation by defining two new quantities as given in Eqs. (34.2) and (34.3) and the substitution of them into Eq. (34.1):

$$\psi = \frac{eV}{kT}, \tag{34.2}$$

$$y^2 = \frac{p_x^2}{2mkT}, \tag{34.3}$$

$$f = \frac{1}{2}\left[1 \pm \frac{2}{\sqrt{\pi}}\int_{y=0}^{y=\psi^{\frac{1}{2}}} e^{-y^2}\, dy\right], \tag{34.4}$$

$$f = \tfrac{1}{2}\left[1 \pm P(\psi^{\frac{1}{2}})\right]. \tag{34.5}$$

After the integration of Eq. (34.1), the plus sign corresponds to the emitter region. The integral in Eq. (34.4) has been tabulated under the well-known designation "Probability Integral" defined as:

$$P(\psi^{\frac{1}{2}}) = \frac{2}{\sqrt{\pi}}\int_0^{\psi^{\frac{1}{2}}} e^{-y^2}\, dy. \tag{34.6}$$

35. Definition of distance unit x_1. In order to solve simultaneously Eqs. (33.1), (33.2), and (33.3) it is desirable to introduce a unit of distance which is exactly the same as that used in Eq. (22.4) except for an additional numerical factor of $\sqrt{2}$. The similarity of these unit distances can be seen more clearly by the following relation:

$$x_1^2 = 2\left[\frac{kT\varepsilon_0}{e^2 n_0}\right]\frac{e n_0 (kT/2\pi m)^{\frac{1}{2}}}{I}. \tag{35.1}$$

or

$$x_1^2 = \frac{2\varepsilon_0 (kT)^{\frac{3}{2}}}{e(2\pi m)^{\frac{1}{2}} I} = 2.370\times10^{-12}\frac{T^{\frac{3}{2}}}{I} = 2.963\times10^{-6}\frac{V_T^{\frac{3}{2}}}{I}. \tag{35.2}$$

Note that in Eq. (35.1) the constant current density I is expressible directly in terms of the density of electrons n_0 that can give exactly this current density for those electrons of a complete MAXWELLian distribution which cross a boundary. The actual concentration of electrons at the potential minimum is given by Eq. (33.2) and allows one to write the following:

$$v_0 = \tfrac{1}{2}\, n_0 . \tag{35.3}$$

The direct substitution of these relations in Eq. (33.1) results in the single differential equation that follows:

$$\frac{d^2\psi}{d\chi^2} = -\left[1 \pm P(\psi^{\frac{1}{2}})\right] e^{\psi} . \tag{35.4}$$

In this equation the plus sign is used for the emitter region and the minus sign for the collector region illustrated in Fig. 7. With the unit of distance defined by Eq. (35.2), the distance parameter χ is defined as (x/x_1) and x is measured from the potential minimum.

36. Solution to give electric intensity. Even though an explicit algebraic solution to Eq. (35.4) cannot be formulated, a step toward that solution can be made and the result is the following:

$$\frac{d\psi}{d\chi} = \sqrt{2}\left\{\left[1 \pm P(\psi^{\frac{1}{2}})\right] e^{\psi} - \left(1 \pm \frac{2}{\sqrt{\pi}}\,\psi^{\frac{1}{2}}\right)\right\}^{\frac{1}{2}} . \tag{36.1}$$

The next step in the complete solution of the problem would normally require the solving of Eq. (36.1). To find this solution explicitly seems to be impossible, but, of course, it can be accomplished by numerical integration. The solution by this method is given in Table 3.

By using a combination of theoretical forms as well as the results recorded in the table, the author has developed empirical equations which represent the results with considerable accuracy. These equations will be given in Sect. 37.

Eq. (36.1) permits the computation of the electric field at any point at which the potential is known. Note that the field is given by the following equation:

$$E = -\frac{dV}{dx} = -\left(\frac{kT}{e\,x_1}\right)\frac{d\psi}{d\chi} . \tag{36.2}$$

In this calculation the temperature is characteristic of the problem and the distance parameter x_1 is computed by Eq. (35.2). The emission current density I carried across the diode must be known.

37. Empirical equations that represent the solution to the LANGMUIR equation. In the emitter region the solution to Eq. (36.1) can be represented with good accuracy by the two equations given here as Eqs. (37.1) and (37.3). Notice that each applies for a specific range.

Range $0 \leqq \chi_s \leqq 1.4$ (Emitter Region)

$$\psi_s = \frac{\chi_s^2}{2} + 0.6\,(e^{0.32\,\chi_s^{3.17}} - 1) , \tag{37.1}$$

$$\psi_s = \frac{\chi_s^2}{2} + 0.6\,(10^{0.139\,\chi_s^{3.17}} - 1) . \tag{37.2}$$

Range $1.4 \leqq \chi_s \leqq 1.806$ (Emitter Region)

$$\psi_s = 2 \ln \left[\cos\,(\chi_s - 0.235)\right]^{-1} , \tag{37.3}$$

$$\psi_s = 4.605 \log_{10} \left[\cos\,(\chi_s - 0.235)\right]^{-1} . \tag{37.4}$$

Attention may be directed to the fact that as χ_s approaches 1.806, the value of ψ_s approaches infinity. The symbol $\chi_m = 1.806$ will often be used for this maximum value.

The inverse relation to the above equations is also of value. Again, a single equation cannot be used for the entire range but the two given below as Eqs. (37.5) and (37.6) give quite accurate results.

Range $0 \lessapprox \psi_s \lessapprox 2.0$ (Emitter Region)

$$\chi_s^2 = 2\psi_s + 0.72\psi_s^{1.46}. \tag{37.5}$$

Range $2 \lessapprox \psi_s$

$$\chi_s^2 = [\arctan (e^{\psi_s} - 1)^{\frac{1}{2}} + 0.235]^2. \tag{37.6}$$

The above equations are presented as empirical results that serve as a solution to Eq. (36.1) when the plus signs are used and are therefore applicable to the emitter region. For Eq. (36.1) to apply to the collector region, the negative signs must be used and under these circumstances the following equations give quite accurate results:

(Collector Region)

$$\psi_c = 1.17 \frac{\chi_c^{\frac{4}{3}}}{1 + \frac{1.68}{\chi_c^{0.681}}}, \tag{37.7}$$

$$\chi_c = 0.8888\, \psi_c^{\frac{3}{4}} \left(1 + \frac{1.413}{\psi_c^{0.475}}\right)^{\frac{3}{4}}. \tag{37.8}$$

The numerical constants of the two equations are, respectively, $(\frac{9}{4}\sqrt{\pi})^{\frac{2}{3}}$ and $(4\sqrt{\pi}/9)^{\frac{1}{2}}$.

38. The CHILD-LANGMUIR space-charge equation. As a step toward the writing of a relation that is the equivalent of the CHILD-LANGMUIR equation, Eq. (37.8) squared may be rearranged as follows:

$$1 = \frac{4\sqrt{\pi}}{9} \frac{\psi_c^{\frac{3}{2}}}{\chi_c^2} \left(1 + \frac{1.413}{\psi_c^{0.475}}\right)^{\frac{3}{2}}. \tag{38.1}$$

This equation rewritten in terms of the symbols introduced as Eqs. (34.2) and (35.2) takes on the familiar form as follows:

$$I = \frac{4\varepsilon_0}{9} \left(\frac{2e}{m}\right)^{\frac{1}{2}} \frac{V_c^{\frac{3}{2}}}{x_c^2} \left(1 + \frac{1.413}{\left(\frac{eV_c}{kT}\right)^{0.475}}\right)^{\frac{3}{2}}. \tag{38.2}$$

It is clear from this equation that under many experimental conditions the applied potential may be very nearly equal to that shown in Fig. 7 as V_c and that the distance x_c may be very nearly equal to w. For large values of applied voltage, the last factor of the equation is practically unity and the equation then reverts to that of the CHILD-LANGMUIR equation. The constant of that equation is given as follows:

$$K_L = \frac{4\varepsilon_0}{9} \left(\frac{2e}{m}\right)^{\frac{1}{2}} = 2.334 \times 10^{-6}. \tag{38.3}$$

It will be useful to define the ψ_c function of Eq. (38.1) by the symbol $F(\psi_c)$ given as follows:

$$F(\psi_c) = \psi_c \left(1 + \frac{1.413}{\psi_c^{0.475}}\right). \tag{38.4}$$

The true numerical values, that this function was developed to give, can be derived as indicated by Eq. (38.1) from the tabular values of χ_c, since the relation is given as follows:

$$F^{\frac{3}{2}}(\psi_c) = \frac{9}{4\sqrt{\pi}}\chi_c^2 = 1.269\,\chi_c^2. \tag{38.5}$$

Two equations very useful in computation that are the equivalent of Eq. (38.2) are given as Eqs. (38.6) and (38.7):

$$I = K_L \frac{F^{\frac{3}{2}}(\psi_c)}{x_c^2} V_T^{\frac{3}{2}}. \tag{38.6}$$

$$I = N \frac{\chi_c^2}{x_c^2} V_T^{\frac{3}{2}}. \tag{38.7}$$

The numerical value of a constant N may be computed from basic physical quantities as follows:

$$N = \varepsilon_0 \left(\frac{2e}{\pi m}\right)^{\frac{1}{2}} = 2.963 \times 10^{-6}. \tag{38.8}$$

A final and closely related expression which serves to link directly the properties in the emitter region to those in the collector region is given in equation form as:

$$x_1^2 = \frac{x_s^2}{\chi_s^2} = \frac{x_c^2}{\chi_c^2} = N \frac{V_T^{\frac{3}{2}}}{I}. \tag{38.9}$$

Even though it may be said that solutions to the space-charge problem are given by these various equations it is not easy to apply them to laboratory results. There are basically five independent variables which may be listed as follows:

1. The *diode spacing* w. The spacing to the potential minimum is related to w in that the sum of x_s and x_c is always equal to w.

2. The emitter temperature expressed either as T or its equivalent V_T [see Eq. (46.9)].

3. The *zero field* (at the emitter) *electron emission* current density of the emitter. This may be related to the temperature by an empirical equation of the form of Eq. (9.1) in which the two constants a and Φ constitute a description of the emitter.

4. The *applied difference in potential* which is directly controllable by the observer.

5. The *contact difference in potential* including its temperature coefficient, which depends both upon the properties of the emitter and the collector. Even though the temperature variation of the contact potential must be expected to be nonlinear, observations generally apply to such a limited range that it will be assumed at the start of the analysis that the contact difference in potential may be expressed as:

$$P_T = P_0 + V_T \frac{dP}{dV_T}. \tag{38.10}$$

The remaining sections of this theoretical analysis relate in one way or another to the bridging of the gap between the basic space-charge equations and their application to the interpretation of experimentally obtained results.

39. Application of the theory to boundary conditions. The equation which represents the thermionic emission current as a function of the temperature for stable cathodes was given as Eq. (9.1) and is reproduced as follows:

$$I = a\,e^{-\frac{e\Phi}{kT}} = a\,e^{-\frac{\Phi}{V_T}}. \tag{39.1}$$

This equation applies over that range in temperature for which the potential distribution between the emitter and the collector lies between curve (I) and curve (II) of Fig. 6a. At a very critical temperature $T = \Theta$ the potential gradient at the emitter is zero and this critical current I_0 is given by Eq. (39.2).

$$I_0 = a\, e^{-\frac{e\Phi}{k\Theta}}. \tag{39.2}$$

In order for this critical temperature to be determined with accuracy, the emitter must be very uniform, in regard to both its surface composition and its temperature.

A specific use to which Eq. (38.2) may be applied is that of determining for a given electrode spacing and given applied voltage v between the electrodes, the current I_0 that will flow when the critical temperature Θ is reached. Under these conditions V_c is related to the applied potential according to Eq. (32.1). Note that V_s is zero. The distance x_c is identically equal to the spacing w. With the temperature $T = \Theta$ yet to be determined precisely, a first approximation for the space-charge limited current can be obtained by neglecting the correction term involving the temperature in Eq. (38.2). If the cathode properties are known and specified by Eq. (39.2), it is easy to determine the temperature at which the approximate value of current density will be obtained. This temperature, now identified as Θ' may be used in the correction term of Eq. (38.2) and a corrected value of the current density computed. Having thus determined the most suitable I_0, one may make a very small correction to determine the exact temperature Θ from Eq. (39.2) that will yield a self-consistent set of data.

40. Determination of value of potential minimum. As the temperature increases above the critical value Θ, the potential minimum develops and the equation for the current is the following:

$$I = a\, e^{-\frac{e(\Phi + V_s)}{kT}}. \tag{40.1}$$

If ΔT is the increase in temperature above the critical value Θ then Eqs. (39.2) and (40.1) may be combined to give the appropriate value for the difference in potential between a point just outside of the emitter and the potential minimum illustrated in Fig. 7.

$$V_s = \Phi \frac{\Delta T}{\Theta} - \frac{kT}{e} \ln\left(\frac{I}{I_0}\right). \tag{40.2}$$

An inspection of this equation shows at once that if the current density I did not change at all with an increased temperature above its critical value I_0, then the potential minimum would increase in value in direct proportion to the temperature excess above the critical value Θ. The constant of proportionality is the work-factor Φ. Under well-controlled experimental conditions the current I will exceed I_0 by only a small amount ΔI for a considerable increase in temperature. Under these conditions an approximate form of Eq. (40.2) may be written by which the correction term may be evaluated most readily:

$$V_s \approx \Phi \frac{\Delta T}{\Theta} - \frac{T}{11\,600} \cdot \frac{\Delta I}{I_0} = \Phi \frac{\Delta T}{\Theta} - V_T \frac{\Delta I}{I_0} \tag{40.3}$$

where V_T is defined as $(T/11\,600)$.

This equation is useful in its application to experimentally realizable emitters under most circumstances, since the distance to the space-charge minimum x_s is generally smaller than the radius of curvature of the emitter. The steps by which this critical distance is determined follow.

41. Determination of distance to potential minimum. The first step is to compute the value of ψ_s:

$$\psi_s = \frac{eV_s}{kT} = \frac{\Phi e}{k\Theta} \cdot \frac{\Delta T}{T} - \ln \frac{I}{I_0}. \tag{41.1}$$

This value can be computed from observable quantities which are specifically: 1. the work-factor Φ; 2. the critical temperature Θ; 3. the absolute temperature T; 4. the excess temperature ΔT; 5. the current ratio (I/I_0). The corresponding value χ_s may be computed directly from Eq. (37.5) or Eq. (37.6), depending on the numerical value of ψ_s computed from Eq. (41.1). Since the current density and the temperature are known, the correct value for the distance from the cathode surface to the potential minimum may be computed directly from Eq. (35.2) or Eq. (38.9) and the definition of χ_s.

42. Application of theory to the retarding potential problem. In the retarding potential problem illustrated by Fig. 6b and Fig. 8 the magnitude of the retarding potential applied is constant and given by

$$V_r = V_s - V_c. \tag{42.1}$$

The expression that corresponds to Eq. (40.2) of the previous example is given as follows:

$$V_s = \frac{\Delta T}{\Theta}(\Phi + V_r) + V_r - V_T \ln \frac{I}{I_0}. \tag{42.2}$$

The procedure outlined above for the calculation of the distance to the potential minimum can be carried through in an analogous manner.

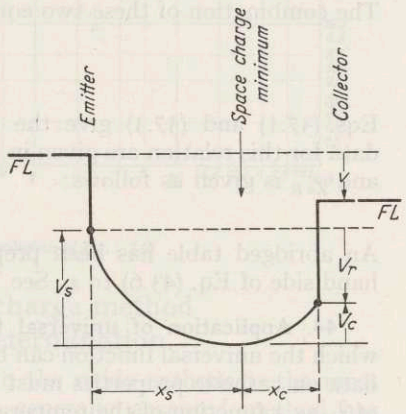

Fig. 8. Electrostatic potential with a space-charge minimum between the emitter and the collector for an applied retarding potential.

An inspection of Fig. 8 and qualitative considerations permit one to conclude that if the retarding potential, V_r, were increased while at the same time the temperature and properties of the cathode were held constant the potential minimum would shift toward the collector until at a particular value of retarding potential the electric field is exactly zero at this surface. If it is assumed that there are no reflection effects at the collector, space charge will have no influence on the emission current for still greater values of retarding potential. It is of some importance to devise a means for determining this critical value of retarding potential at which the onset of space-charge limitation takes place. A review of the "Pillbox Theory" given in Sect. 24 shows that the method of computation should follow much the same procedure.

43. Limiting retarding potential for onset of space charge. Eqs. (37.1) and (37.3) are directly applicable to this problem. The fact that χ_s cannot exceed 1.806 permits one to write two important relations which form the basis for the method of calculation to follow. The numerical factor comes from Eq. (35.2). These relations are given as:

$$(1.806)^2 \times 2.370 \times 10^{-12} = \frac{I_R}{\Theta^{\frac{3}{2}}} \delta^2 = 7.729 \times 10^{-12} \tag{43.1}$$

and

$$7.729 \times 10^{-12} = \frac{I_m}{\Theta^{\frac{3}{2}}} w^2. \tag{43.2}$$

$$9.664 \times 10^{-6} = \frac{I_m}{V_\Theta^{\frac{3}{2}}} w^2 = N \chi_m^2. \tag{43.3}$$

Eq. (38.8) defines N.

In Eq. (43.1) the current (I_R) is the actual current measured at the collector. The distance δ is the measure of the diode spacing for a diode of unlimited emission current capacity which would yield the current, I_R, actually observed. In Eq. (43.2) the current I_m is the maximum current which can flow across a diode of the actual spacing w and still achieve zero potential gradient at the collector. These two equations lead to the next which is

$$z^2 = \frac{w^2}{\delta^2} = \frac{I_R}{I_m}. \tag{43.4}$$

If the emission current capability of the emitter at zero field over the surface of the emitter is defined as I_0, then the current I_R will be given by the following relation:

$$I_R = I_0 \, e^{-\frac{eV_R}{k\Theta}} = I_0 \, e^{-\psi_{sR}}. \tag{43.5}$$

The combination of these two equations is the following:

$$\frac{I_0}{I_m} = z^2 \, e^{\psi_{sR}}. \tag{43.6}$$

Eqs. (37.1) and (37.3) give the relation between ψ_{sR} and χ_{sR}. More accurate data for this relation are given in Table 3 E. Note also that the relation between z and χ_{sR} is given as follows:

$$\chi_{sR} = 1.806\, z. \tag{43.7}$$

An abridged table has been prepared which relates the function on the right-hand side of Eq. (43.6) to z. See Table 4.

44. Application of universal function to problem solution. The method by which the universal function can be used will be outlined as follows. Experimental data on cathode properties must be depended upon to yield the numerical value of I_0 as a function of the temperature in terms of the two empirical constants (a) and (Φ) as given in Eq. (39.2). At any specified temperature and for a diode of specified dimensions Eq. (43.2) establishes the current density, I_m. The properties of the cathode and the spacing of the diode permit one to write the current ratio, (I_0/I_m), needed in Eq. (43.6). The plot given in Fig. 9 or the tabular data in Table 4 allow for the determination of the correct value of z to satisfy Eq. (43.6). As soon as z is known, then Eq. (43.4) permits the correct determination of the actual current I_R. A knowledge of this current and the specified temperature will permit the determination of the precise retarding potential at which space-charge limitation will begin. Ideally, for all values of retarding potential greater than the one that satisfies these equations the current received at the collector will be governed by the exponential relation similar to Eq. (43.5), with the current I less than the limiting one associated with the solution to this problem. This method of solution properly adapted also permits the user to determine the temperature at which the onset of space-charge limitation occurs for a given retarding potential V_r.

Table 4 has been computed over the middle range for which an explicit expression for z cannot be written. The following equation will serve as a means of establishing the correct value for the very small values of z.

Range $(I_m/I_0) > 100$

$$z = \frac{\left(\frac{I_0}{I_m}\right)^{\frac{1}{2}}}{1 + 0.8\left(\frac{I_0}{I_m}\right)}. \tag{44.1}$$

For the highest range of z from 0.98 to 1.0 the following equation should be used:

Range $(I_0/I_m) \leqq 800$

$$z = 1 - \frac{2}{(\pi + 0.47)} \left(\frac{I_m}{I_0}\right)^{\frac{1}{2}} = 1 - 0.554 \left(\frac{I_m}{I_0}\right)^{\frac{1}{2}}. \tag{44.2}$$

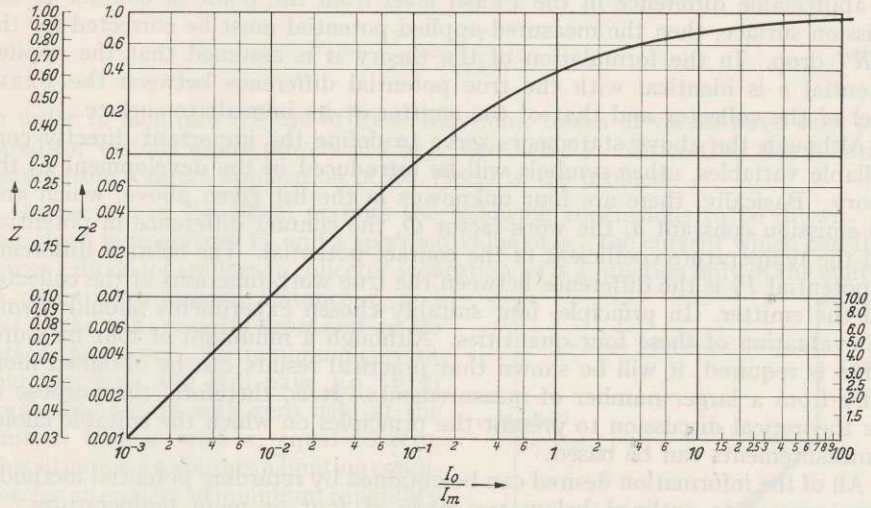

Fig. 9. Plot of data in Table 4 for solution of Eq. (43.6).

V. Idealized use of space-charge method for cathode property determination.

45. Statement of the problem. Even though the oxide cathode is the most important thermionic emitter of electrons, no generally accepted method has been developed for the evaluation of cathode properties under conditions that approach those used in most practical applications. This section will develop the theoretical background for the application of the space-charge equations to cathode evaluation. A brief outline of the fundamental principles involved may facilitate the direct application of the theory.

The following statements will serve to define the symbols used and the experimental conditions directly controllable.

1. The initial development of the theory will apply to a plane-parallel diode with the emitter to collector distance w small compared with other dimensions.

2. The emission properties of the emitter may be expressed by the empirical relation of Eq. (39.1) for which the emission constant a and the work-factor Φ are to be determined.

3. The absolute temperature of the emitter is T and this must be capable of determination either by thermocouple measurements, by pyrometry or by the investigation of the electron energy distribution with very high retarding fields.

4. The temperature and the emission properties of the emitter must be uniform.

5. The collector must have a uniform work-function and be a perfect receiver for the electrons that come to it.

6. The actual current density of the electrons, that cross the diode and therefore constitute the collector current per unit area, will be represented by I and will be directly measurable under any specified conditions.

7. The applied voltage v will be directly measurable and will represent the difference in energy between the FERMI levels of the collector and the emitter. Notice that if there is a sufficient resistance between the emission surface and the point of contact used for the applied potential measurement so that there is an appreciable difference in the FERMI level from the point of contact to the emission surface, then the measured applied potential must be corrected for the "IR" drop. In the formulation of the theory it is assumed that the applied potential v is identical with the true potential difference between the FERMI level of the collector and that of the emitter at its immediate surface.

Although the above statements serve to define the important directly controllable variables, other symbols will be introduced in the development of the theory. Basically, there are four unknowns in the list given above, which are: the emission constant a, the work-factor Φ, the contact difference in potential, and the temperature coefficient of the contact potential. The contact difference in potential P_T is the difference between the true work-functions of the collector and the emitter. In principle, four suitably chosen experiments should permit the evaluation of these four quantities. Although a minimum of four measurements is required, it will be shown that practical results can be obtained more easily from a larger number of measurements. It is, therefore, the purpose of this theoretical discussion to present the principles on which the suitable choice of measurements can be based.

All of the information desired can be obtained by retarding potential methods, if measurements outlined below are made at four or more temperatures. A second avenue of approach depends on a similar set of measurements made with accelerating fields applied. The final method to be discussed depends on a combination of the first two; it involves making observations at only three temperatures with suitably chosen applied potentials that give both retarding potential and accelerating potential data.

a) Emitter evaluation by accelerating potential methods.

46. Basic space-charge equations. The potential distribution between the emitter and the collector is shown by the curve of Fig. 7 for a given applied potential difference v. The relation between the applied potential and the other potentials pertinent to Fig. 7 and analysis of this problem is given in the following equation:

$$v = V_c - V_s + P_T. \tag{46.1}$$

Eq. (38.2) may be rewritten in a more useful form as:

$$I = K_L \frac{F^{\frac{3}{2}}(\psi_c)}{w^2\left(1-\frac{x_s}{w}\right)^2}(V_T)^{\frac{3}{2}}. \tag{46.2}$$

The following equations serve as definitions of the symbols used here:

$$K_L = \frac{4\varepsilon_0}{9}\left(\frac{2e}{m}\right)^{\frac{1}{2}} = 2.334\times10^{-6}, \tag{46.3}$$

$$N = \varepsilon_0\left(\frac{2e}{\pi m}\right)^{\frac{1}{2}} = 2.963\times10^{-6}, \tag{46.4}$$

$$\chi_m = 1.806 \text{ [from (37.4)]}, \tag{46.5}$$

$$\psi_c = \frac{eV_c}{kT}, \tag{46.6}$$

$$F_{\frac{3}{2}}(\psi_c) = \frac{9}{4\sqrt{\pi}}\chi_c^2 = 1.2694\,\chi_c^2, \tag{46.7}$$

$$F(\psi_c) = \psi_c\left(1 + \frac{1.413}{\psi_c^{0.475}}\right), \tag{46.8}$$

$$V_T = \frac{kT}{e} = \frac{T}{11600}. \tag{46.9}$$

In order to facilitate the use of these functions, tables of values have been prepared for various useful powers of $F(\psi_c)$. See Table 5. Notice that this function results from a direct application of Eq. (38.2) to the problem.

Inspection of Eq. (46.2) permits the following conclusions to be drawn. At any given temperature V_T and a specified value of ψ_c, the current which can flow across a diode (of emitter to collector separation w) is a function only of the emitter to potential minimum distance x_s and *this is the only variable dependent on the cathode properties*. The minimum current that can flow and still have Eq. (46.2) applicable occurs with zero field at the emitter, that is, with x_s equal to zero. This situation establishes a limiting condition for an emitter of minimum capability at a particular temperature. For a given emitter let this temperature be represented by the symbol Θ.

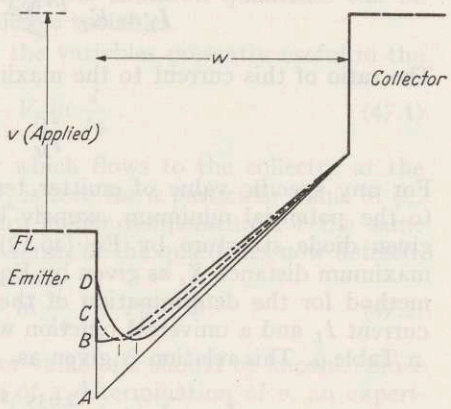

Fig. 10. Potential distributions for four different cathode conditions, constant temperature and applied potential. *A* Very low emission. *B* Critical condition of zero field at emitter. *C* Partial activation. *D* Highest activation.

Fig. 10 has been prepared to show qualitatively the change in the distribution in potential between an emitter held at a constant temperature and a collector maintained at a fixed *applied potential* v. An emitter of very low emission capability is identified by condition *A* of this figure and the current is not limited by space charge. An activation process may lower the work-function to condition *B* and the critical situation of zero field at the emitter is shown by this curve. Further lowering of the work-function to conditions *C* and *D* results in the development of the space-charge minimum and its progression across the interelectrode space toward the collector.

The above description applied specifically to a change in emitter activation and to no change in the *applied* potential. The analysis of experimental data that will lead to an evaluation of emitter properties can be simplified by taking the potential difference V_c in the collector space as constant instead of the applied potential. Under this condition and with a constant emitter temperature it follows that, as the emission capability increases, the potential difference V_s across the emitter region increases at a slightly lower rate than P_T (the contact difference in potential) in order to permit an increase in current without a change in V_c. This result follows because the emitter region distance x_s increases, and it is evident from Eq. (46.1) that the applied potential v must be increased.

As the activation process continues, Eq. (37.6) becomes a controlling factor and x_s approaches a maximum value of X_s which may be computed by Eq. (46.10), as it will be shown. The following equation may be derived by the elimination

of the parameter x_1 between Eqs. (37.6) and (37.8) and it serves as a direct means of making the calculation of

$$X_s = \frac{w}{1 + \frac{2\pi^{\frac{1}{4}}}{3\,(1.806)} F^{\frac{3}{4}}(\psi_c)} = \frac{w}{1 + 0.4914\, F^{\frac{3}{4}}(\psi_c)} = \frac{w}{1 + \frac{\chi_c}{\chi_m}}. \tag{46.10}$$

The numerical constant is written out to show the direct connection with Eqs. (37.6) and (37.8).

The maximum current is given by the following equation:

$$I_M = 7.729 \times 10^{-12} \frac{T^{\frac{3}{2}}}{X_s^2} = 9.664 \times 10^{-6} \frac{V_T^{\frac{3}{2}}}{X_s^2}. \tag{46.11}$$

Let the current I_L represent some of the factors in Eq. (46.2) and be expressed as

$$I_L = K_L \frac{F^{\frac{3}{2}}(\psi_c)}{w^2} (V_T)^{\frac{3}{2}} = N \frac{\chi_c^2}{w^2} (V_T)^{\frac{3}{2}}. \tag{46.12}$$

The ratio of this current to the maximum current may be expressed as follows:

$$\frac{I_L}{I_M} = \left(1 - \frac{X_s}{w}\right)^2. \tag{46.13}$$

For any specific value of emitter temperature and collector potential relative to the potential minimum, namely V_c, the current I_L can be computed for a given diode structure by Eq. (46.12). The introduction of the value for the maximum distance X_s as given by Eq. (46.10) in Eq. (46.13) gives an alternative method for the determination of the maximum current as the product of the current I_L and a universal function which has also been computed and recorded n Table 6. This relation is given as

$$I_M = I_L \left(1 + \frac{2.035}{F^{\frac{3}{4}}(\psi_c)}\right)^2 = I_L\, f(\psi_c) = I_L \left(1 + \frac{\chi_m}{\chi_c}\right)^2. \tag{46.14}$$

47. Application of basic equations to cathode evaluation. As the basic equations are applied to determine emitter properties the only two directly controllable and observable variables are the emitter temperature and the applied difference in potential. The unknowns which it is the purpose of the study to evaluate quantitatively may be listed as follows:

1. The work factor Φ.
2. The RICHARDSON work-function φ_R.
3. The thermionic constant a.
4. The critical temperature Θ or its equivalent V_Θ which is the minimum temperature at which a given emitter will operate with the current limited by space charge for a specified value of V_c.
5. The contact difference potential P_T at any temperature.
6. The temperature coefficient of the contact difference in potential which is also the negative of the temperature coefficient of the true work-function of the emitter.
7. The contact potential P_0 which is the value at absolute zero of temperature determined by a linear extrapolation from the observational temperature region to absolute zero. For stable emitters with emission current given by either Eq. (39.1) or the RICHARDSON type of equation, the temperature variation of the work-function is dominated by the first power term. It will be shown in

Sect. 81 that for oxide cathodes higher power terms are needed. The present analysis depends on the use of a suitably chosen average temperature coefficient and a corresponding P_0.

There are still other quantities which can be considered as indirect variables. The analysis depends on the arbitrary choice of two or more values for ψ_c. If it is assumed that this analysis applies to the evaluation of an oxide cathode, or its equivalent, then the choice of values of ψ_c between 15 and 50 will correspond to the application of accelerating potentials such that the energy with which the electrons bombard the collector will lie between 1.5 and 5 electron volts. For a particular choice of ψ_c, Eq. (46.12) permits the preparation of a table of values of I_L as a function of the temperature. In particular these values should be computed for the normal temperature of operation represented by V_n and for a range of lower temperatures. The value of I_M may also be computed directly with the aid of the tabulated function expressed in Eq. (46.14) as $f(\psi_c)$. The analysis which follows will show the method by which the unknown quantities can be related to the directly and indirectly controllable variables.

Eq. (40.2) may be rewritten in terms of the variables presently useful in the analysis, as follows:

$$V_s = \Phi \frac{V_T - V_\Theta}{V_\Theta} - V_T \ln \frac{I}{I_\Theta}. \tag{47.1}$$

In this equation I_Θ is the current density which flows to the collector at the critical temperature Θ when the value of V_s is zero for a particular value of ψ_c. The current I is the current density at any higher temperature for the same value of ψ_c. Eq. (46.1) may be rewritten in terms of the quantities now defined, as follows:

$$v = V_T \left(\psi_c + \frac{dP}{dV_T} - \frac{\Phi}{V_\Theta} + \ln \frac{I}{I_\Theta}\right) + P_0 + \Phi. \tag{47.2}$$

For this equation to hold exactly, the correct value of I should be known. Since its value cannot be determined in advance of a determination of v, an experimental procedure must be used.

With good cathodes, the current I will be very nearly equal to I_M for an appreciable range in temperature above and below the normal operating temperature expressed as V_n. The experimental procedure is to compute I_M as well as I_L for each temperature and the specified value of ψ_c. One establishes by experiment the applied potentials v'' and v' which are observed to be required to give diode current densities of I_M and I_L, respectively. The equation for the I_M characteristic curve is the following:

$$v'' = V_T \left[\psi_c + \frac{dP}{dV_T} - \frac{\Phi}{V_\Theta} + \ln \left[f(\psi_c)\right] + \frac{3}{2} \ln \left(\frac{V_T}{V_\Theta}\right)\right] + P_0 + \Phi \tag{47.3}$$

since

$$\ln \frac{I_M}{I_\Theta} = \ln \frac{I_M}{I_L} \left(\frac{V_T}{V_\Theta}\right)^{\frac{3}{2}} = \ln \left[f(\psi_c)\right] + \frac{3}{2} \ln \left(\frac{V_T}{V_\Theta}\right). \tag{47.4}$$

Over the high-temperature range the characteristic curve for the I_L data follows an equation identical to Eq. (47.3) except that a lower value of ψ_c is applicable. It is possible to compute this lower value of ψ_c but it does not serve a useful purpose in the present analysis. The more useful result to keep in mind is that a linear relation between an observable quantity and the temperature can be formulated from Eq. (47.3). This relation depends on an observable voltage quantity defined by the following:

$$v^{**} = v'' - V_T \left[\frac{3}{2} \ln \frac{V_T}{V_\Theta} + \ln f(\psi_c)\right]. \tag{47.5}$$

Note that the computation of the correction term depends on an estimate of the critical temperature V_Θ. The means for making this estimate will be described in connection with the discussion of the data presented in Fig. 11.

With this definition of the voltage v^{**}, the following equation may be written:

$$v^{**} = V_T\left[\psi_c + \frac{dP}{dV_T} - \frac{\Phi}{V_\Theta}\right] + P_0 + \Phi. \tag{47.6}$$

At the critical temperature V_Θ, Eq. (47.2) relates to the observations made along the I_L characteristic curve and satisfies the requirement as expressed in the following equation:

$$v'_\Theta = V_\Theta\left(\psi_c + \frac{dP}{dV_T} - \frac{\Phi}{V_\Theta}\right) + P_0 + \Phi. \tag{47.7}$$

A comparison between Eqs. (47.6) and (47.7) shows that the purpose of this analysis is to establish an accurate value for the critical temperature V_Θ. The straight line described by the plotted values of v^{**} as a function of the temperature V_T over the high-temperature range intersects the voltage scale at the zero value of V_T to give a measure of $(P_0 + \Phi)$. At the critical temperature, v^{**} is identical to v'_Θ which establishes the fact that the intersection of the straight line described with the observed I_L characteristic curve, as shown in Fig. 11, determines the exact value of V_Θ to be used.

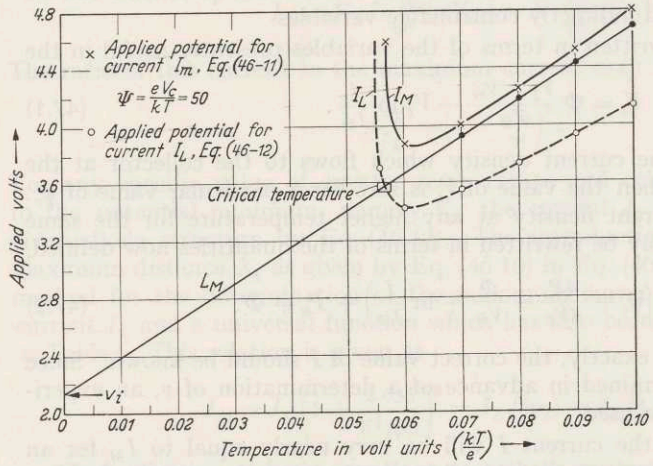

Fig. 11. Applied potentials for emitter evaluation at $\psi_c = 50$.

It is to be anticipated that in carrying out the experiment, observations would not be made at this exact temperature, and yet, if the observations were made at temperatures slightly above and below this temperature, it is easy to interpolate between the observation points and determine the suitable value of V_Θ. The insertion of this value of temperature in Eq. (46.12) gives an accurate measure of the zero field emission capability of the emitter. This result is expressed as follows:

$$I_0 = I_{L\Theta} = N\,\frac{\chi_c^2}{w^2}\,(V_\Theta)^{\frac{3}{2}}. \tag{47.8}$$

The application of these principles can be illustrated best by the numerical data presented in Figs. 11 and 12. For these curves, typical values of all of the constants are assumed in advance so that the curves can be drawn to scale.

The solid and the dashed curves of Figs. 11 and 12 join a set of points that represent, as a function of temperature, the directly observable applied potentials needed so that the computed current densities I_M and I_L are the ones actually observed. Note that Fig. 11 applies to a value of ψ_c of 50 and Fig. 12 is for ψ_c of 16. Before the corrections can be applied that correspond to the application of Eq. (47.5), an estimated value of the critical temperature V_Θ must

be determined. A sufficiently accurate choice may be made by drawing a tangent to the smooth curve designated as I_M at the highest temperature and then determining the intersection of this tangent with the dashed curve designated as I_L. This approximate value of the critical temperature, V_Θ, can be used in Eq. (47.5) to locate the points identified in these figures by solid dots. An inspection of Eq. (47.6) shows that a straight line drawn through these points has an intercept v_i on the voltage axis at the zero of temperature. The intersection of the straight line designated L_M, with the dashed experimental curve is indicated by the square □ on each of the figures. The exact value of the critical temperature, V_Θ, is determined by this intersection. It is anticipated that this exact value of the critical temperature will not differ enough from the previously determined approximate value to make it necessary to re-evaluate the potentials computed by Eq. (47.5).

This analysis of experimental data as illustrated by Figs. 11 and 12, should yield a single value of the intersection potential v_i for both choices of ψ_c of 50 and 16. If the initial analysis of the data for the two cases gives slightly different values for v_i, an average value should be taken and new straight lines should be drawn to correspond to the best representation of the entire set of data. A lack of self-consistency will generally indicate a failure to satisfy the uniformity requirements either with respect to emitter temperature or the surface conditions of the emitter and collector.

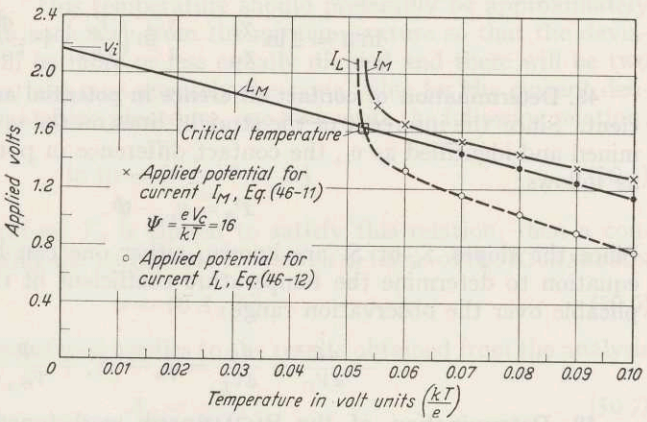

Fig. 12. Applied potentials for emitter evaluation at $\psi_c = 16$.

If the contact potential variation with temperature cannot be represented well enough by Eq. (38.10), then experimental points will not fall exactly on a straight line but may deviate systematically. This may indicate that the best straight line will give a good mean value of the temperature coefficient and the corresponding P_0 that will be useful only over the observational range in temperature.

The slope of the line L_M is given by the terms contained within the square brackets of Eq. (47.6). There are essentially two unknowns in this expression for the slope; they are the temperature coefficient of the contact potential and the work-factor. The acquisition of data at the two chosen values of ψ_c identified here as ψ_a and ψ_b, instead of 50 and 16, permits the determination of the work-factor by the following relation:

$$\Phi = \frac{(S_a - S_b) - (\psi_a - \psi_b)}{\frac{1}{V_{\Theta b}} - \frac{1}{V_{\Theta a}}}. \tag{47.9}$$

Use may be made of Eq. (47.8) and an alternative method of computing the work-factor Φ may be employed as in the following equation:

$$\Phi = \frac{2 \ln \frac{\chi_a}{\chi_b} + \frac{3}{2} \ln \frac{V_{\Theta a}}{V_{\Theta b}}}{\frac{1}{V_{\Theta b}} - \frac{1}{V_{\Theta a}}}. \tag{47.10}$$

In this equation the values of χ_a and χ_b are those found in Table 3C corresponding to the selected values of ψ_a and ψ_b. A direct calculation of the thermionic constant expressed as $\ln a$ may be made from either set of data taken at ψ_a or ψ_b. The following equation will be written in terms of the choice of ψ_a and is:

$$\ln a = \ln\left[N \frac{\chi_a^2}{w^2} V_{\Theta a}^{\frac{3}{2}}\right] + \frac{\Phi}{V_{\Theta a}}. \tag{47.11}$$

To facilitate calculation, it will be convenient to define a characteristic "temperature" that in effect describes the diode spacing. This symbol is defined by the following equation:

$$V_w^{\frac{3}{2}} = \frac{w^2}{N \chi_m^2}. \tag{47.12}$$

The substitution of the symbol V_w in Eq. (47.11) gives the form by which the thermionic constant can be computed most easily.

$$\ln a = 2 \ln \frac{\chi_a}{\chi_m} - \frac{3}{2} \ln\left(\frac{V_w}{V_{\Theta a}}\right) + \frac{\Phi}{V_{\Theta a}}. \tag{47.13}$$

48. Determination of contact difference in potential and its temperature coefficient. Since the intercept of the straight lines on the ordinate axis can be determined and identified as v_i, the contact difference in potential may be computed as follows:

$$P_0 = v_i - \Phi. \tag{48.1}$$

Since the slopes S_a or S_b are known, either one can be used in the following equation to determine the temperature coefficient of the contact potential applicable over the observation range

$$-\frac{dP}{dV_T} = \frac{d\varphi}{dV_T} = \psi_a - \left(S_a + \frac{\Phi}{V_{\Theta a}}\right). \tag{48.2}$$

49. Determination of the RICHARDSON work-function and the true work-function. If the work-factor Φ is known, it is easy to calculate the most appropriate value for the RICHARDSON work-function φ_R that will best represent the data over any specified temperature range, as shown in the next section. Assume for this calculation that V_n represents the highest temperature of interest and that V_m corresponds to the lowest temperature of interest. The RICHARDSON work-function is then given by the following equation:

$$\varphi_R = \Phi - (V_n + V_m). \tag{49.1}$$

With the temperature coefficient of the work-function known from Eq. (48.2), the best value for the true work-function is given as follows:

$$\varphi = \varphi_R + V_T\left(\frac{d\varphi}{dV_T}\right). \tag{49.2}$$

50. Determination of the RICHARDSON constant A_R and its relation to the thermionic constant a. When they are considered as empirical equations to represent the temperature-dependence of thermionic emission, the simplified equation and the RICHARDSON form are equally valid. These two equations are written as follows:

$$I = a e^{-\frac{\Phi}{V_T}}, \tag{50.1}$$

$$I = A_R T^2 e^{-\frac{\varphi_R}{V_T}}. \tag{50.2}$$

Since the range of temperature of practical interest is generally less than two to one, it is possible to express relations between the empirical constants such that either equation will represent the experimental data within the accuracy of the temperature scales used. By differentiation it may be shown that the slope of the simplified equation plot is related to the RICHARDSON slope by the following equation:

$$\Phi = \varphi_R + 2\,V_T. \tag{50.3}$$

Since the average temperature over the range of interest is $(V_n + V_m)/2$ it is appropriate to take this value for V_T of Eq. (50.3) and the following relation is obtained:

$$\Phi = \varphi_R + V_n + V_m. \tag{50.4}$$

With this relation between the work-factor Φ and the RICHARDSON work-function φ_R, the thermionic constants a and A_R should be chosen so that the two equations give exactly the same values of current density at some intermediate temperature T_0. This temperature should preferably be approximately one-quarter of the range each way from the midtemperature so that the deviations that must exist will be more or less equally divided and there will be two points at which the equations give precisely the same value for the current density. As a result of this matching procedure, one may write the following relation:

$$\ln 10 = \frac{T_n + T_m}{T_0} = 2.3 \tag{50.5}$$

If the matching temperature T_0 is chosen to satisfy this relation, then a convenient means of calculating the thermionic constant a in terms of the RICHARDSON constant A_R follows:

$$a = 10\,A_R\,T_0^2. \tag{50.6}$$

The inverse relation is useful as it applies to the results obtained from the analysis of Sect. 47:

$$A_R = \frac{a}{10\,T_0^2}. \tag{50.7}$$

Although the name "work-factor" has been found to be a convenient term for Φ as Eq. (50.1) is applied specifically to thermionic emission data, an equation of this form has been used as a means of expressing the conductivity of semiconductors as a function of the temperature. In the conduction process, there is also the problem of the temperature coefficient of the FERMI level. In the discussion in Sect. 65 it is shown that the temperature exponent of the theoretical equation that best represents results is $-(\frac{3}{4})$ instead of 2 as in the RICHARDSON empirical formula given here as Eq. (50.2) and therefore a more general conversion formula is needed. In the application of Eq. (50.1) to these conduction problems the quantity Φ has acquired the name "activation energy"[1, 2]. Actually, it is no more a direct measure of the true activation energy in the conduction case than it is a measure of the true work-function in the emission case. In both analyses it is simply an empirical constant.

Since data found in the literature are often expressed this way, however, it will be convenient to write general forms for the conversion of the empirical constants representing data according to Eq. (50.1) to suitable choices for the empirical constants in the generalized equation given as follows:

$$I = A_v\,T^v\,e^{-\frac{\varphi_v}{V_T}}. \tag{50.8}$$

[1] N. B. HANNAY, D. MACNAIR and A. H. WHITE: J. Appl. Phys. **20**, 669 (1949).
[2] R. LOOSJES and H. J. VINK: Philips Res. Rep. **4**, 449 (1949).

This equation gives the same variation in the quantity $\ln I$ with respect to V_T^{-1} as that given by Eq. (50.1) at the temperature V_T if the following condition is satisfied:

$$\varphi_\nu = \Phi - \nu V_T. \tag{50.9}$$

The two equations will give the same value for the quantity I at a chosen temperature if the relation between a and A_ν is given by

$$A_\nu = \frac{a}{e^\nu T_0^\nu}. \tag{50.10}$$

One generally wishes to choose the constants so that they will give comparable results over a specific range in temperature. If the extent of that range can be bracketed by V_n and V_m (or T_n and T_m) which carries the interpretation now that the first of these temperatures is the maximum temperature of the range and the second the minimum temperature of the range, then the best choice for the relations between the empirical constants may be written according to the following two equations:

$$\varphi_\nu = \Phi - \frac{\nu}{2}(V_n + V_m), \tag{50.11}$$

$$T_0 = \tfrac{1}{2}(T_n + T_m). \tag{50.12}$$

b) Emitter evaluation by retarding potential methods.

51. Basic space-charge equations. A general statement covering the objectives of this theory of cathode evaluation is given in Sect. 45 and should be referred to in order that such limitations as necessarily exist will be clearly understood. Oxide cathodes generally operate at a temperature for which the emission current is strongly limited by space charge and, therefore, it is appropriate to present a theory of cathode evaluation which depends on the direct application of space-charge theory to this practical problem. The basic equation has already been worked out by which one can calculate the maximum current which can flow across a diode of given dimensions if the cathode is operated at a specified temperature and the *potential gradient at the collector is exactly zero.* This equation was first presented as Eq. (43.3) and may be written in terms of notation presently useful as follows:

$$I_m = 7.729 \times 10^{-12} \frac{T^{\frac{3}{2}}}{w^2} = 9.664 \times 10^{-6} \frac{V_T^{\frac{3}{2}}}{w^2}. \tag{51.1}$$

For a good oxide cathode this equation gives the observed current when zero field exists at the collector for the temperature range higher than 800° K. For lower temperatures the actual current obtained under the zero field condition is lower than I_m and the ratio of these currents is defined as in Eq. (43.4) as follows:

$$z^2 = \frac{I_R}{I_m}. \tag{51.2}$$

The analysis which follows shows the means by which the correct value of z can be determined. With z known, it is possible to give a quantitative value to the true retarding potential that exists across the space between a point just outside of the emitter and the corresponding point outside of the collector. When this retarding potential is known, the emission capability of the emitter will also be known at the specific temperature at which z has been evaluated.

The current received at the collector can be expressed in terms of cathode properties as follows:

$$I_R = a\, e^{-\frac{\Phi + V_R}{V_T}}. \tag{51.3}$$

In this equation the constant, a, is a measure of an emitter property and is to be determined by the series of experiments to be described. The work-factor is

Φ, and the true retarding potential is V_R. It is to be noted that the symbol V_R is appropriate, since it measures the true difference in potential across the emitter space as described in Sect. 31. In the present example there is no collector space, since the zero gradient of the potential distribution occurs at the collector. The relation between the applied difference in potential v and the true retarding potential V_R is the following:

$$v = P_T - V_R. \tag{51.4}$$

The true contact difference of potential including the temperature variation of the emitter work-function is P_T. See Sects. 45 and 47. These relations permit the following equation to be written:

$$v - V_T \ln I_m = V_T \left[\frac{dP}{dV_T} - \ln a - \ln \frac{1}{z^2} \right] + \Phi + P_0. \tag{51.5}$$

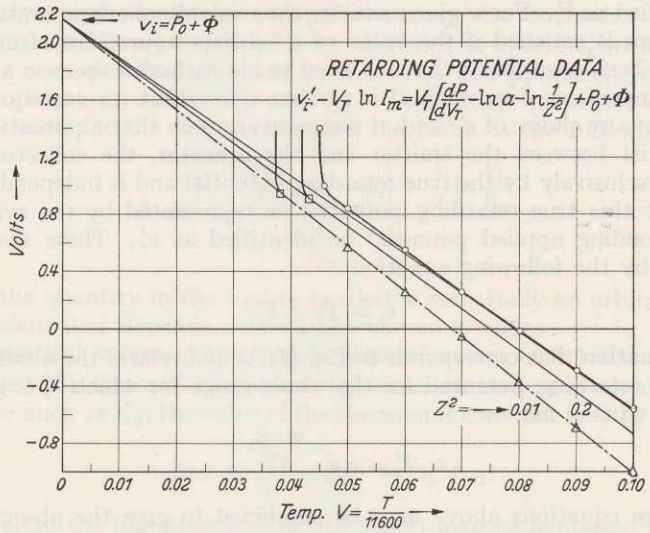

Fig. 13. Emitter evaluation by retarding potential methods.

52. Application of basic equations to cathode evaluation. Over the high-temperature range of approximately 800° to 1200° K for oxide cathodes it is to be expected that Eq. (51.5) can be simplified to read as follows:

$$v_1 - V_T \ln I_m = V_T \left[\frac{dP}{dV_T} - \ln a \right] + \Phi + P_0. \tag{52.1}$$

Over this range z^2 is so near unity that its logarithm can be neglected. The experimental observations grouped on the left-hand side of the equation involve first, the computation of I_m by means of Eq. (51.1) and the observation of the applied voltage v_1 required at each temperature to give the corresponding current density I_m in the test diode. The voltage v_1^* can be defined as in the following equation and a plot made of this voltage as a function of the temperature

$$v_1^* = v_1 - V_T \ln I_m. \tag{52.2}$$

Computed points typical of observational data are shown in Fig. 13. A tangent may be drawn through the points in the high-temperature range and the intercept of this line on the voltage axis may be identified as follows:

$$v_i = \Phi + P_0. \tag{52.3}$$

As the temperature is lowered, the observed points will deviate very gradually as shown in Fig. 13. At each of the known emitter temperatures, observed applied voltages may be determined to give a set of points corresponding to some arbitrarily chosen values of z^2. For example, 0.2 and 0.01 may be selected. The current that is observed in the experiment can be related to the computed current I_m by the following equation:

$$I'_r = z'^2 I_m. \tag{52.4}$$

The reason for the change in notation from I_R to I'_r is that, in the first case, the current flow I_R indicated that particular value for which zero gradient existed at the collector for a known or specified value of z^2. In that case, the true retarding potential between the emitter and the collector would be identical to the emitter potential relative to the space-charge potential minimum which has been identified as V_s. For a given emitter there is only one temperature at which this condition is satisfied if the value of z'^2 differs appreciably from unity. It has already been mentioned that for good oxide cathodes there is a very useful range in temperature for which z^2 is so near unity that its variation is not detectable. For any choice of z'^2 and of temperature such that a potential minimum does *not* exist between the emitter and the collector, the collector current is controlled exclusively by the true retarding potential and is independent of space charge. Let this true retarding potential be represented by the symbol V_r and the corresponding applied potential be identified as v'_r, These two potentials are related by the following equation:

$$v'_r = P_T - V_r. \tag{52.5}$$

The new equation that corresponds to Eq. (51.3) and relates the observed current to the true retarding potential for the whole range for which V_r is greater than V_s, may be written as:

$$I'_r = a\, e^{-\frac{\Phi + V_r}{V_T}}. \tag{52.6}$$

The three equations above may be combined to give the observed relation between the temperature expressed as V_T and the observed applied potential v'_r which yields the observable current I'_r after a definite choice has been made for the value of z'^2

$$v'_r - V_T \ln I_m = V_T \left[\frac{dP_T}{dV_T} - \ln a - \ln \frac{1}{z'^2}\right] + \Phi + P_0. \tag{52.7}$$

It is to be seen that this equation has exactly the same form as Eq. (51.5) and it indicates that observed points will fall on a straight line of slope $S_{z'}$ as defined by the following equation:

$$S_{z'} = \frac{dP}{dV_T} - \ln a - \ln \frac{1}{z'^2}. \tag{52.8}$$

Note that all lines should be expected to have a negative slope increasing in value as z'^2 decreases and all lines intersect at the same voltage point v_i, as given by Eq. (52.3).

Under ideal conditions of emitter uniformity the observed points will fall on the straight lines described for all temperatures in excess of the critical temperature for which the condition of zero gradient at the collector is satisfied. As the temperature is lowered, below the critical value, the observed points break away sharply from the straight lines, as shown in Fig. 13. With these critical temperatures known for two or more values of z' appreciably less than unity,

the properties of the emitter may be specified by the methods given in the following section.

53. Interpretation of results. The location of corresponding critical temperatures, collector currents, and z' values leads first to a determination of true retarding potentials applicable in Eq. (51.3). Since this equation involves the two unknowns a and Φ, their numberical values can be determined from data obtained at two temperatures. These temperatures and the corresponding currents may be determined as described in Sect. 52. The next step, to determine the relation between V_R and z, still remains to be completed. Eq. (43.7) gives the relation between χ_s and z and Eq. (37.1) relates ψ_s to χ_s for the smaller values of χ_s. Thus, for values of z less than 0.77 or z^2 less than 0.6, Eq. (37.1) will be found satisfactory for most calculations. The data in Table 3 E combined with an accurately prepared plot for interpolation may also be used.

Let the two arbitrary values of z' be identified as z'_1 and z'_2 with z'_1 being the larger. The corresponding values of ψ_s will be ψ_1 and ψ_2 and the corresponding critical temperatures will be V_{z1} and V_{z2}. With these quantities defined, it is possible to solve for the work-factor and the result is the following:

$$\Phi = \frac{\left[\ln\left(\frac{z'^2_1}{z'^2_2}\right) + \psi_1 - \psi_2\right] + \frac{3}{2}\ln\frac{V_{z1}}{V_{z2}}}{\frac{1}{V_{z2}} - \frac{1}{V_{z1}}}. \tag{53.1}$$

Note that the quantity in the square bracket is essentially an arbitrary constant of the problem that depends only on the chosen z values.

The numerical values of this constant for z^2 values of 0.2 and 0.01 is 3.409.

With the work-factor Φ known and the emission current given at a particular temperature such as V_{z1}, the value of the thermionic constant may be expressed as:

$$\ln a = \frac{\Phi}{V_{z1}} + \psi_1 + \ln\left(z'^2_1 I_{m1}\right). \tag{53.2}$$

The slope of the line described by Eq. (52.7) may be expressed by Eq. (52.8) and is a directly measurable quantity. This equation contains only the temperature coefficient of the contact potential as an unknown and therefore it may be evaluated. The temperature coefficient of the work-function is the negative of the quantity (dP/dV_T). The intercept on the voltage axis is a directly measurable quantity and, combined with the work-factor as in Eq. (52.3), serves to evaluate the effective contact difference in potential at the zero of temperature.

54. Criticism of the retarding potential method of cathode evaluation. In Sects. 51 through 53 the theory of cathode evaluation by retarding potential methods has been presented in order to prepare for the use of certain of its elements in the theory which follows. The next sections show the most practical means of evaluating an electron emitter under conditions nearly identical to those under which an oxide cathode is most likely to be used in practical applications.

The principal objection to the retarding potential method of cathode evaluation involves the critical nature of the emission current and temperature measurements at the low end of the temperature scale. The most basic quantity, namely, the work-factor, depends so strongly on these temperature measurements and on the identification of the critical temperature that cathode inhomogeneities can be expected to interfere seriously with the accuracy of the results. Of the three methods of cathode evaluation presented here the retarding potential

method is the least satisfactory. The theory presented above, however, is basic to an understanding of the combination method, undoubtedly the best of the three, which will be described in the next section.

c) Emitter evaluation by a combination of retarding and accelerating potential methods.

55. Statement of the problem. Practical electron emitters such as oxide cathodes cannot be expected to be perfect surfaces of uniform emission efficiency. Any method of cathode evaluation which does not assess the cathode in the presence of space charge under conditions similar to those of its practical operation may very well yield misleading results. Evaluation methods that depend only on the drawing of saturation current by means of an accelerating field at the cathode evaluate patches of low work-function area, since these are likely to yield a disproportionate fraction of the emission current. It follows that a method which will permit evaluation of the emitter and which will include information obtained at normal operating temperatures and with very low fields can be expected to yield the most reliable information. It is the purpose of the next few sections to present new methods for emitter evaluation by taking full advantage of the space-charge theory[1].

The quantities to be determined are (1) the work-factor Φ, (2) the thermionic constant a, (3) the average temperature coefficient of the work-function, and (4) the contact difference in potential. These four quantities may be determined by measurements made at a minimum of three different temperatures.

The method to be described depends on measurements made in both the retarding potential and the accelerating ranges. Some previous knowledge of the general properties of the emitter is presupposed in order that the temperatures most suitable for study may be selected. The highest temperature used can be that associated with the normal operation of the emitter. For oxide cathodes this would be approximately 1160° K. Temperatures of approximately 660° and 580° K are generally suitable for the other two temperatures. The analysis requires that these temperatures be known quite accurately and, therefore, thermocouple measurements combined with electron energy distribution measurements should be used in their determination.

The methods of cathode evaluation, described in Sects. 45 to 54, required observations made at five or six different values of temperature and a knowledge of the diode spacing, with considerable accuracy, in order to obtain reliable results. The method to be presented is more practical, since it depends on the accumulation of data, for subsequent analysis, by making a large number of current measurements as a function of applied voltage while the temperature is held constant. It is for this reason that importance is attached to this phase of the theoretical analysis.

To obtain the most accurate results, it is necessary to measure the emission as a function of the applied voltage from currents of approximately 10^{-9} amp/cm.^{2} to values of about 4×10^{-3} amp/cm.^{2} for a diode of approximately 1 mm. spacing. The normal procedure is to cover the range in the accelerating field region to

[1] Although the author read the article by W. R. FERRIS [RCA Review **10**, 134 (1949)], some years ago, the present analysis has been developed independently. Since the author's objective is cathode evaluation, it has been necessary to go into far more detail in the theory. It will be shown that FERRIS' concept of a "Universal diode characteristic" is practically the equivalent of the "Master Curve" described here. The theory is extended to make it applicable to the evaluation of emitters with any ratio of (I_0/I_R) and a means of adapting it to the cylindrical diode is provided.

an applied voltage of approximately 6 volts. It is necessary for the cathodes to be very stable and the measurements must be reproducible with high accuracy to indicate such stability.

56. Methods of comparison between theory and experiment. A graphical method of analysis is the most appropriate means of comparing the observations with the theory. In this manner the current flow under the various critical conditions may be determined by experiment. The first of these conditions to be discussed will be that associated with zero gradient at the collector for each of the temperatures. This condition may be defined as that for $\varphi_c = 0$. Two other critical conditions involve the determination of the collector potential at which zero gradient exists at the emitter for two or more of the lower temperatures chosen for investigation.

The first step in the procedure is to prepare a plot of the logarithm of the emission current as a function of the observed applied potential expressed in the dimensionless unit of (v/V_T). Let this ratio define the quantity, s, as follows:

$$s = \frac{v}{V_T}. \tag{56.1}$$

Depending on the polarity of v, the quantity s may be positive or negative.

The emission current density characteristic of the emitter itself, which it is the purpose of this analysis to determine, is given by the following equation:

$$I_0 = a\, e^{-\frac{\Phi}{V_T}}. \tag{56.2}$$

With the true retarding potential, defined as V_r, the emission current density which arrives at the collector may be expressed as follows:

$$\ln I = \ln I_0 - \frac{V_r}{V_T}. \tag{56.3}$$

Since it is generally more convenient for the graphic analysis to use semilogarithmic paper, Eq. (56.3) may be written in terms of common logarithms as

$$\log_{10} I = \log_{10} I_0 - 0.4343\, S. \tag{56.4}$$

In this equation, the dimensionless form of the absolute value of the retarding potential expressed as S is related to the observable quantity defined by Eq. (56.1) by the following relation

$$|S| = -\frac{P_T}{V_T} + \frac{v}{V_T} = -\frac{P_T}{V_T} + s. \tag{56.5}$$

Even though the current I_0 and the true contact difference in potential P_T at the temperature T are unknown, it is nevertheless possible to compare the theory with experiment by noting that the observed currents plotted as a function of s on semi logarithmic paper yield a straight line of slope 0.4343. This straight-line relation applies over the entire range for which there is no potential minimum between the emitter and the collector. At a critical value of s, a departure from the straight line can be detected. This departure serves as an approximate indication of the maximum current which can flow across the diode under the condition of zero gradient at the collector. The use of a nonuniform collector surface can cause some uncertainty in the correct identification of the applied potential required to give zero gradient at the collector. The more serious difficulty standing in the way of a simple interpretation of experimental results is the reflection effect at the collector. This effect makes the recorded current

at the critical condition of zero gradient less than the true emission current, since additional space charge is created by the reflected electrons as they approach and leave the collector without being recorded. Evidence for this enhanced space charge will be presented in Sect. 83.

To establish a more suitable identification of the applied voltage which would have been correct for $\psi_c = 0$ in the absence of reflection, it is necessary to observe the rise in current with applied voltage through a sufficient range of positive values of ψ_c so that the observed curve can be matched by the theoretical curve. The matching of curves in this region by the technique described in the following sections makes it possible to evaluate accurately the ideal critical current I_R for the zero value of ψ_c. The method also permits an evaluation of I_0 over the lower range in temperature. See Sect. 67 for the detailed application of this theory to experimental data.

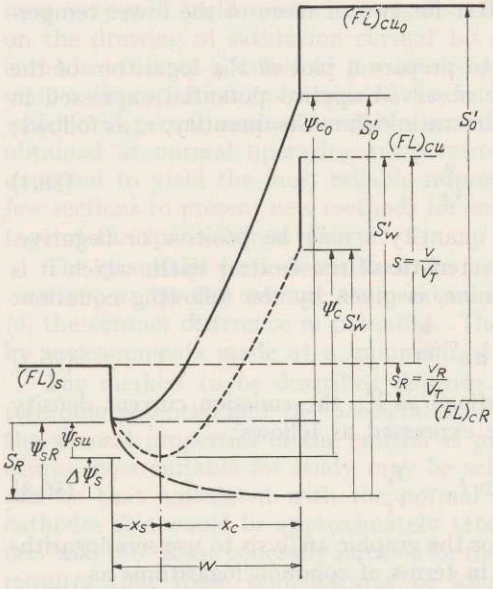

Fig. 14. Graphical illustration of symbols related to theory of the universal limiting curve.

57. The onset of space-charge limitation and the universal limiting curve. For any given temperature and emission property of the emitter, let the critical value of applied voltage for which zero gradient occurs at an ideal collector be identified as v_R and the corresponding value of s as s_R. These quantities are related as in Eq. (56.1). In Sect. 56 the absolute value of the surface potential of the collector relative to the emitter was defined as S and the true retarding potential was equal to S as long as no space-charge minimum existed between the emitter and the collector. At a certain critical valu of s zero field develops at the collector and this value of S is identified in Fig. 14 as S_R. As S becomes smaller than S_R the current increase no longer follows Eq. (56.4) because of the limitation by space charge which then sets in. With this critical condition as a reference potential, the quantity $S' \gtrless 0$ may be defined by the following equation:

$$S' = s - s_R = \frac{v - v_R}{V_T}. \tag{57.1}$$

Although the actual value of s_R will not be known until the analysis is carried further, it is to be expected that a "universal" relationship may be found between the current expressed as a ratio and the value of S' (Sect. 58). Thus the logarithm of the current ratio as a function of S' will create a curve which will serve as a means of determining the location of the exact value of s_R. The relation between the observed current and s determined experimentally may be plotted on semi-logarithmic paper and for comparison with theory may be superpositioned on the plotted set of "Master curves" described in Sect. 58. It will be the purpose of the next few paragraphs to derive this relation from space-charge theory.

The relation between S' and other quantities of interest is best illustrated by Fig. 14. Three curves are shown. The dashed line represents the distribution

in potential for $S' = 0$, that is, the whole difference in potential in the space is exactly ψ_{sR}. The applied difference in potential expressed in dimensionless units is s_R. As the applied potential is changed to a more positive value by an amount S' as expressed in Eq. (57.1), the potential at the surface of the collector changes exactly the same amount and is related to the change in the emitter region potential $\Delta\psi_s$ and to the change in the collector region potential ψ_c, by the relation given as follows:

$$S' = \Delta\psi_s + \psi_c. \tag{57.2}$$

The intermediate potential distribution to which this equation applies is shown by the dotted curve of Fig. 14. This change in the emitter region potential results in an increase in current from the critical value I_R to the new value I given as

$$\ln (I/I_R) = \Delta\psi_s = \ln u^2. \tag{57.3}$$

Eq. (57.3) serves to define the quantity u^2 which is (I/I_R).

A very important limiting condition of potential distribution is illustrated by the solid line of Fig. 14. A cathode of finite emission capability I_0 has zero field at its surface when the current carried across the diode is exactly equal to I_0. This condition may be related to the previously defined critical situation of zero gradient at the collector by the following equation:

$$\frac{I_0}{I_R} = u_0^2 = e^{\psi_{sR}}. \tag{57.4}$$

Since the current I_R is directly related to the emission capability I_0, this property of the emitter establishes the zero reference for the quantity S' defined by Eq. (57.2) and illustrated in Fig. 14. With space-charge theory dominating, the maximum permissible value for S' occurs when the current flow across the diode is I_0 and is associated with zero gradient at the emitter. Let this maximum value of S' be represented by S'_0. A very important universal curve relates u_0^2 to S'_0, since both of these quantities relate specifically to the emission capability I_0. This relation is to be derived.

From the basic considerations expressed as Eq. (38.9), the following three equations may be written directly:

$$I_0 = N \frac{\chi_{c0}^2}{w^2} (V_T)^{\frac{3}{2}}, \tag{57.5}$$

$$I_R = N \frac{\chi_{sR}^2}{w^2} (V_T)^{\frac{3}{2}}, \tag{57.6}$$

$$\frac{I_0}{I_R} = \frac{\chi_{c0}^2}{\chi_{sR}^2} = u_0^2. \tag{57.7}$$

It is with the help of Eq. (57.7) that the relation may be written that ties together the two critical values of χ as given in the following equation:

$$\chi_{c0} = u_0 \chi_{sR} = \chi_{sR} e^{\psi_{sR}/2}. \tag{57.8}$$

This equation illustrates the plan of calculation by which the desired relation can best be computed. The steps in the calculation and the results obtained are given in Table 7. Note that χ_s and ψ_s combined as in Eq. (57.8) yield a table of values for χ_{c0}. From accurately made plots of the LANGMUIR data of Table 3C or from Eq. (37.7) rewritten below as Eq. (57.9) the corresponding values of ψ_{c0} may be obtained:

$$\psi_{c0} = 1.172 \frac{\chi_{c0}^{\frac{4}{3}}}{1 + \frac{1.68}{\chi_{c0}^{0.681}}}. \tag{57.9}$$

With the knowledge of the appropriate values of ψ_{sR} and ψ_{c0}, the correct value of S_0' may be written as follows:

$$S_0' = \psi_{sR} + \psi_{c0}. \tag{57.10}$$

The desired universal curve is obtained as a plot of the quantity u_0^2 of Eq. (57.7) on semi-logarithmic paper as a function of S_0' of Eq. (57.10). This curve has been plotted on Figs. 16 and 17 and is designated the "Universal Limiting Curve".

The basic purpose for this universal curve is to serve as the means by which the correct value of I_0 may be assigned as it applies to an experimentally measured current-voltage characteristic. It is therefore equally important that a set of master curves he developed to be used in association with this Universal Limiting Curve so that the best value for the current I_R can be established for a particular case. At the same time a most appropriate value of I_0 will be obtained at the intersection of the observed current-voltage characteristic with the Universal Limiting Curve. The next section shows the means for deriving the required master curves.

58. Equations and tables for the master curves. The first step in the derivation leading to the desired set of master curves is to obtain the limiting curve applicable to cathodes so copious in their emission that they become the "ideal emitters" of essentially unlimited emission capability. This master curve will form an upper boundary, illustrated in Figs. 16 and 17, to the set of master curves applicable to emitters of limited emission capability. The first part of this section will develop the theory by which the current voltage characteristic applicable to the "ideal emitter" may be computed.

Even though the emitter has practically unlimited electron emission available in the presence of a retarding field, it was shown in Sect. 43 that there is a maximum current I_m that can flow across a diode of spacing w with an emitter at a temperature V_T and have a zero gradient at the collector. The value of this current is given by the following equation which is essentially the same as Eq. (43.3):

$$I_m = \chi_m^2 N \frac{V_T^{\frac{3}{2}}}{w}. \tag{58.1}$$

For any positive value of ψ_c there is also a maximum current that can flow across a diode from an ideal emitter. This current may be computed directly from the following equation which is derived from the combination of Eqs. (46.10) and (46.11):

$$I_M = \chi_m^2 N \frac{V_T^{\frac{3}{2}}}{w} \left(1 + \frac{\chi_c}{\chi_m}\right)^2. \tag{58.2}$$

These two equations may be combined to define the quantity U^2 as in the following equation:

$$\frac{I_M}{I_m} = U^2 = \left(1 + \frac{\chi_c}{\chi_m}\right)^2. \tag{58.3}$$

The present objective is to express the relationship between U^2 and a variation in the applied voltage with reference to the zero value established when zero gradient occurs at the collector. When ψ_c is zero, U^2 is unity. Voltages expressed in dimensionless units are best illustrated by Fig. 15 which, it will be noted, is very similar in its construction to Fig. 14 except that, in this case, the condition of zero gradient at the emitter is never reached. This figure will also define symbols used in the following equations.

The increase in current expressed in terms of the current ratio U^2 is related to the *change* in the potential across the emitter region by the following equation:

$$U^2 = e^{\Delta\psi_s}. \tag{58.4}$$

With the change in applied potential represented by the symbol Σ, the following equations may be written:

$$\Sigma = \psi_c + \Delta\psi_s = \psi_c + \ln U^2, \tag{58.5}$$

$$\Sigma = \psi_c + \ln\left(1 + \frac{\chi_c}{\chi_m}\right)^2. \tag{58.6}$$

The "master curve" that forms the limiting set is obtained from a plot of the corresponding values of U^2 and Σ; its value is computed by Eq. (58.6). These corresponding values are given in Table 8.

All real emitters have finite emission capability and yet practical emitters, such as oxide cathodes operated at their normal temperature, can be expected to have such high emission capability that their operation is characterized by a z_R^2 value close to 0.998, as defined in the following equation:

$$\frac{I_R}{I_m} = z_R^2. \tag{58.7}$$

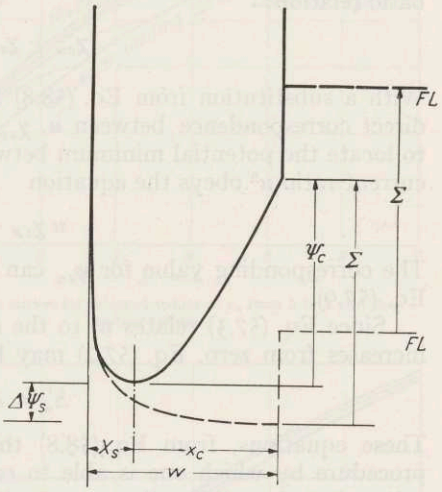

Fig. 15. Potential distribution for an emitter of unlimited emission.

Eq. (44.2) and an estimated value for the emission capability of an oxide cathode operating at 1160° K of 10 amp/cm.² was used to determine this value of z_R^2 that approaches so near unity. The value of z_R^2 for a good cathode operated at one-half its normal operating temperature will be close to 0.66. These figures are quoted to show that over a considerable range in temperature, practical oxide cathodes of good quality can be expected to approach in their performance very close to that of the ideal emitter of unlimited capability.

For every value of I_0 expressed in terms of u_0^2, as in Eq. (57.4), there is a corresponding value of z_R^2 and a characteristic current-voltage relation that covers the range of current from I_R to I_0. The parameter u^2 expressed as follows serves as a measure of the current I.

$$\frac{I}{I_R} = u^2. \tag{58.8}$$

Just as it was the purpose of the previous paragraphs to find the relation between U^2 and Σ, the following analysis is designed to show the method of calculating the relation between u^2 and S'. The steps for obtaining this relation are rather involved and yet, because the result is so important, the details are given.

Again Fig. 14 serves as the reference by which the variation of the potentials and the current may be linked in a simple and yet completely correct manner.

From Eq. (57.4) the following relation may be written:

$$\psi_{sR} = \ln u_0^2. \tag{58.9}$$

When the potential difference between the emitter and the collector is exactly ψ_{sR}, the value of S' is zero and the value of ψ_c is also zero. As the potential of the collector is made more positive with respect to this limiting value, a difference in potential of an amount which is symbolized by ψ_{cu} develops between the potential minimum and the collector. Under the same conditions of current flow, identified by a particular value of u, there is also a difference in potential of ψ_{su} between the emitter and the potential minimum. The relation between the measured current I and the emission capability I_0 is given by the following equation:

$$\ln \frac{I_0}{I} = \ln \frac{u_0^2}{u^2} = \psi_{su}. \tag{58.10}$$

Eqs. (38.9) and (57.6) may be combined and solved to form the following basic relation:

$$\chi_{cu} + \chi_{su} = \left(\frac{I}{I_R}\right)^{\frac{1}{2}} \chi_{sR}. \tag{58.11}$$

With a substitution from Eq. (58.8) in Eq. (58.11), it is possible to express the direct correspondence between u, χ_{su} and χ_{cu}. In principle this relation serves to locate the potential minimum between the two electrodes when the particular current ratio u^2 obeys the equation

$$u\,\chi_{sR} - \chi_{su} = \chi_{cu}. \tag{58.12}$$

The corresponding value for ψ_{cu} can be obtained either from Table 3C or from Eq. (57.9).

Since Eq. (57.3) relates u^2 to the change in the emitter space potential as S' increases from zero, Eq. (57.2) may be rewritten as follows:

$$S'_u = \Delta\psi_{su} + \psi_{cu}. \tag{58.13}$$

These equations, from Eq. (58.8) through Eq. (58.13) form the basis for the procedure by which one is able to calculate characteristic curves of current as a function of applied collector potential for emitters of all capability, as measure by the parameter u_0^2 expressed by Eq. (57.4).

The method of calculation involves nine steps and these are outlined very briefly as follows:

1. An arbitrary choice is made of the u_0^2 for which the calculation is to be made. Calculations have been made for a set of selected values of u_0^2 between 2 and 200 as shown in Table 9.

2. Each selection of u_0^2 gives by Eq. (58.9) a specific value of ψ_{sR} and also a corresponding value of χ_{sR}.

3. Corresponding values of ψ_{su} and χ_{su} may be copied from Table 3E for the range $0 < \psi_s \gtrsim 1.0$ to make a good working table for the best choice of u^2 values.

4. It follows from Eq. (58.10) that a suitable set of u^2 values may be obtained from the following relation

$$u^2 = u_0^2\, e^{-\psi_{su}}. \tag{58.14}$$

5. A reference work, such as BARLOW's Tables[1], serves as an excellent aid in converting these u^2 values to u.

6. The operation described by Eq. (58.12) is performed to obtain the corresponding set of χ_{cu} values.

[1] BARLOW's Tables, Edited by L. J. COMRIE, 4th ed. New York: Chemical Publishing Co., 1944.

7. The χ_{cu} values may be converted by means of Table 3C or by Eq. (57.9) to obtain the corresponding ψ_{cu}.

8. Logarithm tables may be used to determine $\ln u^2$ values corresponding to those recorded as step 4.

9. Since $\ln u^2$ is related to $\Delta\psi_{su}$ by Eq. (57.3), all of the data are at hand to perform the addition indicated in Eq. (58.13) and thus to obtain the correct value of S'_u.

The desired curve that relates u^2 to S'_u for a particular value of u_0^2 is thus available. The manner in which the master curves are used as they apply to experiment will be described in the next sections. Typical master curves are plotted in Figs. 16 and 17.

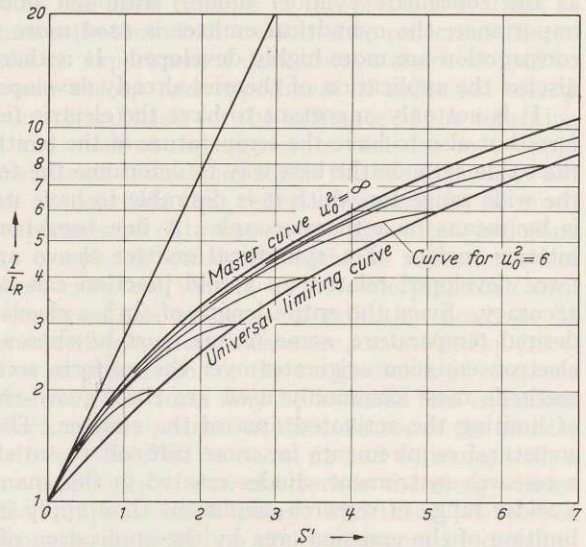

Fig. 16. Master curves for selected values of u_0 from 2 to 8 and the limiting curves.

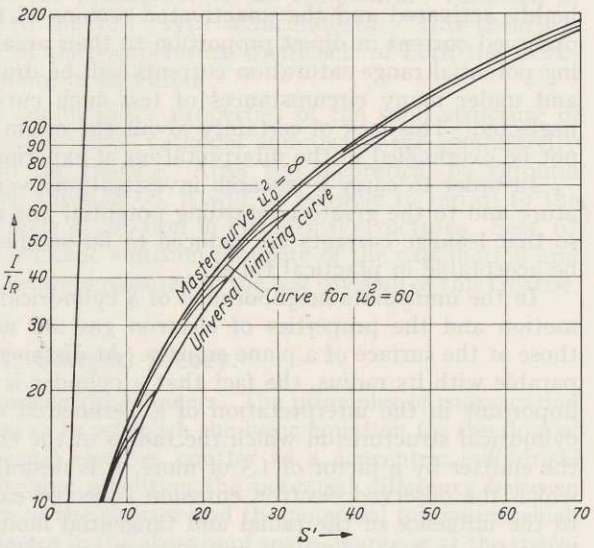

Fig. 17. Master curves for selected values of u_0 from 16 to 200 and the limiting curves.

59. General discussion of the application of theory to experiment. It has been the plan of this treatise to begin at Sect. 14 and to present as much as possible of the theoretical structure of the science of thermionic emission with a minimum of references to specific experimental results. The theories have been developed with the ultimate objective of applying them directly to the experiments to be described in later sections. It now becomes necessary to discuss, in a general way certain specific features of experimental research to justify the development of more specialized features of the theory in advance of the application of the entire theory to the interpretation of experimental research.

Basically, nearly all researches on oxide cathodes are performed with diode tube structures. There are only two practical forms of the diode structure that lend themselves to a complete theoretical analysis: (1) a diode formed between parallel planes and (2) a diode formed by concentric cylinders. The fundamental reason for this limitation in structure is that only these tube structures can

yield a uniform field at the emitting surface and at the collecting surface for a fixed applied difference in potential between them. Although the plane parallel electrode system is easier to deal with theoretically, it is not as easy to construct as the concentric cylinder diode. Although both structures are of practical importance, the cylindrical emitter is used more widely and techniques for its construction are more highly developed. It is therefore considered significant to discuss the application of theories already developed to the cylindrical structure.

It is not only important to have the electric fields within the test diode uniform but also to have the temperature of the emitter uniform and known. With the oxide cathode the best way to determine the temperature of the emitter over the wide range for which it is desirable to have its value determined accurately is by means of a thermocouple. A fine tungsten wire may be welded to the interior surface of a cylindrical emitter sleeve and the thermal electromotive force developed relative to a cold junction can be calibrated with satisfactory accuracy. Since the entire length of such a sleeve cannot be maintained at the desired temperature, some means must be chosen to assure that the measured electron emission originates over the uniform section of the emitter. The two methods most commonly used are the "guard-ring" method and the method of limiting the activated area of the emitter. The guard-ring method involves structural requirements far more difficult to satisfy than the other and yet, as a research instrument, diodes created in this manner yield reliable results over a wider range of research conditions than apply if the observer depends on the limiting of the emission area by the application of the oxide coating to just the central portion. The objection to the latter method becomes evident especially in the retarding potential range. At a sufficiently high retarding potential the highly activated and the unactivated regions of the cathode contribute to the observed current in direct proportion to their areas. In the intermediate retarding potential range saturation currents will be drawn from the unactivated area and under many circumstances of test such currents are small enough to be neglected. This lack of certainty about the origin of the observed current must not be overlooked in the interpretation of experimental observations.

In order to carry a research investigation over the widest range in temperature and to the greatest retarding potential one must design the test structure so that leakage currents are reduced to far smaller values than would normally be acceptable in practical tubes.

In the immediate neighborhood of a cylindrical emitting surface, the electron motion and the properties of electron gas are not appreciably different from those at the surface of a plane emitter. At distances away from the emitter comparable with its radius, the fact that a cylinder is used becomes more and more important in the interpretation of experimental data. Therefore, for practical cylindrical structures in which the radius of the collector is greater than that of the emitter by a factor of 1.5 or more, it is desirable to work out the theory by which the observed electron emission collected can be interpreted with respect to the influence of the radial and tangential momenta of the electrons as they leave the emitter. Sect. 60 will present an outline of the theory and indicate some of the methods by which tabulated functions presented there may be used.

Even though a given cylindrical diode structure is created with a well-defined collector to emitter ratio of radii, in the application of space-charge theory to the electron flow, the potential minimum crosses the diode as the collector space potential expressed as ψ_c increases from zero to very moderate values of approximately 10 units of V_T. In order to understand the increase in current expected at the collector region as the potential is made positive, it is necessary

to combine the theory for the electron flow in a cylindrical structure with an evaluation of the location of the potential minimum between the emitter and the collector. These relations will be presented in Sect. 61.

It was appropriate to develop the basic theories in the previous sections as they would apply to emitters and collectors which exhibited no reflection effects. The application of these theories to experimental data always seems to lead to unexpected disagreement between theory and experiment if reflection effects are neglected. At this time a theoretical basis for the existence of the reflection effect has not been developed and most of the arguments that one may apply in a classical manner to the transmission of electrons across the boundary between a solid and a vacuum lead one to conclude that reflection cannot be of much importance. Since all of the experimental data known to this writer, including those of FAN[1] and HUNG[2], are completely consistent with the reflection-effect hypothesis—even though in some cases the writers do not interpret their own results in that manner—the theory of the influence of reflection needs to be presented. In the examples for which quantitative data are available, Eq. (26.4) offers the most satisfactory form of expression for the transmission of electrons out of an emitter or into a collector. This form may be assumed and equations may be derived to interpret reflection effects either at the collector or the emitter or at both. These equations will be presented in Sects. 62 and 63 along with a discussion of the influence that a deficiency of slow electrons in the energy distribution will have on the application of space-charge theory. This theory, developed on the basis of LANGMUIR'S equations, depended on the electron energy distribution being MAXWELLian.

Sect. 64 will be devoted to the evaluation of the temperature variation of the FERMI level as it applies to the "N" type semiconductor. This theory is essential to the interpretation of the temperature coefficient of both the work-function and the contact difference in potential.

Sect. 65 will relate to the conductivity properties of the solid structure of the semiconductor typical of oxide-coated cathodes and also to the conductivity through the occluded pores in the coating. After the theoretical background has been developed in Sects. 60 through 66, it will be possible to return to the discussion of the theory of cathode evaluation in cylindrical structures. Sect. 67 will complete the theory of thermionic emission requisite of the explanation and discussion of the experimental results presented in the last division of this treatise.

VI. General theory.

60. Electron flow between concentric cylinders. The principles of conservation of energy and of momentum serve to establish the basic equation for the flow of emission current from an internal electron emitter to a concentric cylindrical collector. To establish this limiting condition the potential difference between a point just outside the surface of the emitter and the potential minimum which occurs at the surface of the collector in the absence of space-charge or at the space-charge minimum, when one exists between the electrodes, is expressed as V_s (see Figs. 8, 10, and 14). The surface of the emitter is thus V_s positive with respect to the cylindrical surface at which the limiting condition for electron arrival is being expressed. This surface either coincides with the collector or lies between the emitter and the collector. The tangential (p_θ) and the radial (p_r)

[1] H. Y. FAN: J. Appl. Phys. **14**, 552 (1943).
[2] C. S. HUNG: J. Appl. Phys. **21**, 37 (1950).

momenta are related to the potential difference and to the initial values of these momenta at the emitter by the following equation:

$$\frac{p_\vartheta^2}{2m} + \frac{p_r^2}{2m} + eV_s = \frac{p_{\vartheta s}^2 + p_{rs}^2}{2m} = \text{const}. \tag{60.1}$$

This equation expresses the conservation of energy and the following expresses the conservation of momentum:

$$r\,p_\vartheta = r_s\,p_{\vartheta s}. \tag{60.2}$$

Since the limiting condition is that associated with p_r being zero, the following relation gives the limiting values of the momenta p_{r1} and $p_{\vartheta 1}$ at the emitter for electrons to arrive at the potential point V_s negative with respect to the emitter at a radius of R:

$$2m\,e\,V_s = p_{r1}^2 + \left(1 - \frac{r_s^2}{R^2}\right) p_{\vartheta 1}^2. \tag{60.3}$$

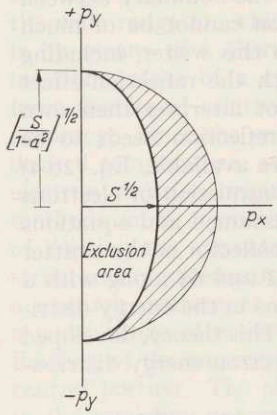

Fig. 18. Momentum space illustration of exclusion area for cylinders of (1/a) ratio of 1.2 as used in Eq. (60.4).

The basic equation for the calculation of current is Eq. (26.7) and for the present purpose it will be best to compute the integral on the basis that the transmission coefficient expressed by Eq. (26.4) is one, or that ω of that equation is zero. The method of integration which must be employed can be illustrated best by the momentum space diagram of Fig. 18.

At the surface of the emitter the radial component of the momentum is interchangeable with the x component used in Eq. (26.7) and the tangential component is the equivalent of the y component of that equation. The exclusion area in the momentum space of Fig. 18 is bounded by an ellipse the equation of which is Eq. (60.3). The integration method found most convenient involved first, the evaluation of the integral in the entire area of positive p_x values outside of the circle drawn with a radius of $(2m\,e\,V_s)^{\frac{1}{2}}$; then, to this value is added the contribution represented by the cross-hatched area of Fig. 18 which lies between the exclusion boundary and the circle. The results of this integration are expressed as follows:

$$I = I_{00}\left\{1 + \frac{2}{\sqrt{\pi}}\sqrt{\frac{S}{1-a^2}}\,e^{-S/(1-a^2)} - \frac{2}{\sqrt{\pi}}\int_0^{\sqrt{\frac{S}{1-a^2}}} e^{-x^2}\,dx + \right.$$
$$\left. + \frac{2}{\sqrt{\pi}}\int_{\sqrt{S}}^{\sqrt{\frac{S}{1-a^2}}} \frac{2x^2\left(1 - \frac{S}{x^2}\right)^{\frac{1}{2}}}{a}\,e^{-x^2}\,dx\right\}. \tag{60.4}$$

The two parameters of this equation, S and a, are defined by the following:

$$S = \frac{V_s}{V_T}, \tag{60.5}$$

$$a = \frac{r_s}{R}. \tag{60.6}$$

It is to be noted that when a^2 is small compared with unity, Eq. (60.4) reduces to the essential part of Eq. (26.11) which was derived by SCHOTTKY for the limiting case of a small filament coaxial with respect to a collector of large radius. As a approaches one, Eq. (60.4) becomes identical with the simple BOLTZMANN relation expressed as follows:

$$I = I_{00}\,e^{-S}. \tag{60.7}$$

For arbitrary choices of the ratio of radii, represented by the parameter a, the function shown as Eq. (60.4) has been evaluated by numerical integration for the entire useful range of S from zero to 20. These results are summarized in Table 10.

Smooth curves drawn through plotted points that represent the data given in Table 10 are shown in Fig. 19 for selected values of $(1/a)$ of 1, 1.5, 2.5 and

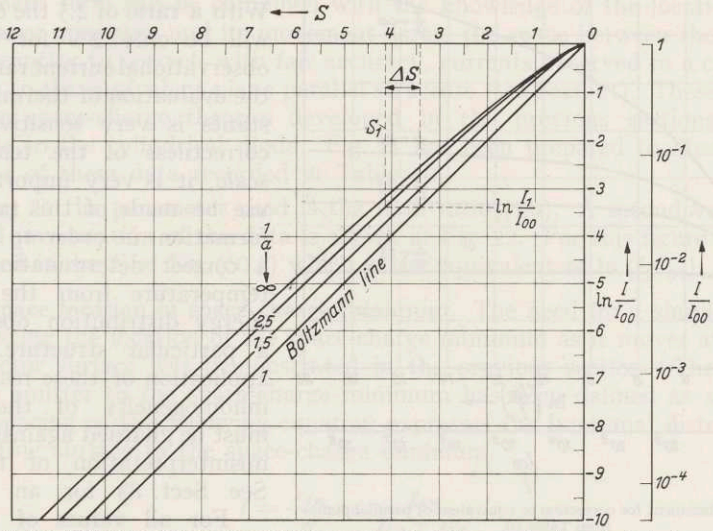

Fig. 19. Plots from Table 10 and illustration of displacement method of conversion to equivalent of parallel planes.

infinity. An inspection of these curves leads to the following conclusions: (1) for small values of $(1/a)$ the lines rapidly become parallel to the BOLTZMANN line, and (2) the larger the values of $(1/a)$ the greater is the displacement of the curve from the BOLTZMANN line.

Mention has been made of the fact that the temperature of the emitter can be determined by an analysis of the electron energy distribution at high retarding

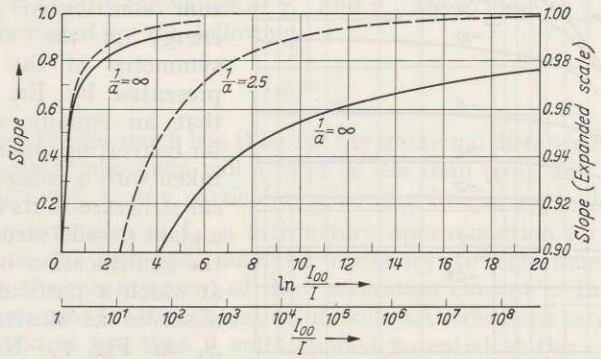

Fig. 20. Slope correction factor from Table 10.

fields applied to a plane parallel structure. These results show that the electron temperature may also be determined in a similar manner for a cylindrical structure if the observed average slope is corrected by the slope factor characteristic of the radius ratio $(1/a)$ of the tube in which the observations were made. In Table 10 the slopes are given for the various values of $(1/a)$ as a function of the quantity $\ln(I/I_{00})$. Smooth curves drawn through the computed points for the two cases of $(1/a)$ of 2.5 and infinity are shown in Fig. 20. These curves are offered by way

of illustration of the usefulness of the data in Table 10. For very large values of $(1/a)$ they show graphically that the apparent electron temperature will be 7% higher than the true temperature if the average slope of experimental data is determined for the range of current ratio (I/I_{00}) of 10^{-2} to 10^{-4}. With a ratio of 2.5 the correction will be only 2% for the same observational current range. Since the evaluation of thermionic constants is very sensitive to the correctness of the temperature scale, it is very important that use be made of this tabular information in order to arrive at a correct determination of the temperature from the electron energy distribution observed in a particular structure. In the application of these results gross inhomogeneity of the emitter must be guarded against to avoid misinterpretation of the data. See Sect. 83 for an example.

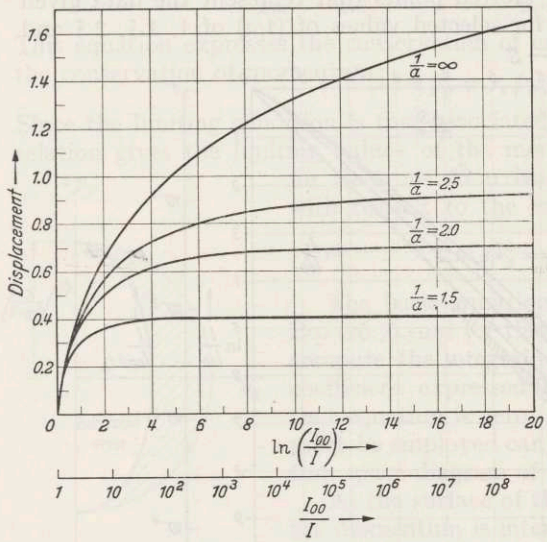

Fig. 21. Displacement for correction to equivalent of parallel planes from Table 10.

For all values of the radii ratio $(1/a)$, the lines illustrated in Fig. 19 are displaced to the left relative to the BOLTZMANN line. Note that at any particular value of S the excess of the current over the corresponding value on the BOLTZMANN line is a direct measure of the contribution to the current that arrived at the collector or at the space-charge minimum because tangential initial momentum contributed to the total energy of the electron. The symmetry of the function represented by Eq. (60.4) shows that an equally valid method for converting observational data taken with a concentric cylindrical structure to its equivalent for a plane parallel structure involves the identification of the S-value at which a particular current is observed as illustrated at point S_1 in Fig. 19. Note that the horizontal displacement shown there as ΔS permits the determination of the applied potential which would yield the same emission current (I_1) from an emitter which had identical properties to that used in the observation but was an equivalent parallel plane diode structure.

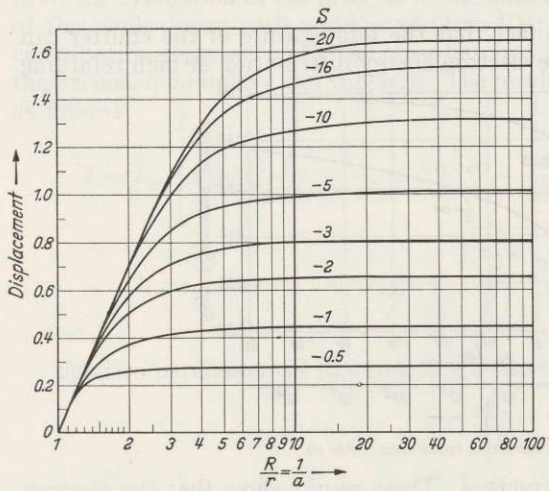

Fig. 22. Displacement as related to shift in space-charge minimum.

For a particular ratio of radii such as 2.5 for example, the displacement ΔS is a function of the ratio (I/I_{00}) given by the separation between the "2.5" line

and the BOLTZMANN line. In general, there will be a value of I at which space charge will set in and following that the effective radii ratio will decrease rapidly from 2.5 to a value near to unity. As $(1/a)$ approaches unity, tangential components of momentum will no longer contribute to the initial kinetic energy needed to pass the space-charge minimum. The data derivable from Table 10 for the displacement term can be combined with the knowledge of the location of the space-charge minimum and its movement across the space between the collector and the emitter to correct, with fair accuracy, currents observed in a cylindrical structure to the equivalent plane parallel structure (see Sect. 61). These methods make the space-charge theories developed in the previous sections directly applicable to the cylindrical diode. Fig. 21 has been prepared to illustrate the usefulness of these data recorded in Table 10.

In Fig. 21 the parameter used is the radii ratio $(1/a)$. A second very useful graphical presentation of the data is shown in Fig. 22. For this figure the parameter used is the S of Eq. (60.7) which is the equivalent of $\ln (I/I_{00})$.

61. Space location of space-charge minimum. The need for a simple method of calculating the location of the space-charge minimum as it moves away from the collector surface was demonstrated in the previous section. The distance from the emitter to the space-charge minimum has been defined as x_{su}. With a diode spacing w, the following equation expresses the fractional distance from the emitting surface to the space-charge minimum.

$$f = \frac{x_{su}}{w} = \frac{\chi_{su}}{\chi_{cu} + \chi_{su}}. \tag{61.1}$$

This equation may be combined with Eq. (58.11) to give the following results:

$$f = \frac{\chi_{su}}{u\,\chi_{sR}}. \tag{61.2}$$

The details of the method by which this equation is used will be outlined below. It is of interest to note that for emitters of very high emission capability which have $u_0^2 = (I_0/I_R) > 10^3$, the values of χ_{su} and χ_{sR} are so close to χ_m that Eq. (61.2) is well approximated by the following:

$$f_M = \frac{1}{u}. \tag{61.3}$$

When the value of u_0^2 is much less than 10^3 the fractional distance from the emitter to the space-charge minimum will always be less than $(1/u)$, and it may be computed with accuracy at any particular value of u by the method to be outlined.

For the lower values of I_0, a satisfactory approximation for u_0^2 may be obtained without the complete analysis necessary to determine this quantity accurately by the measurement of the "saturation current". In most practical diode structures used for the evaluation of oxide cathodes such saturation currents will be observed at less than 6 volts applied potential at the collector relative to the emitter. With ψ_{sR} given by Eq. (58.9) the corresponding value of χ_{sR} is obtained from Table 3 E. At intermediate values of u between unity and u_0 the appropriate value of ψ_{su} is given by Eq. (58.10) and the corresponding value of χ_{su} may be obtained from Table 3 E. With these quantities determined, the fractional distance from the emitter to the space-charge minimum in a plane parallel diode structure is given accurately by Eq. (61.2). Experiments with cylindrical structures indicate that the same formula gives an excellent approximation for the location of the space-charge minimum as it progresses from the

collector surface toward the emitter surface as the collector is made more and more positive with respect to the critical potential at which zero gradient is established at the collector. This analysis, combined with the tabular information developed in the previous section goes far to bridge the gab between the exact theories applicable to the plane parallel structure and their use in association with cylindrical diodes.

62. Influence of multiple electron reflection on diode currents. In spite of the fact that electron reflection effects at the boundary between solids and vacuum are not generally accepted as fact, there are no published experimental data that demonstrate conclusively the absence of reflection effects. GERMER[1] interpreted his experiment to indicate that reflection effects are absent, but NOTTINGHAM's studies[2] show that GERMER's experimental data are in excellent agreement with the reflection hypothesis. HUTSON's experiments[3] to be described in more detail in Sect. 72 are most easily explained by the reflection hypothesis and in fact yield a transmission coefficient in excellent agreement with NOTTINGHAM's. HUNG[4] made a careful study of the electron energy distribution from an oxide cathode source and interpreted the deviation between his observations and those to be expected in the absence of reflection as the result of patchiness of the emitter surface. It is true that patchiness can cause similar discrepancy.

It is the purpose of this section to make available the theoretical background by which reflection can be included in the analysis of experimental data if the observer finds it necessary. Sect. 81 will show that electron emission properties of oxide cathodes, both in the presence and absence of space charge, can best be understood if the reflection hypothesis is integrated with the theoretical interpretation of the experimental data.

The most convenient expressions that best fit the quantitative data available for the transmission and reflection of electrons at a solid surface are repeated from Sect. 26 as follows:

For transmission:

$$D(p'_x) = \left(1 - e^{-\frac{(p'^2_x/2m)}{\omega}}\right). \tag{62.1}$$

For reflection:

$$R(p'_x) = e^{-\frac{(p'^2_x/2m)}{\omega}}. \tag{62.2}$$

In these expressions for transmission and reflection, the quantity $(p'^2_x/2m)$ is the kinetic energy associated with an electron which has a component of momentum p'_x perpendicular to the barrier at the surface of the solid as the electron passes so close to the barrier that the principal forces acting are the mirror-image forces. Although it might be anticipated that the empirical constant ω entering into these equations might very well be expected to be dependent on the externally applied surface field, the researches of HUTSON show that the constant does not change appreciably for moderate field strength.

An emitter in the presence of a strong retarding potential can be expected to deliver across its barrier all of the electrons that would be predicted in the absence of any reflection effect. Over the energy range of 0.2 electron volts and less, strong reflection effects would normally be expected. In the presence of a retarding field, an electron atmosphere is built up outside the emitter with

[1] L. H. GERMER: Phys. Rev. **25**, 795 (1925).
[2] W. B. NOTTINGHAM: Phys. Rev. **49**, 78 (1936).
[3] A. R. HUTSON: Phys. Rev. **98**, 889 (1955).
[4] C. S. HUNG: J. Appl. Phys. **21**, 37 (1950).

exactly that concentration that would be found without reflection effects, because in a region of this kind transmission and reflection exactly compensate so that the normal density is maintained. The situation is different at the collector, since electrons arrive there with a distribution of energy such that many of them cross the collector barrier with a very small energy. These electrons, if reflected, return to the emitter with such high energy that they should be expected to be completely reabsorbed by the emitter surface without multiple reflection. Unless there are unexpected localized energy regions characteristic of the crystal structure of the emitter which would result in a transmission characteristic far more complex than that described by Eq. (62.1), an observer must expect to find a variation in current received with retarding potential changes that will follow the BOLTZMANN relation and therefore seem to indicate an absence of reflection at the collector. This failure to show reflection even though it may exist results from the fact that the energy distribution of the electrons arriving at the collector is independent of the retarding potential. The number of electrons arriving depends on the retarding potential. The fraction reflected will be independent of the retarding potential.

The situation reverses when observations are made in the presence of a small accelerating field. If the minimum energy of the electrons arriving at the collector is in excess of one electron volt and if there are no reflection maxima not described by Eq. (62.1), then practically all of the electron current that arrives at the collector will be absorbed by it. This statement holds true for that range in applied potential for which secondary electron emission effects are negligible.

Even in the absence of space-charge, multiple reflections can occur when the retarding or accelerating fields are very weak. The equations which are to be developed in this section are capable of providing a description of the current-voltage relation to be anticipated under geometrical conditions that involve an equality of transmission and reflection effects at the emitter and the collector boundaries. In the presence of space charge, the problem becomes somewhat more involved, but the same principle is used. Over the retarding potential range and before a space-charge minimum develops, a constant fraction of the electrons that arrive at the collector will be reflected back and reabsorbed by the emitter. As the space-charge minimum develops, the electrons which pass over this minimum will have a higher transmission probability of entering the collector, since the very slowest electrons will be received at the collector with and energy of V_c at the surface. Again, the space-charge which develops in the immediate neighborhood of the emitter will be fully equal to that which would be expected in the absence of a reflection effect, because of the self-compensating action that takes place at the emitter barrier for the electrons passing into space with insufficient energy to go over the space-charge potential minimum. As the value of this potential between the surface of the emitter and the potential minimum as expressed by V_s decreases, the space-charge density will decrease and finally become characteristic of the electron energy distribution which actually comes from the emitter. This distribution will contain an abnormally high proportion of high-energy electrons in comparison with the distribution that would exist in the absence of a reflection effect.

It should be evident from this preliminary discussion of the problem that, if reflection effects are present, they would show in diode studies first because a deviation from the BOLTZMANN distribution should be observed at a smaller current that would be predicted by the computation called for in Sect. 43. Experiments to be described in Sect. 83 will show that such a deviation is found. Many other evidences in these studies of space-charge in diodes are entirely

consistent with the reflection hypothesis and the features made available by this hypothesis are needed to explain the observations. The computation which follows applies directly to the circumstance and temperature range for which space-charge effects are negligible.

In the formulation of this problem, there are two ranges of interest, designated as the "retarding range" and the "accelerating range". It is to be anticipated that the equations which are derived and are applicable to each of these ranges individually will yield exactly the same answer at zero field. The voltages that enter into the equation will be designated V_s or V_c. The first will give the potential difference of the emitter surface relative to the collector surface and will therefore represent the actual magnitude of the retarding potential (see Fig. 23). Over the accelerating potential range the symbol will be V_c for the voltage difference between the collector surface and the emitting surface (see Fig. 24). Under this circumstance, the potential will be an accelerating potential for the electrons emitted at the surface. The equation for the retarding range will be developed first.

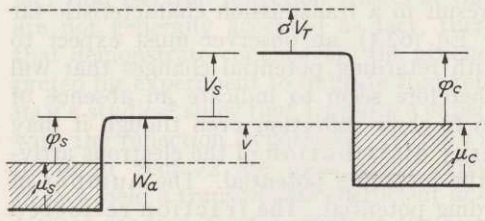

Fig. 23. Symbols used for multiple reflection theory with retarding potentials.

Electrons which are emitted from the surface with sufficient energy to pass across the diode and approach the collector will have a certain probability of acceptance by the collector which is expressed by Eq. (62.1). Those reflected, with a probability expressed by Eq. (62.2), will return to the emitter where, again, there will be a certain probability of acceptance by the emitter given by Eq. (62.1) and a certain probability of reflection to the collector. The final equation for the current delivered from the emitter to the collector must represent the sum of an infinite series which, under most circumstances, converges so rapidly that three or four terms in the series are sufficient to give high accuracy. This series is expressed as follows:

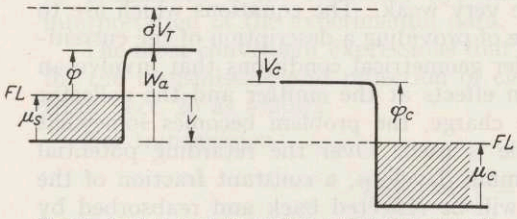

Fig. 24. Symbols used for multiple reflection theory with accelerating potentials.

$$I = I_{00} \sum_{n=0}^{\infty} \int_{\sigma=0}^{\infty} e^{-\left(\frac{V_s}{V_T}+\sigma\right)} \left(1 - e^{-\frac{V_s+\sigma V_T}{\omega}}\right)\left(1 - e^{-\frac{\sigma V_T}{\omega}}\right) e^{-n\left(\frac{V_s+2\sigma V_T}{\omega}\right)} d\sigma. \quad (62.3)$$

In this equation the quantity σ is best defined by Fig. 23 in which it is shown to be the energy of an electron in excess of that needed for entrance across the motive maximum V_s and is expressed in dimensionless units. The quantity I_{00} is defined by the following relation:

$$I_{00} = \frac{4\pi m k^2 e}{h^3} T^2 e^{-\frac{\varphi}{V_T}} = A T^2 e^{-\frac{\varphi}{V_T}}. \quad (62.4)$$

In this equation φ is the *true* work-function (not the RICHARDSON work-function) and the current density expressed is that which impinges on the interior surface for the group of electrons energetic enough to escape. The constant A of this equation is the universal constant from the theory and it should apply to emission from all substances.

Inspection of Eq. (62.3) shows that, for each value of the parameter n, there will be four terms in the final equation. These may be combined algebraically to give the following results:

$$I = I_{00}\, e^{-\frac{V_s}{V_T}} \sum_{n=0}^{\infty} F(V_s, V_T, n) \tag{62.5}$$

with

$$F(V_s, V_T, n) = \frac{e^{-\frac{n V_s}{\omega}}}{\frac{\omega}{V_T} + 4n + 1 + 2n(2n+1)\frac{V_T}{\omega}} - \frac{e^{-(n+1)\frac{V_s}{\omega}}}{\frac{\omega}{V_T} + 4n + 3 + (2n+1)(2n+2)\frac{V_T}{\omega}}. \tag{62.6}$$

The diagram which shows the symbols appropriate to the analysis of the multiple reflection problem with accelerating fields is shown as Fig. 24. The formulation of the problem is exactly analogous to that required for Eq. (62.3) except for the definition of (σV_T) which for the application of an accelerating field measures the kinetic energy associated with the electron motion as it passes over the emission barrier instead of the collection barrier as was illustrated in Fig. 23. With this change of symbolization the new equation is of exactly the same general form and is given as follows:

$$I = I_{00} \sum_{n=0}^{\infty} \int_{\sigma=0}^{\infty} e^{-\sigma} \left(1 - e^{-\frac{\sigma V_T}{\omega}}\right) \left(1 - e^{-\frac{V_c + \sigma V_T}{\omega}}\right) e^{-\frac{n}{\omega}(2\sigma V_T + V_c)}\, d\sigma. \tag{62.7}$$

After integration, the solution is very similar to that given as Eq. (62.5) and is the following:

$$I = I_{00} \sum_{n=0}^{n=\infty} F(V_c, V_T, n). \tag{62.8}$$

Since the function $F(V_c, V_T, n)$ is exactly the same as that given above as Eq. (62.6) except for the substitution of V_c for V_s this function will not be written out in detail. Although in Eqs. (62.1) and (62.2) ω is expressed in energy units of joules, it is far more convenient for computational purposes to express ω in electron volts. The value of this constant which seems to fit the experiments best is 0.191 electron volts or its equivalent 3.06×10^{-18} joules.

Although these relations have been worked out specifically for the plane parallel electrode structure, they are applicable to the cylindrical structure if the radii ratio is close enough to unity so that a large fraction of the electrons reflected from the collector return to the emitter. If the emitter is of very small radius compared with the collector then multiple reflection effects are unimportant even though consideration must be given to the reflection effect at the emission surface. The reason multiple effects are negligible for this geometry is that, after an electron leaves the emitter, there is very small probability that it will return to the emitter without having made many excursions to the collector with a finite probability that it will be accepted there and record as observed current each time it returns. The usual structures for emitter testing with oxide cathodes make it necessary to include in the analysis the concept of multiple reflection. The application of these theories to the analysis of electron flow in the presence of space charge introduces still more complications.

For high values of V_s or V_c, Eq. (62.6) has a value only for the $n = 0$ term. The value of the function is given as follows:

$$f(V_c, V_T, 0) = \frac{1}{\frac{\omega}{V_T} + 1}. \tag{62.9}$$

It follows that, for high retarding potentials, the current is given by Eq. (62.10) and for high accelerating potentials it is given by Eq. (62.11) if one neglects the reduction in work-function that results from the SCHOTTKY effect discussed in detail in Sect. 27:

$$I = I_{00}\, e^{-\frac{V_c}{V_T}} \frac{1}{\frac{\omega}{V_T} + 1} \tag{62.10}$$

(Range of retarding potentials $V_s > 3\omega$).

$$I = I_{00} \frac{1}{\frac{\omega}{V_T} + 1} \tag{62.11}$$

(Range of accelerating potentials $V_c > 5\omega$).

Since the observed currents in both the retarding-potential range and the accelerating-potential range are lowered by the same factor which is given by Eq. (62.9), the intersection of the extrapolated retarding-potential line and the saturation-current line in the absence of space-charge will nevertheless give a rather accurate determination of the "zero-field" condition. HUNG[1] observed this intersection point as a function of the temperature. Although he did not point out that he had measured the temperature coefficient of the work-function in this manner, the discussion of this problem in Sect. 81 will indicate that his value of the temperature coefficient of the work-function for oxide cathodes is typical of that expected for a well-activated cathode over the temperature range of his observations.

63. Average energy of electrons transmitted across the mirror-image field reflection barrier. For high retarding potentials, it has already been pointed out that the reflection effect leaves the distribution in electron energy unaltered. However, an analysis of the statistics shows that the average energy associated with the component of momentum perpendicular to a surface across which electrons travel with a MAXWELLian distribution of velocity will be given in the following equation:

$$\bar{\varepsilon}_x = \frac{\overline{p_x'^2}}{2m} = kT = eV_T. \tag{63.1}$$

To calculate the average energy associated with the component of momentum p_x' in the presence of a reflection effect boundary one may write the following basic equation:

$$\bar{\varepsilon}_x = \frac{\int_0^\infty \frac{p_x'^2}{2m} \frac{p_x'}{m} e^{-\frac{\varepsilon_x}{kT}} \left(1 - e^{-\frac{\varepsilon_x}{\omega}}\right) dp_x'}{\int_0^\infty \frac{p_x'}{m} e^{-\frac{\varepsilon_x}{kT}} \left(1 - e^{-\frac{\varepsilon_x}{\omega}}\right) dp_x'}. \tag{63.2}$$

This equation, evaluated, gives the following result:

$$\bar{\varepsilon}_x = kT \frac{1 + 2\frac{\omega}{kT}}{1 + \frac{\omega}{kT}}. \tag{63.3}$$

[1] C. S. HUNG: J. Appl. Phys. **21**, 143 (1950).

If the average energy is expressed in electron volts, the equation takes on the following form:

$$\bar{\varepsilon}_x = V_T \frac{1 + 2\frac{\omega}{V_T}}{1 + \frac{\omega}{V_T}}. \tag{63.4}$$

This equation shows that there is a significant change in the average energy of electrons emitted through a reflection barrier compared with the nonreflection barrier. With the expected value of ω taken as 0.191 electron volts combined with the normal value of V_T of 0.1 electron volts it shows that the average energy under these circumstances is 66% higher than the usual kT value. The difference is still greater if one applies this equation to a lower value of V_T such as 0.05. Under this circumstance the average energy is 80% above the usually accepted value.

The indications are that over the average temperature range important for oxide cathodes, it is to be expected that space-charge effects and other phenomena that depend on the energy distribution of the electrons should be examined in the light of the fact that the average energy of escaping electrons will be significantly higher than the value usually assigned of kT or, in electron units, V_T. As space charge develops with an increase in temperature for a given emitter, the reflection effect alteration of the average energy of the electrons diminishes gradually and finally becomes small enough to be negligible for most practical purposes.

64. Temperature coefficient of the FERMI level in N type semiconductors and the FOWLER thermionic equation. As a starting point for this discussion, Sects. 14, 15 and 16 should be reviewed, since the derivation of the basic equation, Eq. (16.1). depended on that material. This equation is repeated as the following:

$$N(\varepsilon_x)\, d\varepsilon_x = 2\frac{(2\pi m kT)}{h^3} \ln\left(1 + e^{-\frac{\varepsilon_x - \mu}{kT}}\right) d\varepsilon_x. \tag{64.1}$$

In this equation, the variable ε_x is the kinetic energy[1] associated with an electron whose x component of momentum is perpendicular to the surface across which $N(\varepsilon_x)$ electrons cross in the positive direction per unit area per unit time per unit energy range in ε_x. This equation gives the random current which crosses the boundary at the stated energy value with respect to the zero of kinetic energy in the conduction band. If the conductor is reduced to absoiute zero, then the highest occupied electronic state in the conductor is a direct measure of the FERMI level at absolute zero of temperature. It is most convenient to assign the energy at this level its value with respect to the zero of kinetic energy in the conduction band. For all of the common metallic conductors, the FERMI level designated in this equation by μ is positive and decreases in absolute value as the temperature increases. The rate of decrease is dependent on both the electron concentration and the expansion properties of the crystal.

In all of the semiconductors of particular interest as they relate directly to thermionic emission, the concentration of electrons in the conduction band at absolute zero is generally zero and the FERMI level is negative. Although one might consider the approach to absolute zero in the semiconductor problem to yield an indeterminante value for the FERMI level, it is possible to show that

[1] If the temperature-energy kT is expressed in joules as in Eq. (64.1) then ε_x and μ, and later μ' and E, are expressed in joules but if the temperature-energy is expressed in its electron volt equivalent then ε_x, μ, μ' and E are expressed in electron volts.

at the zero of temperature, the FERMI level is exactly halfway between the zero state in the conduction band and the highest occupied impurity level. The energy level diagram of Fig. 25 will serve to relate the quantities mentioned here.

As the temperature increases from absolute zero, the position of the FERMI level changes in a manner that depends on the donor concentration n_D and on the energy level or levels of these donors expressed in the diagram as E_D. Although equations[1] may be worked out by which the temperature variation of the FERMI level can be computed for a multiplicity of donor levels (two such levels are shown in Fig. 25), it will simplify the calculations to treat first the problem for a single, well-defined set of donors. Fig. 26 may be used to describe the situation at an intermediate temperature between absolute zero and the maximum at which structural changes can occur in the semiconductor. This range

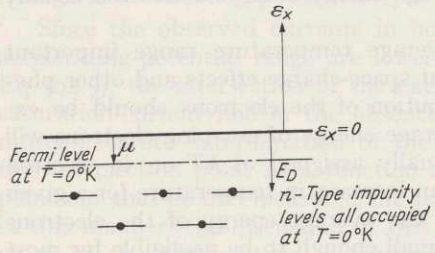

Fig. 25. Energy states in a semiconductor.

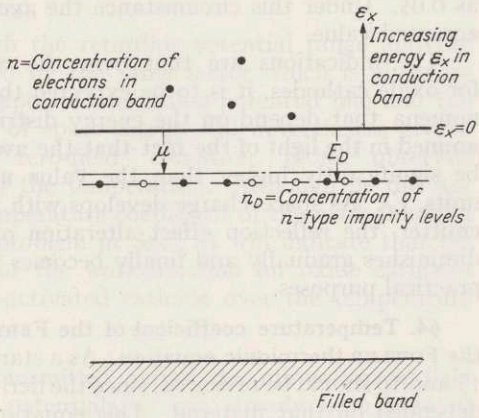

Fig. 26. An N type semiconductor at a high temperature.

in temperature for the oxide cathode lies below approximately 1200° K. As the temperature is increased from absulute zero, electrons transfer from the donor states into the conduction band to maintain a steady state situation at each temperature for which the rate of transfer from the donor states to the conduction band is exactly equalized by the return of electrons from the conduction band to the donor states.

If the experimental evaluation of the theory depended on exact knowledge of the true distribution of the electrons in the conduction band, then a quantum theory analysis of the wave functions suitable for the particular crystals and crystallographic direction of the solid would be demanded before any further progress could be made in the discussion of the temperature variation of the FERMI level. Such details are not necessary for the present purpose. since in the final analysis, the center of interest relates to the random current rather than to the true distribution of the electrons which gives rise to that current.

Since crystals having very different distributions in available quantum states can be formed in intimate contact with each other and under thermal equilibrium conditions there is no net flow of electricity across the boundary, the random current flow in the interiors of the separate crystals must each be exactly that called for by Eq. (64.1) or else the random flow must be exactly zero in one or the other of the crystals. In the application of this principle, the FERMI level is continuous across the boundary and therefore it is to be expected

[1] R. A. HUTNER, E. S. RITTNER and F. K. DUPRÉ: Philips Res. Rep. **5**, 188 (1950).

that for dissimilar substances, the location of the energy state $\varepsilon_x = 0$ will be different in the two crystals. The FERMI levels in those crystals expressed relative to the $\varepsilon_x = 0$ of the individual crystal will differ in magnitude. These points are illustrated in Fig. 27.

In Fig. 27 an energy diagram is shown that is applicable to a contact between a metallic conductor and an N type semiconductor. This contact is considered to be in thermodynamic equilibrium with no net current flowing across the boundary layer lying between the planes $A-A$ and $B-B$. These planes are taken sufficiently far inside of each of the conductors so that the presence of the boundary does not influence the random currents within the interiors of the two conductors. In the metal, the FERMI level μ_1 is positive, whereas in the semiconductor its value is negative. The algebraic difference between these FERMI levels is equal to the sum of their absolute values and measures the displacement in energy of the reference levels at the bottoms of each of the conduction bands. Since no conduction takes place in the semiconductor below the level designated as $\varepsilon_{x2} = 0$, all electrons that impinge on the boundary $A-A$ as they move from left to right will be totally reflected without changing energies at the boundary potential and will return into the metal. Thus the net current over this energy band remains zero, in spite of the fact that there is no corresponding current in the semiconductor. The electrons which move from left to right across $A-A$ with energy well above the motive maximum shown in the diagram will pass directly across the boundary layer and enter the semiconductor at its boundary $B-B$. In order to maintain zero net current across these boundaries an exactly equal number of electrons must return from the semiconductor into the metal no matter how complex the energy band structure of either the semiconductor or the metal may be. For that electron group which has energy within the metal greater than $\Delta\varepsilon$ (shown in the figure) and less than that corresponding to the maximum in the motive shown between A and B, there will be a partial transmission from the metal into the semiconductor. Exactly the same reflection and transmission properties must be assigned to this barrier for the electrons which approach from right to left within the semiconductor. It follows that the random current in both the metal and the semiconductor, even in this energy band of incomplete transmission, must be exactly the same and may be computed by the introduction of the correct values of the FERMI level relative to the zero energy state in the individual conductor by Eq. (64.1).

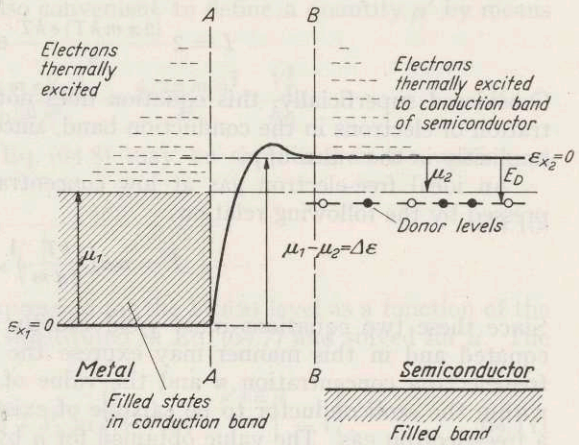

Fig. 27. A contact between a semiconductor and a metal.

This discussion concerning the universality of the random current found in all conductors gives the basic condition upon which the simplifications needed, to avoid the impossible problem of working it out exactly as it would apply to a practical oxide-coated, rests. The exact method would demand a detailed examination of the distribution in quantum states that would come from a wave-mechanical analysis.

Subject only to the restriction that there are no forbidden bands in the energy-level system above $\varepsilon_x = 0$, the random current density in any conductor is given by the following formula:

$$I = 2\frac{(2\pi m kT)\, e}{h^3} kT \int_{\varepsilon_x=0}^{\infty} \frac{\ln\left(1 - e^{-\frac{\varepsilon_x - \mu}{kT}}\right)}{kT} d\varepsilon_x. \tag{64.2}$$

In all cases of importance to thermionic emission from semiconductors, μ is negative and its absolute value is large compared with kT. Under these circumstances, the exponential part of Eq. (64.2) is small in comparison with unity over the entire range of ε_x from zero to infinity. This fact permits the integration of Eq. (64.2) to give the following result:

$$I = 2\frac{(2\pi m kT)\, e\, kT}{h^3} e^{\frac{\mu}{kT}}. \tag{64.3}$$

Considered superficially, this equation does not appear to contain the concentration of electrons in the conduction band, since the concentration appears only implicitly in the value of μ.

An ideal free-electron gas at low concentration has a random current expressed by the following relation:

$$I = n e \left(\frac{kT}{2\pi m}\right)^{\frac{1}{2}}. \tag{64.4}$$

Since these two equations must yield exactly the same current, they may be equated and in this manner may express the functional relation between the free-electron concentration n and the value of μ required for the electron gas within the semiconductor to be capable of existing in thermal equilibrium with a free-electron gas. The value obtained for μ by this procedure is the following:

$$\mu = -kT \ln \frac{2(2\pi m kT)^{\frac{3}{2}}}{n h^3}. \tag{64.5}$$

In an "N" type semiconductor, the number of electrons which make transitions from the filled valence band into the conduction band at the temperatures encountered with oxide cathodes is so small in comparison with those which transfer from the donor levels to the conduction band that only the latter need to be considered. Since the FERMI factor [Eq. (15.1)] expresses the probability that an electronic state will be occupied, the following equation will give the concentration of electrons as a function of the temperature, the donor concentration, and the energy level of the donors expressed relative to the conduction band reference at $\varepsilon_x = 0$

$$n = n_D\left(1 - \frac{1}{e^{\frac{E-\mu}{kT}} + 1}\right) = \frac{n_D}{1 + e^{-\frac{E-\mu}{kT}}}. \tag{64.6}$$

This equation may also be solved for μ to obtain the following results:

$$e^{-\frac{\mu}{kT}} = \frac{e^{-\frac{E}{kT}}}{\left(\frac{n_D}{n} - 1\right)}. \tag{64.7}$$

Eq. (64.5) and (64.7) may be combined to obtain an explicit expression for the electron concentration as a function only of the temperature for a given

donor density (n_D) located in a level at E with respect to the bottom of the conduction band. The equation obtained without the introduction of any approximation is the following:

$$n = \frac{2n_D}{1 + \left[1 + \frac{2n_D h^3 \, e^{-\frac{E}{kT}}}{(2\pi m k T)^{\frac{3}{2}}}\right]^{\frac{1}{2}}}. \tag{64.8}$$

For the purposes for which these theories are being developed the approximate forms of this equation[1] are not suitable.

Eq. (64.8) may be put into a more useful form for the purpose of computation by expressing the energy E in electrons volts. At the same time one may use to advantage the electron-volt equivalent of the temperature expressed here as V_T defined by Eq. (46.9). It is also convenient to define a quantity μ' by means of the relation shown as:

$$e^{\frac{\mu'}{V_T}} = \frac{2(2\pi m e V_T)^{\frac{3}{2}}}{(n_D/2) h^3} = \frac{4(2\pi m e)^{\frac{3}{2}}}{h^3} \cdot \frac{V_T^{\frac{3}{2}}}{n_D}. \tag{64.9}$$

With the above substitutions, Eq. (64.8) may be simplified in its writing as follows:

$$n = \frac{2n_D}{1 + \left[1 + 8\, e^{-\frac{\mu' + E}{V_T}}\right]^{\frac{1}{2}}}. \tag{64.10}$$

In order to obtain a direct expression for the FERMI level as a function of the temperature, Eq. (64.10) can be substituted in Eq. (64.7) and solved for μ. The result is given as follows:

$$\mu = E - V_T \ln 2 + V_T \ln \left\{\left[1 + 8 e^{-\frac{\mu' + E}{V_T}}\right]^{\frac{1}{2}} - 1\right\}. \tag{64.11}$$

The first step in the quantitative use of this equation involves the computation of μ'. Constants in Eq. (64.9) have been combined to permit the easy calculation of μ' by the following relation:

$$\mu' = V_T \left[\ln \frac{1.208 \times 10^{28}}{n_D} - \frac{3}{2} \ln V_T^{-1}\right]. \tag{64.12}$$

In order to assist in the use of these equations, values of the various functions presented here are given in Table 11 for a wide range of values of n_D and E. A very important equation is that for the temperature coefficient of the FERMI level which is given by the differentiation of Eq. (64.11) with respect to V_T. The result of this differentiation is the following:

$$\frac{d\mu}{dV_T} = \frac{\mu - E}{V_T} - \frac{\left(\frac{3}{2} - \frac{E}{V_T}\right) 8 e^{-\frac{\mu' + E}{V_T}}}{2\left[\left(1 + 8 e^{-\frac{\mu' + E}{V_T}}\right)^{\frac{1}{2}} - 1\right]\left[1 + 8 e^{-\frac{\mu' + E}{V_T}}\right]^{\frac{1}{2}}}. \tag{64.13}$$

In reviewing these equations, practically the only assumption which has been made is that the numerical value of $|\mu/V_T|$ be approximately 5 or more.

To satisfy this condition without at the same time having a very small concentration of donor states, the value of (E/V_T) must be of the order of 10. If the value of μ' as computed by Eq. (64.12) can be related to the temperature and

[1] F. SEITZ: The Modern Theory of Solids, p. 188. New York: McGraw-Hill 1948.

be found to give (μ'/V_T) a value greater than 5, then E may have practically any value and the requirement that $|\mu/V_T|$ be greater than 5 will be satisfied.

The combination of symbols described in the following equation occurs so often in the use of all of the equations in this section that it will be used to define a quantity K as follows:

$$K^{-2} = 8e^{-\frac{\mu'+E}{V_T}}. \tag{64.14}$$

In this work, the principal application of Eq. (64.13) comes in the close relation to the temperature coefficient of the work-function. If the electron affinity W_a is practically independent of the temperature, then the temperature coefficient of the FERMI level is a direct measure of the temperature coefficient of the work-function.

This important phase of the basic theory of thermionic emission from oxide cathodes has received very little attention and yet it will be shown in later sections that by making a suitable choice of the donor density n_D and the associated energy E, excellent correlation is found between the temperature variation of the FERMI level and the temperature variation of the contact difference in potential. See Sect. 81 and 83. Eq. (64.13) can be adapted to permit a direct calculation of the temperature coefficient without the previous determination of the numerical value of the FERMI level. The equation written in this form is:

$$\frac{d\mu}{dV_T} = \frac{\ln 2}{2} - \frac{\mu'+E}{2V_T} + \ln\left[(K^2+1)^{\frac{1}{2}} - K\right] - \frac{\left(\frac{3}{2} - \frac{E}{V_T}\right)}{2\left[K^2+1-K(K^2+1)^{\frac{1}{2}}\right]}. \tag{64.15}$$

With this equation it is possible to write expressions for the extreme variation in the temperature coefficient of the FERMI level, since for very low temperatures K is very small, whereas for very high temperatures K is large. In the high-temperature range, for which the approximate expression gives very accurate results, the value of K should be 5 or more. The following equations result from this analysis:

High temperature range:

$$\frac{d\mu}{dV_T} \approx -\left(\frac{\mu'}{V_T} + \frac{3}{2} - \ln 2\right) = -\left(\frac{\mu'}{V_T} + 0.8069\right). \tag{64.16}$$

Low temperature range:

$$\frac{d\mu}{dV_T} \approx -\frac{1}{2}\left(\frac{\mu'}{V_T} + \frac{3}{2} - \ln 2\right) = -\frac{1}{2}\left(\frac{\mu'}{V_T} + 0.8069\right). \tag{64.17}$$

The significance of these two equations stands out strongly after the substitution is made from Eq. (64.12) for the definition of μ'. Again for the two ranges, equations may be written as follows:

High temperature range:

$$\frac{d\mu}{dV_T} \approx -\left[\ln\frac{1.208\times 10^{28}}{N_D} - \frac{3}{2}\ln(V_T^{-1}) + 0.8069\right]. \tag{64.18}$$

Low temperature range:

$$\frac{d\mu}{dV_T} \approx -\frac{1}{2}\left[\ln\frac{1.208\times 10^{28}}{N_D} - \frac{3}{2}\ln(V_T^{-1}) + 0.8069\right]. \tag{64.19}$$

The two main points of this result are: (1) the total range in the variation of the temperature coefficient of the FERMI level can be very little more than

a factor of two and (2) the temperature coefficient depends *only* on the concentration of donors and the temperature and is completely independent of the energy level from which the donors arrive. This latter result is of major significance as it relates to the emission properties of oxide cathodes and related semiconductor phenomena.

Various experiments on oxide cathodes which will be discussed in Sect. 81 and 83 indicate that the probable range in *average* temperature coefficient of the work-function as expressed in the units used in these equations lies between 5 and 9 for well-activated, normal oxide cathodes. Since the probable value of E is approximately 0.7 electron volts negative with respect to the bottom of the conduction band, the low temperature range requirement is satisfied with V_T approximately 0.05. With the donor concentration of 5×10^{22} donors per m.^{3}, the value of the temperature coefficient is 4.3. Since the average coefficient can be expected to be approximately 1.5 times greater, this calculation yields an average value of 6.5. An increase in donor concentration by factor of 10 would reduce the average coefficient to 4.2 and a decrease in concentration by a factor of 10 would increase the average coefficient to 8.8. The indication is that for normal oxide cathodes, the expected range of donor concentrations will be 5×10^{21} to 5×10^{23}. It remains to be shown, in the next section, that conductivity data can be used to advantage to estimate the location of the energy level to be associated with these donors.

FOWLER[1] derived an emission equation applicable to the "N-type" semiconductor under specifically limited conditions. Note, first, that the introduction of the BOLTZMANN relation in Eq. (64.3) yields the true RICHARDSON equation, which is Eq. (18.5) and is written here as follows:

$$I = 2 \frac{(2\pi m k T)\, e k T}{h^3} e^{-\frac{W_a - \mu}{kT}} . \tag{64.20}$$

In this equation, W_a is the electron affinity of the semiconductor and, under the conditions of special interest as they relate to oxide cathodes, μ is actually a negative number. The true work-function, which is $(W_a - \mu)$ is, therefore, the numerical sum of these two quantities. The equations given in this section show clearly that μ is a function of the temperature and, therefore, the true work-function will be very temperature dependent. It could be said that the purpose of the FOWLER equation is to take account of the temperature variation of the work-function in a more satisfactory manner than to assume that its average value will be a constant. Since his equation has often been used for the analysis of thermionic emission data, observed with the oxide cathode, it will be worthwhile to derive this formula to show very clearly the restrictions which the user should impose but sometimes does not[2].

An examination of Eq. (64.8) shows, that, under the conditions of a high donor concentration (n_D) and low temperatures, the concentration of electrons in the conduction band can be small in comparison with the number of donors. This condition holds when the principal term in the denominator is very large compared with unity. Under these conditions, the concentration of electrons in the conduction band may be expressed by the following equation:

$$n = n_D^{\frac{1}{2}} \frac{\sqrt{2}\,(2\pi m k T)^{\frac{3}{4}}}{h^{\frac{3}{2}}} e^{\frac{E}{2kT}} . \tag{64.21}$$

[1] R. H. FOWLER: Statistical Mechanics, 2nd edit., p. 402. Cambridge Univ. Press 1936.
[2] J. NAKAI, Y. INUISHI and Y. TSUNG-CHE: J. Phys. Soc. Japan **10**, 437 (1955).

This equation, when combined with the current Eq. (64.4), gives a good approximation for the random current that crosses any boundary within the interior of the semiconducting crystal. This random current, reduced by the BOLTZMANN factor $\exp(-W_a/kT)$, gives the current density in the immediate neighborhood of the crystal surface, when thermodynamic equilibrium applies. Again, there is the problem as to whether or not all electrons which impinge on the boundary from the interior enter the space outside the crystal. In order to include the possibility that some are reflected, the generalized transmission function first introduced in Eq. (26.1) and illustrated further by Eq. (26.4) will be introduced here in the final formulation of the FOWLER emission equation.

$$I = \overline{D(p, B)}\, n_D^{\frac{1}{2}} \left[\frac{e\sqrt{2}\,(2\pi m)^{\frac{1}{4}} k^{\frac{5}{2}}}{h^{\frac{9}{2}}}\right] T^{\frac{5}{4}} e^{-\frac{W_a-(E/2)}{kT}}. \tag{64.22}$$

The symbol $\overline{D(p, B)}$ is designed to call attention to the fact that the transmission will depend on the electron energy and the barrier itself. An example will shown of the use of this equation in Sect. 81 and 83. In order to assist in computation, the universal constant included in the brackets is evaluated as follows:

$$\frac{e\sqrt{2}\,(2\pi m)^{\frac{1}{4}} k^{\frac{5}{2}}}{h^{\frac{9}{2}}} = 1.726\times 10^{-5}. \tag{64.23}$$

The units are such that, if the donor concentration is expressed in the number per m.^{3} and the temperature given on the KELVIN scale, then the current density will be expressed in amp/m^2.

Although Eq. (64.22) can be used as an empirical equation in exactly the same manner as the RICHARDSON form of equation, its most useful purpose is that of determining an estimated value of the donor concentration. Assume that it is possible to measure experimentally the zero-field thermionic emission current density from a semiconducting surface such as an oxide-coated cathode and construct a plot of $\log_{10}(I/T^{\frac{5}{4}})$ as a function of $(1/T)$. The slope of such an experimentally obtained curve will determine $(W_a - 0.5E)$. It should be clear from the method by which this equation was derived that this quantity really represents the true work-function at absolute zero. The true work-function is of course temperature-dependent and the negative of the temperature coefficient is given by Eq. (64.19). It is assumed that the temperature coefficient of the electron affinity W_a is negligible. After the FOWLER emission plot has been constructed as described above and the slope determined, any point on the plot will serve to determine the value of the numerical constant defined as follows:

$$A_F = 1.726\times 10^{-5}\, \overline{D(p, B)}\, n_D^{\frac{1}{2}}. \tag{64.24}$$

An experimentally determined value (Sect. 81) for the empirical constant A_F is 1.5×10^5 or, if the current is expressed in amp/cm.^{2}, the number is 15 amp per cm$^2\cdot$ deg$^{\frac{5}{4}}$. With a value of $\overline{D}$ of 0.175 (which is not unlikely for the very low temperature range) the donor density n_D is 2.4×10^{21} per m^3. The very accurate data of HUNG are used for this analysis in Sect. 81 and there the reflection effect is introduced as indicated in Eq. (62.11) *before* the plot is made according to Eq. (64.22). The equation form then becomes:

$$I_{00} = 1.726\times 10^{-5}\, n^{\frac{1}{2}} T^{\frac{5}{4}} e^{-\frac{(W_a-(E/2))}{kT}}. \tag{64.25}$$

The FOWLER work-function is given by:

$$\varphi_F = \frac{(W_a - (E/2))}{e}. \tag{64.26}$$

65. Conduction processes in porous semiconductors. LOOSJES and VINK[1] were among the first to call specific attention to the need for a detailed analysis of conduction processes in porous semiconductors to serve as step toward the better understanding of thermionic emission phenomena from oxide cathodes. This section will deal with basic concepts needed for the interpretation of conductivity data applicable to polycrystalline semiconductors.

Practically all experiments show that at very low field strength the conduction current is directly proportional to the average electric field within the test specimen. The basic condition which must be satisfied is that *the energy gained on the average by the electrons between inelastic collisions must be small compared with their thermal energy expressed as kT*. The force acting on an electron in the presence of a field can be expressed as the product (eE_x) and the matter of the sign of the field in relation to the sign of the charge carrier can be omitted for the time being. The average change in momentum is then the force multiplied by the average time between inelastic collisions. This relation is expressed as follows:

$$\overline{\Delta p_x} = e E_x \bar{\tau}. \tag{65.1}$$

If the electron concentration is n and the effective mass that of a free electron, the conductivity may be expressed as follows:

$$\sigma = \frac{\overline{\Delta p_x}}{m E_x} e n = \frac{e \bar{\tau}}{m} e n. \tag{65.2}$$

The factor $(e\bar{\tau}/m)$ is the electron mobility which will be identified as M_s for the electron mobility within the solid structure and as M_p for the electron mobility in the porous structure. These definitions expressed in equation form are the following:

For crystalline structure:

$$M_s = \frac{e \bar{\tau}_s}{m}. \tag{65.3}$$

For pore conduction:

$$M_p = \frac{e \bar{\tau}_p}{m}. \tag{65.4}$$

Studies of the conductivity of oxide-coating material as a function of the temperature and the previous history (which would include activation processes) serve as the best means of gaining information concerning the conduction mechanism. LOOSJES and VINK have identified three ranges in temperature, two of which are associated with the conductivity of the free electrons in the pores of the porous structure. The third is dominated by the conduction through the solid. These two conduction mechanisms may be thought of as parallel conductors. Eq. (65.2) is suitable for the computation of each and depends on a knowledge of the electron concentration n and the average time between inelastic collisions $\bar{\tau}$. These two quantities will differ many orders of magnitude depending on whether one is dealing with the conduction in the solid or in the pore. The theoretical background for these two cases will be presented very briefly in this section. Conductivity in the crystalline structure will be discussed first.

Since Eq. (64.8) or (64.10) may be relied upon for the calculation of the electron density in an N-type semiconductor as a function of temperature, it remains only to discuss $\bar{\tau}_s$ to establish the conductivity characteristic. The use

[1] R. LOOSJES and H. J. VINK: Philips Res. Rep. **4**, 449 (1949).

of either classical or FERMI statistics, as it applies to a free electron concentration of low density, permits one to write an expression for the average speed of electrons in an electron distribution characterized by a specific temperature. The expression for the average speed is the following:

$$\bar{v} = 4\left(\frac{kT}{2\pi m}\right)^{\frac{1}{2}}. \tag{65.5}$$

One of the factors that must enter into the calculation of the time between inelastic collisions is the average speed of the electrons and the time should be inversely proportional to the speed. A second factor which must enter is the distance between collision centers and its dependence on temperature. At the relatively high temperature associated with thermionic emission there can be little doubt that the thermal vibration of the molecules of the structure sets up a disorder of the potential function through which the electrons travel in their random motions. Therefore the average distance of "free flight" must decrease as the temperature increases. Even if quantum mechanics could be applied to solve this problem of the lattice scattering of the electron waves for a pure barium oxide crystal, it is doubtful that the solution would apply more than approximately to the barium-strontium-oxide crystals employed in all thermionic emitters of this classification. One may assume, therefore, for the purposes of the present discussion, that the average "free flight" distance in the solid structure is inversely proportional to the temperature and that an experimental determination of the electron mobility will be depended upon to determine the order of magnitude of the proportionality constant and, in turn, the approximate distance between scattering points. With these assumptions the following equation may be written:

$$\tau_s = \frac{l_s}{\bar{v}} = \frac{l_{s0}\,T_0}{T} \cdot \frac{1}{4} \cdot \left(\frac{2\pi m}{kT}\right)^{\frac{1}{2}}. \tag{65.6}$$

In this equation the proportionality constant is written as $(l_{s0}\,T_0)$ with l_{s0} the average free flight distance at some low temperature T_0 above which it is assumed that the free flight distance is inversely proportional to the temperature. Eq. (65.6) may be combined with Eq. (65.3) to obtain the following expression for the mobility:

$$M_s = \left(\frac{\pi e}{8m}\right)^{\frac{1}{2}} l_{s0}\,\frac{V_{T0}}{V_T^{\frac{3}{2}}} = 2.63\times 10^5\,\frac{V_{T0}}{V_T^{\frac{3}{2}}}\cdot l_{s0}. \tag{65.7}$$

The equation has been put in the above form in order to make it ready for easy numerical calculation. Rather than assume a value of l_{s0} it is of more direct interest to take the value for the mobility given by PELL[1] for electrons in barium-oxide single-crystals which was 5×10^{-4} m.^{2} per v-sec. If it is assumed that this value is appropriate at a temperature V_{T0} of 0.04 (464° K) and the value of l_{s0} is computed it is 3.8×10^{-10} m. Calculations based on the molecular weight and density figures for barium and strontium oxide lead to the conclusion that this distance is exactly equal to the average molecular distance in the solid. If one considers the high temperature at which this mobility measurement was made and the fact that it could very well have been twice as great since there was considerable uncertainty in the exact value to be chosen, the fact that the free flight distance in an ionic crystal is equal to one or two intermolecular distances seems altogether reasonable and justifies the use of Eq. (65.7). With the introduction of these numbers, one obtains a mobility equation which follows:

$$M_s = \frac{4\times 10^{-6}}{V_T^{\frac{3}{2}}}\ \text{m.}^2/\text{v-sec}. \tag{65.8}$$

[1] E. M. PELL: Phys. Rev. **87**, 457 (1952).

This expression for the mobility of electrons in a barium-strontium oxide crystal may be combined as in Eq. (65.2) with the expression for electron density as a function of the temperature given in Eq. (64.10) to express the conductivity of typical crystals used in oxide cathodes so that the prediction of the equation can be compared with experiment and in that manner an appropriate value for the donor energy level E can be derived. The equation so derived is the following:

$$\sigma = \frac{1.82 \times 10^{-24} C_s n_D V_T^{-\frac{3}{2}}}{1 + \left[1 + 8\, e^{-\frac{(\mu' + E)}{V_T}}\right]}. \tag{65.9}$$

The constant C_s is introduced to correct for the fact that a porous structure will have a smaller conduction cross section than the same volume of solid crystalline material.

The usual experimental procedure is to plot the logarithm of the conductivity σ as a function of $(1/V_T)$ and use the average slope of this plotted curve as a measure of the "activation energy". The value of E is then often taken as twice the activation energy. The analysis to follow shows that, although this procedure is approximately correct, it is necessary to analyze the results more critically if accuracy is desired.

A quantity K has been defined by Eq. (64.14) and the evaluation of this number indicated that K is generally small for the range of temperature, electron concentration, and energy level E of greatest interest in thermionic emission. With this restriction, Eq. (65.9) may be written as follows:

$$\sigma = \frac{1.82 \times 10^{-24} C_s n_D V_T^{-\frac{3}{4}} K}{1 + K}. \tag{65.10}$$

This equation may be modified still further by the introduction of the value of K as expressed in Eq. (64.14) into the numerator of the above equation and the conductivity relation becomes the following:

$$\sigma = \frac{7.07 \times 10^{-11} C_s n_D^{\frac{1}{2}} V_T^{-\frac{3}{4}} e^{\frac{E}{2V_T}}}{1 + K}. \tag{65.11}$$

The main purpose of measuring the conductivity of an oxide cathode as a function of the temperature is to evaluate the effective energy difference E between the bottom of the conduction band and the energy levels occupied by the donors. It should be clear from the above equation that this can be accomplished best by plotting $\ln(\sigma V_T^{\frac{3}{4}})$ as a function of $(1/V_T)$. The form of the equation is the following:

$$\ln(\sigma V_T^{\frac{3}{4}}) = \ln(7.07 \times 10^{-10} C_s n_D^{\frac{1}{2}}) + \frac{E}{2} V_T^{-1} - K. \tag{65.12}$$

This equation makes use of the fact that the value of K is small. The slope of the straight line obtained from this plot should give the best obtainable value for $(E/2)$, since the temperature variation of K is very small in comparison with $(E/2)$.

In most examples given in the literature, it is the activation energy that has been evaluated and this has been defined by the following relation:

$$\frac{d(\ln \sigma)}{d(V_T^{-1})} = E_a. \tag{65.13}$$

By the direct differentiation of Eq. (65.9) one obtains the complete expression for the activation energy which is clearly not independent of the temperature, as the following analysis will show:

$$E_a = \frac{3}{2} V_T - \frac{\frac{3}{2} V_T - E}{2(K^2+1)^{\frac{1}{2}} \left[K + (K^2+1)^{\frac{1}{2}}\right]}. \tag{65.14}$$

Since the principal range of interest is that for which K^2 is very small in comparison with unity, this equation may be simplified as follows:

$$E_a = \frac{E}{2} + \frac{3}{4} V_T - \left(\frac{E}{2} - \frac{3}{4} V_T\right) K. \tag{65.15}$$

In general, the last term of this equation is very small and, therefore, within the accuracy of most available measurements, an improved value for the true energy of the donor state would be given in terms of the activation energy E_a by the following equation:

$$E = 2E_a - \tfrac{3}{2} V_T. \tag{65.16}$$

The range in activation energy reported in the literature and discussed in Sect. 77 lies between -0.25 and -0.4 ev., with some dependence on the state of activation of the test specimen. The only activation energies that are appropriate for comparison with this theory are those taken over such a low temperature range that the electron conductivity through the pores contributes a negligible proportion of the total conductivity of the specimen. An average value of V_T for this low temperature range is 0.05. Eq. (65.16) shows that if the activation energy E_a is -0.31 the effective location of the donor state will be at 0.7 ev below the bottom of the conduction band.

With a very densely packed crystalline structure, the constant C_s of Eq. (65.9) could presumably approach the value of 1.0. Since the equations as they have been developed apply to the conductivity of single crystals, they do not take into account the fact that in a practical oxide cathode less than 50% of the superficial cross section is occupied by crystals. Furthermore, these crystals make contact at very small surface areas compared with the crystal cross section. It is practically impossible to generalize, therefore, about the best choice of C_s to fit a specific test specimen which will permit a direct comparison between theory and experiment. Under the circumstances, the best procedure is to evaluate the energy E which measures the location of the donor levels by means of the temperature variation in the conductivity over the low temperature range, as has been described in this section. The best means of determining the most suitable concentration of donors has been demonstrated in a previous section to depend on a measurement of the temperature coefficient of the contact difference in potential, which in turn, is the negative of the temperature coefficient of the true work-function. With the donor density and the energy level known, observations of the conductivity analyzed according to Eq. (65.9) yield a direct value for C_s. Again, the published material for comparison with theory is very meager, but the indications are that a value of C_s of the order of 0.05 to 0.1 is needed to be consistent with experimental values unless the mobility of the electrons in the single crystals of barium-strontium oxide is smaller than the PELL[1] value of 5×10^{-4} m.^{2} per v-sec. Since a choice of C_s within the range described here seeems reasonable, confidence should be placed in these equations and in this analysis until better data become available to justify the development of an alternative theoretical analysis.

[1] E. M. PELL: Phys. Rev. **87**, 457 (1952).

The conductivity of the open structure between the particles of an oxide cathode will become more and more important as the temperature increases. The theory to be developed in the following paragraphs shows that the conduction through the pores will be directly proportional to the electric field within the porous structure provided that the energy gained from the field in the time of one free flight of the electron across the pore is small compared with the thermal energy V_T (or kT). The analysis will show that at very high field strength comparable to that associated with pulse emission studies, the conduction will increase as the square root of the field as LOOSJES and VINK[1] have shown experimentally. The conductivity in the pore will be given by Eq. (65.2) in which the density of the electrons within the pore will be relatively uniform over the lower temperature range but will become non-uniform in a manner that can best be evaluated by the theory presented here in Sect. 21 to 24, inclusive. This development of space charge within the pore influences both the determination of $\bar{\tau}_p$ and the value of electron density n. These factors control the conductivity-temperature function in the high-temperature range, and it will be different from the function followed over the low-temperature range of pore conductivity. These phenomena account very satisfactorily for the two high-temperature ranges in conductivity first reported by HANNAY, MACNAIR, and WHITE[2] and identified by LOOSJES and VINK as ranges II and III.

In the application of Eq. (65.2) to the conductivity of the pores, the computation of the average time of flight of an electron will depend mainly on the electron speed and the effective path length for the low-field condition. As the intensity of the electric field increases, the energy gained by an electron in one free flight across the pore can eventually exceed its temperature energy under which condition the time of flight is greatly shortened and is field-dependent. It is only necessary to formulate the problem for these two extremes, if one realizes that between these extremes the average time of flight can take on any intermediate value.

If the temperature range is that in which pore conduction predominates and measurement shows that the current is directly proportional to the field, sufficient indication is given that the energy gained per free flight is small enough in comparison to the thermal energy and that the time of flight computed by the following equation is the proper choice.

$$\bar{\tau}_{p\,\mathrm{II}} = \left(\frac{\pi m}{8e}\right)^{\frac{1}{2}} \frac{l_p}{V_T^{\frac{1}{2}}}. \tag{65.17}$$

In this equation, the number II is applied as a subscript on $\bar{\tau}_p$ to indicate that this equation applies over the temperature below approximately 0.09 ev equivalent (1044° K). In this equation l_p corresponds to the free-flight distance averaged over all of the electron trajectories within the pore. This free-flight distance is, in general, smaller than the average dimension of the pore but is the same order of magnitude. For example, if the pore were spherical, then l_p would be approximately 64% of the diameter. The relation given in Eq. (65.17) can be used to calculate the mobility for this low-field condition and the result is given as follows:

$$M_{p\,\mathrm{II}} = \left(\frac{\pi e}{8m}\right)^{\frac{1}{2}} \frac{l_p}{V_T^{\frac{1}{2}}} = 2.63 \times 10^5 \frac{l_p}{V_T^{\frac{1}{2}}}. \tag{65.18}$$

[1] R. LOOSJES and H. J. VINK: Philips Res. Rep. **4**, 449 (1949).
[2] N. B. HAANNAY, D. MACNAIR and A. H. WHITE: J. Appl. Phys. **20**, 669 (1949).

This equation combined with the evaluation of the electron density gives the conductivity of the pore

$$\sigma_{p\,\mathrm{II}} = n_0\, e \left(\frac{\pi e}{8m}\right)^{\frac{1}{2}} \frac{l_p}{V_T^{\frac{1}{2}}} = 4.21\times 10^{-14}\, n_0 \frac{l_p}{V_T^{\frac{1}{2}}}. \tag{65.19}$$

Eq. (24.7) is the most suitable one for the computation of the electron density in the immediate neighborhood of the surface boundary of the pore. This equation, with the universal constants evaluated, and the temperature expressed in its electron-volt equivalent, is the following:

$$n_s = 6.04\times 10^{27}\, V_T^{\frac{3}{2}}\, \mathrm{e}^{-\frac{\varphi}{V_T}}. \tag{65.20}$$

In this equation, the symbol φ represents the *true work-function*. The true work-function depends to some extent on the state of activation, principally through the alteration of its average temperature coefficient which decreases as the concentration of donors increases. A formula which applies as a satisfactory approximation for a limited range in temperature for a well-activated oxide cathode is the following:

$$\varphi = \varphi_0 + \alpha V_T. \tag{65.21}$$

For these oxide cathodes the range in φ_0 is 0.9 to 1.2 and for α it is 5 to 9.

Over the range of conductivity characteristic below 1000° K the pore concentration of electrons n_0 is practically equal to the electron concentration at the surface of the pore. The temperature at which there is an appreciable difference between these concentrations depends on the pore size and can be determined quite well by the theory presented in Sect. 24. There the space charge relations were computed for a pillbox like pore with the small dimension w between parallel planes. Qualitative considerations indicate that the use of l_p, which is defined as the *effective* average distance of free flight within the pore, is the equivalent to the use of w in Eq. (24.4). With this condition considered, the following equation gives the maximum density of electrons which one can expect in the central region of a pore of this size:

$$n_{0\,m} = 1.09\times 10^{9} \frac{V_T}{l_p^2}. \tag{65.22}$$

The actual density n_0 in the central region of a pore the boundaries of which are characterized by a definite value of the true work-function is related to this maximum possible value for the density through the parameter z expressed by:

$$n_0 = n_{0\,m}\, z^2. \tag{65.23}$$

Since both n_s and $n_{0\,m}$ can be computed from a knowledge of the temperature, the pore size, and the true work-function, the expression given as Eq. (24.6) permits the direct evaluation of z^2 from the ratio of these two concentrations with the help of Table 4 or of the curve shown as Fig. 9. Since the main purpose of this calculation is to estimate the upper limit for the temperature range identified by II, Eq. (24.9) serves as a satisfactory means of computing z, since it is only for z values less than 0.1 that n_0 and n_s are essentially equal. Eq. (24.5) shows that the reduction in concentration at the center of the pore under this condition is 2.5%. Since n_s increases very rapidly with the temperature after this particular temperature has been reached, the transition from conduction region II to III is quite sharp. With this value of z as the arbitrary criterion for the determination of the transition temperature, the following relation may be written:

$$1.8\times 10^{-21} = l_p^2\, V_T^{\frac{1}{2}}\, \mathrm{e}^{-\frac{\varphi}{V_T}}. \tag{65.24}$$

If the characteristic pore dimension l_p is 2.5×10^{-6} m. (2.5 microns), this equation is satisfied at the value of V_T of 0.0833 (970° K). This calculation is mentioned at this point to indicate that the above equation is in excellent agreement with the temperature limit that marks the separation between regions II and III found by LOOSJES and VINK. The variation of the critical temperature with activation will be discussed in Sect. 77.

The introduction of Eq. (65.20) into Eq. (65.19) completes the calculation of the expression for the pore conductivity as a function of the pore dimension, the temperature, and the true work-function for that range of temperature which lies within range II:

$$\sigma_{p\,\mathrm{II}} = 2.54 \times 10^{14} V_T \, \mathrm{e}^{-\frac{\varphi}{V_T}} l_p . \tag{65.25}$$

If the true work-function is known only through its approximate representation given as Eq. (65.21), then:

$$\sigma_{p\,\mathrm{II}} = 2.54 \times 10^{14} \, \mathrm{e}^{-\alpha} V_T \, \mathrm{e}^{-\frac{\varphi_0}{V_T}} l_p . \tag{65.26}$$

A plot of $\ln \sigma_{p\,\mathrm{II}}$ as a function of V_T^{-1} yields an activation energy Φ_σ which is related to φ_0 by Eq. (50.11) which yields:

$$\varphi_0 = \Phi_\sigma - \frac{V_n + V_m}{2} \tag{65.27}$$

in which V_n and V_m are the voltage equivalents of the maximum and minimum temperatures of range II.

Although Eq. (65.25) represents the conductivity of a pore of characteristic dimension l_p, the quantity usually measured is the conduction per unit area, as exemplified by the researches of LOOSJES and VINK. The following equation serves to describe this function in which g is the conduction of a specimen of thickness L over which a potential difference of V is applied:

$$\frac{g}{A} = 2.54 \times 10^{14} \frac{V}{L} C_p V_T \, \mathrm{e}^{-\frac{\varphi}{V_T}} l_p . \tag{65.28}$$

Two additional symbols are introduced in this equation, which are A, for the area, and C_p, for a constant introduced in this equation to account for some of the structural factors similar to those considered, just as the corresponding constant, C_s, was introduced in Eq. (65.9). Before this theoretical equation is compared with experimental results, an estimate must be made for the value of C_p. The higher the degree of porosity, the greater the value of C_p. Even though the known porosity might be 50%, the choice of a value of 0.5 would be too large for two reasons. First, the conduction through the pores will follow a devious route, even though it might be direct from pore to pore. Second, some conduction will be through solid structure in series with the pores. This resistance will reduce the conduction. It is estimated, therefore, that the value of C_p to be used for comparison with experiment should be 0.1 to 0.4 for the usual coating structure.

A question may be raised as to why Eq. (65.20) is used for the electron density instead of Eq. (64.21), since it was the latter that led to the FOWLER equation for thermionic emission. The latter formula is not appropriate, even though it was used by NAKAI, INUISHI and TSUNG-CHE[1]. The purpose of Sect. 64 was to show that the temperature variation of the FERMI level could be incorporated n the theory of the FOWLER emission equation under the restriction that the

[1] J. NAKAI, Y. INUISHI and Y. TSUNG-CHE: J. Phys. Soc. Japan **10**, 437 (1955).

range of temperature for which it is applied be sufficiently low. The simplified equation used as a substitute for the exact equation, namely, Eq. (64.10), is thus limited in its range of application. It is therefore more appropriate to use Eq. (65.20), even though it involves the true work-function and this, in turn, may have to be represented by its approximate form given as Eq. (65.21).

66. Conductivity with high internal field strength. Experiments have been carried out by LOOSJES and VINK[1] and by others[2] in which sufficiently high fields were applied to an oxide coating to pass beyond the linear part of the conduction characteristic. The first deviation in the linearity should appear when the energy gained from the field is comparable with the temperature energy V_T or (kT). The experiments of LOOSJES and VINK show that, in the lower temperature range which is still high enough so that pore conductivity may be separated from crystal conductivity, the conduction current is proportional to the square root of the total voltage applied across the specimen. The following equation indicates the conditions under which this result may be anticipated.

$$\left(\frac{e E_x l_p}{2 m \lambda l_p}\right) \tau^2 + \left(\frac{8 e V_T}{\pi m l_p^2}\right)^{\frac{1}{2}} \tau = 1 . \tag{66.1}$$

An explanation of this equation will be given. The average time of flight τ enters the quadratic equation in two terms. The first term relates to the energy acquired by an electron in traveling a distance λ in the presence of a field of electric intensity E_x. A suitable value for λ will be close to one half of the characteristic pore dimension defined in the previous section and represented by l_p.

The second term comes from the average thermal speed, as in Eq. (65.17). Two extremes may be considered, depending on the value of $(E_x l_p)$. In the low-field range for which the first term of this equation is very small, the free-flight time may be computed by the second term to obtain the result already given as Eq. (65.17). As E_x increases, the solution to the quadratic equation above gives an ever decreasing value of the flight time τ, and more and more importance must be attached to the first term of this equation. Finally, when it becomes large compared to the second term, the average flight time τ_E becomes:

$$\tau_E = \left(\frac{2 m \lambda}{e E_x}\right)^{\frac{1}{2}} = \left(\frac{2 m \lambda l_p}{e V_p}\right)^{\frac{1}{2}} . \tag{66.2}$$

Here, V_p is the drop in potential over a single "effective" pore distance. Note that the flight time is inversely proportional to $E_x^{\frac{1}{2}}$ (or $V_p^{\frac{1}{2}}$) and proportional to a characteristic distance $(l_p \lambda)^{\frac{1}{2}}$. At moderately low temperatures, this distance should be approximately 0.4 of the average pore dimension. As the temperature increases and/or the field increases, additional complications enter into the computation of the flight time and the conduction equation.

Assume first that the field is not quite strong enough to wipe out all of the effects of space charge, but nearly sufficient to do so. Under this condition, Eq. (65.2) may be combined with Eq. (65.20) to yield an equation for the pore conduction per unit area with a moderately strong field and not too high a temperature. The result is the following:

$$\frac{g}{A} = 5.75 \times 10^{14} C_p \lambda^{\frac{1}{2}} \left(\frac{V}{L}\right)^{\frac{1}{2}} V_T^{\frac{3}{2}} e^{-\frac{\varphi}{V_T}} . \tag{66.3}$$

This equation is similar in many respects to that given as Eq. (65.28) and is the one most suitable for comparison with experiment, as will be shown in Sect. 77.

[1] R. LOOSJES and H. J. VINK: Philips Res. Rep. **4**, 449 (1949).
[2] See footnote 1, p. 91.

The conduction per unit area is g/A for an applied voltage difference of V over a specimen of thickness L. Thus, the average field within the specimen is V/L. The quantity C_p must be estimated, since it depends on the actual physical structure of the specimen investigated. In general, the porosity of practical cathodes is close to 0.5, although somewhat smaller and larger values than this have often been studied. As in the previous section, it is indicated that the conduction through pores may follow devious routes and in some circumstances may even have to be considered to be in series with a very small thickness of the solid structure. The crystalline solid has a higher resistance and therefore interferes slightly with the conduction attributed to the pores alone. These considerations lead to the establishment of a probable range for C_p of 0.1 to 0.4. Applications will be made of this equation in the discussion of experiments with oxide cathodes given in Sect. 84.

An inspection of Eq. (66.1) shows that the maximum value of the time of free flight is associated with the lowest value of the internal field. As the field increases, the first term of the equation becomes more and more important until it finally dominates, under which condition the time of free flight is inversely proportional to the square root of the field. At some particular field, the two terms will contribute equally, that is, the value of each will be exactly 0.5. The relation between the field and the temperature for this special circumstance is given in the following equation:

$$\frac{E_x l_p}{V_T} = \frac{V_p}{V_T} = \frac{8}{\pi}\frac{\lambda}{l_p} \approx 1.3 . \tag{66.4}$$

In this equation, the product $(E_x l_p)$ is the potential drop over a characteristic pore length and is symbolized by V_p. Since electrons enter the pore at various positions along its x direction, the distance λ should be approximately one half of the characteristic distance l_p. Subject to this assumption, a numerical value of the ratio is approximately 1.3. It follows, therefore, that if the potential V_p is just 1.3 V_T, then the conduction will be exactly half of that calculated by Eq. (65.28). Again, inspection of Eq. (66.1) shows that under this condition of (V_p/V_T) of 1.3, the conduction will be 70% of that calculated by Eq. (66.3). The fact that this analysis of the variations in conduction with field is in good agreement with the experiments of Loosjes and Vink will be shown in Sect. 77.

Implicit in the derivation of Eq. (66.3) was the assumption that the concentration of electrons in the immediate neighborhood of the pore surface at which they enter will be independent of the electric intensity superimposed on the space within the pore. This condition is satisfied if the emission current into the pore is limited by the space-charge within it. As the field is increased, space-charge limitations will gradually be removed and the supply of electrons needed to maintain the anticipated current density will be too small. If the only influence of the field were that of shortening the transit time as indicated in Eq. (66.2), then the conductivity would be inversely proportional to the square root of the field and the conduction directly proportional to $E_x^{\frac{1}{2}}$. After the supply of available electrons decreases, a "saturation" effect will set in gradually and the conduction will rise even less rapidly than is indicated by Eq. (66.3). Nakai, Inuishi and Tsung-che[1] attributed the lack of complete saturation of the conduction current to a lowering of the work-function on the interior of the pore surface by the Schottky effect (see Sect. 27). The application of this theory depends on the assumption that the emission increase results *only* from the cancellation of mirror-image forces by the external field. The total lack of uni-

[1] J. Nakai, Y. Inuishi and Y. Tsung-che: J. Phys. Soc. Japan **10**, 437 (1955).

formity of field over the surface of the interior of the pore makes this assumption inappropriate. More details concerning these experiments will be given in Sect. 79.

The application of these equations to the interpretation of the experiments of LOOSJES and VINK yields a value of the characteristic pore length of 2.8×10^{-6} m. and C_p of 0.18 for the lower temperature range. The presence of space-charge over the high-temperature range interferes with the direct application of this theory. As space-charge effects set in, the effective pore length decreases, since this length depends on the distance of free flight and the presence of space-charge limits it. As the temperature is increased, and the externally applied electric intensity E_x is maintained constant, the product $(E_x\, l_p)$ which defines the quantity V_p decreases, and therefore the range in applied field for which the conduction increases linearly with the voltage is extended enough to be clearly measurable, and is shown by LOOSJES and VINK.

Even though the theory is capable to indicating quantitatively the dependence of pore conduction on field and temperature in this high field, high-temperature range, its application would depend upon the choice of pore structures not realizable in actual experiments. It is therefore sufficient to show by this qualitative discussion, the relation between theory and observation for these experimental conditions.

67. Emitter evaluation in a diode having concentric cylinders. In the previous sections, space-charge theory as it applies to thermionic emission observations in diodes of parallel-plane construction has been formulated and the results of the theory adapted for direct application to experiment either in equation form or tabular form. The theory has also been developed for the flow of electrons from a cylindrical emitter across the space to a cylindrical collector for all ratios of collector to emitter radii. In order to determine the property of an emitter, it is necessary to combine these two divisions of thermionic emission theory in the manner that is to be outlined here.

A concentric cylinder diode can be constructed with practically any arbitrarily chosen ratio of radii. A practical choice for test purposes would be (R_c/r_s) of 2.5. The collector radius is defined as R_c and the emitter radius r_s. For the idealized application of the theory, all parts of the emitter that deliver electrons to the collector must have a single value of the true work-function at the temperature of test and the emitter must be uniform in its temperature. This condition can be realized in the laboratory by the use of the "guard ring" principle of tube construction. In a properly constructed diode having practical dimensions there will be a sufficient range of applied voltage over which the potential at the surface of the collector will be so negative with respect to that at the emitter that the presence of space-charge will not interfere with the flow of electrons from the emitter to the collector. An estimate of the maximum current density which can flow without space-charge interference may be computed by Eq. (51.1). The use of this equation may be illustrated best by a numerical example in which the effective diode spacing is taken as 1.0 mm. and the extremes in temperature are 580 and 1160° K. The corresponding current densities are respectively: 10.8 and 30.5 microamp/cm.^{2}. With these values serving as an indication of the maximum current flow without space-charge interference, there will be a range of lower current values extending through many orders of magnitude for which curves of the type shown in Fig. 19 will be directly applicable.

A well-activated oxide cathode operating at 1160° K should be capable of an electron emission density of 10 amp/cm.^{2} which is a factor of 3×10^5 greater

than the approximate current density required to develop the zero field condition at the collector. Reference to Fig. 21 shows that the displacement of the observed points over the entire range of retarding potentials negative with respect to the critical value will be close to 0.9.

Fig. 28 has been prepared to illustrate the use of the displacement theory in combination with "master curve $u_0^2 = \infty$" shown in Figs. 16 and 17. In Fig. 28 the current density values that would be obtained in an experiment are plotted on semi-logarithmic paper as a function of the applied voltage in

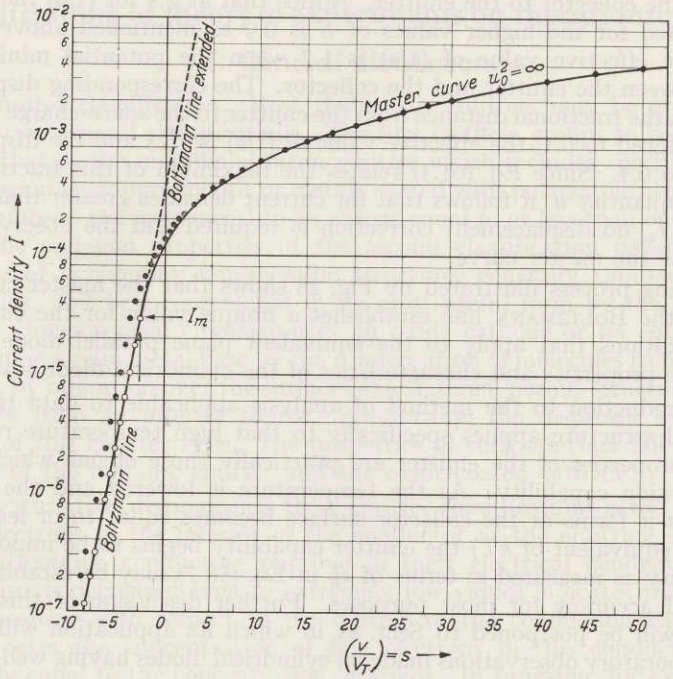

Fig. 28. The application of space-charge theory and the displacement method to evaluate an emitter in a concentric cylindrical diode.

dimensionless units defined by (v/V_T). The current density value designated I_m marks the maximum value of the current density expected at the onset of space-charge limitation. The displacement theory calls for a displacement to the right of 0.9 for each of the observed points for which the current density is less than I_m. These displaced points are shown by open circles. The purpose of this displacement is to establish the proper location of the straight line designated the "BOLTZMANN Line" which is the correct extrapolation of the "master curve" for values of u^2 defined as (I/I_K) which are less than unity. This is the range of current ratio for which there is no space-charge minimum between the emitter and the collector. The analysis shows that this displacement process converts experimental data obtained in a cylindrical diode to a set of points appropriate to represent the emission properties of the same cathode had they been determined in a parallel-plane diode. For the data shown in Fig. 28 the BOLTZMANN Line crosses the critical current value at -2.5 on the "s" scale. This corresponds to an applied potential after correction of -0.25 volts. The actual applied potential for this current would be -0.34 volts. As the actual applied voltage is made more positive than this -0.34 volts, a potential minimum develops first very

close to the collector and then moves with each increase in applied voltage across the space until it approaches very close to the emitter surface. As this transition takes place, the tangential components of momentum with which the electrons left the emitter become less and less effective as contributors to the total kinetic energy required for an electron to pass the potential minimum and ultimately register as collector current.

Fig. 22 may be referred to as the quantitative means by which the correct displacement may be computed as the space-charge minimum moves across the diode from the collector to the emitter. Notice that at 2.5 for $(1/a)$ the displacement indicated for the higher values of S is 0.9 as mentioned above. In this example, the effective value of $(1/a)$ is 1.7 when the potential minimum lies halfway between the emitter and the collector. The corresponding displacement is 0.5. When the fractional distance from the emitter to the space-charge minimum has been reduced to 0.1, the effective value of $(1/a)$ is 1.15 and the displacement is reduced to 0.1. Since Eq. (61.3) relates the maximum of this fractional distance to the quantity u, it follows that for current densities greater than approximately $100\, I_m$ no displacement correction is required and the observed points should follow the master curve.

This fitting process illustrated by Fig. 28 shows that the master curve combined with the BOLTZMANN line establishes a unique value for the current and voltage conditions that apply to the equivalent plane parallel diode that has precisely the properties and characteristics of the cylindrical diode investigated.

This introduction to the method of analysis applicable to data taken with a cylindrical structure applies specifically to that high temperature range over which the properties of the emitter are practically those of one which has unlimited emission capability. As the temperature is lowered and the potential minimum as it forms at the collector surface becomes equal to or less than V_T (that is the equivalent of kT) the emitter capability begins to be important and this capability as measured in terms of z_R^2 in Eq. (58.7) may be established with the required accuracy for most purposes. Further discussion of this phase of the theory will be postponed to Sect. 83 in which its application will be made to actual laboratory observations made on cylindrical diodes having well-activated and stabilized thermionic properties.

68. Thermionic emission theory. Concluding remarks. The theories presented in Sects. 14 to 66 are the necessary background for the interpretation of experimental researches in thermionic emission. Much of the theoretical work presented here may be found scattered in the literature and therefore it forms a body of uncoordinated information. It is one of the present objectives of this writing, not only to coordinate, but to present the subject in a manner that will permit its use as effective reference material without the demand on the reader that he master all the phases of the subject at one time. Its greatest usefulness depends on one's being able to open the study at the particular section of special interest and derive from it the information desired.

The phases of the theory that have been purposely omitted and yet may be relevant to the detailed understanding of thermionic emission phenomena include the analysis of electronic band structure in solids; the corresponding calculations at the surface boundaries and the present-day theories of the transmission of electrons over and through barriers as these relate to the waves associated with the interaction of electrons with atoms that form solid structures. The more important experiments on thermionic emission reported in the present-day literature and during the past twenty-five years require for their explanation

only those phases of the theory that are presented here. Additional experiments that relate specifically to the emission of electrons from single crystals and their absorption by single crystals are likely to demand additional theoretical development. With these exceptions, it is hoped that the theories presented here will be sufficiently comprehensive to satisfy all of the important needs of those who come to this source for information related specifically to the theoretical problems of thermionic emission.

D. Applications of theory to experiments on thermionic emission.

I. General discussion.

69. Emitter classification. Most thermionic emitters may be grouped under either of two general classifications. The first of these groups to be discussed in detail is that of the metallic electron emitter which includes specifically thermionic emission from pure metals or metals coated with polarizable atoms adsorbed to the surface of the pure metal to an extent equal to or less than one monatomic layer. The emission properties of the second classification depend upon the adherence of a complex non-metallic structure, generally thousands of atom layers thick, and best represented in its most useful form by the oxide-coated cathode. Under special circumstances an oxide cathode or its equivalent may be built upon a pure metal base by the condensation of molecules from an external source or, by migration over the surfaces of a sintered, porous structure of metallic crystallites from an interior source. Specifically, the dispenser cathode is an example of this emitter type. The properties of such emitters fall between the extremes of the metallic emitter and the oxide-coated cathode.

The feature that distinguishes these emitter classifications is the *concentration* of free electrons in the interior of the conductor at the emitting surface. The fact that metallic conductors improve in their electrical conductivity as the temperature is decreased even to extremely low values indicates that the FERMI level is positive with respect to the bottom of the conduction band and that in most cases the concentration of free electrons in this conduction band is practically equal to the concentration of atoms. In tungsten, for example, there are approximately 6.3×10^{28} atoms per cubic meter, and with the number of free electrons in the conduction band being approximately equal to this value, the FERMI level is located positive with respect to the bottom of the conduction band 5.7 ev. Since the true work-function of tungsten, as will be shown in Sect. 72, is between 4.4 and 5.3 ev depending on the crystallographic configuration of the exposed surface, the electron affinity (W_a) is close to 10.5 ev again depending on the exposed crystallographic surface. Over the entire operating range of temperature, the concentration of free electrons in the interior of tungsten crystals will remain high and not change significantly. The equation most suitable for the calculation of the FERMI level as a function of the temperature is given in Appendix 3.

Eq. (18.5) shows that the emission properties of a specific surface do not depend on the absolute values of the electron affinity (W_a) and the FERMI level (μ_s) but depend on the difference between these quantities which is, by definition, the true work-function. It is expected that for all metallic surfaces free from adsorbed layers, that the electron affinity will decrease slightly as the temperature increases. Furthermore, the value of the FERMI level also decreases and therefore depending only on the relative rates of decrease, the true work-function may increase or decrease with the temperature. In all known cases of metallic

emitters free from adsorbed layers these changes in the true work-function with temperature are relatively small.

The demand for increased electron emission densities for the same input of power, that is, the same temperature, stimulates the search for a practical means of lowering the true work-function. The adsorption onto the surface of a tungsten crystal of a fraction of a monolayer (approximately 0.7) of electropositive polarizable atoms such as thorium or cesium results in an effective lowering of the electron affinity in direct proportion to the *average dipole moment per unit area.* This method of increasing electron emission efficiency is made use of in all practical devices that depend on thoriated tungsten ribbons or filaments as their electron emission sources. For metals there is no evidence to indicate that practical electron emitters can be improved in their efficiency by the introduction into the interior of alloying impurities which are capable of increasing the concentration of free electrons and in that manner appreciably alter the value of μ_s.

Electron emission from poor conductors of which the oxide-coated cathode is the most important example is predominantly characterized by factors that in most respects are exactly opposite to those important for metallic emitters. First, the electron affinity (W_a) is low, that is, generally less than 1 ev. Secondly, the free electron concentration in the interior of the crystal near its surface is generally lower by a factor of 10^6 and at very low temperatures the concentration of free electrons approaches zero. Under these low temperature conditions, the FERMI level will lie almost exactly halfway between the bottom of the conduction band and the highest occupied electronic level within the crystal. Such levels are shown schematically in Figs. 25, 26 and 27. As the temperature is increased, the magnitude of μ increases very appreciably and this change in the value of μ therefore *increases* the value of the true work-function and decreases the emission compared with the emission that would have been realized had there been no change in the FERMI level.

With these poor conductors, the number of free electrons in the conduction band is therefore dependent not only on the concentration of donor centers (which are probably oxygen vacancies in the oxide cathode), but also it is very dependent on the temperature. The equation which relates the value of the FERMI level to the concentration of donors and to the temperature is Eq. (64.11). An oxide cathode in a thoroughly deactivated state would have no excess of barium over oxygen and the FERMI level would fall at an energy value approximately 2 ev below the bottom of the conduction band. The introduction of a barium excess of as little as 1 part in 10^7 would result in a shifting in the FERMI level to a value halfway between the energy E_D as in Fig. 25 and the bottom of the conduction band if the temperature is sufficiently low. The introduction of such a very small impurity content into an otherwise perfect ionic crystal does not change the electron affinity but does make a very significant reduction in the true work-function because of the important reduction in the magnitude of the FERMI level value μ.

An increase in the concentration of donors by a factor of 100 or more will not change the electron energy level E_D associated with a particular donor type such as, for example, an oxygen vacancy. The really significant factor that is influenced by the increase in the concentration of the donors is the temperature coefficient of the FERMI level. The exact value of this coefficient may be computed by Eq. (64.13) as was done in the preparation of the data given in Table 11 for selected values of donor concentration and donor energy level.

This discussion may be summarized by the statement that the high emission efficiency of oxide cathodes is achieved by the use of a non-metallic emitting

surface having a very low electron affinity and the introduction into the crystalline structure of this emitter of a sufficiently high concentration of donor centers to reduce the temperature coefficient of the FERMI level. With this combination the work-function has an acceptably small value at the normal operating temperature. Any changes in the crystalline structure such as those associated with the addition of a high concentration of strontium to form a solid solution of barium-strontium oxide crystals can presumably make some change in the donor level relative to the bottom of the conduction band or it may make a change in the maximum donor concentration that can be incorporated into the solid structure of the crystal.

The experimental evidence which forms the basis of these introductory remarks will be presented in the later sections of this treatise. These researches will be discussed in the order of increasing complexity which is first, emission from pure tungsten; second, the emission from tungsten in the presence of cesium vapor; third, the emission from thoriated tungsten; and fourth, the emission and conduction properties of oxide cathodes.

70. General studies of thermionic emission from tungsten. Of all of the pure metals which have been studied to determine their thermionic emission properties, tungsten has received the most attention. Because of the economic importance of tungsten in the lamp industry, the major metalurgical problems associated with the production of high-quality filaments were solved many years ago. It will be shown in Sect. 71 that there is no unique value of the true work-function that can be associated with any crystalline material without the specification of the particular crystallographic surface across which the electrons are escaping into the evacuated space. Reproducibility of average emission properties from tungsten is attained only after sufficient heat treatment in a completely inert atmosphere (high vacuum or inert gas) to recrystallize the microcrystals into much larger ones and at the same time drive out and evaporate off occluded impurities which had been purposely introduced in order to facilitate the production of the wire.

The evaluation of the thermionic emission properties of polycrystalline wire is basically an engineering problem rather than a problem in physics. The conventional method of expressing the results in a useful form is to quote the experimentally determined empirical constants suitable for use in the RICHARDSON type of equation [Appendix I and Eq. (50.2)]. A practical choice of these constants is $\varphi_R = 4.5$ ev and $A_R = 60$ amp per cm.^{2} degree^2. NICHOLS[1] has measured the average RICHARDSON constants for various samples of wire and compared his results with those previously obtained on similar samples less well defined in terms of their impurity content. The expected average values of these constants have been obtained by computations based on the known variation of true work-function with crystallographic direction and assumptions with regard to the probable distribution of the particular elemental areas associated with specific crystallographic orientations over the entire surface of the specimen.

The empirically determined work-functions expressed as φ_R are suitable only for the calculation of the average electron emission density as a function of the temperature at an applied potential which is nominally zero. If the average electric intensity at the surface of the emitter can be computed from geometrical considerations then the SCHOTTKY relation given as Eq. (27.13) may be used for the calculation of the average current density obtainable in the presence of a moderately strong accelerating field.

[1] M. H. NICHOLS: Phys. Rev. **78**, 158 (1950).

Theoretical relations applicable in the field of surface chemistry often demand a knowledge of the work-function of the surface at which the reaction takes place. The use of the empirical quantity φ_R for this work-function should be avoided if accuracy is of importance. In all probability no part of the real surface will have a true work-function of this value since some areas conceivably of the order of 50% of the superficial surface may have a slightly lower work-function while the remaining area can very well have a work-function higher than the thermionic average by as much as 1 electron volt. Since work-functions are generally measured at high temperatures, the surface will often be "self cleaning" and give a result which is characteristic of a clean surface even though it may not be an homogeneous one. As the temperature is lowered, polarizable atoms or molecules condense on the surface very quickly unless the partial pressure of condensable gases is maintained at extremely low values (of the order 10^{-13} mm. or less). These adsorbed gases may form a monolayer which will be quite stable under well-defined conditions and give reproducible results. It must be emphasized that reproducibility is not a reliable indication of the absence of surface contamination.

A detailed analysis of thermionic emission data by SEIFERT and PHIPPS[1] aimed at a more accurate determination of the RICHARDSON work-function of tungsten led them to the discovery of the *periodic deviation effect.* If the best of experimental conditions are maintained, measurements show that the rise in average emission current from a polycrystalline test specimen does not follow precisely along the straight line predicted by the SCHOTTKY theory [Eq. (27.13)] but shows small periodic deviations from this line. This effect has been studied most extensively by COOMES and his collaborators[2] and the theory has been developed by GUTH and MULLIN[3] and by HERRING and NICHOLS[4]. Even though this periodic deviation effect is so small that it is insignificant as it relates to practical problems of thermionic emission, it is an effect so well established by experiment that any detailed theory for the transmission of electrons from the interior of the metal across an uncontaminated barrier into a vacuum must include a satisfactory explanation of this phenomenon and at the same time not introduce assumptions that conflict with other known properties of the emitter.

In order to illustrate the major points of this section by carefully taken experimental data, Fig. 29 has been prepared. Two sets of data are shown on the figure. The solid circles apply to data taken at 1373° K while the open circles show results at 1790° K. The logarithm of the observed current is plotted as a function of the square root of the electric field at the surface of the emitter. At a field of approximately 6.4 kv per cm., the currents differ by a factor of exactly 10^4. With the corresponding displacement vertically, the two curves cross each other at this field and they can, therefore, be displayed on the same figure. This method of display permits the graphic illustration of a number of points important for the understanding of thermionic emission from clean, polycrystalline tungsten in the presence of a strong applied field. After a brief description of the method of measurement, the points illustrated by these data will be explained.

A long filament of GE 218 wire was polished to remove all die marks and scratches and its diameter was measured by an interferometer method to be

[1] R. L. E. SEIFERT and T. E. PHIPPS: Phys. Rev. **56**, 652 (1939).

[2] R. J. MUNICK, W. B. LABERGE and E. A. COOMES: Phys. Rev. **80**, 887 (1950). — D. W. JUENKER, G. S. COLLADAY jr., and E. A. COOMES: Phys. Rev. **90**, 772 (1953).

[3] E. GUTH and C. J. MULLIN: Phys. Rev. **61**, 339 (1942) and earlier papers.

[4] C. HERRING and M. H. NICHOLS: Rev. Mod. Phys. **21**, 185 (1949).

4.24×10^{-3} cm. The filament was mounted accurately on the axis of a set of five cylinders, each having an inside diameter of 2 cm. The center collector was 3 cm. in length and the currents measured correspond to the arrival of electrons at this collector. The tube was so constructed that applied voltages up to 10000 volts could be used without appreciable leakage or spurious current. At this voltage, the surface field was 0.76×10^6 volts per cm. which was sufficient to give a very measurable field emission with the filament at room temperature. This contribution due to field emission is clearly evident in curve *a* of Fig. 29 at a field strength of 0.2×10^6 volts per cm. The deviation of the three highest points from the extrapolated straight line, shown on this figure, corresponded quite precisely with the field emission observed at room temperature. For the high temperature data, shown as curve *b*, the field emission over the range shown was not important since the measured thermionic currents at the higher temperature were 10000 times greater than those observed for curve *a*.

Eqs. (27.5) and (27.13) were used to calculate the field at the surface of the emitter and determine the slope of the two straight lines, shown in Fig. 29, associated with curves *a* and *b*. These lines are both drawn to fit the observed data points in the very high field range. This choice is quite arbitrary and depends on the assumption that even with these strong fields, the penetration of electrons through the modified mirror-image barrier is of minor significance. An inspection of the location of the data points in comparison with these lines shows that over the range of field of 4×10^4 volts per cm. and higher, the deviation of the plotted points with respect to the straight line is practically independent of the temperature of the emitter. At lower fields the curves show quite graphically that the deviation of the observed points is very measurably greater the lower the temperature. This fact alone indicates that space charge is playing no important part in the control of the electron flow from the emitter to the collector.

If the periodic deviations are neglected and an approximate average slope is determined, the departure from the theoretical SCHOTTKY lines is close to 8%. It is evident from these data that average slopes that might be used to represent experimental data according to the so-called "SCHOTTKY plot" will deviate more and more from the theoretical slope the lower the field and the lower the temperature.

These deviations are consistent with the explanation that long range surface fields are produced because of the non-uniformity of the work-function exhibited by the specimen of tungsten used for this study. Undoubtedly, the crystals were large and exhibited a variation in work-function depending on the crystallographic direction. The minimum value was approximately 4.3 and the maximum was about 5.3 volts. Although patch theories have been worked out[1] for special geometrical arrangements of patches, it is hardly worthwhile to do more than indicate that a choice of patches may be made which is capable of accounting for characteristics similar to those shown in Fig. 29. Although the patch effect is important, such an explanation leaves much to be desired and serves relatively little purpose since the details concerning the specimen used for observations are generally lacking.

These data may be taken as typical and represent thermionic emission from polycrystalline tungsten wire at two temperatures. It is conventional, as has already been explained, to use the intercepts of straight lines of the type shown in Fig. 29 as appropriate data for the RICHARDSON equation. The limitations as well as the usefulness of the empirical constants A_R and φ_R have been discussed.

[1] J. A. BECKER: Rev. Mod. Phys. **7**, 95 (1935). — W. B. NOTTINGHAM: Phys. Rev. **49**, 78 (1936). — C. HERRING and M. H. NICHOLS: Rev. Mod. Phys. **21**, 185 (1949).

Computation shows that the empirical constants as given in Appendix I may be used to compute the intercepts expected for these two temperatures. These observed data show a deviation in current density observed of only 20% from that expected for curve *a* and 40% for curve *b*. Lack of agreement with the average predicted current density for tungsten of this magnitude is typical.

A careful examination of the data shown in Fig. 29 serves to establish the fact that the data points deviate systematically from a straight line. Clearly, these deviations are small and stand out strongly only when accurately taken data permit the direct plotting of the deviation from the theoretical straight line as a function of the field. The data shown in this figure, in addition to other data taken at the same time at other temperatures provide the information on which maxima and minima in the deviation can be indicated. In this figure the minima are indicated by arrows pointing downward and the maxima by arrows pointing upwards. One striking fact that came from these observations is that the fractional magnitude of these deviations is practically independent of the temperature and the location of the maxima and minima also seems to be practically independent of the temperature. These results were reported very briefly by NOTTINGHAM[1].

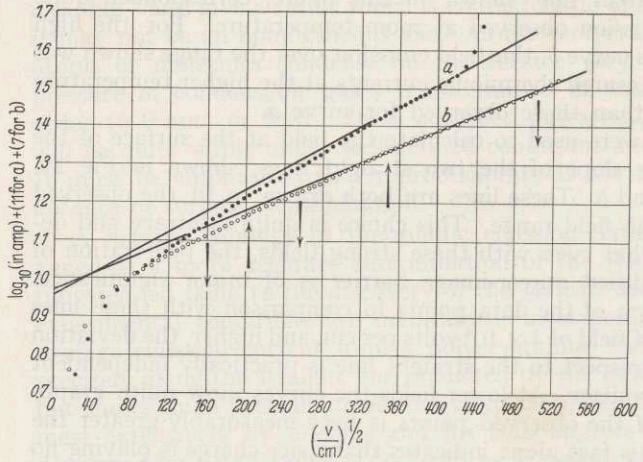

Fig. 29. Electron emission from tungsten as a function of field at two temperatures. Curve *a* for 1373° K; *b* for 1790° K. Straight lines represent SCHOTTKY mirror-image theory. Maxima of periodic deviation ↑; Minima ↓.

The work of DUSHMAN and others[2] led to the erroneous conclusion that the experimentally determined value of the thermionic constant A_R should be 60.2 amps per cm.^{2}-degree^2 and therefore agreed exactly with the value of the theoretical constant which he computed. This value is now recognized to have been in error by a factor of 2. The factors that enter into the correct calculation of the thermionic constant A are given in Eq. (18.6). Contributing to this difference between the observational value of 60 and the computed value of 120 are three factors not previously taken into account. These are:

1. For tungsten, practically all the emission comes from approximately 50% of the superficial area of the emitting filament;

2. The effective temperature coefficient of the true work-function of the important emitting areas is not only uncertain as regards its actual value but even the sign, remains in doubt;

3. The observed deficiency in the number of slow electrons emitted from the surface must also be given consideration.

The combination of these last two factors would seem to indicate that the average temperature coefficient of the true work-function of the strongly emitting areas is small and negative so that the combination of all factors gives an empirical value of the constant A_R of 60 amps per cm.^{2}-degree^2.

[1] W. B. NOTTINGHAM: Phys. Rev. **57**, 935 (1940).
[2] S. DUSHMAN: Rev. Mod. Phys. **2**, 381 (1930).

II. Emission from single crystals.

71. Thermionic emission properties of single crystals of tungsten. The pioneering work of MÜLLER[1] showed by the use of his electron projection microscope that the field emission properties of a tungsten single crystal were very dependent on crystallographic direction. Shortly before MÜLLER's work, thermionic electrons were projected in a similar manner from a filamentary source to a surrounding cylindrical fluorescent screen and thus indicated at least qualitatively the variation in the emission properties of a single crystal of tungsten as a function of crystallographic direction. Following a series of researches by JOHNSON and SHOCKLEY[2], NELSON[3], and MARTIN[4], NICHOLS[5] made the first quantitative measurements of the thermionic emission from a single crystal of tungsten as a function of its crystallographic direction.

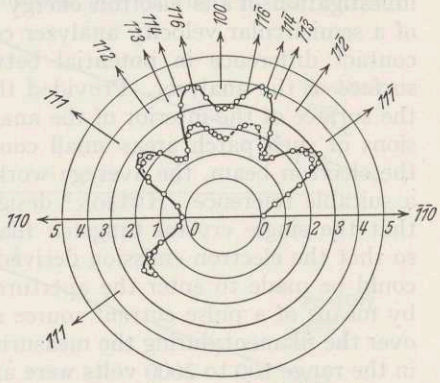

Fig. 30. Polar diagram of thermionic emission current as a function of angle as observed by NICHOLS at 1880° K, applied surface field of 60 kv per cm. Solid line shows emission from a cleaner surface after the crystal was heated to 2500° K.

In the NICHOLS experiment, a polished tungsten filament in which a single crystal 9 cm. long had been grown was mounted on the axis of a cylindrical electron collector system. The filament was supported on a frame with bearings accurately aligned so that the filament could be rotated about its own axis through more than 180°. A slot in the collector system defined an opening through which a beam of electrons could be delivered to a shielded collector for measurement. Cold working of polycrystalline tungsten wire previous to its first heating tends to line up the 110 direction of the crystallites along the axis of the wire. Such wires invariably grow crystals with this orientation. The polar diagram shown as Fig. 30 is a reproduction of the one presented by NICHOLS. The diagram shows weak emission areas in the 110 and the 112 direction. Maxima occur in the 111 and 116 directions. The minimum in the 100 direction is sometimes not as pronounced as that found by NICHOLS.

Table 71.1.

Direction	NICHOLS		SMITH	
	φ_R	A_R	φ_R	A_R
(111)	4.39	35	4.38	52
(112)	4.69	125	4.65	120
(116)	4.39	53	4.29	40
(100)	4.56	117	4.52	105
(110)[7]	4.68	15	4.58	8

The NICHOLS tube was reconstructed by SMITH[6] and very extensive additional measurements were made on a new crystal. These measurements included a study of the emission as a function of surface field. Although the SMITH measurements were in substantial agreement with NICHOLS, analysis showed that the electron current observed with the crystal oriented with the 110 face in direct line with the measurement slot was almost entirely spurious. Work-function difference evaluations by

[1] E. W. MÜLLER: Z. Physik **106**, 541 (1937); **108**, 668 (1938).
[2] R. P. JOHNSON and W. SHOCKLEY: Phys. Rev. **49**, 439 (1936).
[3] R. B. NELSON: M. I. T. PhD Thesis 1938.
[4] S. T. MARTIN: Phys. **56**, 947 (1939).
[5] M. N. NICHOLS: Phys. Rev. **57**, 297 (1940).
[6] G. F. SMITH: Phys. Rev. **94**, 295 (1954).
[7] Emission in this direction is spurious and the corresponding A_R and φ_R do not represent the RICHARDSON constants truly characteristic of this surface direction.

HUTSON (Sect. 72) show that the true work-function associated with this direction is so high that the currents measured by NICHOLS and by SMITH were correctly identified by SMITH to be the result of secondary effects and not a valid measurement of the primary emission in that direction. The results of both of these studies are best summarized by the Table 71.1.

72. Velocity analysis of thermionic emission from single crystals of tungsten. A study[1] that required a homo-energetic beam of electrons indicated that an investigation of the electron energy distribution from a hot filament by means of a semicircular velocity analyzer could yield an accurate determination of the contact difference in potential between the emitter surface and the interior surface of the analyzer. Provided that the local work-function differences over the surface of the interior of the analyzer were sufficiently small and the dimensions of such patch areas small compared to the distance from the surface to the electron beam, the average work-function of the analyzer interior serves as a suitable reference. HUTSON[2] designed a tube similar to the NICHOLS tube in that the single crystal tungsten filament could be rotated about its own axis so that the electron emission derived from well-defined crystallographic surfaces could be made to enter the aperture of the analyzer. The filament was heated by means of a pulse current source so that there would be no drop in potential over the filament during the measuring half cycle. Electron accelerating voltages in the range 100 to 2000 volts were applied between the filament and the co-axial cylinder. The slot in the cylinder subtended a very small angle at the filament and therefore permitted electrons to enter it from a well-defined area. A carefully designed electron-optical system provided a means for slowing down the electrons so that they entered the 180° velocity analyzer with an energy of about 3 ev. Depending on the strength of the uniform magnetic field, a precisely known energy group passed around the analyzer and out the exit slit to the shielded electron collector. The data shown in Fig. 31 are typical of the results obtained. In this figure the current observed is plotted on a logarithmic scale as a function of the kinetic energy, expressed as V_p, of the electrons at the emission surface. The current and energy values are not shown in this diagram since they were normalized by vertical and horizontal displacements in order to match the three sets of observed data which were taken with the extremes in applied voltage of 150 to 2000 volts.

It was possible to establish that no change had occurred in the average work-function of the interior of the analyzer during the time required for a set of measurements, and therefore the horizontal displacements required to bring the various curves similar to those shown in Fig. 31 into alignment are a direct measure of the changes in the true work-function with electric field. The observed changes for three of the important crystallographic directions are plotted in Fig. 32. The SCHOTTKY theory of the change in true work-function with field was presented in detail in Sect. 27 and Eq. (27.11) shows that the change in work-function should be proportional to the square root of the electric intensity at the surface of the emitter.

In Fig. 32 the work-function change is plotted as a function of the square root of the surface field and the straight lines are drawn with the theoretical slope required by the SCHOTTKY theory. This study therefore stands as the first direct observation of the SCHOTTKY effect reduction in work-function by the influence of an external field. All previous verifications of the SCHOTTKY theory

[1] W. B. NOTTINGHAM: Phys. Rev. **55**, 203 (1939).
[2] A. R. HUTSON: Phys. Rev. **98**, 889 (1955).

have depended on the assumption not previously established that the energy distribution of the electrons transmitted across the maximum of the potential barrier remained independent of the applied field. HUTSON's experiments demonstrate this independence separately from the direct observation of the shift in the work-function which is established by these data to be exactly that predicted by the SCHOTTKY theory within the experimental error. Fig. 33 illustrates the fact that the energy distribution at a constant temperature of 2000° K and a constant accelerating anode voltage is independent of the crystallographic

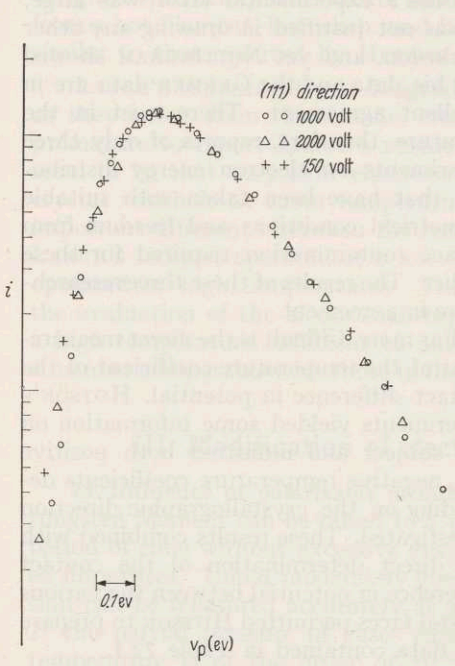

Fig. 31. Superposition of energy distributions obtained by HUTSON at 2000° K for three different anode potentials and electron emission in the 111 direction. Initial energy of electron is V_p in ev.

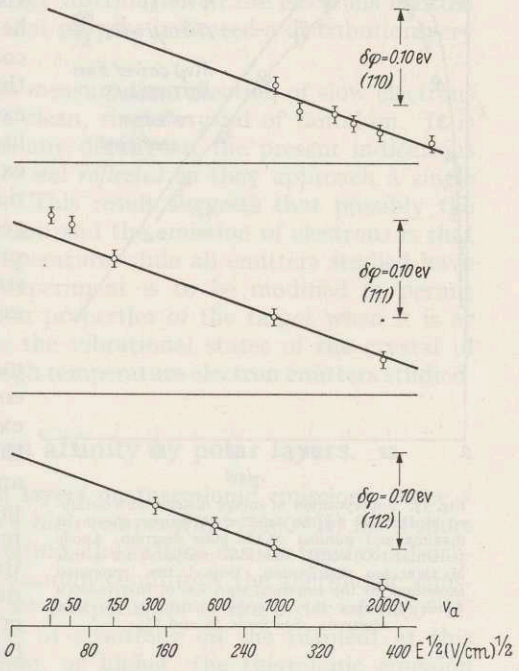

Fig. 32. Change of work-function with applied field as observed by HUTSON from the relative voltage displacements required to superpose distributions illustrated by Fig. 31. Solid lines are drawn with a theoretical slope required by SCHOTTKY's mirror-image theory.

direction and furthermore that there is a very marked deficiency of slow electrons. This result is indicated by the lack of agreement between the observed points illustrated there and the solid line which represents the results that would have been obtained had the electrons been emitted from the hot filament with a perfect MAXWELLian distribution.

Electron energy distributions determined by the retarding potential method by NOTTINGHAM[1] indicated a similar departure from a MAXWELLian distribution for electrons emitted from tungsten filaments and from thoriated tungsten filaments. Patch effects on the tungsten filaments interferred with the accurate reproducibility of the retarding potential curve but did not interfere with the results obtained with thoriated filaments. An empirical relation discussed in Sect. 26 and given by Eq. (26.4) served as an accurate representation of the retarding potential data. This relation would predict the distribution function

[1] W. B. NOTTINGHAM: Phys. Rev. **49**, 78 (1936).

represented by the dotted line of Fig. 33. Since the method by which the electron energy distribution was determined by NOTTINGHAM was inherently less accurate than that of HUTSON. There is no significant disagreement between these studies.

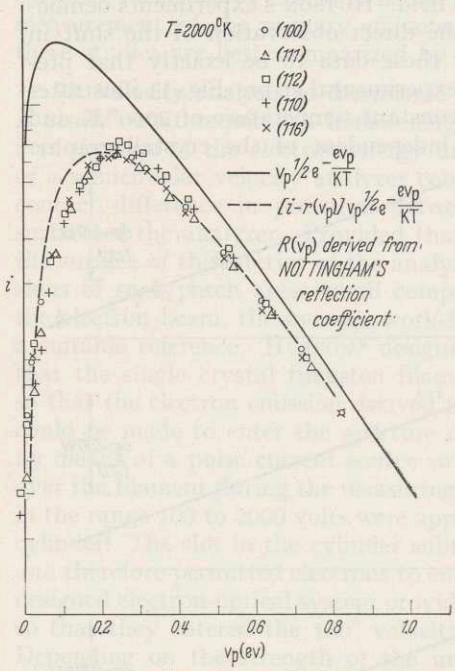

Fig. 33. Superposition of energy distributions obtained by HUTSON for the selected directions shown at maxima and minima of the polar diagram. Anode potential 1000 volts. Solid line computed for a true MAXWELLian distribution. Dotted line computed according to the empirical equation of NOTTINGHAM which describes the observed deficiency of slow electrons. See Sects. 26 and 75.

The retarding potential measurements made by GERMER[1] are often cited as proof that electrons are emitted from tungsten with a MAXWELLian distribution. Since GERMER'S experimental error was large, he was not justified in drawing any other conclusion, and yet NOTTINGHAM showed that his data and the GERMER data are in excellent agreement. There exist in the literature, therefore, reports of only three experiments on electron energy distribution that have been taken with suitable geometrical conditions and freedom from surface contamination required for these studies. The results of these three researches are in agreement.

Far more difficult is the direct measurement of the temperature coefficient of the contact difference in potential. HUTSON'S experiments yielded some information on this subject and indicated both positive and negative temperature coefficients depending on the crystallographic direction investigated. These results combined with the direct determination of the contact difference in potential between the various crystal faces permitted HUTSON to prepare the data contained in Table 72.1.

Table 72.1.
HUTSON'S *estimates of the true work-functions for a tungsten crystal in the temperature range 1700 to 2000° K.*

Direction	φ in ev	φ in ev
111	$4.3 + (3 \times 10^{-5})\,T$	$4.3 + 0.36\,V_T$
112 (Note 1)	$4.57 - (5 \times 10^{-5})\,T$	$4.57 - 0.6\,V_T$
112 (Note 2)	$4.66 - (8 \times 10^{-5})\,T$	$4.66 - 0.9\,V_T$
116 (Note 3)	$4.20 + (3 \times 10^{-5})\,T$	$4.2 + 0.36\,V_T$
116 (Note 3)	$4.31 + (3 \times 10^{-5})\,T$	$4.31 + 0.36\,V_T$
100	$4.44 - (2 \times 10^{-5})\,T$	$4.44 - 0.24\,V_T$
110 (Note 4)	$5.09 \pm$ (uncertain)	

Note 1: Assume no effect of spurious current similar to that found for 110 orientation
Note 2: Based on observed temperature coefficient.
Note 3: Range thought to be result of heat treatment.
Note 4: Best estimate for crystal at 2000° K.

Since HUTSON was not prepared to make a direct determination of the absolute value of any of the RICHARDSON work-functions with an accuracy comparable with that of NICHOLS and of SMITH, those given in Table 72.1 depend on the acceptance of the NICHOLS and SMITH work-function determined for the 111direction.

Because of the fact that no theory has been devised to account for the observed deficiency of slow electrons emitted thermionically from hot surfaces, experimentally unsupported criticism has followed the publication of the experimental

[1] L. H. GERMER: Phys. Rev. **25**, 795 (1925).

results that show the deficiency. The latest is that offered by SMITH[1] in criticism of the work of HUTSON. SMITH makes the hypothesis that, for reasons unknown, the resolution of HUTSON's velocity analyzing equipment was a factor of 10 poorer than the value claimed by HUTSON. All attempts to identify a cause for this lack of resolution assumed by SMITH have failed and independent evidence by LANGE[2] indicates that his analyzer, which was similar in construction to that of HUTSON, has practically the resolution expected from it according to calculations similar to those applied by HUTSON. LANGE's experiment was not designed specifically to evaluate the energy distribution of the electrons emitted from a hot filament, but when used for that purpose indicated a distribution very similar to that reported by HUTSON.

LANGE's experiment was designed to measure the reflection of slow electrons as they enter, from the outside, into a clean, single crystal of tantalum. It is premature to report LANGE's results in any detail, but the present indications seem to be that very slow electrons are *not reflected* as they approach a single crystal which is at room temperature. This result suggests that possibly the important difference between the reception and the emission of electrons is that LANGE's receiver operated at a low temperature while all emitters studied have operated at high temperatures. The experiment is to be modified to permit the evaluation of the electron absorption properties of the target when it is at a high temperature sufficient to excite the vibrational states of the crystal in a manner comparable with those in the high temperature electron emitters studied.

III. Modification of electron affinity by polar layers.

73. Influence of polarizable adsorbed layers on thermionic emission. Since a tungsten filament can be raised to a very high temperature (3000° K) for a short period of time without excessive evaporation, the surface can be freed of adsorbed impurities. Under moderately good vacuum conditions the thermionic emission can be measured accurately at a test temperature of the order of 1400° K. If the partial pressure of gases capable of adsorbing on the filament at this temperature is of the order of 10^{-10} mm. or higher, the thermionic emission from the test filament usually decreases with the time. This phenomenon often described as "emitter poisoning" is characteristic of the adsorption onto the filament of electro-negative gases such as oxygen. Since the electro-negative adsorbed layers are difficult to control and reproduce, they have not been investigated in terms of their influence on thermionic emission to the extent that adsorbed layers of electro-positive material have been studied.

The adsorption of films on the surface of a single crystal of tungsten and its influence on the thermionic emission is exhibited dramatically by the researches of MARTIN[3]. A large single crystal of tungsten was cut and polished to form a hemispherical cap which could be heated by radiation and electron bombardment from a filament mounted in a cavity in this cap. This structure was located at the center of a spherical bulb coated with a phosphor so that the pattern of light observed at the surface of the phosphor served as a qualitative measure of the distribution of electron emission over the surface of the tungsten emitter. It was not possible to control nor measure the quantity of adsorbed material on the tungsten, but it was possible to establish that the adsorption and emission

[1] G. F. SMITH: Phys. Rev. **100**, 1115 (1955).
[2] W. J. LANGE: Unpublished researches at M. I. T.
[3] S. T. MARTIN: Phys. Rev. **56**, 947 (1939).

properties of the surface varied in an extremely complex manner and yet maintained symmetries that were determined by the known crystallographic directions of the single crystal specimen. These studies of MARTIN's demonstrated the futility of attempting to interpret, in much more than a qualitative manner, the influence of adsorbed films on thermionic emission. For this reason, Sect. 74 will give a very brief review of the researches of TAYLOR and LANGMUIR[1] which was the latest and most comprehensive study of the properties of cesium films on tungsten. Sect. 75 will deal with some of the properties of tungsten when activated by a partial layer of thorium as produced on a thoriated tungsten filament.

The forces that act on an electron as it leaves the interior of a metallic conductor and escapes across the conducting boundary into free space are complex and understood in some detail only after the very short-range forces become reduces in importance in comparison with the long-range mirror-image force. The integral of all of the forces that act on an electron as it escapes is measured by the quantity W_a known as the "electron affinity". The true work-function of a surface as discussed in Sect. 19 is not the electron affinity itself, but the difference between two quantities both measured from the same reference and given by Eq. (19.1). Additional discussion will be found in Sect. 27.

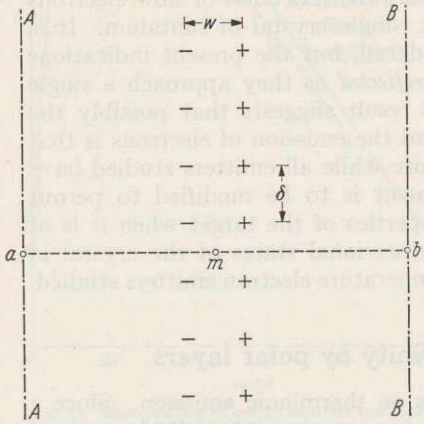

Fig. 34. Infinite plane of dipoles for computation of difference in potential from a to b.

The adsorption of polarizable atoms in the form of a film less than one mono-molecular layer in thickness can have no influence on the location of the FERMI level μ_s, but can act directly to reduce (or even increase) the average value of the electron affinity W_a. The effect of a dipole layer can be evaluated quantitatively by first considering that the problem is closely related to that of computing the difference in potential between the sheets of charge that reside on the surfaces of a parallel plane capacitor with a separation between the surface charges of w and a charge per unit area of σ. The following equation expresses that difference in potential:

$$\Delta V = \frac{w\sigma}{\varepsilon_0}. \tag{73.1}$$

If the system of charges is considered to be the equivalent of the grouping shown in Fig. 34, then an electron at point a in the plane AA will experience practically no net force acting on it due to the presence of the dipoles if the distance $a - m$ is large compared with the average distance between the dipoles shown in the figure as δ. The net force on the electron at point b also vanishes under these same conditions. However, as the electron approaches close to the sheet of dipoles, it is acted upon by forces which, because of the negative charge accelerate the electron across the space. In other words, it would have fallen through a difference in potential expressible by an equation similar to Eq. (73.1) as follows:

$$\Delta V = \frac{\overline{m} n_a}{\varepsilon_0}. \tag{73.2}$$

[1] J. B. TAYLOR and I. LANGMUIR: Phys. Rev. **44**, 423 (1933).

In this equation $\overline{m}$ is the average dipole moment per atom and is defined as the average displaced charge within the polarized atomic or molecular unit multiplied by the average distance of displacement. The quantity n_a is the number of adsorbed molecules per unit area. On the basis of this reasoning, it is an accurate statement to say that the reduction in the true work-function that results from the adsorption of an electro-positive substance to the extent of one monolayer or less is directly proportional to the average dipole moment per unit area that results from the adsorption of this layer.

The arrangement of charges shown in Fig. 34 suggests at once that the adsorbed dipoles should generally repel each other and therefore act in their motion over the surface of a crystal as a two-dimensional gas. When the average distance between dipoles is large compared with atomic spacings, then the dipole moment per atom or molecule should be independent of their concentration. As the number on the surface increases, however, the dipoles react upon each other and reduce the dipole moment per atom. As it will be shown in Sects. 74 and 75, this fact accounts for the linear reduction in work-function with increased concentration when a small fraction of the surface is covered.

With larger concentrations, the dipole moment per atom decreases to such an extent that a maximum dipole moment per unit area occurs with approximately 70% of the surface covered and not when a complete monolayer is formed.

For a given concentration of adsorbed atoms, it is to be anticipated that the dipole moment per atom will decrease as the temperature increases. Because direct measurements of the temperature coefficient of the contact potential are difficult, although not impossible, there exist no quantitative data on the net increase in work-function with temperature. Indirect measurements by NOTTINGHAM[1] would indicate a maximum of 28.5×10^{-5} volts per degree for thorium on tungsten. This factor, when converted to the units used in Eq. (38.10), gives the value of (dP/dV_1) of 3.3. The thermionic constant A_R for surfaces activated by electropositive fractional monolayers is low, and this fact is a direct indication that this positive temperature coefficient of the work-function is influencing the emission-*versus*-temperature relation.

The opposite effect is observed when the surface is contaminated by electronegative atoms or molecules. Again, the first direct indication comes from the fact that the empirical A_R values for those contaminated surfaces are very high compared with the theoretical A given by Eq. (18.6).

74. The properties of cesium films on tungsten. The properties of fractional monolayers of cesium adsorbed to tungsten have been studied experimentally and analytically in the greatest detail by TAYLOR and LANGMUIR[2]. The principal tube used for their study had two "well-aged" tungsten filaments, each of 30 cm. total length mounted close to the axis of a three-electrode collector system. The central 10 cm. sections of these filaments were straight and 10 cm. of filament at each end were wound in a tight spiral so that the center section would heat very uniformly. The collectors were formed by evaporation onto the glass wall of the tube so that the entire structure except for the filaments themselves could be maintained accurately at a pre-assigned temperature in the range from about 270 to 300° K. The concentration of cesium in the vapor phase was controlled by the regulation of this temperature.

[1] W. B. NOTTINGHAM: Phys. Rev. **49**, 78 (1936).

[2] J. B. TAYLOR and I. LANGMUIR: Phys. Rev. **44**, 423 (1933). — I. LANGMUIR: J. Amer. Chem. Soc. **54**, 2798 (1932).

LANGMUIR and KINGDON[1] showed that all cesium atoms which strike a high-temperature tungsten filament leave as positive ions and the measurement of this ion current is a direct indication of the arrival rate of cesium atoms at the filament. As the temperature of the test filament is reduced, atoms tend to adsorb on the filament until a sufficient layer is built up so that the rate of evaporation from the surface is exactly equal to the rate of arrival of atoms at the surface. For a wide range of surface concentrations that approached closely to a monolayer, TAYLOR and LANGMUIR determined rates of evaporation of atoms, positive ions and electrons as a function of the temperature. LANGMUIR based his theoretical analysis on the assumption that 99.5% of the entire surface of his "aged" filaments was 110 surface. This hypothesis was well supported by the self-consistency of the data, but was never verified by actual observation of the emission pattern by the electron projection tube method later used so successfully by JOHNSON and SHOCKLEY and by MARTIN[2] to show that the filament actually had developed an etched structure such that only 110 surfaces were exposed. ROBINSON[3] made a vigorous attempt to follow the techniques of TAYLOR and LANGMUIR to produce a test specimen of uniform surface structure, but found it impossible.

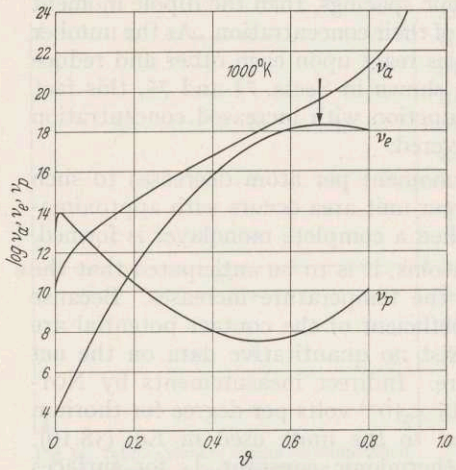

Fig. 35. Atom (ν_a), ion (ν_p), and electron (ν_e) evaporation rates at 1000° K with zero-field as observed by TAYLOR and LANGMUIR as a function of the fraction of the surface covered ϑ.

In spite of the uncertainty in the true nature of the underlying crystallographic structure of the tungsten specimen studied by TAYLOR and LANGMUIR, there can be no doubt concerning the broader aspects of their results. These will be summarized very briefly by the following statements.

1. The adsorption of cesium on a tungsten surface reduces the work-function in direct proportion to the number of cesium atoms adsorbed for coverages less than approximately 15% of the number of cesium sites available to a monolayer of adsorbed atoms. LANGMUIR's determination gives 4.8×10^{14} atoms per cm.^{2} for complete coverage.

2. A maximum reduction in average work-function of approximately 3 volts takes place if the surface covered is 0.67 of a monolayer. This maximum occurs because the dipole moment per atom decreases at a greater and greater rate so that in spite of an increase in cesium concentration above this critical value, the average dipole moment per unit area actually decreases.

3. The relative rates of atom evaporation, electron evaporation and positive ion evaporation at 1000° K are best illustrated by Fig. 35. In this figure, the fraction of the surface covered is represented by the symbol ϑ and the evaporation rates are expressed in terms of units per cm.^{2} per sec. This figure shows that, for very small concentrations the ion evaporation is very large compared with

[1] I. LANGMUIR and K. H. KINGDON: Science, Lancaster, Pa. **57**, 52 (1923). — Proc. Roy. Soc. Lond., Ser. A **107**, 61 (1925).

[2] R. P. JOHNSON and W. SHOCKLEY: Phys. Rev. **49**, 436 (1936). — S. T. MARTIN: Phys. Rev. **56**, 947 (1939).

[3] C. S. ROBINSON: Unpublished research. Dept. of Physics, M. I. T.

either atom evaporation or electron evaporation. As the surface coverage increases, ion evaporation drops to practically negligible proportions, whereas the atom evaporation continues to increase and as a monolayer is approached, the atom evaporation increases so rapidly that at this high filament temperature it is practically impossible to form even a small part of a second layer of cesium on the surface. Electron evaporation is shown to have a maximum at a ϑ value of 0.67.

These studies of TAYLOR and LANGMUIR have contributed more than any other single investigation to an understanding of the properties of adsorbed films on an underlying metallic structure. The results are best accounted for by the statement that the adsorption of an electropositive layer modifies the electron affinity in direct proportion to the dipole moment per unit area. The adsorbed layer reduces the work-function and permits the thermionic emission of enormously more electrons than would otherwise obtain. This is one of the clearest examples of catalytic action since the cesium itself assists in the "reaction" without in any way being used up in the process.

75. Some properties of thoriated tungsten emitters. In the early days of lamp manufacture, improved ductility of tungsten was obtained by the introduction of thorium oxide to the extent of about one percent along with the tungsten powder before sintering and wire production. Before heating to a high temperature, wires containing thorium oxide are practically indistinguishable by inspection from pure tungsten wires. Upon the first high-temperature heating, however, there is a very great difference in the average crystal size of the heated wire. Pure tungsten invariably develops large crystals that generally extend as single crystals across the entire diameter of the wire, while thoriated tungsten develops many small crystals per wire diameter that seem never to grow to develop large crystals in later heating. Hundreds of pockets of thorium oxide are formed in the interstices between the tungsten crystals in a centimeter of wire length. LANGMUIR and ROGERS[1] discovered that, after a suitable sequence of heating, thoriated tungsten wires yielded tens of thousands greater electron emission density at a favorable operating temperature in comparison with pure tungsten at that same temperature. The main features of the phenomena of thorium oxide reduction and diffusion to the surface were studied by LANGMUIR[2] and BRATTAIN and BECKER[3].

From these and other studies it has become clear that thorium oxide is reduced to some extent by the evoluation of oxygen in excess of the thorium when the filament is flashed to a high temperature, preferably between 2800 and 3000° K. After a flash of the order of one minute at this high temperature, the concentration of thorium averaged over the entire surface of the tungsten is practically negligible and the emission properties of the specimen are very close to those of pure tungsten. In order to activate this filament, it must be maintained in an evacuated tube from which all active gases have been removed, either by pumping or by the "getter action" of some material such as barium. For quantitative researches, it is necessary to reduce the partial pressure of these active gases to less than 10^{-14} mm.

If the filament is maintained, preferably with no applied electron accelerating field, at a temperature of 2100° K, thermionic emission tests made at some fixed test temperature such als 1400° K or less show that the emission capability

[1] I. LANGMUIR and W. ROGERS: Phys. Rev. **4**, 544 (1914).
[2] I. LANGMUIR: Phys. Rev. **22**, 357 (1923).
[3] W. H. BRATTAIN and J. A. BECKER: Phys. Rev. **43**, 428 (1933).

of the filament will increase through many orders of magnitude and finally stabilize after approximately 30 min. of activation at a value which is independent of further activation heating

For a quantitative investigation of the activation procedure, it is more instructive to choose a lower activation temperature such as 1900° K and a test temperature of 1200° K or less. After the filament has been aged by repeating the activation procedure a few times, it may be flashed to a high temperature for 30 sec. and a detailed study of the rise in emission with time of activation may be made. Since a decrease in true work-function as a result of activation is a direct measure of the average dipole moment per unit area that results from the presence of the thorium on the tungsten surface, the following equation gives the relation between the observed emission current and the time:

$$\ln I = \ln I_0 + \frac{e}{\varepsilon_0 k T_s} \int_{t=0}^{t=t} \bar{m}_0 \left[1 - f(n_a/n_1)\right] \left(\frac{dn_a}{dt}\right)_{T_a} dt. \qquad (75.1)$$

This equation is written in this form in order to bring out certain features of the phenomena involved. Consider first the time rate of increase in the density of adsorbed atoms represented by $(dn_a/dt)_{T_a}$. For a temperature of activation T_a as low as 1900° K, the evaporation of thorium atoms is practically negligible until the surface concentration builds up to 0.8 of a monolayer. Under that condition this factor is controlled by the diffusion of thorium from a large number of relatively active spots between crystals out of which the thorium atoms stream and spread (because of their mutual repulsive forces) over the entire surface of the thoriated tungsten filament. For the most accurate results, the thorium atoms should be given an opportunity to disperse uniformly over the entire emitter by holding it at a temperature of approximately 1400° K for a considerable period of time after each activation period before the emission observations are made at 1200° K. Other factors in the equation include $\bar{m}_0$ which is defined as the average dipole moment per thorium atom when the concentration is less than 5% of a monolayer and the second factor of the equation is written in this form to indicate that the average dipole moment per atom is known to decrease as the concentration increases. In other words, the function $f(n_a/n_1)$ would start out for small concentrations to be practically zero, but as the concentration increases, this function will gradually increase until it approaches the concentration of a monolayer specified as n_1. It follows from this discussion that if the arrival rate of thorium atoms is initially constant, and if the function $f(n_a/n_1)$ is small compared with 1, then $\ln I$ should be a linear function of the time. Initially it can be assumed that the evaporation rate can be neglected in comparison with the rate of arrival of thorium atoms from the interior, and that this rate of arrival is governed by an exponential temperature relation. Studies of the initial rise in emission current for small surface concentrations should permit a determination of the dipole moment $\bar{m}_0$. The exact rate of arrival at a given activation temperature T_a could differ from sample to sample, but it would be expected that the dipole moment per atom would be reproducible. Tests of this kind have not been made with all factors of the problem under control.

Having once determined a suitable value for $\bar{m}_0$ and the rate of arrival for a given low temperature of activation T_a, then it should be possible to determine more specifically the interaction function $f(n_a/n_1)$.

As regards this process of activation, it is sufficient to say that a surface concentration of approximately 0.7 of a monolayer yields the highest emission current at a given test temperature and that the addition of extra thorium

atoms actually results in a lower emission as measured at zero field since, because of the interaction of one dipole on its neighbor, the average dipole moment per unit area decreases with an increase in thorium concentration above the 0.7 value.

Fundamental to the understanding of the physics of thermionic emission is knowledge concerning the energy distribution of the electrons emitted. NOTTINGHAM[1] developed a circuit for the pulse heating of a thoriated filament in order to study its emission properties as a function of applied voltage without the results being distorted by the presence of a drop in potential over the length of the filament that delivered current to the collector. Extensive and detailed research yielded information that indicated an unmistakable departure from the anticipated MAXWELLian distribution. By means of analytic methods described in detail in Sect. 26, it was possible to show that, over a very wide range in activation and in temperature, the empirical equation given as Eq. (26.8) and discussed in Sect. 26, was an excellent representation of the data. This result is illustrated by Fig. 36, which is a composite of electron energy distributions for 9 states of activation which covered a very wide range of emission capabilities. The test temperature was 1160° K.

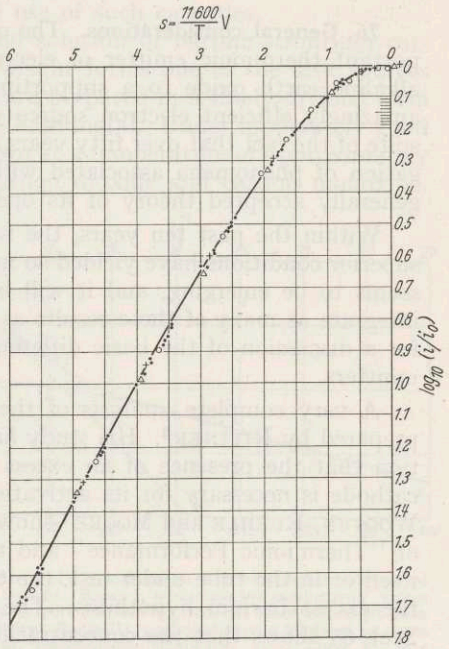

Fig. 36. Composite of the electron energy distributions observed by NOTTINGHAM for nine states of activation. Circle, $\vartheta = 0.032$; Cross, $\vartheta = 0.18$; Triangle, $\vartheta = 0.9$. Other states of activation not identified. Solid line computed with $\omega = 3.05 \times 10^{-20}$ joules or 0.191 ev. i_0 = current at zero-field. $T = 1160°$ K.

The extent of this deficiency in slow electrons is best illustrated by the curves of Fig. 4, which apply to three selected temperatures. The statement has been made by HERRING and NICHOLS[2] that the observed deficiency in slow electrons can be accounted for on the basis of a hypothetical distribution of nonuniformities. In reply to this suggestion, it may be stated that it seems highly improbable that a single sample of thoriated filament wire in so many different states of activation would have effectively the same distribution of nonuniformity and furthermore, that all samples investigated with the same degree of care as the one under present discussion show the same energy distribution. All that can be said is that all of the known data at present capable of giving an answer to this question of the electron energy distribution yield the same answer and further more, this answer is in excellent agreement with HUTSON's data, discussed in Sect. 72.

The influence of patches and the details of their development can be studied by observing the thermionic emission with an accelerating field. Typical data covering this phase of the subject are given in NOTTINGHAM's paper. The most significant conclusion that can be drawn from these studies is that although the long-range forces between the parallel dipoles formed by the adsorption of thorium atoms are repulsive forces, the experimental evidence indicates that there are strong, short-range attractive forces which permit patch areas of large

[1] W. B. NOTTINGHAM: Phys. Rev. **49**, 78 (1936).
[2] C. HERRING and M. H. NICHOLS: Rev. Mod. Phys. **21**, 185 (1949).

groups of thorium atoms to accumulate together and form local regions of high thorium density separated by regions of very low density. In other words, the "surface phase postulate" of LANGMUIR that "all the properties of an adsorbed film on an underlying surface of given composition are uniquely determined by ϑ and T" is not fulfilled with thorium and, in all probability, is not as perfectly satisfied for cesium on tungsten as TAYLOR and LANGMUIR[1] thought.

IV. The oxide-coated cathode.

76. General considerations. The oxide-coated cathode is by far the most important thermionic emitter of electrons. The fact that the application of an alkaline earth oxide to a supporting metallic conductor converted it into an amazingly efficient electron source was discovered in 1903 by WEHNELT[2]. In spite of the fact that over fifty years of research have been applied to the investigation of phenomena associated with the oxide cathode, a comprehensive and generally accepted theory of its operation has not been developed.

Within the past ten years, the results of many researches carried on under superior conditions have yielded so much new material that a fairly clear picture seems to be emerging, and it will be the purpose of the following sections to integrate as many of these results as possible into a unified theory. See Sect. 69 for a discussion of the basic difference between the oxide emitter and metallic emitters.

A very complete analysis of the chemistry of the oxide cathode has been prepared by RITTNER[3]. His study has been made with the background assumption that the presence of an excess of barium within the crystal of the oxide cathode is necessary for its activation. In spite of the fact that the results of WOOTEN, RUEHLE and MOORE[4] show no correlation between their measurements of "Thermionic Performance" and the free barium found either in the coating itself or in the tube under test, the theory to be presented here also depends on the excess barium hypothesis. The application of the equations developed in Sect. 65 shows that the concentration of excess barium need not be more than a few parts per million and that a variation in this concentration has a more direct bearing on the temperature coefficient of the true work-function than it does on the work-function derived as an empirical constant from the RICHARDSON formula (see Sect. 81).

RITTNER's analysis of the chemistry of the oxide cathode shows that pure nickel reacts with barium and strontium oxide to such an extremely small extent that it is the impurities intentionally introduced into the nickel base that are are the most efficient reducing agents in practical cathode nickel to develop and maintain the needed excess barium. It would carry this discussion too far afield to go into all the details of the thermo-chemistry involved. It must be summarized simply by stating that reducing agents such as aluminum, silicon, magnesium and titanium are favored in practical applications. Good production procedure demands a combination of elements so that the initial activation can proceed rapidly and possibly exhaust a strongly acting reducing agent such as

[1] J. B. TAYLOR and I. LANGMUIR: Phys. Rev. **44**, 423 (1933). — I. LANGMUIR: J. Amer. Chem. Soc. **54**, 2798 (1932).

[2] A. WEHNELT: Verh. dtsch. phys. Ges. **5**, 255, 423 (1903). — Ann. Phys. **14**, 425 (1904).

[3] E. S. RITTNER: Philips Res. Rep. **8**, 184 (1953).

[4] L. A. WOOTEN, A. E. RUEHLE and G. E. MOORE: J. Appl. Phys. **26**, 44 (1955). — L. A. WOOTEN, G. E. MOORE and W. G. GULDNER: J. Appl. Phys. **26**, 937 (1955). — G. E. MOORE, L. A. WOOTEN and J. MORRISON: J. Appl. Phys. **26**, 943 (1955).

magnesium within the first few hours of cathode operation. The excess barium thus produced would soon leave the crystals in the course of life unless some slower process of BaO reduction continued the maintenance of the required excess barium concentration. Silicon and titanium alloyed into the base nickel seem to serve this function. An excessive use of silicon results in the development of an interface layer identified by x-ray analysis[1] as barium ortho-silicate. Although the formation of the compound results in the liberation of barium, the interface thus developed may have an extremely high resistance which is in general very objectionable in the practical use of such cathodes.

Practical experience teaches that a solid solution of barium-strontium carbonate in proportions close to 50—50 by weight forms one of the best sources for oxide cathode material. These crystals are prepared in a finely divided form mixed with a binder and sprayed on to the base metal. Under moderately good vacuum conditions the carbonate breaks down at a temperature of approximately 1200 to 1300° K with the evoluation of carbon dioxide and carbon monoxide. The most detailed descriptions concerning manufacturing procedure available in the literature are given by HERRMANN and WAGENER[2]. Even though the discussion and details given in that book are very helpful, it must be recognized that manufacturers of oxide cathodes have developed the art as it applies particularly to their own environment and generally maintain their procedures as "company confidential".

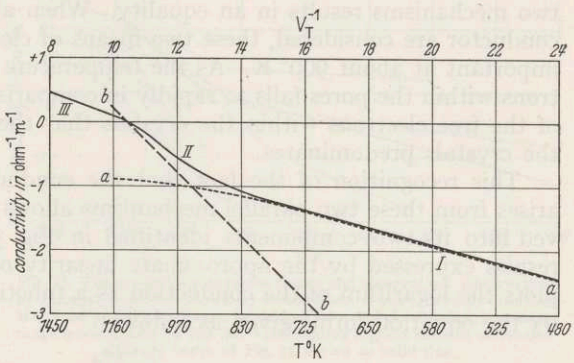

Fig. 37. Conductivity of a typical barium-strontium coating as computed by theories of Sect. 65. Range I, semiconductor conductivity within crystals. Range II, pore conductivity becomes more important than crystal conductivity. Range III pore conductivity inhibited by space charge. Curve *aa*, semiconductor conduction alone, Curve *bb*, pore conduction alone without space charge.

77. General discussion of the electrical properties of the coating. LOOSJES and VINK[3] were probably the first to present the most acceptable generalized description of the electrical properties of an oxide coating. Their description and data apply more specifically to the uniform and regular features of the coating than they do to the distorted and complex situations associated with cathodes in which a non-uniform distribution of the donor centers exists. The maintenance of high electron emission currents always develops some nonuniformity in the coating because of the high internal electric field. With well-activated coatings the internal field within the semiconductor coating is often so small as the electron current is drawn that the ionic flow of the impurity center in the presence of this field can be neglected. Although it will be necessary to discuss the evidence which is directly related to the properties of cathodes with a nonuniform distribution of donors, it will be best to postpone that complication until after the basic properties have been described.

The conductivity characteristic of an oxide cathode may be divided into three ranges, which are identified in Fig. 37 by the numbers I, II and III. The

[1] A. S. EISENSTEIN: Adv. Electronics **1**, 24 (1948).

[2] G. HERRMANN and S. WAGENER: The Oxide-Coated Cathode, vol. 1. London: Chipman & Hall 1951.

[3] R. LOOSJES and H. J. VINK: Philips Res. Rep. **4**, 449 (1949).

very low temperature range (I) is dominated by the mechanism of electronic conductivity through the solid structure of the crystalline semiconductor of which the coating is made. In parallel with these conducting paths through the crystals and their contacts with each other is a second means of conduction. This additional mechanism is the conduction by electrons which can escape from the crystalline surfaces into the pores between crystals and thus carry current by the unimpeded flow of the electrons across the pores. Approximate expressions for the electron mobility associated with these two mechanisms were presented as Eqs. (65.8) and (65.18). These formulae show that, if the average free-flight distance of an electron in a pore is three microns, then at 1000° K the mobility of an electron in the pore is well over 16000 times greater than the mobility for electrons in the crystalline solid. It will be shown that, at about 1000° K the expected ratio of electron density in the pore compared to that of the free electrons within the crystal is also about 16000 to one but in the reverse manner such that the product of the mobility and the electron density for these two mechanisms results in an equality. When all of the properties of a porous conductor are considered, these two means of electrical conductivity are equally important at about 900° K. As the temperature is lowered, the density of electrons within the pores falls so rapidly in comparison with the decrease in density of the free electrons within the crystals that the semiconducting mechanism of the crystals predominates.

This recognition of the fact that the conduction over the ranges I and II arises from these two parallel mechanisms allows the observed curve to be resolved into its two components identified in Fig. 37 as *aa* and *bb*. The empirical results expressed by the approximate linearity of these two components as one plots the logarithm of the conduction as a function of $(1/T)$, can be represented by the equation forms given as follows:

$$\sigma_A = a_A \mathrm{e}^{-\frac{e\Phi_A}{kT}} = a_A \mathrm{e}^{-\frac{\Phi_A}{V_T}}, \tag{77.1}$$

$$\sigma_B = a_B \mathrm{e}^{-\frac{e\Phi_B}{kT}} = a_B \mathrm{e}^{-\frac{\Phi_B}{V_T}}. \tag{77.2}$$

These equations are of exactly the same form as a simplified thermionic equation first presented as Eq. (9.1). They also serve the same purpose which was to yield two numbers by which a set of observation data points can be correlated. When the basic electronic mechanism responsible for the conduction behavior can be identified, the generalized conversion equations of Sect. 50 are most useful.

The empirical constants Φ_A and Φ_B are expressed in energy units of "electron volts". By analogy with certain chemical reactions, these quantities have often been referred to as "activation energies". In view of the detailed theory already presented in Sect. 65, it is to be expected that the activation energy Φ_B could very well be identified as the work-factor associated with the surfaces of the pores. More details on this point are given in Sect. 86. In order to relate the activation energy Φ_A to such details of a specific electronic conductor as the donor concentration and energy level, it is necessary to identify the conducting mechanism. If it is that of conduction through the N-type semiconductor, the equation form given as Eq. (65.11) is the best one to use. In the low temperature range, experiment can give a good value of Φ_A for conduction through the crystalline structure, and since Eq. (65.11) involves the temperature in a manner such that $\nu = -\frac{3}{4}$, then Eq. (50.11) may be applied to evaluate the location of the donor level. The result is given as follows:

$$E = -2\left[\Phi_A + \tfrac{3}{8}(V_n + V_m)\right]. \tag{77.3}$$

In this equation the highest temperature of the range over which Φ_A has been evaluated is V_n in its electron volt equivalent and the lowest temperature of the range is V_m in the same units.

Conduction curves which have all of the characteristics of the calculated curve shown in Fig. 37 by the solid line have been observed[1] with oxide cathodes. Fig. 38 presents the experimental data of two of these observers and the theoretical curve of Fig. 37 is superimposed. A reader familiar with the difficulty associated with the experimental determination of the conductivity of the oxide coating as a function of temperature will not be surprised at the relatively large differences in the experimentally determined characteristics, and he will recognize that the theoretical curve shown is in satisfactory agreement with the experimental determinations. It is therefore in order to explain in considerable detail the model on which the theoretical curve depended so that the necessary precautions may be taken to avoid the drawing of unwarranted conclusions from experimental data.

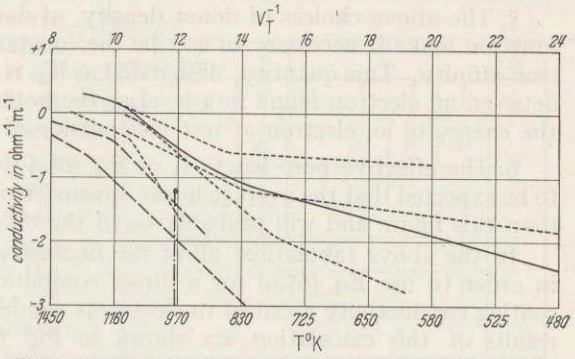

Fig. 38. The comparison between theory and observation. Observations by Loosjes and Vink shown by dotted lines. Observations by Hannay, MacNair and White shown by dashed lines and the dot-dash line shows range covered also by Fig. 40. Circle shows highest state of activation. Theory curve of Fig. 37 shown as solid line.

The theoretical calculations for the curves in Fig. 37 assume properties of the oxide coating structure tabulated as follows:

1. The oxide coating is a porous structure of small crystallites in contact with each other to give an average density of approximately 50% of that which would be obtained for the solid crystalline structure of the composition used. Thus the total volume of the pores is approximately one-half of that of the coating as a whole.

2. The conductivity and the emission properties are to be computed on the basis that the electrons are in thermal equilibrium with a concentration of donors of 5×10^{22} per m.^{3} located at an energy level 0.7 ev negative with respect to the bottom of the conduction band.

3. At very low temperatures, the conductivity of the coating is attributed to the electronic conductivity of the crystals only, since the concentration of electrons in the pores between the crystals is completely negligible in that temperature range. This conductivity for the actual coating will be taken to be a factor of 10 lower than that computed by the theory for this system of donors in order to correct for the fact that the true average cross-sectional area of the conduction paths will be reduced because of the presence of the voids and because of the fact that the crystals will make contact with each other over surface areas small compared with the crystal cross-sections. In addition, the conduction paths will be longer because the electrons will have to follow devious routes. It is not possible to evaluate these corrections separately and therefore they are all lumped together and approximated by this factor of 10. This factor was introduced into the theoretical equations as C_s of Eq. (65.9).

[1] R. Loosjes and H. J. Vink: Philips Res. Rep. **4**, 449 (1949). — N. B. Hannay, D. Mac Nair and A. H. White: J. Appl. Phys. **20**, 669 (1949). — R. Forman: Phys. Rev. **96**, 1479 (1954). — J. R. Young: J. Appl. Phys. **23**, 1129 (1952). — J. Nakai, Y. Inuishi and Y. Tsung-Che: J. Phys. Soc. Japan **10**, 437 (1955).

4. A measurement of the temperature coefficient of the contact difference in potential, to be described in more detail in Sects. 81 and 83, served to establish the magnitude of the donor density to be associated with a well-activated oxide cathode. It must be assumed that a slightly higher density is to be found close to the interior surfaces of the pores. Since the exact density actually located there in an experimentally observable structure of the oxide cathode is unknown, it is assumed that the temperature coefficient of the true work-function at the surfaces of the pores and averaged over the important temperature range is (6.3). This coefficient (α) is defined in the units described by Eq. (65.21). The value of φ_0, associated with that same equation is taken as 1.05 ev and may very legitimately be compared with tabulated values of the RICHARDSON work-function as observed and reported in the literature for well-activated oxide cathodes.

5. The above choices of donor density, of donor energy level and true work-function make it necessary to ascribe the constant value of 0.875 ev to the electron affinity. This quantity, designated as W_a, is defined as the energy difference between an electron found in a level at the bottom of the conduction band and the energy of an electron at rest just outside of the emitting surface.

6. The effective pore length l_p of Eq. (65.17) is taken as 2.5×10^{-6} m. It is to be expected that the average linear dimension of the pore will be slightly greater than this figure and will probably be of the order of 3 to 3.3 microns.

In the above tabulation, all of the necessary quantities have been specified in order to use Eq. (65.9) for a direct computation of the contribution to the coating conductivity ascribed to electronic conduction through the crystals. The results of this calculation are shown in Fig. 37 by curve *aa*. A comparison between this calculated curve and the composite curve shows that over the range of temperature below 725° K conductivity is entirely dominated by this component. Note that curve *aa* is not a straight line and when it is combined with the conductivity component attributed to the pores, the apparent straight line range extends to higher temperatures. Note also that the "activation energy" Φ_A for the temperature range identified as the LOOSJES-VINK range I is 0.315 ev. The conversion formula given either as Eq. (77.3) or Eq. (65.16) permits the evaluation of the energy level of the donors to be 0.7 ev.

As the temperature increases, range II is clearly evident. LOOSJES and VINK in their analysis extrapolate linearly from range I and deduce what they consider a suitable representation of pore conductivity by analysis of the difference between the actually observed curve and the extrapolated straight line. It is evident from Fig. 37 that theory indicates a curve for the range *aa* instead of a straight line and therefore over region II the conductivity of the electrons through the pores plays a still more important part than was attributed to it by LOOSJES and VINK. Eq. (65.26), derived from theoretical considerations and with the constants called for in the tabulation above, serves as the means for the calculation of the pore conductivity as shown in Fig. 37 by the line *bb*. Note that a line drawn tangent to the composite curve in the range II would have yielded an apparent activation energy of 0.84. This value, it will be noted, has no obvious significance at all. If the correct procedure is followed, however, of establishing the location of line *bb* by subtracting the contribution really due to conduction through the crystalline structure, then the "activation energy" associated with this line is 1.14 ev. Eq. (65.27) furnishes the means by which this activation energy can be converted to obtain the correct value of φ_0.

It is more difficult to obtain precision in a theoretical calculation that applies to range III. It is easy to make use of Eqs. (65.20), (65.22) and (65.23) to establish

certain limits for the conductivity expected in the pores after space charge within them becomes an important limiting factor. The curve shown in Fig. 37 has been drawn to fall more or less midway between those computable limits. Again, it is possible to calculate a so-called "activation energy" for this range and the value obtained is 0.43 ev. This result is in good agreement with the values reported by HANNAY, MACNAIR and WHITE. This reduced rate of increase in conductivity with temperature is the result of the building up of space charge within the pores and the shortening of the time of free flight. The term "activation energy" has no physical significance under these conditions except to express that rate as an empirical constant.

An analysis has been made of the electronic structure of barium oxide by HENSLEY[1]. His energy level diagram is shown as Fig. 39. It is to be noted that he does not include a donor state nearer to the conduction band than 1.4 ev. Practically all experiments on the conductivity of well-activated oxide cathodes show "activation energies" for the low-temperature range between 0.25 and 0.4 ev. The analysis presented here in Sect. 65 indicates that there must therefore be a donor state close to 0.7 ev below the conduction band. The presence of this state may be difficult to establish by methods that are completely independent of thermionic studies since the important concentration range for this donor state lies below a few parts per million. It is probable that the presence of other states such as those shown by HENSLEY is indicated by the higher values of activation energy associated with poorly activated cathodes.

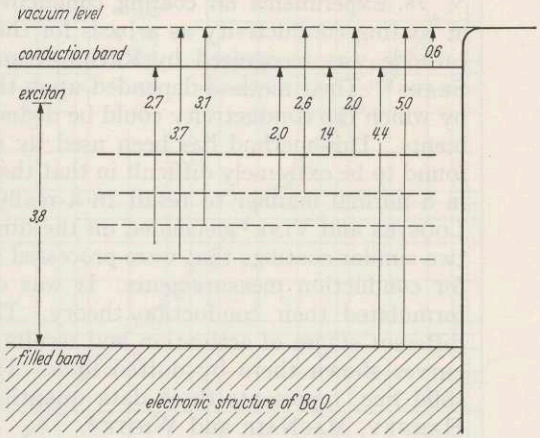

Fig. 39. Energy level diagram for barium oxide as prepared by HENSLEY. Energies expressed in ev.

It has not been possible to establish unambiguously the nature of the important donor center. The choice seems to be either it is an oxygen vacancy or an interstitial barium atom. Experiments on electron emission which are interpreted in terms of the local depletion of the donor concentration have been interpreted by FROST[2] to indicate that the activation energy for the diffusion process of the donor is about 0.4 ev. Since this energy is so low and the concentration of donors needed for activation so small, it seems quite likely that an electron in an oxygen vacancy may be the important donor level. The resolution of this problem of donor identification will probably have to depend on a theoretical analysis of the properties of excess barium as it is incorporated into the crystal in this way.

Although most of the conduction properties of oxide cathodes are accounted for quantitatively by the application of the LOOSJES and VINK model of the porous conductor, the experimental observation of electron mobility as a function

[1] E. B. HENSLEY: Report on the M. I. T. 15th Annual Conference on Physical Electronics, Cambridge, Mass., p. 18, 1955.

[2] H. B. FROST: Transient Changes in Oxide Cathodes. ScD Thesis, M. I. T. 1954; also H. B. FORST: Report on the M. I. T. Annual Physical Electronics Conference, Cambridge, Mass., p. 1, 1955.

of temperature as reported by FORMAN[1] contributes additional facts in favor of this model. The direct observation of mobilities through the interpretation of conductivity combined with the measurement of the HALL-effect emf is subject to many difficulties. The observed value of mobility over the high-temperature range was about 30 m.^{2} per v-sec. With FORMAN's estimated mean-free path within the pores of his test sample as 10 microns, Eq. (65.18) gives a mobility anticipated for the pore conduction model of about 10 m.^{2} per v-sec. at 1000° K. This direct observation of electron mobility in the high-temperature range and its corresponding fall to much lower values as the temperature is lowered serves as strong evidence in favor of the LOOSJES and VINK pore-conduction hypothesis. A very high magneto-resistive effect has also been observed by FORMAN in oxide cathode test samples.

78. Experiments on coating conductivity. The importance of measurements of coating conductivity as a basis for the development of a theory of the oxide cathode was recognized by REIMANN and MURGOCI and also by BECKER and SEARS[2]. Their method depended upon the imbedding into the coating of probes by which the conductivity could be deduced from potential and current measurements. This method has been used by many other investigators and has been found to be extremely difficult in that the processed coating very seldom activates in a normal manner to result in a really active cathode. The method used by LOOSJES and VINK[3] depended on the direct measurement of conductivity across two similar coatings that were processed in a normal manner and pressed together for conduction measurements. It was on the basis of these results that they formulated their conduction theory. They made observations on coatings in different stages of activation and results are summarized in Fig. 38 by the three curves shown there by dotted lines. The theoretical curve, shown there as a solid line, represents these data quantitatively better than it does the data of HANNEY, MACNAIR and WHITE[4].

These experimenters developed a tube of unusual design in which the oxide coating was deposited upon a magnesium oxide base which, in turn, was heated by an internally located tungsten heater. Four electrical connections were made to the coating by means of platinum wires mounted in grooves cut in the ceramic. These wires served as connections and potential leads so that the conductivity could be measured by the observation of the drop in potential over a well-defined length of the coating of about one centimeter. Since the coating could not be activated in the usual manner, a heat treatment in an atmosphere of methane served as a reducing agent to bring about activation. Many observations were made at a standard temperature of approximately 970° K and the conductivity was found to vary over three orders of magnitude as it depended on the activation and aging process. These points are represented by the vertical dot-dash line of Fig. 38. The most favorable state of activation reported gave a conductivity of 6×10^{-2} ohm^{-1} m.$^{-1}$. This state of activation is represented by the circle shown in the figure. In view of the difficulty of accomplishing full activation by this process, it is not surprising that the observed maximum conductivity is approximately a factor of four below that obtained by LOOSJES and VINK at the same temperature.

[1] R. FORMAN: Report on the M. I. T., Annual Physical Electronics Conference, Cambridge, Mass., p. 10, 1955; and Phys. Rev. **96**, 1479 (1954).

[2] A. L. REIMANN and R. MURGOCI: Phil. Mag. **9**, 440 (1930). — J. A. BECKER and R. W. SEARS: Phys. Rev. **38**, 2193 (1931).

[3] See ref. 1, p. 117.

[4] See ref. 1, p. 117.

In addition to the extensive measurements made at 970° K, others were made over the high temperature range extending up to about 1400° K. These results are summarized by the dashed lines of Fig. 38. The indications are that the coating material was not fully activated at the 0.7 ev donor level and therefore because of the high temperature coefficient of the work-function, the conductivity in the pores of the structure was low, and the electronic conductivity in the crystals also sufficiently low so that it did not show its contribution over the range of temperature studied . In spite of this lower state of activation, clear evidence exists in these studies for the space-charge limitation on conductivity as the temperature increases above 1160° K.

In addition, HANNAY, MACNAIR and WHITE [1] measured electron emission at the same temperature of 970° K at which conductivity measurements were made as mentioned above. Under all conditions that corresponded to a uniform distribution of activating centers throughout the specimen, exact proportionality existed between conduction and emission and the results are reproduced here as Fig. 40. Although HANNAY, MACNAIR and WHITE interpreted their results to prove that in their experiments the conductivity through the crystalline structure was more important than the conductivity through the pores, it will be shown in Sect. 86 that their constant proportionality factor between emission current and conductivity is in satisfactory agreement with the one computed from the theories presented here. It will then be shown that these experiments do not conflict with the pore conduction model of the oxide cathode.

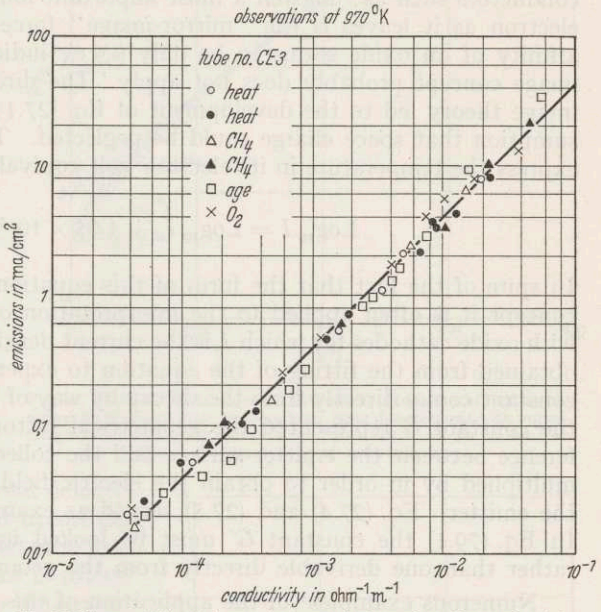

Fig. 40. Linear relation between electron emission and coating conductivity as observed by HANNAY, MACNAIR and WHITE at 970° K.

79. An analysis of emission current measurement methods. Not only is the theory of the oxide cathode a very controversial subject, but an equally unresolved problem is that of the evaluation of cathode-electron emission. It will be the purpose of this section to review some of the more important methods of cathode emission evaluation and discuss the basic principles which must be considered in the interpretation of data obtained by the various laboratory procedures used. Although references will be made to specific examples of the uses to which these various methods have been put, the references to these examples will, of necessity, be very limited.

Five methods of emission evaluation will be described. These methods are tabulated as follows and will be discussed in that order

1. SCHOTTKY plot (*dc* or pulse method) and RICHARDSON plot evaluation;
2. Deviation form the $\frac{3}{2}$ power space charge line;

[1] See ref. 1, p. 117.

3. Analysis of retarding potential data and the use of FOWLER's equation;

4. Indirect methods including harmonic analysis and changes in transconductance;

5. Voltage current characteristics with a detailed evaluation by space-charge theory.

The theory applicable ot the SCHOTTKY concept that the work-function of an electron emitter is reduced through the application of an external field was discussed in detail in Sect. 27. This theory depended on the fact that for good conductors such as tungsten a most important long range force that acts on an electron as it leaves is the "mirror-image" force. The fact that the electron affinity of an oxide seems to be only 0.9 ev indicates that the simple mirror-image concept probably does not apply. The direct application of the mirror-image theory led to the development of Eq. (27.13) which depended on the assumption that space charge could be neglected. This equation reformulated to express the temperature in its electron volt equivalent (V_T) is written as follows:

$$\mathrm{Log}_{10} I = \mathrm{Log}_{10} I_0 + 1.65 \times 10^{-5} \frac{G'^{\frac{1}{2}}}{V_T} (V_c)^{\frac{1}{2}}. \tag{79.1}$$

In spite of the fact that the form of this equation depends on the mirror-image concept it is often applied to the interpretation of experimental data observed with oxide cathodes for which I is the current density, I_0 is an empirical constant obtained from the fitting of the equation to experimental data. The numerical constant comes directly from the theory by way of Eq. (27.13). In that equation, the constant G represented the geometrical factor by which the potential difference between the emitter surface and the collector surface (V_c) needed to be multiplied by in order to obtain the electric field intensity near the surface of the emitter. Eq. (27.4) and (27.5) served as examples for the calculation of G. In Eq. (79.1) the constant G' must be looked upon as an empirical constant rather than one derivable directly from the geometry.

Numerous examples[1] of the application of this equation to emission currents from oxide cathodes lead to the result that G' is always larger than the true geometrical constant G by a factor of 3 to 10. At least four factors contribute to this lack of agreement between G' and G. First, the surfaces of most examples to which this equation has been applied have many sharp points and edges that correspond to the sintered crystallite structure of which the cathode surface is made. Secondly, the very low work-function areas which at a given temperature contribute a large fraction of the observed emission current do not experience a uniform field over the whole emission area and therefore no one simple geometrical factor can be applied. Furthermore if these surfaces are within pores their emission may be space-charge limited within such localized areas. Thirdly, in the neighborhood of low work-function areas the surrounding high work-function areas inhibit the emission because of the local contact difference in potential field and this effect is reduced as the field is increased. Fourth, the mirror-image concept may not apply.

In view of the above restrictions, the method by which Eq. (79.1) is usually applied involves the plotting of $\mathrm{Log}_{10} I$ as a function of $V_c^{\frac{1}{2}}$ or better yet, as a function of $(V_c^{\frac{1}{2}}/V_T)$. The advantage in the second choice is that if the value of G' remains constant as the temperature is varied then the slopes of the plotted

[1] C. S. HUNG: J. Appl. Phys. **21**, 37 (1950). — T. ARIZUMI and S. NARITA: J. Phys. Soc. Japan, **6**, 118 (1951). — J. NAKAI, Y. INUISHI and Y. TSUNG-CHE: J. Phys. Soc. Japan, **10**, 437 (1955). — L. S. NERGAARD: RCA-Rev. **13**, 464 (1952).

curves will all have the same value or vary in a systematic way as for example, in the experiments of HUNG[1]. With either method of plotting, the observed currents invariably fall below the line represented by Eq. (79.1) as the applied voltage is lowered. Typical data are illustrated in Fig. 41. In some examples departure from the straight line results from the influence of space charge, whereas in other examples where the observations are made at such a low temperature that space charge cannot possibly influence the result, the departure from the straight line is attributed to "patch effect", that is, a lack of homogeneity of the emitting surface.

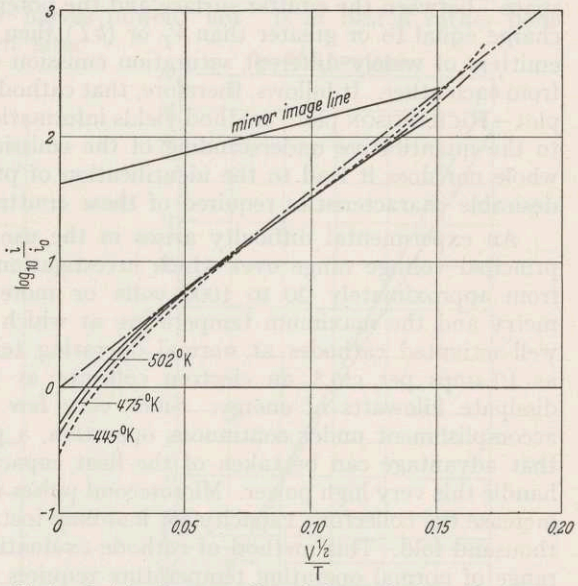

Fig. 41. Emission from an oxide cathode as a function of field as observed by HUNG at three temperatures. Note disagreement with mirror-image slope and other evidence for patch effect. Slope of dot-dash line is 3.1 times slope of SCHOTTKY line.

The straight line extrapolation from the high voltage range in spite of the obvious departure serves to establish the empirical value of I_0 which in turn is often taken to be the "zero-field" current density appropriate for further analysis according to the RICHARDSON or the FOWLER equation. An example of such a plot is shown in Fig. 42. This plot serves to determine the two other empirical constants A_R and φ_R or A_F and φ_F.

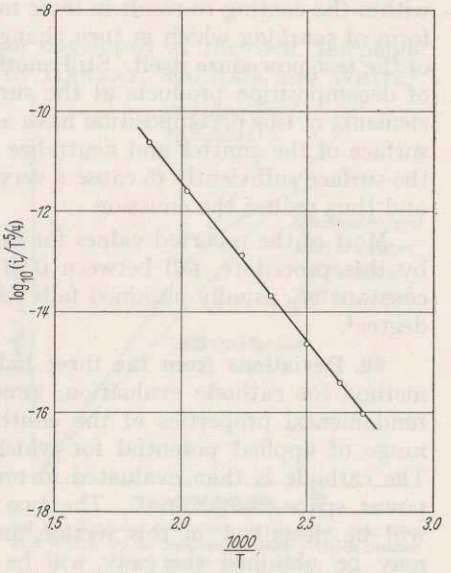

Fig. 42. Empirical representation of HUNG's observations as fitted to the FOWLER equation. $\varphi_F = 1.25$ ev.

Basically this method of analysis yields four empirical constants by which the emission properties of the particular cathode under investigation can be described in the high field region by the RICHARDSON type of equation given as Eq. (50.2) or the FOWLER Equation (64.22) and the SCHOTTKY form given as Eq. (79.1).

Although this method of data analysis has been used more extensively than others it has not been successful as a means for distinguishing between cathodes as they are used and therefore does not serve as a reliable method of emission evaluation. The objections to this method of cathode study deserve some elaboration. Most applications of oxide cathodes involve their use under the condition that the emission is limited by space charge. The theory presented in Sect. 58

[1] See ref. 1, p. 122,

shows that if the electron emission under all conditions of normal tube operation is adequate to maintain a potential difference across the "emitter space" between the emitter surface and the potential minimum created by space charge equal to or greater than V_T or (kT) then in terms of tube performance emitters of widely different saturation emission capability are indistinguishable from each other. It follows, therefore, that cathode evaluation by the "SCHOTTKY plot—RICHARDSON plot" method yields information which is neither well adapted to the quantitative understanding of the emission process of the cathode as a whole nor does it lead to the identification of processes most likely to give the desirable characteristics required of these emitters in practical applications.

An experimental difficulty arises in the use of these methods because the principal voltage range over which investigations must be carried out extends from approximately 20 to 1000 volts or more depending on the tube geometry and the maximum temperature at which the test is to be made. Since well-activated cathodes at normal operating temperatures can yield as much as 10 amps per cm.^{2}, an electron collector at 1000 volts may be required to dissipate kilowatts of energy. Since very few structures are capable of this accomplishment under continuous operation, a pulse method of test is used so that advantage can be taken of the heat capacity of the collector in order to handle this very high power. Microsecond pulses repeated thirty times per second increase the collector's capacity for handling instantaneous power by over thirty thousand fold. This method of cathode evaluation if it is to be applied for the range of normal operating temperature requires powerful, accurately calibrated and controlled pulse equipment. To cover the entire range of study both dc equipment and pulse equipment are needed. The drawing of the needed large currents through the cathode coating creates a sufficiently high electric intensity within the coating to result in ionic migration or even cathode destruction in the form of sparking which in turn changes the properties of the emitter as a result of the test procedure itself. Still another difficulty is associated with the creation of decomposition products at the surface of the collector. The electro-negative elements of this decomposition have a poisoning effect as they condense upon the surface of the emitter and neutralize the effectiveness of the donor centers near the surface sufficiently to cause a very objectionable change in cathode properties and thus reduce the emission.

Most of the reported values for the RICHARDSON work-function Φ_R, obtained by this procedure, fall between 0.94 and 1.1 ev. The RICHARDSON thermionic constant A_R usually obtained falls within the range 0.01 and 0.5 amp per cm.^{2}-degree^2.

80. Deviations from the three halves power line. The second most popular method for cathode evaluation, aimed principally at an understanding of the fundamental properties of the emitter, depends on observations taken over a range of applied potential for which the current is limited by space charge. The cathode is then evaluated in terms of a departure from the "three-halves power space-charge line". The two methods of analysis of data usually used will be described in this section and a critical discussion of the results that may be obtained this way will be presented. A third very closely related method not known to be in present use is described in Sect. 82.

Coordinate paper is available which has a linear scale across the abscissa and a two-thirds power scale along the ordinate. This paper is used, as illustrated in Figs. 43 and 44, by one's plotting the applied voltage along the linear scale and the corresponding observed current along the two-thirds power scale. Plots of

carefully taken observed data according to this method yield fairly straight lines as long as the current is limited by space charge, but never yield truly straight lines because the three halves power "law" is at best a rather poor approximation as will be shown later in this section.

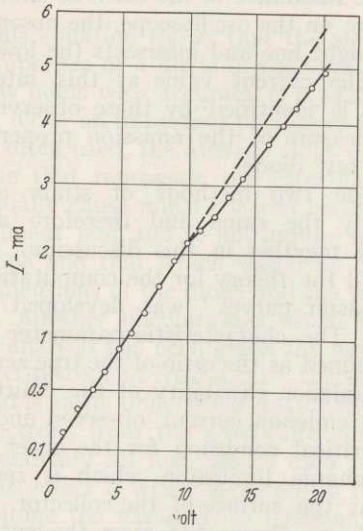

Fig. 43. Observations of NERGAARD [1] plotted on $\frac{3}{2}$ power paper illustrating distortion caused by "high-speed 10-volt effect".

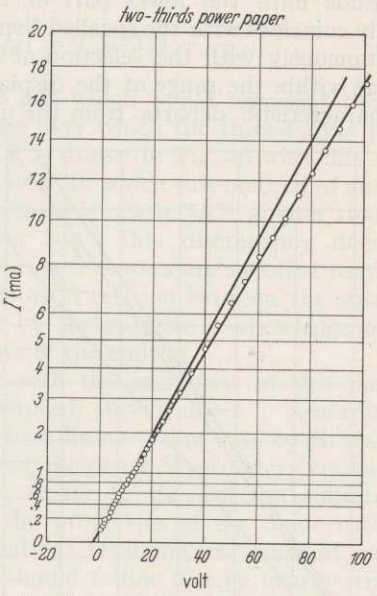

Fig. 44. NERGAARD's use of $\frac{3}{2}$ power paper with an extension into the higher voltage range.

The second method of analysis has been developed at the Bell Telephone Laboratories and is described very briefly by HANNAY, MACNAIR and WHITE [2]. Fig. 45 reproduced from that paper, serves as the best means of describing their method, which involves the following steps.

The diode under test receives a single, one-half cycle voltage pulse applied to the electron collector with respect to the emitter and derived from the 60-cycle power line. In four milliseconds, the applied potential rises to a maximum and then falls to zero in the next four milliseconds. The current, conducted through the tube, produces a small $I\,R$ drop through a calibrated resistance and after amplification is applied to an oscilloscope in a manner to make the vertical deflection of the spot an accurate measure of the current through the test diode. A special sweep circuit has been designed so that at each instant of time the horizontal deflection of the oscilloscope beam is directly proportional to the three-halves power of the applied voltage. On the

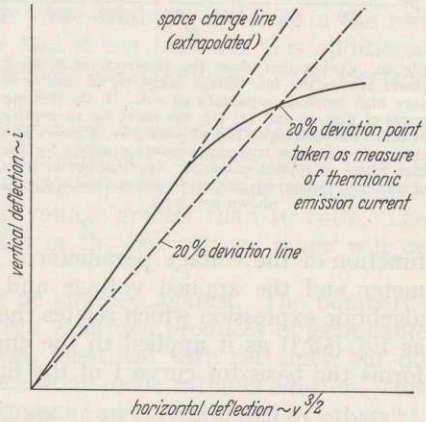

Fig. 45. Emission evaluation by HANNAY, MACNAIR and WHITE by an oscilloscope display which utilized a $\frac{3}{2}$ power voltage axis.

[1] L. S. NERGAARD: RCA-Rev. **13**, 464 (1952). Curves are reproductions of NERGAARD's, Figs. 14 and 15.

[2] See ref. 1, p. 117.

face of the oscilloscope is a ruled coordinate system that is illustrated by Fig. 45. Drawn across the coordinates are straight lines which differ in slope by 20%. The observer uses this equipment by his adjusting the horizontal deflection amplitude until the lower part of the curve produced by the electron beam exactly coincides with the socalled "space-charge line". This adjustment is made simultaneously with the selection of a suitable resistance in the cathode circuit so that within the range of the displayed figure on the oscilloscope, the observed characteristic departs from the upper straight line and intersects the lower one. The current value at this intersection is identified by these observers as a measure of the emission property of the test diode.

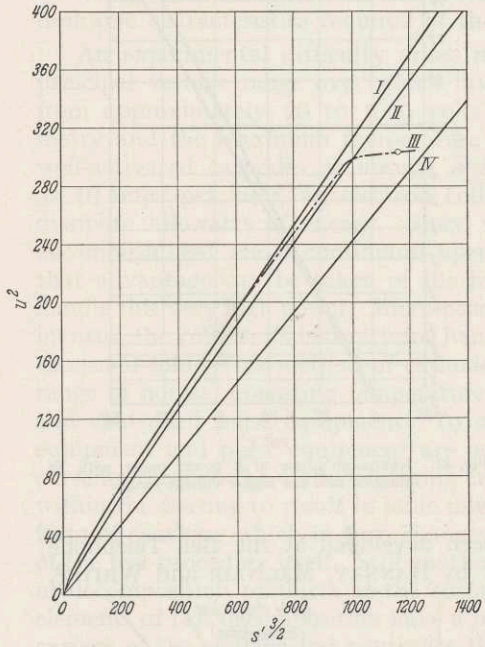

Fig. 46. Curves that show the incorrectness of the $\frac{3}{2}$ power law in the low voltage range. I, an emitter of very high emission capability $u_0^2 = \infty$; II, the limiting curve of Figs. 16 and 17; III, the curve for an emitter of finite emission capability $u_0^2 = 300$; IV, $\frac{3}{2}$ power line that represents the true space-charge equation for the high range of applied potential. Approximate location of zero-field current by 20% deviation method of Fig. 45 shown by circle.

These two methods of study are basically the same and therefore are treated together in this discussion. In Sect. 58 the theory for the computation of "master curves" was developed in detail. The characteristic parameter u_0^2 was defined as the ratio of the true zero-field emission capability of the emitter to the emission current observed under that critical condition for the onset of space-charge limitation which is zero-field at the surface of the collector. It was shown there that over the entire range of the master curves, corresponding to various values of u_0^2 from approximately 5 to infinity, they cannot be distinguished from each other until a sufficiently high accelerating field is applied to the collector to reduce the value of the space-charge minimum to V_T or less. Fig. 46 has been prepared to illustrate the application of the correct theory to the interpretation of data plotted according to the three-halves power method.

From computed data found in Tables 7, 8 and 9, three curves are plotted as a function of the voltage parameter $S'^{\frac{3}{2}}$. The precise relation between this parameter and the applied voltage and temperature is given by Eq. (57.1). The algebraic expression which relates the value of U^2 to the quantity χ_c was derived as Eq. (58.3) as it applied to the emitter of unlimited capability and therefore forms the basis for curve I of the figure. This equation is repeated as follows:

$$U^2 = \left(1 + \frac{\chi_c}{\chi_m}\right)^2. \tag{80.1}$$

The assumption that the three-halves power law will give the same emission current at very high values of applied potential is the equivalent of writing the following relation:

$$U^2 = \gamma\,(\psi_c)^{\frac{3}{2}}. \tag{80.2}$$

In this equation, the proportionality factor γ determines the slope of the line drawn between the origin of the diagram in Fig. 46 and any specified point on

line I. If it is assumed that the value of ψ_c is practically equal to S' over the important range to which this analysis is usually applied, this approximation is satisfactory. These equations may be combined with Eq. (37.8) to yield the following relation:

$$\gamma = \frac{4\sqrt{\pi}}{9} \cdot \frac{1}{(1.806)^2} \cdot \left(1 + \frac{1.413}{\psi_c^{0.475}}\right)^{\frac{3}{2}} = 0.2422 \left(1 + \frac{1.413}{\psi_c^{0.475}}\right)^{\frac{3}{2}}. \qquad (80.3)$$

This equation shows that the slope of the line which would represent the true properties of a diode in the very high range over which the three-halves power law holds with accuracy is 0.2422. Line IV is drawn in Fig. 46 with this slope.

Over an important portion of the range in S' to which this method of analysis is often used, the average slope of the *true curve* is nearly 30% greater than the line that represents the three-halves power law. This discrepancy does not usually cause much concern because many experimenters are satisfied to obtain a linear plot and to not inquire into the detailed relation between the observed slope and that which would be computed by theory from a knowledge of the dimensions of the diode and the temperature of the emitter.

Another phenomenon which interferes with the usefulness of this method of analysis has been given the name "high-speed, 10-volt effect". According to MATHESON and NERGAARD[1], this effect was first discovered in 1935 by H. NELSON and is easily understood qualitatively as being the result of secondary emission of electrons from the composite surface that exists on the electron collector of practically all test diodes used to study the properties of the oxide cathode. This effect is well illustrated by Figs. 43 and 44. Over the low range of applied voltage the variation in emission current should follow a very nearly straight line relation even though it does not have the correct slope as long as the emission is really limited by a space-charge minimum greater than V_T. In the range of applied voltage between 8 and 12 volts, slow secondary electrons are emitted from the collector and increase the space-charge in the neighborhood of the collector enough so that the observer needs to apply additional voltage to the extent of one or two volts or more in order to re-establish the field in the rest of the tube that would have existed there had it not been for this additional group of slow-moving electrons in the immediate neighborhood of the electron collector.

This effect is a property of the collector and can be expected to be different in detail from tube to tube independent of the emitter properties under investigation. It makes the application of space-charge theory to oxide emitter properties difficult to interpret with an applied voltage greater than 10 volts. The fact that very useful data may be obtained in the low-voltage range will be demonstrated in Sect. 83.

There is still another effect which must be guarded against. The bombardment of the electron collector by high-energy electrons produces objectionable decomposition products which have not been identified with certainty but do react in an unfavorable manner at the surface of an oxide cathode emitter. This effect was first reported by HEADRICK and LEDERER[2] and investigated by others[3, 4]. Even though JACOBS' identification of the reaction products is not generally accepted, practically all experiments indicate that the onset occurs at approximately 6 volts electron energy and that the lower the temperature of the emitter,

[1] R. R. MATHESON and L. S. NERGAARD: RCA-Rev. **12**, 258 (1951).
[2] L. B. HEADRICK and E. A. LEDERER: Phys. Rev. **50**, 1094 (1936).
[3] H. JACOBS: J. Appl. Phys. **17**, 596 (1946).
[4] J. D. HOBBS: M. I. T. Thesis "Energy Dependence of Electron Produced Poisoning of Oxide Cathodes". 1954.

the easier it is to detect the influence of this poisoning. The higher the electron energy, the greater is the supply of poison[1] and therefore it is possible to explain the results reported by NERGAARD[2] which indicated that the higher the temperature of the oxide cathode, the higher the energy required to produce sufficient poison to give a measurable reaction at the surface of the cathode.

The current ratio represented by the symbol u^2 was defined in Eq. (57.3). The ordinate scale in Fig. 46 is therefore essentially a current scale with the unit of current that which flows across the test diode at the specified temperature and creates zero field at the surface of the collector. In most examples, this unit of current represented by the symbol I_R is indistinguishable from the maximum current that can flow across such a diode which was represented by the symbol I_m and given quantitatively for the plane parallel diode by Eq. (51.1). The theoretical evaluation of the relation between the radial dimensions of the elements of a diode made with concentric cylinders and the "effective spacing" represented by w of Eq. (51.1) has not been worked out but experiment shows that for a ratio of radii of 2.5, the effective value of w is 0.83 mm. when the actual difference in the radii for the true spacing is 1.0 mm. (see Sect. 83). As the ratio of radii approaches one, the effective spacing should approach the true spacing. This result came from an experiment applied to the low-voltage range and seemed to be independent of the temperature. The LANGMUIR[3] formula, which would be applicable at best to the very high voltage range would give 0.68 mm. for this structure. Really accurate fittings to the theoretical curves in the low-voltage range have not been made except for studies with cylindrical structures and reported in Sect. 83. The ideal structure for the application of theory is the plane parallel one and an excellent design has been fabricated by the Bell Telephone Laboratories and is described in detail in Sect. 84. Test diodes are often made with oval electron collectors instead of cylindrical ones. Although superficially, the dependence of observed current on applied potential may follow so close to the theoretical curves over the low-voltage range that an "effective-spacing" can be established by experiment, the prediction of theory is that such a diode would be unsuitable for the general purpose of emitter evaluation except under very specialized conditions.

The equation which yields the data for the plotting of the "limiting curve" II of Fig. 46 is the combination of Eqs. (57.7) and (57.10). These equations serve as the basis for Table 7. If the experimental data are not distorted by spurious effects, then observed points should follow curve I very closely until approximately half of the maximum zero-field emission from the cathode is obtained. A very gradual deviation from curve I takes place and continues, as shown by curve III, until this curve intersects the limiting curve II. This intersection establishes the true value of the zero-field current for this particular emitter. Since the emission increases very slowly after zero-field has been established, the choice of the 20% point as is Bell Laboratory practice and illustrated in Fig. 45 and 46 is not very much in error.

81. Analysis by retarding potential data and the application of FOWLER'S and RICHARDSON'S equations. The study of thermionic emission from an oxide cathode in the transition range from retarding potentials through to accelerating potentials by HUNG[4] will be used exclusively as the basis for this discussion, since it is one

[1] See ref. 4, p. 127.

[2] L. S. NERGAARD: RCA-Rev. **13**, 464 (1952).

[3] I. LANGMUIR and K. T. COMPTON: Rev. Mod. Phys. **3**, 191 (1931) p. 245.

[4] C. S. HUNG: J. Appl. Phys. **21**, 37 (1950). For greater detail see M. I. T. Thesis, Department of Physics 1948.

of the most carefully executed studies reported in the literature. His data are shown in Fig. 47. The diode used for this study contained a cylindrical coated cathode 0.2 cm. in diameter and 4.5 cm. long concentric with a cylindrical collector system which had a central section one cm. long insulated from the rest so that the current to this collector came from the most uniform part of the emitter. The temperature of the emitter was determined by a calibrated thermocouple. The collector was movable so that evaporation products normally found on such collectors were eliminated. The ratio of the collector to the emitter diameter was four. The spacing between collector and emitter was three mm.

In Fig. 47, experimental results are compared with the solid lines which are the theoretical curves that show the rise in current as a function of applied voltage as computed for the tube geometry used. An idealized FERMI distribution of emitted electrons is assumed (see Sect. 60 and Table 10). The application of the space-charge equations indicates that over the temperature range covered the effect of space charge is negligible even very close to zero-field. HUNG's evidence is very clear that there was a deficiency of electron current at zero field and he interpreted his results on the hypothesis that a lack of uniformity of work-function over the emitting surface was responsible for this deficiency. The detailed theory of multiple reflection as it applies to a diode has been presented in Sect. 62. One of the results of that analysis was that, over a wide range in the retarding potential part of the characteristic, the shape of the curve is unaltered by the reflection effect since every observed point is reduced in current value by exactly the same fraction. Furthermore, this same fractional reduction applies also on the accelerating side [see Eqs. (62.10) and (62.11)]. Although it cannot be taken as a proof of the reflection effect, detailed calculations show that HUNG's experimental points are in excellent agreement with the curve computed by the multiple reflection equations and it is not necessary to make an ad-hoc assumption concerning patchiness to explain his results. Patch structure has a far more important influence on the emission observed with strong accelerating fields. Zero-field observations made at 563° and 610° K show still more deviation from theory which is contrary to prediction from patch theory but this result would be expected because of the space charge created by the extra multiply reflected electrons. Further evidence for this effect will be given in Sect. 83.

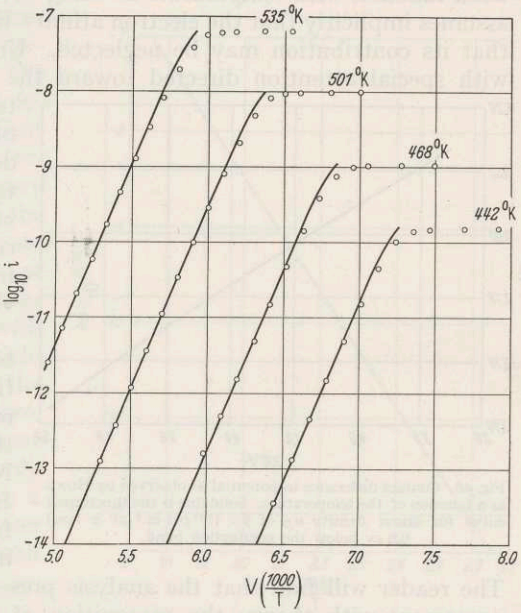

Fig. 47. Current measurements by HUNG as a function of applied potential at four temperatures. Termination of theoretical lines locates zero-field point.

If the reflection hypothesis is assumed, then the procedure used by HUNG for establishing the applied potential required to create zero field in the space between the emitter and the collector is precisely the one that should be used. His table of values of the contact potential as a function of the temperature

serves as a direct observation of the temperature change of the work-function. These results are shown in Fig. 48.

Since the change in measured current as a function of applied voltage is so rapid as the field changes from retarding to accelerating, there can be little doubt about the choice of the emission value as a function of the temperature that characterized his specimen. HUNG plotted his data in accordance with the FOWLER emission equation derived in Sect. 64 and given there as Eq. (64.22). It was shown in that section that FOWLER attributes the entire change in the work-function with temperature as being due to variation of the FERMI level and assumes implicitly that the electron affinity W_a changes so little with temperature that its contribution may be neglected. Until precise measurements are made with special attention directed toward the experimental determination of the temperature variation of W_a, it may be assumed that the electron affinity decreases very slightly as the temperature increases, but that the amount of this decrease is offset by the very considerable increase in the work-function because of the temperature variation of the FERMI level.

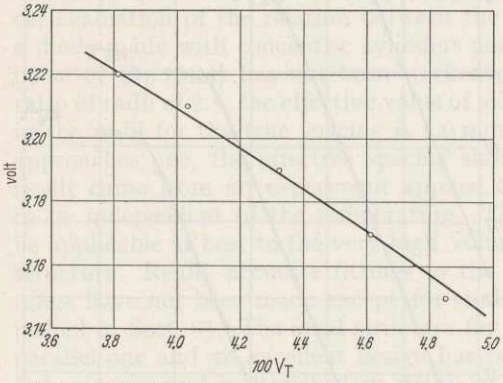

Fig. 48. Contact difference in potential as observed by HUNG as a function of the temperature. Solid line is the theoretical curve for donor density n_D of 3×10^{21} per m.^{3} at a level 0.6 ev below the conduction band.

In the analysis that follows, the basic experimental data depend entirely on the results of HUNG'S study reported in much greater detail in his thesis than in the published paper. None of this analysis was made by HUNG because he did not accept the fact that his data are in good agreement with the reflection hypothesis. The reader will find that the analysis presented here demands for its excellent agreement with theory the recognition of Eq. (62.11) as a suitable means of correcting the observed current to compute the value I_{00} which is the current density which would have been observed at zero field in the absence of any deficiency of slow electrons which Sects. 72 and 75 have shown.

The curves of Fig. 47 show that the measured emission current is very accurately represented by the theoretical curves applicable to this geometry and characterized by the temperature for each curve as measured by a calibrated thermocouple. Consistent with the theories presented in Sect. 62, the applied potential for zero field and the zero-field emission can be established with high accuracy in spite of the deviation from the theoretical non-reflection curve. The curve computed by the theory of multiple reflection does pass through the experimental points, but since the remaining part of this analysis depends only on the knowledge of the zero-field emission and the measured contact difference in potential as well as its variation with temperature, the needed data are all illustrated by Fig. 47. HUNG has reported five contact potential measurements instead of just the four shown in this figure, and zero-field emission current measurements at seven temperatures. It will be these values that are used in the rest of this analysis.

The five observed contact potential measurements of Fig. 48 are joined together by the theoretical curve which depends for its location in this figure on the emitter work-function value of 1.225 ev. This value is obtained from an analysis of the emission data according to the method described in detail later

in this section. The line also depends on the choice of a collector work-function at a temperature somewhat above room temperature of 4.629 ev. The choice of donor state concentration and its average energy level with respect to the bottom of the conduction band will be discussed.

The observations of zero-field current made by HUNG at seven different temperatures were tabulated in terms of the corresponding current densities and then, with the help of Eq. (62.11), the corresponding value of current I_{00} was calculated for each temperature. These values represent the current density which would have been observed in the absence of any reflection effect and it is this current density which is appropriate for analysis according to the FOWLER equation given as Eq. (64.25). The plot of these points is shown as Fig. 49. All of the points lie on such an excellent straight line that its slope can be determined with high accuracy. The theory which led to Eq. (64.25) established the fact that this slope yields an accurate measure of the *true* work-function at absolute zero. That is the advantage of the FOWLER equation compared with the RICHARDSON T^2 equation which, it will be shown, does not yield the *true* work-function at absolute zero, but gives one determined by a linear extrapolation which would be valid only in case the true work-function were a linear function of the temperature over the entire range. The values obtained from this experimental study are recorded in equation form as follows:

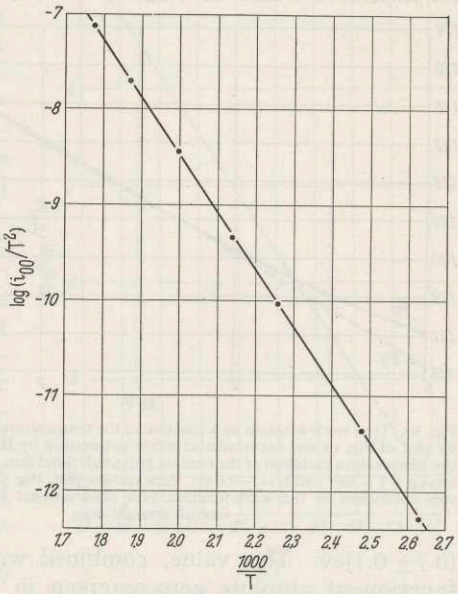

Fig. 49. FOWLER plot based on HUNG's zero-field measurements corrected for a deficiency of slow electrons indicates a true work-function at 0° K of 1.225 ev and a donor concentration n_D of 2.4×10^{21} per m.³.

$$\varphi_F = W_a - \frac{E}{2} = 1.225 \text{ ev}, \tag{81.1}$$

$$1.726 \times 10^{-5}\, n_D^{\frac{1}{2}} = (8.5 \pm 0.2) \times 10^5. \tag{81.2}$$

Note that the unit in Eq. (81.1) is the electron-volt and therefore the electron affinity W_a and the energy level of the donor E are also expressed in electron-volts instead of joules. The donor density which may be calculated directly from the result expressed in Eq. (81.2) is the following:

$$n_D = (2.4 \pm 0.4) \times 10^{21} \text{ per m.}^3. \tag{81.3}$$

This analysis yields a direct measure of the donor density which may be used in association with the theories presented in Sect. 64 to compute the location of the FERMI level at each temperature. The change in FERMI level with temperature with reference to its value at absolute zero may be computed by Eq. (64.11) written as follows:

$$\Delta\mu = \mu - \frac{E}{2} = \frac{E}{2} - V_T \ln 2 + V_T \ln\left\{\left[1 + 8\, e^{-\frac{u' + E}{V_T}}\right]^{\frac{1}{2}} - 1\right\}. \tag{81.4}$$

Although this equation gives the correct change in the FERMI level over the entire range of temperature even beyond that for which the FOWLER equation gives a perfect linear log-plot, the approximation used in deriving his equation

may be applied and the function suitable for accurate computation over the low temperature range is the following:

$$\Delta\mu = \mu - \frac{E}{2} = \frac{V_T}{2}\left[\ln 2 - \ln\frac{1.208\times 10^{28}}{n_D} + \frac{3}{2}\ln\left(V_T^{-1}\right)\right]. \qquad (81.5)$$

Since these equations were used for the computation of Table 11, the data found there for a donor density of 3×10^{21} per m.^{3} and a choice of E of -0.6 ev yielded directly the theoretical curve represented by the solid line of Fig. 50. This line represents the true work-function as a function of the temperature starting at its measured value of 1.225 ev at absolute zero and carrying through to the range of observed contact difference in potential. The points reproduced in this figure come from Fig. 48. Since the data used for this calculation came directly from Table 11 and were not recomputed for the slightly smaller donor density of 2.4×10^{21}, the fit to the data is not quite as good as it would have been if a new curve had been computed with the donor energy level taken at -0.7 ev. These data therefore place the donor energy level at (0.7 ± 0.1)ev. This value, combined with the experimental value of the work-function at absolute zero as given in Eq. (81.1) indicates an electron affinity W_a of 0.875 ev.

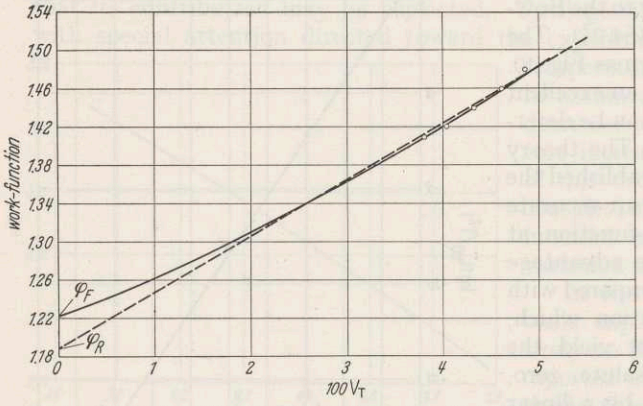

Fig. 50. True work-function as a function of the temperature with φ_F determined by plot of Fig. 49 and experimental points determined by HUNG's observation of the temperature variation of the contact potential. Solid line, the theoretical curve for $n_D = 3\times 10^{21}$ and $E = -0.6$ ev. RICHARDSON plot, Fig. 51. Average temperature coefficient of the work-function over observational range determined by dashed straight line.

Even though this analysis according to the FOWLER equation gives all of the information as a result of the very skillful and direct observation of the electron emission properties of the specimen of an oxide cathode studied by HUNG, it is important to show additional relations by carrying through the analysis according to the RICHARDSON T^2 equation. The same basic data for the emission current density I_{00}, which would have been observed in the absence of reflection, were used to form the plot shown as Fig. 51. The experimental points fall on an excellent straight line since it was demonstrated in Fig. 50 that over the range of observation the temperature variation of the work-function is dominated by the linear term and the average slope is 5.8.

The direct analysis of Fig. 51 gives the following results:

$$\varphi_R = 1.19\,\text{ev}, \qquad (81.6)$$

$$A_R = A_H e^{\left(\frac{d\varphi}{dV_T}\right)} = 3390. \qquad (81.7)$$

Note that the straight line shown in Fig. 50 starting at the RICHARDSON work-function value of 1.19 and drawn with a slope of 5.8 is in excellent agreement with HUNG's observed data on the contact potential changes of his specimen. With this relation, $(d\varphi/dV_T) = 5.8$, the value of the thermionic constant expressed

here as A_H to indicate that it applied specifically to HUNG's data is thus determined experimentally as follows:

$$A_H = 112 \times 10^4 \text{ amp/m.}^2\text{-degree}^2. \tag{81.8}$$

This value is in such excellent agreement with the theoretical value of A which is 120×10^4 amp/m.^{2}-degree^2 that there is very little room for improvement in the application of theory to experiment as it applies to these data.

This demonstration of the application of theory to experimental data should remove the doubt often expressed as to whether or not the RICHARDSON equation or the FOWLER equation should be used for the analysis of emission data as it applies to semiconductors. The answer is that both equations apply perfectly well and give different answers only in that the fundamental theories ask different questions. Thus the difference in the work-functions expressed as Eqs. (81.1) and (81.6) does not in any sense represent an error in their determination since the φ_R represents the *effective* work-function at absolute zero on the basis that a linear extrapolation from that point will give a satisfactory representation of the true work-function in the operating range. Clearly, the most convenient formula for the expression of the true work-function in the operating range as applied to this specimen is based on the RICHARDSON value and given as follows:

$$\varphi = 1.19 + 5.8 V_T. \tag{81.9}$$

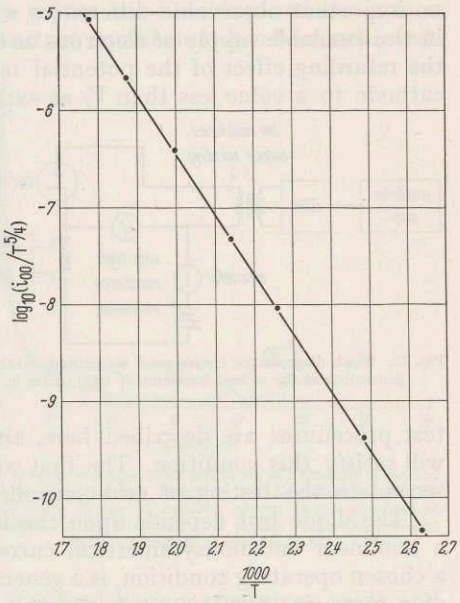

Fig. 51. RICHARDSON plot of HUNG's observations corrected for deficiency of slow electrons gives $\varphi_R = 1.19$ ev and $A_R = 3390$ amp/m.^{2}-degree^2. Combined with average temperature coefficient from Fig. 50 gives $A = 112 \times 10^4$ amps/m.^{2}-degree^2. Theory gives 120×10^4 amps/m.^{2}-degree^2.

The values of the true work-function, calculated from its basic definition ($\varphi = W_a - \mu$) by means of Eq. (64.11) and the experimentally determined value of W_a of 0.875, are in excellent agreement with those given by Eq. (81.9). Since Eq. (81.9) cannot be used for extrapolation to higher temperatures, it is only by means of Eq. (64.11) in its complete form that the *true* work-function can be computed for the whole range in temperature. With the *true* work-function known the emission current in the high range can be computed from the low range data.

Too often in the literature one finds the statement: "Thermionic emission measurements are not capable of deciding the *correct* power of T to be used in emission formulae". Such a statement confuses the issue since it is here demonstrated that it is not a matter of the correctness of the choice of the power of T for the representation but the choice must be made entirely in terms of the information desired. If the emitter is an N-type semiconductor and the range of investigation is that for which the FOWLER equation applies, then its use is appropriate and the basic information obtained rewarding. Both forms are needed for the correct analysis and use of data and *neither* should be used for the empirical representation of data since Eq. (9.1) is far more useful for the purpose.

82. Indirect methods of cathode evaluation including transconductance changes and its theory. Industrial laboratories have need for methods of cathode evaluation that are reliable and simple even though often qualitative, since their tests must apply to production tubes that serve a variety of functions. The tube types include not only simple diodes but complex multigrid structures. With very few exceptions, these practical tubes depend on the flow of electrons across the space-charge minimum for their performance to be within specification limits. Sect. 55 through 59 and especially Sect. 58 develop the application of space-charge theory to the observable emission properties of a cathode to show that no important observable differences will occur as the result of major differences in the available supply of electrons as long as the conditions of test do not reduce the retarding effect of the potential minimum created by space charge near the cathode to a value less than V_T as expressed in electron volts or kT as expressed in joules. The fundamental rule therefore the for evaluation of emission capability is that the test must involve, in one manner or another, an observation which depends upon the tube operation with the space-charge potential minimum *less* than V_T. Two specific test procedures are described here, although there must be many others that will satisfy this condition. The first will relate to the testing of diodes and the second to the testing of grid-controlled tubes.

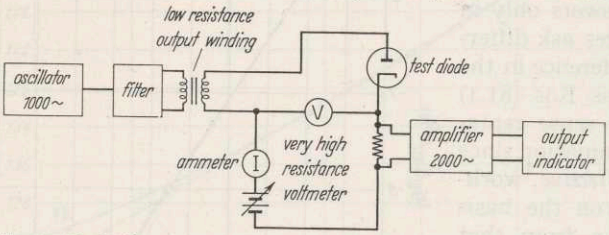

Fig. 52. Block diagram for circuit used for cathode evaluation based on the generation of the second harmonic of 1000 cycles in the test diode.

The diode test depends upon the fact that a circuit element, that has both a nonlinear and nonsymmetrical current voltage characteristic with respect to a chosen operating condition, is a generator of harmonics including even multiples of a pure sine-wave input frequency. A block diagram of the test method is indicated in Fig. 52. The diode under test can be biased to deliver an arbitrarily chosen emission current to the collector that is within the normal operating range for the diode with the current limited by space charge. The circuit provides for a modulation of this bias by a sine wave of controllable amplitude and *high purity*. Since the current-voltage relation in the diode is nonlinear and may be represented by a power series expansion, there will be a second harmonic component of current which can be amplified by means of a narrow band amplifier and the output observed on an oscilloscope or else rectified to produce a direct current proportional to the amplitude of the *second* harmonic. This signal may be observed with a meter or used to actuate a recorder. For a pre-set bias voltage, observations may be made as the temperature of the emitter is lowered. The second harmonic will decrease very slowly until the emission capability of the cathode approaches that critical value at which the space-charge minimum is equal to or less than V_T. Under this condition, the voltage-current relation becomes much more linear and the harmonic output decreases to a minimum and at the same time its phase changes. This dip in the harmonic output serves as a quick index of the fact that the space-charge minimum has decreased to the order of V_T. The heating current required to maintain this condition is a practical measure that can be related to predetermined standards. The time required for the cathode to drop in temperature after the heating power has been removed may also serve as a measure of the critical temperature. The

lower the temperature at which this minimum in second harmonic content occurs, the higher the emission capability of the cathode.

An alternate way of conducting this test requires the setting of the cathode temperature at some arbitrarily chosen value. The applied voltage v of Fig. 52 is increased gradually until the second harmonic output indicator shows a minimum. The observer may record both the critical applied voltage and the corresponding space current as well as the temperature of the emitter. This test serves as an excellent method of determining a current which is very close to the zero-field current capability of the emitter at the specified temperature. Such a test can be made as nearly automatic as desired to reduce the time required for it to a very small fraction of a second after temperature equilibrium has been achieved. With a standardized tube structure and the application of the theories presented here, tests made at two or more temperatures can be analyzed to yield quantitative data concerning many detailed properties of the emitter. Tests made at a single temperature can be used very effectively for production control.

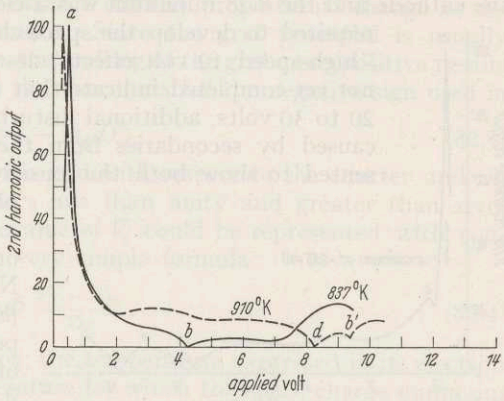

Fig. 53. Harmonic output from test diode as a function of applied volts for two temperatures. Solid line, 837° K; dashed line 910° K. Onset of space charge at collector shown at A; zero-field at emitter shown at B. Minimum at D results "high-speed 10-volt effect". Zero-field at emitter at B'.

Results that may be obtained by the use of this method of second harmonic generation can be illustrated best by the presentation of specific laboratory data. The emitter was an indirectly heated cylinder concentric with respect to a collector with a spacing of 1 mm. and a ratio of radii of 2.5. The central 12 mm. section of the emitter was coated with a standard barium-strontium oxide and on each end beyond this coating the nickel sleeve extended an additional 10 mm. The diode had been processed according to standard methods and had been operated at a temperature of 1160° K for one thousand hours with a space-charge limited current of 55 ma. Additional point-by-point data which show the voltage current properties of this diode will be presented in Sect. 83. Fig. 53 shows the second harmonic output as a function of the applied voltage for two different temperatures. These temperatures were determined by thermocouple measurements of the emitter.

With the emitter maintained at 837° K, the second harmonic was measured as a function of the applied voltage and the gain of the analyzer was adjusted to give an output of 100 units at the maximum located at 0.45 volts (see a of Fig. 53). This maximum was an accurate measurement of the applied potential at which zero gradient occurred at the collector and thus represented the onset of space-charge limitation as discussed in detail in Sect. 57. As the applied potential was made more positive, the harmonic output decreased approximately as the inverse square root of this change in potential. Over this range, the emission current increased with the applied voltage in accordance with the theoretical curves of Figs. 16 and 17. The sharp minimum (b) shown at 4.2 volts was a direct indication of the fact that the space-charge minimum had moved across the diode and was practically coincident with the emitter. The emission current observed with this applied potential was an excellent measure of the "zerofield"

thermionic emission from this cathode at this temperature. The change in potential of 3.75 volts thus observed yields additional information concerning the properties of the emitter.

As the temperature was lowered, the minimum shifted to lower values of applied potential and conversely as the temperature was raised, it moved to higher values. At each temperature, the current flow at the corresponding critical applied potential served as an excellent basis for the determination of the emission properties.

Observed data are shown for the emitter operating at 910° K and two minima are evident, with one at 8.28 volts and the other at 9.3. Detailed study showed that the 9.3 minimum is the one that characterized the emission property of the cathode and the 8.28 minimum was a clear indication of the electron energy required to develop the space-charge distortion effect known as the "high-speed 10-volt effect" described in Sect. 80. Detailed studies not yet completed indicate that at higher electron energies of about 20 to 30 volts, additional disturbances in the space-charge situation caused by secondaries from the collector appear. Fig. 54 is presented to show both the sensitivity of this method of analysis and phenomena which observers of thermionic emission must understand in order not to report misleading data. Note first the two prominent minima (*d* and *f*) at 7.6 and 9.7 volts applied potential. These are the direct result of the "high-speed 10-volt effect" and it will be noted that the location of the first with respect to the condition of zero-field at the collector occurs at exactly the same potential difference of 8 volts as that observed at the lower temperature and shown in Fig. 53. The feature of additional interest and importance is the small sharp minimum (*c*) at zero. Detailed study showed that this minimum was a direct result of the thermionic emission obtained at this temperature (1160° K) from the bare nickel parts of the emitter outside of the central section which was coated. At this temperature and this applied voltage and for all applied voltages more negative than this, the "bare" nickel part of the emitter, because of its larger area, contributed more current to the collector than the central portion. These data are presented in this brief form to stress the need for test diodes designed with guard rings or diodes that use some other method for insuring that the observed emission originates at that part of the emitter which is being investigated.

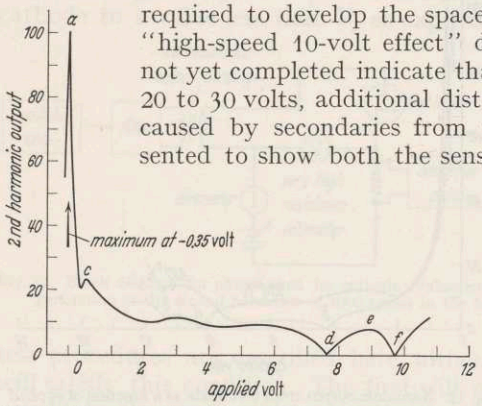

Fig. 54. Harmonic output of test diode at 1160° K. Onset of space charge with zero-field at collector at *A*. Influence of emission from uncoated nickel at *C*. Structure due to "high-speed 10 volt effect" at *D*, *E*, and *F*.

Most grid-controlled vacuum tubes have an electron collector usually called its "plate" which receives a current from the emitter depending upon the potential applied to the control grid. Since the control grid itself receives a negligible part of the emission current, practically all the current which passes the space-charge minimum is received on one or more of the electron collectors. The following relation is basic to the theory concerning the space-charge control of emission discussed in detail in Sect. 57:

$$I = I_0 e^{-\psi_{su}} = I_0 e^{-\frac{V_s}{V_T}}. \tag{82.1}$$

In this equation, I_0 is the zero-field emission current density capability of the emitter at the temperature V_T. The potential in the immediate neighbourhood

of the emitter surface is V_s positive with respect to the potential minimum located a short distance from the emitter. The dimensionless expression for this quantity was used almost exclusively in Sects. 57 and 58 and is given as ψ_{su}. It may be assumed that the change in plate current of interest is either equal to dI or directly proportional to it for all small variations of V_s. The variation in plate current may be expressed by the following equation:

$$\frac{dI}{dV_s} = -\frac{I_0 e^{-\frac{V_s}{V_T}}}{V_T}. \tag{82.2}$$

If the potentials of other electrodes in the tube are held constant, then *small* variations in the grid potential will make a directly proportional change in the potential of the space-charge minimum. Since the grid potential is usually expressed with respect to the emitter, the making of the grid more positive results in a decrease in the value of V_s and thus accounts for the negative sign used in the following equation:

$$dV_s = -m_g dV_g. \tag{82.3}$$

Here, V_g is the applied potential of the grid with respect to the emitter and m_g is the proportionality constant always less than unity and greater than zero. In Eq. (40.3) it was shown that the value of V_s could be represented with considerable accuracy by the following very simple formula:

$$V_s = \Phi \frac{V_T - V_\Theta}{V_\Theta}. \tag{82.4}$$

In this equation, Φ is the work-factor; the temperature expressed in its electron volt equivalent is V_T; and the temperature for which the space-charge minimum is exactly zero for a fixed set of applied conditions is given by V_Θ. The substitution of these equations into Eq. (82.2) gives the following result when it is remembered that definition of I_0 is given by Eq. (39.2):

$$g_m = \frac{dI}{dV_g} A = m_g \frac{a e^{-\frac{\Phi}{V_\Theta}}}{V_T} A. \tag{82.5}$$

Since the definition of a transconductance (or mutual-conductance) g_m is the variation in plate current per unit variation in grid potential expressed as $(dI/dV_g)A$, this equation shows that the transconductance for an emitter of area A and an ideal structure would show a very small increase as the temperature is lowered from its normal operating value to one closer to the critical value V_Θ. This result is not observed in a practical triode because there is no single value of V_Θ applicable to the entire effective area of the emitter.

Since an equation of the form of Eq. (82.5) expresses some of the most basic features of transconductance principles and since no theory including them is found in the textbooks on the theory of vacuum tubes, an illustration of its quantitative usefulness will be given in this paragraph. A plane surface emitter of 0.5 cm.^{2} may be designed into a troide having an emitter to grid spacing of 5×10^{-3} cm. The grid structure is such that its effective capacity at the emitter plane is 6% of the value that it would have if it were a parallel plane instead of a grid structure. With the grid operated sufficiently negative, so that it receives no appreciable part of the emission current the plate of the troide may be sufficiently positive so that the current (i) delivered from emitter to the plate is 25×10^{-3} amps. The minimum temperature V_Θ of a well-activated oxide cathode that can meet the current demand may be computed by the following relation:

$$i = A a e^{-\frac{\Phi}{V_\Theta}}. \tag{82.6}$$

A typical emitter will have $a = 3 \times 10^{10}$ amps per m.^{2} (or 3×10^6 amps/cm.^{2}) and $\Phi = 1.26$ volt. Computation shows that the critical value V_Θ is 7.03×10^{-2} or $\Theta = 816°$ K. The following equation may be used to compute the minimum temperature for satisfactory operation for a given emitter as expressed in terms of the critical temperature (V_Θ) and the work-factor:

$$V_T' = V_\Theta \left(1 + \frac{V_\Theta}{\Phi - V_\Theta}\right). \tag{82.7}$$

The substitution of numbers yields the value 7.45×10^{-2} ev or 865° K. No important change in the transconductance will be observed in a triode operated as described if the temperature of an emitter having these specifications is raised above this value V_T'. The next step for the calculation of m_g of Eq. (82.5) demands a knowledge of the distance from the emitter to the space-charge minimum. For all temperatures above V_T' Eq. (46.11) may be used for calculating the distance to the space-charge minimum. This equation, arranged for direct application is the following:

$$x_s = 3.109 \times 10^{-3} \frac{V_T^{\frac{3}{4}}}{I^{\frac{1}{2}}} = 3.109 \times 10^{-3} \frac{V_T^{\frac{3}{4}}}{(i/A)^{\frac{1}{2}}}. \tag{82.8}$$

Let the distance from the control grid to the emitter be x_g and let the capacitance which one can calculate from the known area and this distance for parallel planes be defined as C_x. By a suitably chosen set of measurements the true capacitance between the grid and the emitter may be determined experimentally. Let its value be C_g. The ratio of these two capacitances (C_g/C_x) is a measure of the effectiveness of the grid in controlling a charge distribution in the immediate neighborhood of the emitter. The fact that the space-charge minimum is at a fractional distance (x_s/x_g) from the emitter makes the modulation of the space-charge minimum by the grid possible. These considerations combine to give an expression for m_g of Eq. (82.5), which is:

$$m_g = \frac{x_s}{x_g} \cdot \frac{C_g}{C_x}. \tag{82.9}$$

These equations may be used to yield the following formula for transconductance:

$$g_m = 3.109 \times 10^{-3} \left[\frac{C_g}{x_g C_x}\right] \cdot \frac{(i/A)^{\frac{1}{2}}}{V_T^{\frac{1}{4}}}. \tag{82.10}$$

In this equation the factor in the square bracket depends on the geometrical configuration of the triode. The current i is the actual emission current which is grid-controlled. Since Eq. (82.10) applies specifically to a structure of parallel planes, the capacitance C_x may be expressed by the following equation:

$$C_x = \frac{\varepsilon_0 A}{x_g}. \tag{82.11}$$

The proportionality factor ε_0 is the permitivity of free space. This equation substituted into Eq. (82.10) yields the following:

$$g_m = 3.109 \times 10^{-3} \frac{C_g}{\varepsilon_0} \frac{(i/A)^{\frac{1}{2}}}{V_T^{\frac{1}{4}}} = 3.511 \times 10^8 C_g \frac{(i/A)^{\frac{1}{2}}}{V_T^{\frac{1}{4}}}. \tag{82.12}$$

In this equation C_g is the true capacitance of that part of the grid which modulates the space-charge minimum and therefore is much less than the input capacitance of an actual triode since the latter includes the coupling of not only the grid wires with respect to all other parts of the structure, but the supports and

the lead-in wires as well. A close-spaced triode of high transconductance has been constructed with the following specifications:

$i = 25 \times 10^{-3}$ amps; $A = 0.5 \times 10^{-4}$ m.^{2}; $C_g = 0.5 \times 10^{-12}$ farad (Estimated)
$x_g = 5 \times 10^{-5}$ m.; $V_T = 0.1$ ev.

With these numbers inserted into Eq. (82.12) the computed transconductance g_m is 7000 microamps per volt which agrees well with laboratory measurements. The quantity least accurately known is C_g, which was estimated from the known input capacitance rating for this triode of 2×10^{-12} farad.

This numerical example has been included here to illustrate the usefulness of the theories of thermionic emission in the presence of space charge which have been presented. It also illustrates the fact that, as the temperature is reduced from its normal value to one that is *between* V_Θ and V_T' as determined by Eq. (82.7), the distance x_s which could be calculated accurately by Eq. (82.8) for the higher temperatures, shrinks very rapidly to zero. Note that this shrinking of x_s reduces m_g to zero as indicated in Eq. (82.9). Since the basic equation for transconductance is Eq. (82.5), it is evident that in this critical range in temperature, transconductance falls rapidly to zero because of the m_g factor.

Although an equivalent of the above theory of transconductance is not widely known judging by the books on tube design, the engineers in the tube industry use a test for emitter quality control which is related to it.

The better the emitter, as measured in terms of the lowering of the work-factor Φ or the increase in the constant a, the lower the critical temperature V_Θ for a given set of operating conditions. These conditions are determined by the potentials applied to all elements of the tube except the heater, which supplies power to maintain the temperature of the emitter. It is not customary to make a direct determination of V_Θ but an indirect measure of it comes by the making of a quantitative determination of the time which elapses between the cutting off of the normal power and the time that the transconductance begins to fall very rapidly. A second method is to permit the heating power to be decreased slowly and determine the minimum value at which the tube under test will maintain a specified fraction of its normal transconductance. A third and less quantitative test involves the measurement of the transconductance at the normal operating temperature and a remeasurement of g_m with a 10% reduction in heater voltage. This method may be used to eliminate very poor emitters but will not distinguish between exceptionally good emitters and only fair ones if the less active surfaces are still able to maintain the potential minimum of the amount V_T over the major part of the emitter surfaces even at the reduced heater power.

83. Voltage-current characteristics with a detailed evaluation of emission according to space-charge theory. Precision measurements that yield quantitative data on electron emission from oxide cathodes have been discussed in detail in Sect. 81. In order to avoid space-charge effects, it was necessary to hold the temperature to less than 600° K. This temperature is so low compared with the normal operating temperature of 1160° K that experiments were undertaken to test the applicability of the space-charge equations as well as the emission equations covering a wide range of temperature for diodes of very simple construction.

The "ideal" diode for scientific study can be designed and built with a few main features which will be mentioned in the following tabulation.

1. The emitter and the collector should be parallel planes.
2. The temperature of each should be measurable by means of thermocouples.

3. A convenient design for the emitter could be a small cylindrical cap, a few millimeters in diameter similar in general construction to that used by the Bell Telephone Laboratories and described in Sect. 84. The part of the collector to which the measured electrons flow should be a pure nickel disc of small diameter guarded by a surrounding sheet of pure nickel to form the parallel plane structure and yet limit the measured emission current to the central part of the emitter.

4. The collector should be capable of being heated to any temperature at least equal to that of the emitter if desired.

5. For fundamental studies, especially of the cathode nickel, all of the parts of the test diode except the emitter should be of the purest nickel available.

6. Leakage current to the collector should be eliminated so that electron currents as small as 10^{-14} amps may be measured with accuracy.

Since the Bell Telephone Laboratories design is the nearest to this ideal, details concerning it will be given in Sect. 84 even though no measurements made with this diode are available for analysis.

The diode on which the test measurements reported in this section were carried out was one produced by the Raytheon Manufacturing Company[1]. It was built with pure nickel parts except for the emitter. The essential dimensions are given in the following tabulation:

Table 83.1.

	Length		Coated band		Outside diameter		Inside diameter	
Emitter	27 mm.	1.06 in.	12 mm.	0.47 in.	1.15	0.045 in.		
Coated					1.35	0.053 in.		
After exhaust .					1.30	0.051 in.		
Collector . . .	19 mm.	0.75 in.					3.35 mm.	0.132 in.

Amer. Soc. Testing Materials **2**, 883 (1952) Designation B 270-52T.

Although a number of specimens built according to this design were investigated in sufficient detail to show that the theoretical analysis developed in the previous sections applied, the data to be presented in this section were taken with great care on one of these diodes which was known from previous measurements to be typical. Before the test was made, it had been operated at the normal operating temperature of 1160° K for 1000 hours with sufficient positive collector potential to give an emission current of about 50 ma which corresponded to a current density of approximately 0.1 amp per cm.^{2}. Throughout the entire set of measurements the emitter temperatures were set and monitored by thermocouple measurements since the emitter had welded to its interior surface a fine tungsten wire. The properties of the tungsten-to-nickel junction for the particular alloy used as the emitter had been studied to obtain the calibration. During a test, the heater power input was maintained constant to better than 0.1%. Voltages were set with potentiometer accuracy and the currents measured with calibrated meters which gave reproducible results to 1%. The emission properties of the cathode were perfectly stabilized and the total range of applied voltage never exceeded 6 volts. All currents were accurately reproducible independent of the temperature sequence used for the investigation. In order to maintain

[1] Raytheon Manufacturing Company, Newton, Massachusetts, U.S.A.

emitter stability during a particular run, a 4 volt applied potential to the collector was maintained at all times, except for the short interval of time required for each individual reading. There were no instabilities that indicated that this precaution was really necessary. After a change in temperature, the electron emission took up its final value as quickly as the temperature could be adjusted. Thereafter, it remained perfectly constant. Because of this reproducibility, it is thought that the physical structure, including the concentration and distribution of donors, remained sufficiently constant over the entire range of time and temperature required for the experiment, so that the analysis, carried out on the basis that all measurements apply to the emitter in a particular state of activation, is justified.

Detailed measurements were made at 9 different temperatures ranging from 689 to 1160° K. Currents were measured as a function of applied voltage both for retarding and accelerating potentials. Over the low temperature range the 6-volt applied potential was sufficient to move the space-charge minimum to the emitter surface and with the help of the curves shown as Figs. 16 and 17, it was possible to determine the zero field emission current with accuracy. On the basis of these data the electron concentration in the immediate neighborhood of the emitter could be computed for the higher temperatures with sufficient accuracy for use in the quantitative determination of the contact difference in potential over the entire temperature range investigated. This evaluation will be illustrated by Fig. 56 and will be discussed in more detail later in this section. The important result is the quantitative determination of the *donor density* in the neighborhood of the emitting surfaces and the determination of the electronic *energy level* associated with the donor. This final step in the analysis comes by the application of the FOWLER and also the RICHARDSON thermionic equations to determine the electron affinity of the emitter and compare the overall results with thermionic emission theory. This paragraph serves to outline the analytic procedure to be followed.

For the diode structure described above, space-charge influences the measured current as it develops to give zero gradient at the collector at about 6×10^{-6} amps for the lowest temperature and about 20×10^{-6} amps for the highest temperature. Since the leakage current was less than 10^{-9} amps, the current flow could be studied as a function of the applied potential over the retarding field range to cover a current ratio of nearly 10^4 without the interference of space charge. Three of the 9 curves have been chosen for Fig. 55 since they serve not only to illustrate the method of analysis but also the complications that arise which must be understood in order not to misinterpret laboratory data.

Observations made with the emitter at 760° K serve as the basis for the plotted points of curve I. The solid line is the theoretical curve which should be expected for this geometry and this temperature. It will be noted that the plotted points follow this line very accurately for currents below 1 microampere. The two points designated *a* and *b* fall below the theoretical line as the result of an influence of space charge at a smaller observed current value than would have been expected if all electrons that impinge on the collector were absorbed by it. This result is a direct indication that electron reflection is taking place at the collector and must be given consideration in the detailed analysis of the observations.

As the applied potential is made more positive than 0.6 volt, the current rise follows that anticipated from space-charge theory for this geometry and temperature as the space-charge minimum moves across the diode and is located at the

emitter surface when the measured current is 220×10^{-6} amps. This method of analysis is illustrated by Fig. 28.

In order to show the relation between the analysis of the point-by-point observations of the current as a function of the voltage compared to the second harmonic method, an additional curve has been drawn in on this figure. This curve shown by the dotted line is a measure of the second harmonic generated in this diode as a function of the applied potential and corresponds to the detailed exploration over the top of the sharp peak shown in Figs. 53 and 54 at *a*. Although

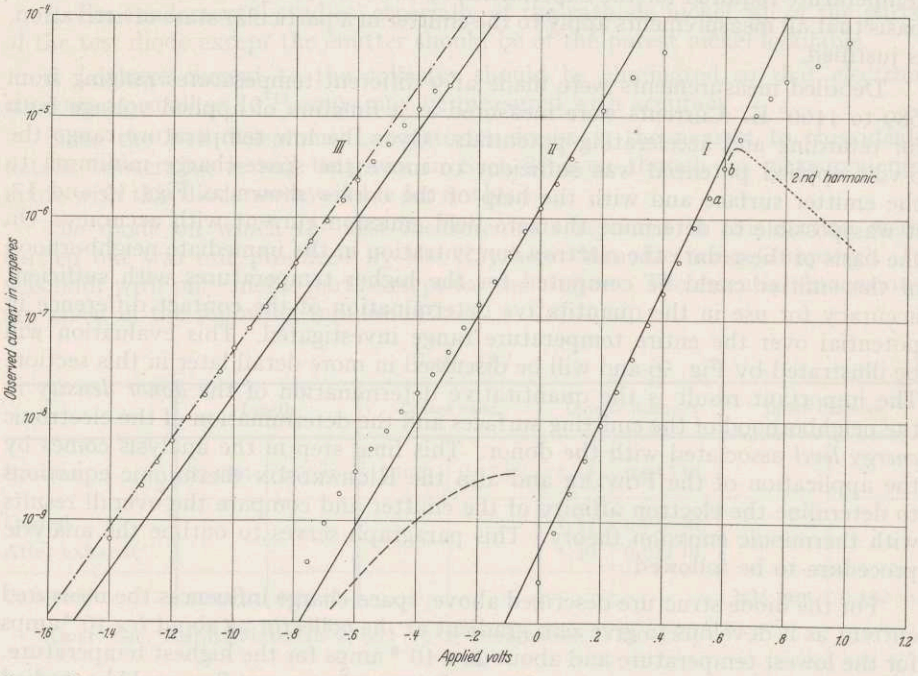

Fig. 55. Retarding potential curves for three temperatures. I. 760° K, dotted line shows second harmonic analysis. II. 956° K, dashed line, emission from bare nickel. III. 1160° K, solid line, emission from coating. Dot-dash line, total emission including bare nickel.

in Fig. 55 the deviation from the solid line was interpreted as the onset of space-charge, it is very clear from the second harmonic curve that the second derivative of the current curve is changing very rapidly at this point.

The data points associated with curve II were observed at a temperature of 956° K. A superficial analysis of the plotted points would indicate that the electron temperature was much higher than the thermocouple temperature. The theoretical curve that represents the true variation in the emission from the oxide coating is again represented by the solid line which is drawn at the theoretical slope for this temperature and geometry. The fact that so many points lie above the predicted line is a direct indication that a contribution to the observed current of major importance is coming from the uncoated areas of the nickel sleeve. This uncoated area seems to have a work-function almost exactly the same as the collector. These work-functions are probably 2.5 and 2.6 respectively. The zero field emission from the uncoated nickel is approximately 3×10^{-9} amps at this temperature. The influence of space-charge is clearly evident for the reading at 0.2 volt under which condition the current flowing is 12×10^{-6} amps.

Again the rise in current follows the curve given by space-charge theory as the space-charge minimum moves across from the collector to the emitter. At this temperature the measured current increases over 1000 fold and the data presented in Table 7 indicate that zero field emission would be observed at 12 to 13 volts applied potential. This prediction was later verified by experiment with the second harmonic method of analysis described in Sect. 82. The complication introduced into the analysis by the existence of the "high-speed 10-volt effect" interfered with the exact determination of the applied voltage required to force the potential minimum to coincide with the emitter.

Curve III which represents observations at 1160° K yields a result which would seem to indicate that the emission changed with applied potential exactly as one would expect for a MAXWELLian distribution characterized by this temperature. The line that represents this distribution is shown as dot-dash. The result which is not so obvious is that the observed distribution follows this line because there is adequate emission from the entire emitter which includes both the coated part and the uncoated part and therefore at each point the currents are larger by about a factor of three than the currents which legitimately belong to the emission properties of the coated part of the emitter. The solid line drawn parallel to the dot-dash line represents the emission from the oxide cathode after the total current has been corrected to subtract out the spurious current. Direct point-by-point observations and also the harmonic analysis illustrated by Fig. 54 shows that the emission from the uncoated area saturates at approximately zero potential. As more and more positive potential is applied, the current is predominantly that emitted from the oxide cathode and it follows very accurately the master curve described by the data of Table 8 after proper consideration is given over the low voltage range to the fact that the observations were made in a cylindrical diode instead of a plane parallel diode. An applied potential of approximately 180 volts would have brought the potential minimum over to the emitter to yield a direct observation of the zero-field emission of this emitter. Under these conditions, the collector would have been required to dissipate about 70 watts. Pulse equipment, not available at the time these measurements were made, would be required to verify this prediction.

On the basis of these analyses, the results presented quantitatively in Table 83.2 summarize the necessary information by means of which an evaluation of the emission is possible.

Table 83.2.

Heater volts	T° K	$100\,V_T$	V_T^{-1}	s_R	$i_R \times 10^6$	i_0 [1]	u_0^2	z^2	Obs. [2] I_m	Cal. [2] I_m	ψ_{SR}	$s_R+\psi_{SR}$	P_T	I_{00}
2.1	689	5.938	16.84	14.9	6.8	30×10^{-6}	4.41	0.52	0.261	0.229	1.8	16.7	0.993	2.35
2.3	729	6.281	15.92	13.6	8.0	110×10^{-6}	13.75	0.718	0.223	0.249	2.7	16.0	1.003	8.0
2.5	760	6.549	15.27	11.4	9.5	220×10^{-6}	23.1	0.780	0.243	0.265	3.36	14.76	0.967	20
3.0	837	7.212	13.87	8.2	12.5	1800×10^{-6}	144	0.910	0.275	0.306	5.04	13.24	0.956	133
3.5	897	7.729	12.94	6.0	15.0	$*6.3\times10^{-3}$	427	0.947	0.317	0.340	6.0	12.00	0.927	
4.0	956	8.237	12.14	3.9	17.5	$*20\times10^{-3}$	1143	0.968	0.362	0.374	6.91	10.81	0.894	
4.5	1003	8.642	11.57	2.7	19.1	$*43\times10^{-3}$	2250	0.977	0.391	0.402	7.64	10.34	0.894	
5.0	1051	9.056	11.04	1.3	21.2	$*91\times10^{-3}$	4670	0.984	0.431	0.429	8.21	9.51	0.861	
6.3	1160	10.00	10	−2.0	25.0	$*380\times10^{-3}$	15200	0.990	0.505	0.505	9.42	7.42	0.742	

[1] High temperature values * obtained by extrapolation according to Eq. (9.1) based on temperature range 689 to 837° K.

[2] Calculated on basis that equivalent plane-parallel diode had spacing $W = 0.78\times10^{-3}$ m.; actual spacing was 1.0×10^{-3} m. between cylinders; range in equivalent spacing observed was $(0.8\pm0.02)\ 10^{-3}$ m.

Based on the observed current at zero field for the four lowest temperatures and a detailed analysis of the effect of multiple reflection developed in Sect. 62, the column headed "I_{00}" represents the average current density which these theories indicate would have been observed in the complete absence of reflection at both the emitter and the collector. These data were used in the FOWLER emission equation given as (64.25) to determine the true work-function at absolute zero and the donor concentration that would yield these results. The graphical analysis is represented by Fig. 56. The FOWLER work-function computed from the slope of this curve is expressed as follows:

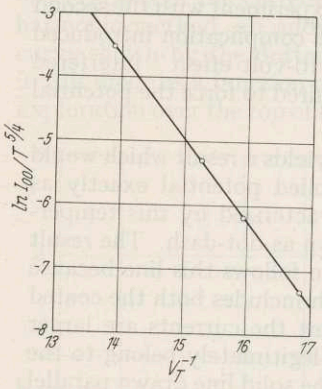

Fig. 56. Plot of emission data according to the FOWLER equation.

$$\varphi_F = W_a - \frac{E}{2} = 1.29 \text{ ev}. \qquad (83.1)$$

These data also yield a FOWLER thermionic constant which determines the donor density as follows:

$$n_D = \left[\frac{1.85 \times 10^6}{1.726 \times 10^{-5}}\right]^2 = 1.15 \times 10^{22} \text{ per m.}^3. \qquad (83.2)$$

If the electron affinity W_a is taken to be 0.88 ev as indicated by HUNG's experiment discussed in detail in Sect. 81, the energy level of the donor is -0.82 ev with respect to the bottom of the conduction band.

With this information available it is possible to compare the computed temperature variation of the work-function with the contact difference in potential observed. With the true work-function at absolute zero known to be 1.29 ev and the donor concentration and donor level known, it is possible to use the data of Table 11 to obtain the true work-function over the entire range in temperature. This result is shown by the solid line in Fig. 57. The choice of an average collector work-function of 2.58 ev places the observed contact difference in potential found at 956° K exactly on the theoretical true work-function line. If it is assumed that the true work-function of the collector is independent of the temperature of the emitter, then all the other nine points of observed contact difference in potential fall as shown in Fig. 57. Even though the agreement between theory and experiment is not exact, it is considered to be practically within experimental error, because the analysis was complicated by the fact that the diode under test was a cylindrical diode without guard rings, and that the correct introduction of the multiple

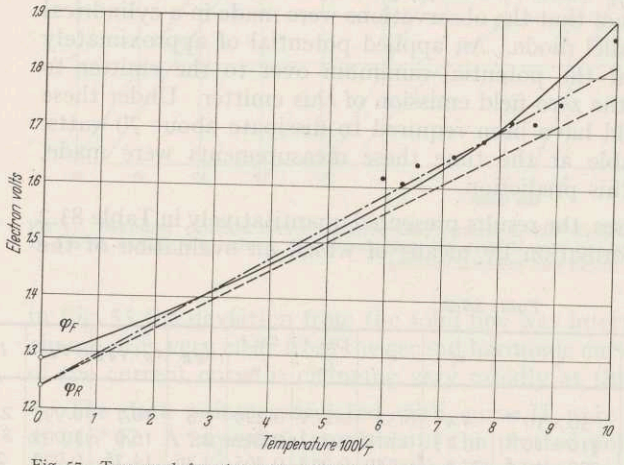

Fig. 57. True work-function with temperature dependence. Open circles, φ_F from FOWLER plot of Fig. 56; φ_R from RICHARDSON plot of Fig. 58. Solid line, theoretical curve computed for n_D of 10^{22} and $E = -0.8$; solid circles, observed contact difference in potential with average collector work-function assumed 2.58 ev; dot-dash line, best straight line through φ_R and experimental points; dotted line, based on choice of temperature coefficient according to RICHARDSON equation.

reflection theory especially as it applies to very low temperature range was not easy to carry through with exactness.

The next step in the analysis involved the application of the RICHARDSON formula to the same data shown in Fig. 56. The RICHARDSON plot is given in Fig. 58. The theories discussed in detail in Sect. 81 show that the slope of this line should give the RICHARDSON work-function which is the one found at absolute zero by linear extrapolation from the observational range. The value obtained for φ_R from this plot is 1.24 ev. This point is plotted in Fig. 57 and identified by φ_R. The straight line drawn from this φ_R point through the data points is shown by a dot-dash line in Fig. 57. The slope of this line is seen to be 5.8 and represents the apparent average temperature coefficient of the work-function in dimensionless units:

Computation based on the data of Fig. 58 gives the RICHARDSON constant A_R a value of 0.63×10^4 amp per m.^{2}-degree^2. If it is assumed that the average temperature coefficient of the work-function can be derived from this RICHARDSON constant and its relation to the theoretical constant A of Eq. (18.6), then the temperature coefficient would be 5.25. The dotted line of Fig. 57 is drawn with this slope. It is evident that if the true work-function of the collector were taken to be 2.54 ev instead of the value chosen of 2.58 ev, the observed points would be in very good agreement with the theoretical line. An inspection of Table 11 as it applies to a donor density of 3×10^{22} shows that a choice of a slightly higher donor density than the one required by Eq. (83.2) would yield slightly better overall self-consistency.

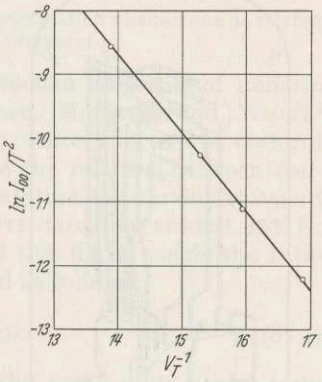

Fig. 58. Plot of emission data according to the RICHARDSON equation.

Since this method of emission analysis has been presented as it was carried through for the first time, the results may be summarized by the statement that the emission properties of this oxide cathode are in excellent agreement with those anticipated by the theories presented here. All factors including reflection effects, correct space-charge theory and analysis of electron flow between concentric cylinders were taken into account. The neglect of any one of these factors would result in a disagreement with theory that would have been outside of the experimental error.

84. Description of Bell Telephone Laboratories M-1949 planar diode. The data presented in Sect. 83 serve to forecast the results which may be obtained by a very careful analysis of voltage, current and temperature relations in diodes having oxide cathodes. The use of a cylindrical structure in contrast to a planar structure is distinctly disadvantageous in that far more effort is required for the analysis of the data. It is therefore important for the advancement of the better understanding of oxide cathodes to design a test structure which is feasible to make and at the same time more adaptable in terms of the theoretical analysis.

The Bell Telephone Laboratories planar diode M-1949 so nearly represents the ideal structure that a description of it is presented here in lieu of the fact that these details are not available in the scientific literature. The following paragraphs are quoted from information supplied by Mr. H. E. KERN of the Bell Telephone Laboratories.

A planar type vacuum tube diode has been designed and built at the Bell Telephone Laboratories for studying the fundamental properties of oxide-coated cathodes. A pictorial view of the diode structure is shown in Fig. 59.

The important structural and material features of this diode are listed below:

1. The cathode is a hat-shaped detail which can be machined from solid rod or formed from sheet material of thicknesses ranging from 0.060 inch to 0.001 or 0.002 inch.

2. The cathode hat is located directly over a hole (not shown) in the top surface of a hollow rectangular cathode heater box and is welded in place along the brim of the cathode hat. The hole in the cathode heater box facilitates removal of gases from beneath the cathode hat.

3. The emission coating is deposited on the top of the cathode hat as indicated by the dotted area. The coated area is 0.05 cm.^{2}.

4. The anode is a hollow rectangular box of exactly the same dimensions as the cathode heater box with the exception of the small hole required for the cathode outgassing.

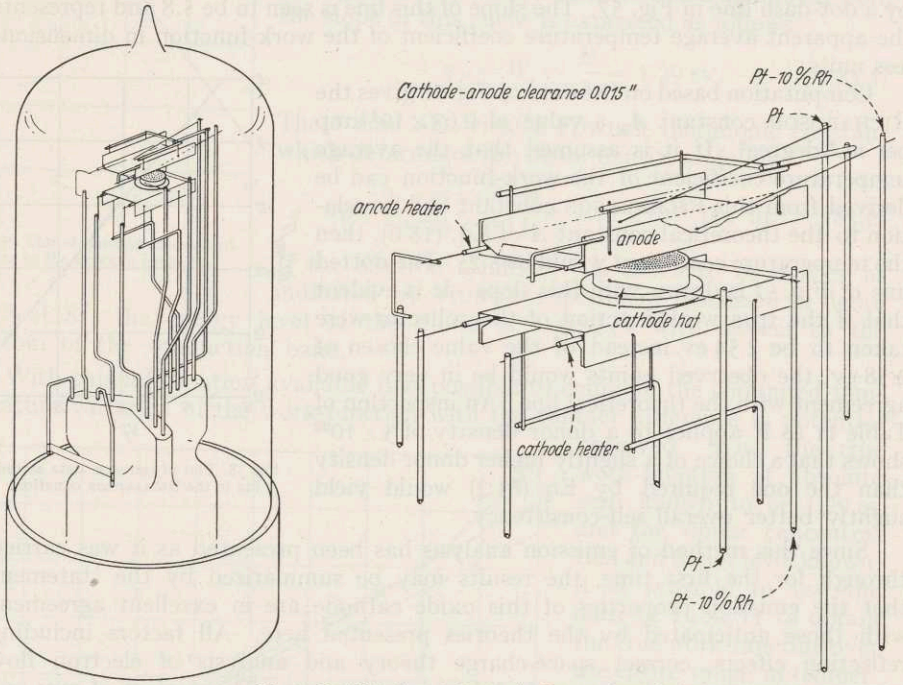

Fig. 59. Bell Telephone Laboratories M-1949 planar diode.

5. A heater is contained in the anode box so that the anode may be heated independently through the same temperature range as the cathode.

6. The anode and cathode heaters are identical and are aluminum-oxide coated-tungsten heaters (RCA-FH-484 H).

7. Platinum and platinum 10% rhodium (0.002 inch diameter) thermocouple wires are separately welded to both the anode box and the cathode hat as shown. An average cathode or anode temperature reading is obtained as a result of the physical separation of the 0.002 inch diameter, Pt and Pt-10% Rh thermocouple wires. This average reading is perhaps of greater interest than a temperature measurement at a single point.

8. The 0.002 inch diameter thermocouple wires are welded to 0.020 inch diameter similar Pt and Pt-10% Rh stem into the soft glass press. In this way reference junctions within the glass envelope are avoided and more accurate temperature measurements can be made.

9. The anode-cathode assembly is mounted on a 12-lead soft glass tripod stem. The dimensions of the completed mount are such that the anode-cathode assembly is approximately 2 inches away from the ultimate seal-in area. This positioning minimizes the possibility of oxidation of parts during seal-in.

10. No ceramics or micas (possible sources of contaminating gases) are contained in this diode.

11. All parts with the exception of the cathode hat and the tungsten heaters are made from high purity vacuum melted nickel.

Some of the advantages of the structure described above are:

1. Fundamental properties of the oxide cathode can be determined over a wide range of temperatures with an exact knowledge of the true temperature of the cathode.

2. The anode can be thoroughly outgassed by means of the anode heater before the carbonates on the cathode are decomposed. During this anode heating, the cathode temperature remains less than the maximum temperature (400 to 450° C) it attained during prior glass bake-out. For example, with the anode at 1000° C true temperature, the temperature of the cathode does not exceed 250° C.

3. A complete temperature *vs.* time record for both anode and cathode can be obtained during all process steps for possible correlation with the emission and life history of the tube.

4. Because of the relatively small coating area and close anode to cathode spacing, life tests can be run at *dc* cathode current densities as high as 500 ma/cm.² without causing excessive anode heating.

5. Cathode current density can be varied over a wide range under conditions of constant anode temperature by making use of the anode heater.

6. A more thorough study can be undertaken of anode deactivation phenomena as related to anode materials, anode processing, and anode operating temperature.

85. Relation between emission properties and conduction properties of uniform oxide-coated emitters. The experiments of HANNAY, MACNAIR and WHITE[1] and also YOUNG[2] serve as examples of researches in which emitters of uniform structural properties were investigated to determine the relation between conduction and emission at an arbitrarily chosen temperature for various states of emitter activation. The HANNAY, MACNAIR and WHITE data, observed at 970° K, are best represented by Fig. 40. An examination of this figure yields the ratio of emission current density to conductivity expressed as follows:

$$\frac{I}{\sigma_{p\,\mathrm{II}}} = 4\times 10^3 \text{ amp-ohm/meter}. \tag{85.1}$$

Results tabulated by YOUNG when expressed in the same units range from 3×10^3 to 25×10^3 amp-ohm per meter for values applicable to studies at 1000° K. The higher value applied to YOUNG's best specimen.

The temperature chosen for both of these studies was sufficiently high to make the conduction mechanism through the coating be dominated by pore conduction in contrast to the direct conduction through the crystals. Eq. (65.28) may be adapted to give an expression for the conductivity through the pores as follows:

$$\sigma_{p\,\mathrm{II}} = 2.54\times 10^{14}\, V_T\, \mathrm{e}^{-\frac{\varphi}{V_T}}\, C_p\, l_p. \tag{85.2}$$

In this expression, the true work-function is expressed as φ; the temperature in its electron-volt equivalent is V_T; and the constants C_p and l_p are determined by the physical structure of the emitter. In both experiments the emission current density figures used were intended to be as accurate a measure of the zero-field emission as it was possible to obtain without detailed analysis. In neither case were the geometrical configurations suitable for an exact evaluation of this current density. The equation that will best represent the emission current density is of the basic type used for the analysis of zero-field data given in Sects. 81 and 83. This equation comes directly from Eq. (18.5) with the modification, which experiment seems to call for, to account for the deficiency in slow electrons. The need for this factor was demonstrated in Sects. 81 and 83. The equation follows:

$$I = \frac{120\times 10^4\times 1.35\times 10^8\, V_T^2\, \mathrm{e}^{-\frac{\varphi}{V_T}}}{1+\frac{0.191}{V_T}}. \tag{85.3}$$

[1] N. B. HANNAY, D. MACNAIR and A. H. WHITE: J. Appl. Phys. **20**, 669 (1949).
[2] J. R. YOUNG: J. Appl. Phys. **23**, 1129 (1952).

In this equation the true work-function is expressed as φ as in Eq. (85.2). These two equations combine to yield the following:

$$\frac{I}{\sigma_{p\,\mathrm{II}}} = \frac{63.8\times10^{-2}\cdot V_T}{\left(1+\frac{0.191}{V_T}\right)C_p\,l_p}. \tag{85.4}$$

This analysis shows that a comparison between theory and experiment can be valid only under the condition that the true work-function applicable in Eq. (85.2) and Eq. (85.3) be the same. In turn this means that averaged over the entire coating, the electron affinity at the surfaces of the pores and the donor concentration found there must be essentially equal to the corresponding quantities at the emission surface. This demands that operation at a constant temperature without the drawing of emission current should precede any measurements. It is also clear that the introduction of poisoning impurities such as oxygen without a period of coating conditioning can increase the true work-function of the emitting surface without at the same time influencing to the same extent the true work-function found at the surfaces of the pores. The experiments of HANNAY, MACNAIR and WHITE are consistent with this view.

The most important factors in Eq. (85.4) that influence the emission current to conductivity ratio are the geometrical constants C_p and l_p. The first of these, as indicated in Sects. 65 and 77, depends on the detailed nature of the porosity of the specimen. Without this information it is not possible to do more than estimate the value of this constant for a given experimental specimen and for the present purposes the estimated value of C_p will be 0.3. Similarly, techniques for the determination of the most suitable value of l_p have not been developed beyond the estimation stage. It is thought that the range in l_p is likely to be from 2 microns to 8 microns. With the assumption that the product of these two constants is 1.5×10^{-6}, the computation of the ratio expressed by Eq. (85.4) gives a value of 11×10^{3} amp-ohm per m. for comparison with experiment. This figure is well within the range of observation made by YOUNG and is less than a factor of 3 larger than that observed by HANNAY, MACNAIR and WHITE as illustrated by Fig. 40.

86. Thermoelectric effects in an oxide coating. The fact that the temperature coefficient of the FERMI level in an oxide cathode is large indicates that the maintenance of a temperature gradient across a coating will result in the production of a measurable difference in potential between suitably placed electrodes. This difference in potential has been observed by YOUNG[1] and found to be directly proportional to the temperature gradient. Although the potential developed depends on the average temperature at which the observation is made, the high temperature electrode is always more positive than the low temperature contact. A typical curve as observed by YOUNG is shown as Fig. 60. The experiment involved the application of a barium-strontium oxide coating to two nickel caps. The coated surfaces were held in contact with each other mechanically, face to face, and each cap could be heated by a suitable internal heater. Thermocouples were used to measure temperatures and temperature differences. Not only could the thermal emf be measured as a function of average temperature, but also the electrical conductivity of the coatings. Fig. 61 presents results obtained by YOUNG for the same specimen as was used for the data of Fig. 60. A comparison between Fig. 61 and Fig. 37 indicates that the LOOSJES and VINK ranges I and II are covered by this study. The very low temperature range therefore is dominated by conductivity in the crystalline substance and the very

[1] J. R. YOUNG: J. Appl. Phys. **23**, 1129 (1952).

high temperature range by conductivity of electrons that build an electron atmosphere in the pores between the crystals. The conductivity data show no indication of important space-charge effects within the pores since range III (see Sects. 77 and 78) is not present. The equations developed in Sects. 64 and 65 may be adapted to the discussion of these thermoelectric effects.

If a temperature gradient is maintained across a single crystal of a substance which has a temperature coefficient of the FERMI level when measured with respect to the bottom of the conduction band, then in the absence of any current flow potentiometer methods permit the measurement of the difference in energy of the FERMI levels at the two points of contact between which the temperature difference exists. In YOUNG'S experiment observations made in the very low temperature range permitted a direct determination of the emf per unit temperature difference averaged over the specimen. Since it is presumed that the temperature difference existed over the same thickness of specimen as that which gave rise to the emf, it was not necessary to know exactly the thickness in order to acquire significant data for comparison with theory.

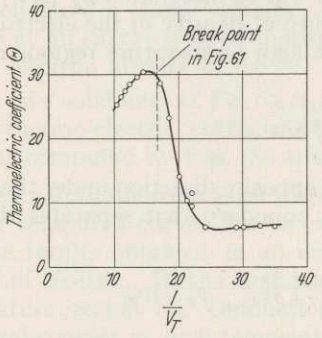

Fig. 60. Thermoelectric coefficient as observed by YOUNG.

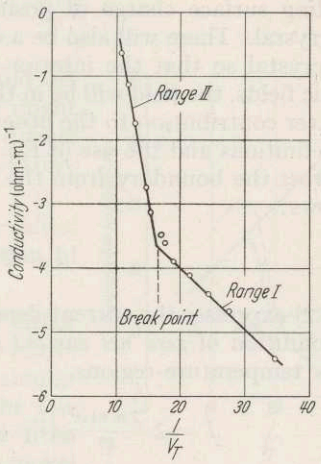

Fig. 61. Conductivity data as observed by YOUNG on same specimen as Fig. 60.

Eq. (64.3) may be used as the starting point for the derivation of an equation which should relate an observable thermoelectric emf to the temperature gradient maintained across a single crystal of activated barium-strontium oxide. The use of "activated" indicates that the theory is applicable only to a crystal in which there are a sufficient number of donor centers close enough to the bottom of the conduction band so that the location of the FERMI level is dominated by the free electron concentration in the conduction band obtained by transitions from the donors and that contributions to the electron density from the valence band are negligible. In the formulation of the theory it is assumed that over a very small distance within the crystal there is a difference in temperature of (ΔV_T) and that over this same distance there is an observable potential difference (Δv). This observable potential difference would have to be measured by potentiometer methods with the help of a potential indicator of the electrometer type since in the very low temperature range the resistance of a practical specimen as it applies to the oxide cathode may be very high. Any appreciable current flow may interfere with the accurate determination of the thermal emf.

The analysis that follows shows that the observable emf may be thought of as being derived from two phenomena. Since the observable emf represents a displacement of the FERMI level in the high temperature region, relative to the

location of the FERMI level in the lower temperature region, the presence of a temperature variation of the FERMI level will contribute a term to the thermal emf. An analysis of Eq. (64.8) as well as purely qualitative considerations show that the concentration of free electrons in the high temperature region will be slightly greater than the concentration of free electrons in the low temperature region. Furthermore, these electrons in the high temperature region will be moving with a greater average velocity as they cross the imaginary boundary between the low temperature and the high temperature region. In order that the time average of the current flowing across this boundary be exactly zero, a true internal field will develop which basically is derived from a small excess of a negative surface charge on the low temperature end of the crystal and a corresponding surface charge of positive electricity at the high temperature end of the crystal. There will also be a distribution of surface charges along the sides of the crystal so that the interior field will be uniform and, in the absence of magnetic fields, the field will be in the same direction as the temperature gradient. This latter contribution to the observable emf will be designated by $(\Delta v')$. With these definitions and the use of Eq. (64.3) a current density of the electrons that flow across the boundary from the low to the high temperature regions is given as follows:

$$I = 2\frac{2\pi m e^3}{h^3} V_T^2 \, e^{\frac{\mu}{V_T}} . \tag{86.1}$$

Eq. (86.2) expresses the current density in the opposite direction under the steady state condition of *zero net current* across the boundary that separates the high and low temperature regions.

$$I = 2\frac{2\pi m e^3}{h^3} (V_T + \Delta V_T)^2 \, e^{\frac{\mu + \Delta\mu}{(V_T + \Delta V_T)}} \, e^{\frac{\Delta v'}{(V_T + \Delta V_T)}} . \tag{86.2}$$

Clearly these equations are valid only in the extreme case of ΔV_T approaching zero. The equations are nevertheless useful since the coefficient of the thermal emf may be defined by the following relation:

$$\vartheta_s = \left(\frac{\Delta v}{\Delta V_T}\right)_{\Delta V_T \to 0} = \left(\frac{\Delta\mu + \Delta v'}{\Delta V_T}\right)_{\Delta V_T \to 0} . \tag{86.3}$$

To solve for the expression of Eq. (86.3), the logarithms of Eq. (86.1) and Eq. (86.2) are set equal to each other and the algebraic solution yields the following result:

$$\vartheta_s = \frac{\Delta v}{\Delta V_T} = -2 + \frac{\mu}{V_T} . \tag{86.4}$$

In the use of this equation, it must be remembered that it applies only for values of μ which are negative, and that the negative sign indicated for the expression as a whole results from the fact that the current carrier is an electron and that the high temperature region is the more positive in the electrostatic sense. In the plot of the theoretical curve as it is compared with YOUNG's experiment, the absolute value of the thermoelectric coefficient will be plotted as a function of $(1/V_T)$.

Note that this expression is identical in basic form to that derived by HENSLEY[1] and does not represent a precisely straight line plot since the location of the FERMI level (μ) is an implicit function of the temperature. Over any short range in temperature the true value of μ may be represented as a linear function of the

[1] E. B. HENSLEY: J. Appl. Phys. **33**, 1122 (1952).

temperature but to do so hardly serves any immediate purpose since Table 11 makes available accurately computed values of μ for a wide range of donor densities and donor energy levels.

It was demonstrated in Sects. 17 and 18 that in the absence of space-charge the potential energy of an electron in a pore differs from that of an electron in the bottom of a conduction band by the electron affinity W_a. Exactly the same principles that are illustrated above serve to give the following equation for the thermoelectric coefficient appropriate to a pore across which there is a small temperature gradient. This equation is the following:

$$\vartheta_p = \frac{\Delta v}{\Delta V_T} = -2 - \frac{W_a - \mu}{V_T}. \tag{86.5}$$

The evidence presented in Sects. 81 and 83 indicate that a well-activated oxide cathode might very well have a donor density of 3×10^{22} donors per m.^{3} at an energy level of approximately -0.6 ev and an electron affinity of 0.9 ev.

The two solid lines of Fig. 62 represent the values of the thermo-electric coefficient as a function of $(1/V_T)$ as computed by Eqs. (86.4) and (86.5)

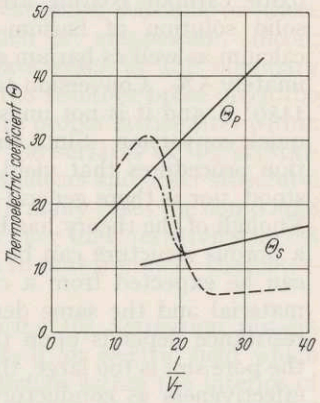

Fig. 62. Comparison between theory and experiment. ϑ_P thermoelectric coefficient for pores; ϑ_s same for crystalline material; dot-dash line, approximate intermediate curve; dotted line, YOUNG's experimental data.

It is an open question as to whether or not either of these computed curves can be expected to represent the results obtained in an experiment similar to that of YOUNG. In the first place over the low temperature region the conduction of heat from the nickel contact at high temperature to the nickel contact at low temperature will be almost entirely that conducted through the multitude of crystals which are sintered together to give contact areas of considerable variability. Of necessity, this results in a nonuniform distribution of temperature gradient, and yet it is not completely unreasonable that for small total temperature differences this nonuniformity will average out satisfactorily. The second difficulty is related to the almost certain lack of similarity between the crystals in direct contact with the nickel surface and those in the interior of the test specimen. Although no obvious interface structure may be present, the thermoelectric behavior of this region might be sufficiently different from the rest of the specimen that it would disturb the results. Finally, in the intermediate temperature range there will be conflict between the two sources of thermal emf since the pores will tend to generate a larger emf than the surrounding solid structure. If the net current averaged over the entire specimen is exactly zero, then in the neighborhood of each pore there will be a circulation of current. This circulation will be in the direction that electrons will flow through the crystalline substance from the low temperature region to the high temperature region, and they will flow in the opposite direction in the pores. The transition region indicated by the dot-dash curve of Fig. 62 will be very dependent on the pore structure and the conduction properties of the specimen under study. No attempt will be made here to derive equations applicable to this intermediate range. The observed results of YOUNG presented in Fig. 60 are reproduced by the dotted line of Fig. 62.

Although qualitative agreement between theory and experiment is evident, the overall picture needs to be clarified. The experiment is not an easy one and therefore it should be duplicated with attention directed toward improvement in the activation of the specimen. The indications are that YOUNG'S specimen was not as well activated as would be desirable. Although YOUNG'S experiment used potentiometer methods for the measurement of the thermal emf, a more sensitive indicator of higher internal resistance than a conventional galvanometer should be used. In spite of this criticism, the experiments of YOUNG contributed valuable information to support the LOOSJES and VINK model of coating conductivity at a time when this theory was less firmly established than at present.

87. Coating activation and related problems. The crystals that constitute an oxide cathode coating are generally formed following the decomposition of a solid solution of barium-strontium carbonate. Some manufacturers include calcium as well as barium and strontium with a proportion of calcium of approximately 5%. Conversion to the oxide takes place rapidly at temperatures above 1150° K and it is not unusual to use temperatures even above 1450° K for very quick conversion. Since the results of detailed studies are not available, production procedures that yield specific advantageous properties are not well understood, nor is there general agreement concerning some of the most basic factors. Enough of the theory has been presented in the previous sections to indicate that a porous structure can be created to have a higher electrical conductivity than can be expected from a crystalline structure having the same total weight of material and the same density of donors. The desired lowering of the coating resistance depends upon the development of pores of optimum dimensions. If the pore size is too large, the presence of space-charge within the pores limits their effectiveness as conductors and if the pores are too small crystalline material interferes with the free flow of the electrons and the resistance of a cathode may increase.

Porosity also plays a part in the liberation of the decomposition products and with the physical strength of the coating. Coating strength in turn relates to coating adherence which is a problem of great practical importance much in need of scientific investigation.

Although the emission properties of an oxide cathode immediately after its formation are generally good enough to yield current densities far in excess of those that would have been available from the base metal, an activation process is necessary to create a really efficient electron emitter. Much evidence points to the fact that activation results from a creation of an oxygen deficiency of approximately 10 to 20 parts per million averaged over the crystalline structure of the coating. As far as the experiments go, the term "oxygen deficiency" is completely analogous to "barium excess". The difference in concept relates specifically to the location of these donors. Excess barium within the crystal in all probability will find itself in normal barium sites and the oxygen atoms that are missing will leave defects within the body of the crystal which serve as trapping centers for the electrons normally associated with the excess barium atom. This trapping of electrons near negative ion sites is well known as it applies to the alkali halides. In potassium chloride, for example, electrons from the excess potassium atoms are trapped near chlorine vacancies and give rise to an absorption band for visible light in the green. A potassium chloride crystal which would otherwise be perfectly clear and transparent appears colored when viewed in

white light because of this absorption band. These trapped electrons are often known as "color centers".

Since the crystal of a barium-strontium oxide cathode has an ionic structure, it is very likely that the donors in an activated cathode are the oxygen vacancies which are capable of delivering one electron per donor to the conduction band by the absorption of energy of approximately 0.7 ev. Direct evidence for this particular transition in an activated oxide cathode is not available although the conduction and emission properties of well-activated cathodes serve as indirect indications of the presence of a donor level at this energy.

The difficulties encountered in the production of the necessary concentration of donors when pure nickel is used as a base metal and great care is exercised to eliminate reducing reactions by the presence of impurities made available from neighboring structures, indicates strongly that the most important chemical reactions responsible for the formation of oxygen vacancies depends on there being present in the base metal reducing agents such as: magnesium, silicon, titanium and manganese[1]. The oxide reduction takes place at the boundary layer between the base metal and the oxide, and if the reaction takes place too rapidly, the excess barium which must be absorbed into proper lattice sites within the crystals in order to be useful may migrate over the surfaces of the crystals and after evaporation from the cathode, deposit on insulators and other structural parts of practical tubes in an objectionable manner. In many cases the compound formed by the oxygen and the reducing agent has a very high resistivity unless this compound itself can hold within it enough donors so that it may be characterized as an "*n*" type semiconductor.

The drawing of an electron emission current during the activation process serves the purpose of creating within the coating itself an electric field which tends to maintain a high concentration gradient of donors within the interior of the coating and inhibit their loss at the exterior surface. With a very small concentration of a very active reducing agent such as magnesium, a high concentration of donors can be created in the first few minutes of the activation schedule and by suitable heat treatment and aging activate the entire coating in a few hours. At least in theory, this quick, initial activation is important from a practical point of view. The ultimate life of an emitter, however, depends on the maintenance of the required donor density throughout the cathode for a very long period of time. The presence of excess donor density in the immediate neighborhood of the vacuum surface of the emitter results in excess barium evaporation. It is therefore necessary to attain a suitable compromise such that the rate of production of excess barium is exactly balanced by its loss either as a result of evaporation or as a result of the neutralization of the oxygen vacancies by the absorption of oxygen or other electronegative elements brought to the surface from the external environment. Constructional and vacuum techniques determine the availability of these poisoning agents. It follows therefore that the achievement of truly long-life reliable cathodes depends on the maintenance of a suitable rate of production of oxygen vacancies over a long period of time and the minimizing of their loss.

Closely associated with this problem of activation is the stability of the emitter under high current drain conditions. Only a few of the many phenomena that depend on current drain can be mentioned here. It has been established by WAYMOUTH[2] that in many examples of moderately high silicon content nickel

[1] E. S. RITTNER: Philips Res. Rep. **8**, 184 (1953).
[2] J. F. WAYMOUTH: J. Appl. Phys. **22**, 80 (1951).

the interface of barium ortho-silicate ($2\,BaO \cdot SiO_2$) will have a low resistance through many hours of emitter life if an electron current is maintained continuously to keep an electric field applied at all times of cathode operation. Such a field inhibits the temperature diffusion of donors out of the interface compound. Without this flow of current, a high internal resistance may develop which could very well interfere with the practical usefulness of such an emitter. The base metal used for emitters in applications for which intermittent service is demanded should contain a minimum of silicon and have substituted in its place reducing agents less prone to develop high resistance in the absence of current flow.

Attention may be directed to the main structure of the oxide cathode, and since one realizes that at the normal operating temperature there is considerable mobility of the atoms that make up such crystals, there is a strong tendency for the donors (probably oxygen vacancies) to become more or less uniformly distributed throughout the interior of each of the crystals if no electron current is flowing. The maintenance of emission current results in an internal electric field within the crystals which interferes with the randomness of temperature diffusion and results in a redistribution of donors with a concentration gradient which in effect balances the electric field. Thus, the higher the emission current, the higher the field and the higher the concentration gradient. In the extreme case of high pulse-emission, the concentration gradient can be so great that the surface crystals increase in work-function so much that a drop in emission may take place. If the emission is too low to maintain a space-charge potential minimum at the surface of the emitter of kT or approximately 0.1 volt for a practical cathode, such an emitter in a vacuum tube may not be sufficiently space-charge limited to maintain in the desired modulation properties.

This increase in work-function is basically the result of the increase in the temperature coefficient of the true work-function as the donor density decreases. The rapidity with which the work-function and its temperature coefficient changes with the reduction in donor concentration is well illustrated by the data in Table 11.

With well-activated cathodes, emission current densities of approximately 5 amps per cm.^{2} may be obtained for reasonable periods of time without prohibitive reduction in donor density at the emission surface. Unless the cathode is well activated and the vacuum environment free from electronegative elements, excessive field develops near the superficial surface which in turn aggravates the situation in that the stronger the field, the greater the difficulty in maintaining a sufficient concentration near the surface.

Although this concept of donor migration in the presence of field dates back at least to the early work of BECKER[1], the most complete recent treatment is that of NERGAARD[2].

These problems of donor concentration, donor distribution and donor mobility in the presence of fields are likely to be the subject of many researches in the near future since these phenomena combined with the control of porosity determine the important emission properties of oxide cathodes.

88. Dispenser cathodes. Dispenser cathodes have been developed to meet the demand for high emission current density under environmental conditions

[1] J. A. BECKER: Phys. Rev. **34**, 1323 (1929).
[2] L. S. NERGAARD: RCA Rev. **13**, 464 (1952).

that would often be considered unfavorable to high emission efficiency. One of the earliest dispenser cathode structures was that proposed by HULL[1]. In this example the emitting surface was molybdenum which received the activating material by evaporation from a closely woven "stocking" of molybdenum wire which contained as a filler a fuzed barya-alumina eutectic (70% BaO, 30% Al_2O_3 by weight). Barium oxide is evaporated from the dispenser and condensed on the molybdenum surfaces presumably with a sufficient concentration of excess barium to maintain a well-activated emission surface for thousands of hours. The thickness of the coatings used was never established by direct experiment, but the properties were so similar to those of a conventional oxide cathode that it may be presumed that a sufficiently thick layer of barium oxide existed to create a multi-layer emitter surface with semiconducting properties.

The development of the "*L*" cathode by LEMMENS, JANSEN and LOOSJES[2] took advantage of a technique by which a porous tungsten plug could be inserted into a molybdenum cup into which had been placed barium-strontium carbonate which was thus sealed into position behind the plug. High temperature operation permitted the conversion of the carbonate to the oxide and the removal of the gaseous products of this reaction. The barium oxide and barium diffuses through the porous tungsten and activates the surface.

HUGHES and COPPOLA[3] have described still another version of the dispenser cathode. In the preparation of this emitter the principle active constituent is barium carbonate which is fuzed with a small amount of calcium carbonate and aluminum oxide (Al_2O_3). After fusion, this material is ground to a fine powder and sintered under high pressure with a powdered refractory material. Typical of this matrix material is the tungsten 25%, molybdenum 75% alloy. The favorable properties resulting from the introduction of calcium were first described by LEVI[4].

Not unrelated to these emitters are those described by MACNAIR, LYNCH and HANNAY[5]. In this example, a plug is formed on a pressed nickel base and contains particles of nickel pressed in special dies with barium-strontium carbonate particles. These molded cathodes, after suitable activation, have an emission efficiency very comparable with well-activated sprayed oxide cathodes.

Still another dispenser cathode has been described by BALAS, DEMPSEY, and REXER[6]. In this case, nickel powder is pressed and sintered to form a cathode matrix. This matrix is filled by water soluble compounds which finally precipitate the barium-strontium carbonate needed for the eventual conversion to barium-strontium oxide. The material contained within the matrix migrates to the surface and activates it. Observations indicate that these emitters have high efficiency and are generally far more able to deliver continuously high current density. They also withstand the temporary admission of oxygen to their surfaces.

Most of the observations with dispenser cathodes are interpreted on the assumption that the surface should be classified as "simple composite". It

---

[1] A. W. HULL: Phys. Rev. **56**, 86 (1939).
[2] H. J. LEMMENS, M. J. JANSEN and R. LOOSJES: Philips Techn. Rev. **11**, 341 (1950).
[3] R. C. HUGHES and P. P. COPPOLA: Phys. Rev. **85**, 388 (1952). — J. Appl. Phys. **23**, 1261 (1952). — Proc. Inst. Radio Engrs. **44**, 351 (1956).
[4] R. LEVI: J. Appl. Phys. **26**, 639 (1955).
[5] D. MACNAIR, R. T. LYNCH and N. B. HANNAY: J. Appl. Phys. **24**, 1335 (1953).
[6] W. BALAS, J. DEMPSEY and E. F. REXER: J. Appl. Phys. **26**, 1163 (1955).

is assumed that a mono-molecular layer of barium oxide reduces the true work-function of an otherwise clean base metal with the resulting high emission efficiency. It should be considered an open question as to whether or not this interpretation is entirely correct since in some cases oxidation of the base metal is a necessary step in the production of an efficient emitter. If this oxide is some 10 to 20 atom layers thick and can be converted into a suitable "*n*" type semiconductor by the presence of the barium oxide, then the concepts associated with the "complex composite" surface may be more appropriate for the explanation of the emission properties.

In order to understand the physics of the emission process for these dispenser cathodes, research data not available in the literature are needed. The general discussion of Sect. 69 indicates broadly the nature of the data wanted. Specifically one may ask the question: can a polarizable monolayer of molecules reduce the work-function as much as is observed? The alternative is that the dispenser cathode should be described as a complex composite surface, and with this statement, it is implied that the surface film is thick enough to have taken on many of the properties of an "*n*" type semiconductor. If this second picture represents the facts, then high emission efficiency results from a very great reduction in the electron affinity and by having present within the complex layer a high concentration of donors. The temperature coefficient of the FERMI level can then be maintained small enough so that a satisfactory true work-function at operating temperature is obtained.

It is not easy to outline the researches which would give an unambiguous answer as to the nature of the surface film on a dispenser cathode. Practically all of the techniques that have been described in Sects. 73 through 83 may be used to yield electrical data that serve to describe the emission properties of these cathodes. Direct measurements of the true work-function over a wide range of temperature should be most helpful. A determination of the temperature coefficient of the work-function as a function of the temperature could very well be useful for the identification of the emission mechanism. Still additional properties may be discovered by the use of a dispenser cathode as a receiver of electrons. In that manner additional direct determinations may be made of the variation of the true work-function with temperature and with activation over a very wide range of these variables. After the electrical properties of various specific types of dispenser cathodes have been determined, they could be compared to the properties of ribbons of the same base metal upon which barium-strontium oxide had been deposited from exterior sources much after the manner of the work of MOORE and ALLISON[1]. They found that a condensation of approximately 10 to 20 molecular layers of barium oxide was required to convert the properties of a tungsten ribbon to those very analogous to a conventional oxide-coated cathode. It seems unlikely that such a large number of layers can be formed by diffusion and molecular migration from the interior of a dispenser cathode. Yet even though the surface may not be covered with that number of layers, if the extent of the coverage is appreciably in excess of a monolayer, the emission properties may be dominated by phenomena associated with the complex layer structure in contrast to the simple composite type. If oxidation of the base metal beyond a monolayer is a fundamental requirement for high efficiency then theories applicable to complex-composite surfaces should apply.

---

[1] G. E. MOORE and H. W. ALLISON: Phys. Rev. **77**, 246 (1950).

89. Concluding remarks and acknowledgements. This treatise has been prepared with the objective that it might serve as a suitable source of basic physics as it relates to thermionic emission. The introduction of many cross-references and the presentation of a glossary of symbols are devices which it is hoped will assist the reader in the acquisition of information in the particular phases of this subject of thermionic emission in which he is most interested. In spite of its length, it touches only lightly on many branches of the subject while at the same time it attempts to discuss with thoroughness, and it is hoped with rigor some of the more important phases of the subject.

Criticism may be made because so much of the writing has been allotted to the analysis and discussion of *space-charge problems*. The justification for this emphasis in an article on thermionic emission is that a thorough mastering of this subject and its intelligent use is needed for the evaluation of thermionic emission and its application in engineering. It is hoped that this better understanding of space-charge theory in its relation to thermionic emission will ultimately assist in the improvement of practical vacuum tubes not only in their performance characteristics but also in their reliability both on a short time and a long time basis.

For similar reasons the *oxide cathode* well deserves the very best effort that any author writing on the subject of thermionic emission can give to it. Millions upon millions of tubes that depend for their usefulness on oxide cathodes have been produced and for some considerable time in the future they will still be needed. It is hoped, therefore, that this treatise will serve as a guide in the formulation of specific means by which the basic problems can be attacked and ultimately solved. The acquisition of new and more reliable information may very well show that the theoretical analysis presented here is not adequate since it does depend on simplifying assumptions. The reader will note that the main effort has been to try to bring together in a simplified manner both experimental and theoretical studies basic to the analysis of thermionic emission from oxide cathodes as it is understood at this time.

Apologies are in order for the very superficial handling of such an important subject as the dispenser cathode. If more time were available for the preparation of this treatise there is no doubt that existing experimental data could be organized and presented in a far better manner so as to establish more clearly the basic phenomena involved.

A number of my colleagues, acquaintances and assistants have aided immeasurably in the production of this treatise. Specifically I wish to acknowledge the help given me by Mr. James Cardell and many of his associates at the Raytheon Manufacturing Company whose studies on the properties of cathode nickel have been most helpful. In addition, this group has made available innumerable test diodes on which studies of cathode material could be undertaken.

Among my students and former students who have helped by their suggestions and criticisms, I wish to mention in particular Andrew R. Hutson, William J. Lange and Haywood Shelton. Without the help of the computing division of the Research Laboratory of Electronics under the directorship of Miss Elizabeth J. Campbell it would have been impossible for me to have prepared the tables, many of which are being made available in this treatise for the first time. It is hoped that this choice of tabular information and its method of presentation will prove useful. Dr. Helen L. Thomas, also of the Research Laboratory of Electronics, assisted in many phases of the editing and the production. Finally I wish to acknowledge the great assistance given me in the preparation of this manuscript by my assistant, Lawrence E. Sprague, who prepared practically all of the drawings. Thanks and credit are due Eveline van Berkum who helped me with much of the original draft and editorial work. My appreciation has been earned by Miss Anne F. Crimmings who prepared all of the final manuscript and helped most effectively in many aspects of the final production.

Table 1. *Density of an electron atmosphere in an enclosed space. (See Sect. 24 for details.)* n_s = electron concentration just outside of surface. n_{0m} = maximum possible density at center of cavity [Eq. (24.4)]. n_0 = true density at center of cavity. $z^2 = n_0/n_{0m}$ [see Eqs. (24.2) and (24.11)]. $V_T = T/11600$ = electron volt equivalent of temperature. V_s = true potential difference in volts between surface and center of cavity.

z	z^2	n_s/n_{0m}	n_s/n_0	V_s/V_T
0.05	25×10^{-4}	2.515×10^{-3}	1.00619	0.00617
0.10	1×10^{-4}	10.25×10^{-3}	1.02508	0.02477
0.15	225×10^{-4}	23.79×10^{-3}	1.05764	0.05604
0.20	400×10^{-4}	44.22×10^{-3}	1.10561	0.10040
0.25	625×10^{-4}	73.22×10^{-3}	1.17158	0.15835
0.30	900×10^{-4}	113.4×10^{-3}	1.25957	0.23077
0.35	1225×10^{-4}	0.1685	1.37555	0.31885
0.40	16×10^{-2}	0.24445	1.52781	0.42383
0.45	20.25×10^{-2}	0.3502	1.72957	0.54787
0.50	25×10^{-2}	0.5000	2.0	0.69315
0.55	30.25×10^{-2}	0.7171	2.3707	0.86318
0.60	36×10^{-2}	1.042	2.8946	1.06281
0.65	42.25×10^{-2}	1.5475	3.6627	1.29821
0.70	49×10^{-2}	2.378	4.8527	1.57954
0.75	56.25×10^{-2}	3.841	6.8287	1.92114
0.80	64.0×10^{-2}	6.701	10.4699	2.3485
0.82	6.724×10^{-1}	8.636	12.8431	2.5528
0.84	7.056×10^{-1}	11.41	16.1729	2.7833
0.86	7.396×10^{-1}	15.54	21.017	3.0453
0.88	7.744×10^{-1}	22.06	28.481	3.3492
0.90	8.100×10^{-1}	33.10	40.861	3.7102
0.91	8.281×10^{-1}	41.71	50.363	3.9193
0.92	8.464×10^{-1}	53.88	63.654	4.1535
0.93	8.649×10^{-1}	71.83	83.050	4.4194
0.94	8.836×10^{-1}	99.77	112.917	4.7267
0.95	9.025×10^{-1}	146.6	162.462	5.0904
0.96	9.216×10^{-1}	233.7	253.60	5.5358
0.97	9.409×10^{-1}	424.0	450.59	6.1104
0.98	9.604×10^{-1}	973.4	1013.53	6.9212
0.99	9.801×10^{-1}	3968.2	4048.7	8.3062

Table 2. *Values of $F(S, kT/\omega)$ for various values of S and kT/ω [see Eq. (26.12)].*

kT/ω	$S\to0$	0.5	1	1.5	2	3	4	5	6	8	10
0	1.0	8.01^{-1}	5.72^{-1}	3.91^{-1}	26.1^{-2}	11.2^{-2}	4.6^{-2}	18.6^{-3}	7.38^{-3}	11.3^{-4}	17^{-5}
0.06	0.943	7.47	5.25	3.51	23.1	9.5	3.78	14.3	5.62	8.4	11.8
0.12	0.893	6.98	4.83	3.18	20.5	8.14	3.12	11.7	4.35	6.05	7.9
0.20	0.833	6.41	4.31	2.81	17.7	6.75	2.45	8.85	3.20	3.99	5.00
0.40	0.714	5.30	3.42	2.09	12.6	4.39	1.47	5.00	1.75	1.96	2.33
0.60	0.625	4.47	2.75	1.62	9.12	2.69	0.974	3.21	1.00	1.12	1.25
0.80	0.556	3.86	2.28	1.29	7.23	2.25	0.70	2.29	0.66	0.751	0.873
1.0	0.500	3.38	1.90	1.05	5.13	1.73	0.538	1.62	0.502	0.578	0.672
1.2	0.455	2.95	1.63	0.872	5.00	1.41	0.401	1.28	0.450	0.461	0.552
1.4	0.417	2.62	1.40	0.739	4.00	1.19	0.331	1.06	0.40	0.386	0.470
1.6	0.385	2.34	1.23		3.37						
2.0	0.337	1.92	0.959		2.61	0.718					
3.0	0.250	1.29	0.611		1.54	0.453	0.143				
5.0	0.167	0.735	0.325		0.879						

Note 1: The row for $kT/\omega = 0$ is $G(S)$ since the first term of Eq. (26.12) reduces to $2S^{\frac{1}{2}}e^{-S}/\sqrt{\pi}$ in the limit. A more complete table of values is given in Table 10.

Note 2: The superscript at the top of each column indicates the power of ten by which the numbers in that column should be multiplied.

Table 3E (Emitter Space). *Numerical solution*[1] *to the* LANGMUIR *equation for epace charge in the Emitter Space [Eq. (36.1)].*

ψ_s	χ_s	χ_s/χ_m	$(\chi_s/\chi_m)^2$	ψ_s	χ_s	χ_s/χ_m	$(\chi_s/\chi_m)^2$
0.005	0.09864	0.05462	0.002983	1.3	1.242	0.6877	0.4731
0.006	0.1080	0.05980	0.003575	1.35	1.258	0.6966	0.4853
0.007	0.1165	0.06451	0.004160				
0.008	0.1244	0.06888	0.004746	1.4	1.273	0.7049	0.4970
0.009	0.1317	0.07292	0.005316	1.45	1.288	0.7132	0.5086
				1.5	1.302	0.7209	0.5197
0.010	0.1387	0.07680	0.005899	1.6	1.330	0.7364	0.5424
0.011	0.1454	0.08051	0.006481	1.7	1.356	0.7508	0.5638
0.012	0.1517	0.08400	0.007055				
0.013	0.1578	0.08738	0.007634	1.8	1.380	0.7641	0.5837
0.014	0.1636	0.09059	0.008204	1.9	1.402	0.7763	0.6028
0.015	0.1692	0.09369	0.008778	2.0	1.423	0.7879	0.6208
				2.1	1.444	0.7996	0.6392
0.02	0.1947	0.10781	0.01162	2.2	1.462	0.8095	0.6552
0.025	0.2169	0.1201	0.01442				
0.03	0.2369	0.1312	0.01721	2.3	1.480	0.8195	0.6714
0.04	0.2721	0.1507	0.02270	2.4	1.497	0.8289	0.6871
0.045	0.2879	0.1594	0.02541	2.5	1.513	0.8378	0.7018
				2.6	1.527	0.8455	0.7150
0.05	0.3027	0.1676	0.02809	2.7	1.541	0.8533	0.7282
0.06	0.3302	0.1828	0.03342	2.8	1.555	0.8610	0.7413
0.07	0.3553	0.1967	0.03869	2.9	1.568	0.8682	0.7539
0.08	0.3783	0.2095	0.04387				
0.09	0.3999	0.2214	0.04902	3.0	1.580	0.8749	0.7652
				3.1	1.590	0.8804	0.7751
0.1	0.4201	0.2326	0.05411	3.2	1.602	0.8870	0.7867
0.15	0.5070	0.2807	0.07879	3.3	1.611	0.8920	0.7956
0.2	0.5777	0.3199	0.10231	3.4	1.621	0.8976	0.8057
0.25	0.6385	0.3535	0.1250	3.5	1.631	0.9031	0.8155
0.3	0.6923	0.3833	0.1469	3.6	1.639	0.9075	0.8235
0.35	0.7396	0.4095	0.1677	3.8	1.655	0.9164	0.8398
0.4	0.7835	0.4338	0.1882	4.0	1.670	0.9247	0.8551
0.45	0.8238	0.4561	0.2081	4.2	1.683	0.9319	0.8683
0.5	0.8605	0.4765	0.2270	4.4	1.694	0.9380	0.8799
0.55	0.8952	0.4957	0.2457	4.6	1.705	0.9441	0.8913
0.6	0.9277	0.5137	0.2639	4.8	1.715	0.9496	0.9017
				5.0	1.724	0.9546	0.9112
0.65	0.9581	0.5305	0.2814				
0.70	0.9871	0.5466	0.2987	5.5	1.742	0.9646	0.9305
0.75	1.014	0.5615	0.3152	6.0	1.756	0.9723	0.9455
0.80	1.039	0.5753	0.3311	6.5	1.767	0.9784	0.9572
0.85	1.064	0.5891	0.3471	7.0	1.776	0.9834	0.9670
0.9	1.088	0.6024	0.3630	7.5	1.783	0.9873	0.9746
0.95	1.109	0.6141	0.3771				
1.0	1.131	0.6262	0.3921	8.0	1.788	0.9900	0.9802
				9.0	1.795	0.9939	0.9878
1.1	1.171	0.6484	0.4203	10.0	1.799	0.9961	0.9921
1.15	1.189	0.6584	0.4335	12.0	1.803	0.9983	0.9967
1.2	1.208	0.6689	0.4473	14.0	1.805	0.9994	0.9989
1.25	1.225	0.6783	0.4602	16.0	1.805	0.9994	0.9899

[1] Based on tables computed by P. H. J. A. KLEYNEN: Philips Res. Rep. **1**, 81 (1946).

Note 1: See Eqs. (37.1), (37.3), (37.5) and (37.6) for empirical equations for these data and the means for extrapolation.

Note 2: The limiting value of χ_s is $\chi_m = 1.806$.

Note 3: Definitions: $\psi_s = V_s/V_T = eV_s/kT$ and $\chi_s^2 = (x_s/x_1)^2$ with $(x_1)^2$ given by Eq. (35.2).

Table 3C (Collector Region). *Numerical solution*[1] *to the* LANGMUIR *equation for space charge in the Collector Region [Eq. (36.1)].*

ψ_c	χ_c	χ_c/χ_m	$(\chi_c/\chi_m)^2$	ψ_c	χ_c	χ_c/χ_m	$(\chi_c/\chi_m)^2$
0.01	0.1440	0.07973	0.006359	5.00	4.320	2.392	5.722
0.02	0.2053	0.11368	0.01292	5.50	4.583	2.538	6.440
0.03	0.2529	0.1400	0.01961	6.00	4.838	2.679	7.176
0.04	0.2933	0.1624	0.02637				
0.05	0.3293	0.1823	0.03323	6.50	5.086	2.816	7.931
				7.00	5.328	2.950	8.703
0.06	0.3621	0.2005	0.04019	7.50	5.564	3.081	9.491
0.07	0.3924	0.2173	0.04721	8.00	5.796	3.209	10.300
0.08	0.4209	0.2331	0.05433	9.00	6.245	3.458	11.957
0.09	0.4477	0.2479	0.06144				
0.10	0.4733	0.2621	0.06868	10.0	6.680	3.699	13.68
				11.0	7.101	3.932	15.46
0.15	0.5866	0.3248	0.1055	12.0	7.510	4.158	17.29
0.20	0.6841	0.3788	0.1435	13.0	7.909	4.379	19.18
0.25	0.7714	0.4271	0.1825	14.0	8.298	4.595	21.11
0.30	0.8515	0.4715	0.2223				
0.35	0.9262	0.5128	0.2630	15.0	8.680	4.806	23.10
				16.0	9.053	5.013	25.13
0.40	0.9965	0.5518	0.3044	18.0	9.780	5.415	29.32
0.45	1.063	0.5886	0.3464	20.0	10.48	5.803	33.67
0.50	1.127	0.6240	0.3894	25.0	12.16	6.733	45.34
0.60	1.247	0.6905	0.4767	30.0	13.74	7.608	57.88
0.70	1.359	0.7525	0.5663	35.0	15.24	8.439	71.21
				40.0	16.68	9.236	85.30
0.80	1.465	0.8112	0.6579				
0.90	1.567	0.8677	0.7527	45.0	18.08	10.011	100.22
1.00	1.663	0.9208	0.8480	50.0	19.43	10.76	115.74
1.10	1.756	0.9723	0.9455	60.0	22.02	12.19	148.7
1.20	1.846	1.0221	1.0449	70.0	24.50	13.57	184.0
1.40	2.018	1.1174	1.248	80.0	26.88	14.88	221.5
1.60	2.181	1.208	1.458				
1.80	2.336	1.293	1.673	90.0	29.17	16.15	260.9
				100.0	31.40	17.39	302.3
2.00	2.486	1.377	1.895	150.0	41.78	23.13	535.2
2.20	2.630	1.456	2.121	200.0	51.25	28.38	805.3
2.40	2.769	1.553	2.351	300.0	68.50	37.93	1439
2.60	2.904	1.608	2.585				
2.80	3.036	1.681	2.826	400.0	84.28	46.67	2178
				500.0	99.04	54.84	3007
3.00	3.164	1.752	3.069	600.0	113.06	62.60	3919
3.20	3.290	1.822	3.319	700.0	126.5	70.04	4906
3.40	3.413	1.890	3.571	800.0	139.4	77.19	5958
3.60	3.533	1.956	3.827				
3.80	3.651	2.022	4.087	900.0	151.9	84.11	7074
				1000.0	164.1	90.86	8256
4.00	3.767	2.086	4.351				
4.50	4.049	2.242	5.026				

[1] Based on tables computed by W. R. FERRIS: RCA-Rev. **10**, 134 (1949).

Note 1: See Eqs. (37.7) and (37.8) for empirical equations for these data and the means for extrapolation.

Note 2: The limiting value of χ_s is $\chi_m = 1.806$.

Note 3: Definitions: $\psi_c = V_c/V_T = eV_c/kT$ and $\chi_c^2 = (x_c/x_1)^2$ with $(x_1)^2$ given by Eq. (35.2).

Table 4. *Emitter region potential and its relation to emitter properties and current flow. (See Sect. 43 and 44 and Fig. 9.)*

ψ_s	z	z^2	u_0	u_0^2	$(I_0/I_m)^{\frac{1}{2}}$	I_0/I_m
0.02	0.1078	0.01162	1.0100	1.0202	0.1089	0.01185
0.025	0.1201	0.01442	1.0126	1.0253	0.1216	0.01478
0.03	0.1312	0.01721	1.0151	1.0305	0.1332	0.01773
0.04	0.1507	0.02271	1.0202	1.0408	0.1538	0.02364
0.05	0.1676	0.02809	1.0253	1.0513	0.1718	0.02953
0.06	0.1828	0.03342	1.0304	1.0618	0.1884	0.03549
0.07	0.1967	0.03869	1.0356	1.0725	0.2037	0.04150
0.08	0.2095	0.04389	1.0408	1.0833	0.2181	0.04755
0.09	0.2214	0.04902	1.0460	1.0942	0.2316	0.05364
0.10	0.2326	0.05410	1.0513	1.1052	0.2445	0.05979
0.15	0.2807	0.07879	1.0779	1.1618	0.3026	0.09154
0.2	0.3199	0.1023	1.1052	1.2214	0.3534	0.1249
0.25	0.3535	0.1250	1.1331	1.2840	0.4006	0.1605
0.3	0.3833	0.1469	1.1619	1.3499	0.4453	0.1983
0.35	0.4095	0.1677	1.1913	1.4191	0.4879	0.2380
0.4	0.4338	0.1882	1.2214	1.4918	0.5299	0.2808
0.45	0.4561	0.2080	1.2523	1.5683	0.5711	0.3262
0.5	0.4765	0.2270	1.2840	1.6487	0.6118	0.3743
0.55	0.4957	0.2457	1.3165	1.7333	0.6526	0.4259
0.6	0.5137	0.2639	1.3499	1.8221	0.6935	0.4809
0.7	0.5466	0.2988	1.419	2.014	0.7758	0.6018
0.8	0.5753	0.3310	1.492	2.226	0.8584	0.7368
0.9	0.6024	0.3629	1.568	2.460	0.9448	0.8927
1.0	0.6262	0.3921	1.649	2.718	1.032	1.066
1.1	0.6484	0.4204	1.733	3.004	1.124	1.263
1.2	0.6689	0.4474	1.822	3.320	1.219	1.485
1.3	0.6877	0.4729	1.915	3.669	1.317	1.735
1.4	0.7049	0.4969	2.014	4.055	1.420	2.015
1.5	0.7209	0.5197	2.117	4.482	1.526	2.329
1.6	0.7364	0.5423	2.226	4.953	1.639	2.686
1.7	0.7508	0.5637	2.340	5.474	1.757	3.086
1.8	0.7641	0.5838	2.460	6.050	1.879	3.532
1.9	0.7763	0.6026	2.586	6.686	2.007	4.029
2.0	0.7879	0.6208	2.718	7.389	2.142	4.587
2.1	0.7996	0.6394	2.858	8.166	2.285	5.221
2.2	0.8095	0.6553	3.004	9.025	2.432	5.914
2.3	0.8195	0.6716	3.158	9.974	2.588	6.699
2.4	0.8289	0.6871	3.320	11.023	2.752	7.574
2.5	0.8378	0.7019	3.490	12.18	2.924	8.549
2.6	0.8455	0.7149	3.669	13.46	3.102	9.623
2.7	0.8533	0.7281	3.857	14.88	3.292	10.834
2.8	0.8610	0.7413	4.055	16.44	3.491	12.19
2.9	0.8682	0.7538	4.263	18.17	3.701	13.70
3.0	0.8749	0.7654	4.482	20.09	3.922	15.38
3.1	0.8804	0.7751	4.712	22.20	4.148	17.21
3.2	0.8870	0.7868	4.953	24.53	4.393	19.30
3.3	0.8920	0.7957	5.207	27.11	4.644	21.57
3.4	0.8976	0.8057	5.474	29.96	4.913	24.14
3.5	0.9031	0.8156	5.755	33.12	5.197	27.01
3.6	0.9075	0.8236	6.050	36.60	5.490	30.14
3.8	0.9164	0.8398	6.686	44.70	6.127	37.54
4.0	0.9247	0.8551	7.389	54.60	6.833	46.69
4.2	0.9319	0.8684	8.166	66.69	7.610	57.91
4.4	0.9380	0.8798	9.025	81.45	8.465	71.66
4.6	0.9441	0.8913	9.974	99.48	9.416	88.67
4.8	0.9496	0.9017	11.023	121.51	10.47	109.6

Table 4. (Continued.)

ψ_s	z	z^2	u_0	u_0^2	$(I_0/I_m)^{\frac{1}{2}}$	I_0/I_m
5.0	0.9546	0.9113	12.18	148.4	11.63	135.2
5.5	0.9646	0.9304	15.64	244.7	15.09	227.7
6.0	0.9723	0.9454	20.09	403.4	19.53	381.4
6.5	0.9784	0.9573	25.79	665.1	25.23	636.7
7.0	0.9834	0.9671	33.12	1096.6	32.57	1060.5
7.5	0.9873	0.9748	42.52	1808.0	41.98	1762.4
8	0.9900	0.9801	54.60	2981.0	54.05	2921.7
9	0.9939	0.9878	90.02	8103.0	89.47	8004.0
10	0.9961	0.9922	148.4	22026.0	147.8	21854.0
12	0.9983	0.9966	403.4	0.16275×10^6	402.7	0.1622×10^6
14	0.9994	0.9988	1096.6	1.2026×10^6	1096.0	1.201×10^6
16	0.9994	0.9988	2981.0	8.8861×10^6	2979.0	8.875×10^6

Note 1: ψ_s and χ_s from Table 3E. $z=(\chi_s/\chi_m)$ from Eq. (43.7). $u_0^2=I_0/I_R=e^{\psi_s}$ from Eq. (43.5). $(I_0/I_m)=z^2\,e^{\psi_s}$ from Eq. (43.6).

Table 5. *Collector region potential and its relation to emitter properties and current Flow. [Use with Eq. (46.2) and related equations.]*

ψ_c	χ_c^2	$[F(\psi_c)]$	$[F(\psi_c)]^{\frac{3}{4}}$	$[F(\psi_c)]^{\frac{3}{2}}$
0.01	0.02074	0.08849	0.16227	0.02633
0.02	0.04215	0.1420	0.23132	0.05351
0.03	0.06396	0.1875	0.28494	0.08119
0.04	0.08602	0.22846	0.33045	0.1092
0.05	0.1084	0.26654	0.37094	0.1376
0.06	0.1311	0.3025	0.40792	0.1664
0.07	0.1540	0.3369	0.44215	0.1955
0.08	0.1772	0.3698	0.47424	0.2249
0.09	0.2004	0.4015	0.50438	0.2544
0.10	0.2240	0.4324	0.53320	0.2843
0.15	0.3441	0.5757	0.66091	0.4368
0.20	0.4680	0.7067	0.77078	0.5941
0.25	0.5951	0.8295	0.86914	0.7554
0.30	0.7251	0.9462	0.95937	0.9204
0.35	0.8578	1.0584	1.0436	1.089
0.40	0.9930	1.1672	1.1229	1.261
0.45	1.130	1.2716	1.1975	1.434
0.50	1.270	1.3748	1.2696	1.612
0.60	1.555	1.5736	1.4050	1.974
0.70	1.847	1.7649	1.5312	2.345
0.80	2.146	1.9542	1.6505	2.724
0.90	2.455	2.1334	1.7652	3.116
1.00	2.766	2.3101	1.8738	3.511
1.10	3.084	2.4840	1.9786	3.915
1.20	3.408	2.6550	2.0799	4.326
1.40	4.072	2.9896	2.2735	5.169
1.60	4.757	3.3163	2.4574	6.039
1.80	5.457	3.6338	2.6319	6.927

Table 5. (Continued.)

ψ_c	χ_c^2	$[F(\psi_c)]$	$[F(\psi_c)]^{\frac{2}{3}}$	$[F(\psi_c)]^{\frac{3}{2}}$
2.00	6.180	3.9482	2.8009	7.845
2.20	6.917	4.2560	2.9631	8.780
2.40	7.667	4.5583	3.1196	9.732
2.60	8.433	4.8559	3.2711	10.70
2.80	9.217	5.1538	3.4205	11.70
3.00	10.011	5.4463	3.5651	12.71
3.20	10.824	5.7367	3.7068	13.74
3.40	11.649	6.0243	3.8453	14.79
3.60	12.482	6.3072	3.9799	15.84
3.80	13.330	6.5908	4.1134	16.92
4.00	14.190	6.8708	4.2438	18.01
4.50	16.394	7.5657	4.5618	20.81
5.00	18.662	8.2486	4.8672	23.69
5.50	21.004	8.9243	5.1633	26.66
6.00	23.406	9.5926	5.4507	29.71
6.50	25.867	10.255	5.7306	32.84
7.00	28.388	10.911	6.0033	36.04
7.50	30.958	11.559	6.2690	39.30
8.00	33.594	12.205	6.5299	42.64
9.00	39.000	13.483	7.0363	49.51
10.0	44.622	14.749	7.5260	56.64
11.0	50.424	16.002	8.0006	64.01
12.0	56.400	17.241	8.4611	71.59
13.0	62.552	18.473	8.9107	79.40
14.0	68.857	19.696	9.3493	87.41
15.0	75.342	20.914	9.7796	95.64
16.0	81.957	22.115	10.198	104.0
18.0	95.648	24.516	11.018	121.4
20.0	109.83	26.885	11.807	139.4
25.0	147.87	32.782	13.700	187.7
30.0	188.79	38.587	15.482	239.7
35.0	232.26	44.294	17.170	294.8
40.0	278.22	49.966	18.794	353.2
45.0	326.89	55.637	20.372	415.0
50.0	377.52	61.236	21.891	479.2
60.0	484.88	72.357	24.809	615.5
70.0	600.25	83.426	27.604	762.0
80.0	722.53	94.400	30.285	917.2
90.0	850.89	105.26	32.863	1080.1
100.0	985.96	116.16	35.378	1252.0
150.0	1745.6	169.97	47.074	2216.0
200.0	2626.6	223.44	57.741	3334.0
300.0	4692.3	328.57	77.175	5956.0
400.0	7103.1	433.22	94.958	9017.0
500.0	9808.9	537.20	111.58	12451.0
600.0	12783.0	640.95	127.39	16227.0
700.0	16002.0	744.48	142.52	20313.0
800.0	19432.0	847.43	157.06	24667.0
900.0	23074.0	950.20	171.14	29290.0
1000.0	26929.0	1053.3	184.89	34184.0

Note 1: Tabular form of Eq. (46.2) comes from relation $[F(\psi_c)]^{\frac{2}{3}} = 1.2694\ \chi_c^2 = (\frac{9}{4}\sqrt{\pi})\ \chi_c^2$.
Note 2: Use Eq. (37.8) or (46.5) for $\psi_c > 1000$.

Table 6. *Relation between maximum and minimum current flow for a given collector region potential. [See Eq. (46.14).]*

ψ_c	$f(\psi_c)$	$\ln f(\psi_c)$	$f^{\frac{3}{2}}(\psi_c)$	$(\frac{3}{2}) \ln f(\psi_c)$
1.0	4.3515	1.47052	2.6654	0.98035
2.0	2.9810	1.09226	2.0713	0.72818
3.0	2.4674	0.90316	1.8260	0.60211
4.0	2.1890	0.78344	1.6859	0.52230
5.0	2.0110	0.69863	1.5932	0.46576
6.0	1.8861	0.63451	1.5266	0.42301
7.0	1.7929	0.58383	1.4758	0.38922
8.0	1.7204	0.54256	1.4358	0.36171
9.0	1.6621	0.50808	1.4032	0.33872
10.0	1.6139	0.47865	1.3759	0.31910
12.0	1.5389	0.43107	1.3329	0.28738
14.0	1.4827	0.39386	1.3003	0.26257
16.0	1.4389	0.36388	1.27455	0.24259
18.0	1.4035	0.33897	1.2536	0.22598
20.0	1.3744	0.31802	1.2362	0.21201
25.0	1.3191	0.27695	1.2028	0.18463
30.0	1.2802	0.24702	1.1790	0.16468
35.0	1.2511	0.22402	1.1611	0.14935
40.0	1.2283	0.20563	1.1469	0.13709
45.0	1.2098	0.19046	1.1354	0.12697
50.0	1.1946	0.17781	1.1259	0.11854
60.0	1.1708	0.15769	1.1109	0.10513
70.0	1.1529	0.14228	1.0995	0.09485
80.0	1.1389	0.13006	1.0906	0.08671
90.0	1.1277	0.12018	1.0834	0.08012
100.0	1.1183	0.11181	1.0774	0.07454
150.0	1.0883	0.08462	1.0580	0.05641
200.0	1.0717	0.06925	1.0473	0.04617
300.0	1.0534	0.05202	1.0353	0.03468
400.0	1.0433	0.04239	1.0287	0.02826
500.0	1.0368	0.03614	1.0244	0.02409
600.0	1.0322	0.03169	1.0214	0.02113
700.0	1.0288	0.02839	1.0191	0.01893
800.0	1.0261	0.02577	1.0173	0.01718
900.0	1.0239	0.02362	1.0159	0.01575
1000.0	1.0221	0.02186	1.0147	0.01457

Note 1: $f(\psi_c) = \left(1 + \frac{\chi_m}{\chi_c}\right)^2$ (Eq. (46.14).

Table 7. *The universal limiting curve of Figs. 16 and 17 is a plot of u_0^2 as a function of S'. (See Sect. 57.)*

			u_0	$u_0 \chi_{sR}$		u_0^2	S'
ψ_{sR}	χ_{sR}	$\psi_{sR}/2$	$e^{(\psi_{sR}/2)}$	χ_{c0}	ψ_{c0}	$e^{\psi_{sR}}$	$\psi_{sR} + \psi_{c0}$
0.02	0.1947	0.01	1.0101	0.1967	0.0180	1.0202	0.038
0.04	0.2721	0.02	1.0202	0.2776	0.0362	1.0408	0.076
0.06	0.3302	0.03	1.0305	0.3403	0.0533	1.0618	0.113
0.08	0.3783	0.04	1.0408	0.3937	0.0703	1.0833	0.150
0.10	0.4201	0.05	1.0513	0.4417	0.0871	1.1052	0.187
0.15	0.5070	0.075	1.0779	0.5465	0.1322	1.1618	0.282
0.20	0.5777	0.10	1.1052	0.6385	0.1750	1.2214	0.375
0.25	0.6385	0.125	1.1332	0.7235	0.223	1.2840	0.473
0.30	0.6923	015	1.1618	0.8043	0.270	1.3499	0.570
0.40	0.7835	0.2	1.2214	0.9570	0.372	1.4918	0.772
0.50	0.8605	0.25	1.2840	1.1049	0.483	1.6487	0.983
0.60	0.9277	0.3	1.3499	1.252	0.605	1.8221	1.205
0.693	0.985	0.347	1.414	1.393	0.732	2	1.425
0.80	1.039	0.4	1.4918	1.550	0.883	2.226	1.683

Table 7. (Continued.)

			u_0	$u_0 \chi_{sR}$		u_0^2	S'
ψ_{sR}	χ_{sR}	$\psi_{sR}/2$	$e^{(\psi_{sR}/2)}$	χ_{c0}	ψ_{c0}	$e^{\psi_{sR}}$	$\psi_{sR}+\psi_{c0}$
1.00	1.131	0.5	1.6487	1.865	1.22	2.718	2.220
1.099	1.169	0.549	1.732	2.025	1.382	3	2.481
1.2	1.208	0.6	1.8221	2.201	1.627	3.320	2.827
1.386	1.267	0.693	2.000	2.534	2.068	4	3.454
1.4	1.273	0.7	2.014	2.564	2.110	4.055	3.51
1.6	1.330	0.8	2.226	2.961	2.690	4.953	4.29
1.792	1.375	0.896	2.449	3.369	3.33	6	5.12
1.8	1.380	0.9	2.460	3.395	3.37	6.050	5.17
2.0	1.423	1.0	2.718	3.868	4.19	7.389	6.19
2.079	1.439	1.040	2.828	4.071	4.55	8	6.63
2.303	1.480	1.151	3.162	4.680	5.69	10	7.99
2.4	1.497	1.2	3.320	4.970	6.28	11.023	8.68
2.773	1.550	1.386	4.000	6.200	8.92	16	11.69
2.8	1.555	1.4	4.055	6.306	9.15	16.44	11.95
2.996	1.580	1.498	4.472	7.065	10.91	20	13.91
3.2	1.602	1.6	4.953	7.935	13.09	24.53	16.29
3.6	1.639	1.8	6.050	9.916	18.40	36.60	22.00
3.689	1.645	1.844	6.325	10.40	19.77	40	23.46
4.0	1.670	2.0	7.389	12.34	25.59	54.60	29.59
4.094	1.675	2.047	7.746	12.98	27.56	60	31.6
4.4	1.694	2.2	9.025	15.288	35.0	81.45	39.4
4.605	1.704	2.303	10.000	17.04	41.0	100	45.6
5.0	1.724	2.5	12.18	20.998	55.7	148.4	60.7
5.298	1.730	2.649	14.142	24.47	70.0	200	75.3
5.5	1.742	2.75	15.64	27.245	81.5	244.7	87.0
6.0	1.756	3.0	20.09	35.278	118	403.4	124.0
7.0	1.770	3.5	33.12	58.821	240	1096.6	247.0
8	1.788	4.0	54.60	97.625	488	2981	496
9	1.795	4.5	90.02	161.59	975	8103	984
10	1.799	5	148.4	266.97	1944	22026	1954
12	1.803	6	403.4	727.33	7490	0.16275×10^6	7500
14	1.805	7	1096.6	1979.36	28800	1.2026×10^6	28800
16	1.805	8	2981	5380.71	110000	8.8861×10^6	110000

Table 8. *Master curve for emitter of unlimited capability* $u_0^2 = \infty$. *(See Sect. 58 and Figs. 16 and 17.)*

ψ_c	U^2	Σ	ψ_c	U^2	Σ
0.02	1.2403	0.23535	35.0	89.09	39.490
0.04	1.3512	0.34099	40.0	104.8	44.652
0.06	1.4412	0.42548	45.0	121.2	49.797
0.10	1.5928	0.56549	50.0	138.3	54.929
0.20	1.9011	0.8424	60.0	174.1	65.160
0.40	2.4080	1.2788	70.0	212.2	75.358
0.60	2.8577	1.6500	80.0	252.3	85.531
1.00	3.6895	2.3055	90.0	294.2	95.684
1.40	4.483	2.9003	100.0	338.0	105.823
2.0	5.648	3.7313	150.0	582.4	156.37
3.0	7.573	5.0246	200.0	863.1	206.76
5.0	11.506	7.4429	300.0	1515.0	307.32
7.0	15.60	9.7473	400.0	2272.0	407.73
10.0	22.08	13.095	500.0	3118.0	508.04
12.0	26.61	15.281	600.0	4045.0	608.31
14.0	31.30	17.444	700.0	5047.0	708.53
16.0	36.15	19.588	800.0	6113.0	808.72
20.0	46.28	23.835	900.0	7244.0	908.89
25.0	59.80	29.091	1000.0	8439.0	1009.04
30.0	74.10	34.305			

Note 1: $U^2 = \left(1 + \frac{\chi_c}{\chi_m}\right)^2$ [Eq. (58.3)]. Note 2: $\Sigma = \psi_c + \ln U^2$ [Eq. (58.5)].

Table 9. *Master curve for emitter of limited capability*

$u_0^2 \rightarrow$ $\psi^s R$ $\chi^s R$	2 0.693 0.985		3 1.099 1.169		4 1.386 1.267		6 1.792 1.375		8 2.079 1.439	
ψ_s	u^2	S'	u^2	S'	u^2	S'	u^2	S'	u^2	S'
0	2	1.425	3	2.509	4	3.456	6	5.11	8	6.629
0.04	1.922	1.126	2.882	2.113	3.843	2.999	5.765	4.5418	7.686	5.9495
0.10	1.810	0.929	2.714	1.836	3.619	2.651	5.429	4.1157	7.238	5.4393
0.15	1.721	0.802	2.582	1.661	3.443	2.436	5.164	3.824	6.886	5.0995
0.2	1.637	0.6918	2.456	1.506	3.275	2.244	4.912	3.568	6.550	4.7895
0.3	1.482	0.508	2.222	1.238	2.963	1.908	4.445	3.127	5.926	4.2424
0.4	1.341	0.3513	2.011	1.015	2.681	1.624	4.022	2.739	5.362	3.7684
0.5	1.213	0.2163	1.820	0.817	2.426	1.376	3.639	2.401	4.852	3.344
0.6	1.097	0.098	1.646	0.6413	2.195	1.134	3.293	2.094	4.390	2.960
0.8	0.899		1.348	0.3459	1.797	0.7723	2.696	1.569	3.594	2.309
1.0	0.736		1.104	0.1035	1.472	0.4615	2.207	1.133	2.943	1.764

Table 10. *Electron current in a retarding field for cylinders of various radii ratios from 1 to ∞ (Sect. 60).*

$$\frac{1}{a} = \infty$$

S	$F_1(S)$	$\ln F_1(S)$	$\log_{10} F_1(S)$	Slope	Disp.
0	1.0000	0	0	0	0
0.5	0.8012	− 0.2216	− 0.0962	0.608	0.2784
1.0	0.5724	− 0.5579	− 0.2423	0.728	0.4421
1.5	0.3916	− 0.9374	− 0.4071	0.787	0.5626
2.0	0.2615	− 1.3414	− 0.5826	0.826	0.6586
3.0	0.1116	− 2.1927	− 0.9523	0.872	0.8073
4.0	4.601×10^{-2}	− 3.0788	− 1.3371	0.898	0.9212
5.0	1.857×10^{-2}	− 3.9864	− 1.7313	0.9157	1.0136
6.0	0.7383×10^{-2}	− 4.9086	− 2.1318	0.9281	1.0914
7.0	0.2905×10^{-2}	− 5.8413	− 2.5368	0.9370	1.1587
8.0	0.1134×10^{-2}	− 6.7820	− 2.9454	0.9444	1.2180
9.0	4.398×10^{-4}	− 7.7291	− 3.3567	0.9501	1.2709
10.0	1.697×10^{-4}	− 8.6812	− 3.7702	0.954	1.3188
12.0	0.2498×10^{-4}	− 10.5974	− 4.6024	0.962	1.4026
14.0	3.632×10^{-6}	− 12.526	− 5.4400	0.967	1.474
16.0	0.5234×10^{-6}	− 14.463	− 6.2812	0.970	1.537
18.0	7.488×10^{-8}	− 16.407	− 7.1255	0.974	1.593
20.0	1.066×10^{-8}	− 18.357	− 7.9723	0.977	1.643

$$\frac{1}{a} = 5.0$$

S	$F(S, a)$	$\ln F(S, a)$	$\log_{10} F(S, a)$	Slope	Disp.
0	1.0000	0	0	0	0
0.5	0.7979	− 0.2257	− 0.0980	0.619	0.2743
1.0	0.5668	− 0.5678	− 0.2466	0.740	0.4322
1.5	0.3854	− 0.9535	− 0.4141	0.800	0.5465
2.0	0.2557	− 1.3639	− 0.5923	0.839	0.6361
3.0	0.1077	− 2.2280	− 0.9676	0.886	0.7720
4.0	4.384×10^{-2}	− 3.1272	− 1.3581	0.911	0.8728
5.0	1.747×10^{-2}	− 4.0475	− 1.7578	0.9286	0.9525
6.0	0.6858×10^{-2}	− 4.9824	− 2.1638	0.9406	1.0176
7.0	0.2664×10^{-2}	− 5.9278	− 2.5744	0.9499	1.0722
8.0	0.1027×10^{-2}	− 6.8811	− 2.9884	0.9566	1.1189
9.0	3.935×10^{-4}	− 7.8405	− 3.4051	0.9622	1.1595
10.0	1.500×10^{-4}	− 8.8050	− 2.8240	0.9667	1.1950

u_0^2 = *selected values. (See Sect. 58 and Figs. 16 and 17.)*

10 2.303 1.480		20 2.996 1.580		40 3.689 1.645		60 4.094 1.675		100 4.605 1.704		200 5.298 1.730	
u^2	S'	u^2	S^2	u^2	S'	u^2	S'	u^2	S'	u^2	S'
10	8.003	20	13.906	40	23.489	60	31.644	100	45.55	200	75.298
9.608	7.2527	19.22	12.9059	38.43	22.0588	57.65	29.9544	96.08	43.5651	192.2	72.2585
9.048	6.6926	18.00	12.0559	36.19	20.7688	54.29	28.2943	90.48	40.707	181.0	68.193
8.607	6.2826	17.21	11.3255	34.43	19.8089	51.64	27.0443	86.47	39.5598	172.1	66.2481
8.187	5.9126	16.37	10.8454	32.75	18.9089	49.12	25.8942	81.87	37.4051	163.7	63.398
7.408	5.2726	14.82	9.8459	29.63	17.3188	44.45	23.7743	74.08	35.0	148.2	58.4985
6.703	4.7226	13.41	8.946	26.81	15.8587	40.22	21.8743	67.03	32.3851	134.1	54.0986
6.065	4.2276	12.31	8.2104	24.26	14.538	36.39	20.1443	60.65	29.9051	121.3	49.9
5.488	3.7776	10.97	7.3651	21.95	13.3287	32.93	18.4944	54.88	27.6051	109.7	46.3
4.493	3.001	8.99	6.0761	17.97	11.2187	26.96	15.2443	44.93	23.5151	89.9	39.5
3.679	2.353	7.36	4.981	14.72	9.3992	22.07	13.2342	36.79	20.0252	73.6	34.2

Table 10. (Continued.)

S	$F(S,a)$	$\ln F(S,a)$	$\log_{10} F(S,a)$	Slope	Disp.
		$\frac{1}{a} = 5.0$ (Continued)			
12.0	0.2154×10^{-4}	−10.7454	−4.6667	0.9733	1.2546
14.0	3.059×10^{-6}	−12.6973	−5.5144	0.9784	1.3027
16.0	0.4307×10^{-6}	−14.6578	−6.3658	0.9821	1.3422
18.0	6.026×10^{-8}	−16.6247	−7.2200	0.9848	1.3753
20.0	0.8386×10^{-8}	−18.5967	−8.0764	0.9872	1.4033
		$\frac{1}{a} = 4.0$			
0	1.0000	0	0	0	0
0.5	0.7960	−0.2281	−0.0991	0.625	0.2719
1.0	0.5635	−0.5736	−0.2491	0.747	0.4264
1.5	0.3818	−0.9628	−0.4182	0.807	0.5372
2.0	0.2524	−1.3768	−0.5979	0.847	0.6232
3.0	0.1056	−2.2482	−0.9764	0.893	0.7518
4.0	4.266×10^{-2}	−3.1544	−1.3699	0.918	0.8456
5.0	1.688×10^{-2}	−4.0817	−1.7727	0.9358	0.9183
6.0	0.6582×10^{-2}	−5.0234	−2.1816	0.9472	0.9766
7.0	0.2541×10^{-2}	−5.9753	−2.5950	0.9566	1.0247
8.0	9.731×10^{-4}	−6.9351	−3.0119	0.9631	1.0649
9.0	3.705×10^{-4}	−7.9007	−3.4312	0.9685	1.0993
10.0	1.404×10^{-4}	−8.8712	−3.8527	0.9725	1.1288
12.0	0.1994×10^{-4}	−10.8230	−4.7004	0.9789	1.1770
14.0	2.801×10^{-6}	−12.7857	−5.5528	0.9836	1.2143
16.0	0.3904×10^{-6}	−14.7562	−6.4085	0.9869	1.2438
18.0	5.410×10^{-8}	−16.7324	−7.2668	0.9893	1.2676
20.0	0.7464×10^{-8}	−18.7132	−8.1270	0.9915	1.2868
		$\frac{1}{a} = 3.0$			
0	1.0000	0	0	0	0
0.5	0.7916	−0.2336	−0.1015	0.640	0.2664
1.0	0.5562	−0.5866	−0.2548	0.762	0.4134
1.5	0.3739	−0.9837	−0.4272	0.823	0.5163
2.0	0.2452	−1.4056	−0.6105	0.863	0.5944
3.0	0.1010	−2.2926	−0.9956	0.907	0.7074
4.0	4.022×10^{-2}	−3.2135	−1.3956	0.933	0.7865

Table 10. (Continued.)

S	$F(S, a)$	$\ln F(S, a)$	$\log_{10} F(S, a)$	Slope	Disp.
		$\frac{1}{a} = 3.0$ (Continued)			
5.0	1.568×10^{-2}	−4.1552	−1.8046	0.9492	0.8448
6.0	0.6034×10^{-2}	−5.1104	−2.2194	0.9609	0.8896
7.0	0.2299×10^{-2}	−6.0752	−2.6384	0.9687	0.9248
8.0	8.701×10^{-4}	−7.0469	−3.0604	0.9747	0.9531
9.0	3.276×10^{-4}	−8.0239	−3.4847	0.9795	0.9761
10.0	1.228×10^{-4}	−9.0050	−3.9108	0.9829	0.9950
12.0	0.1710×10^{-4}	−10.9764	−4.7670	0.9883	1.0236
14.0	2.361×10^{-6}	−12.9564	−5.6269	0.9916	1.0436
16.0	0.3242×10^{-6}	−14.9420	−6.4892	0.9940	1.0580
18.0	4.433×10^{-8}	−16.9316	−7.3533	0.9957	1.0684
20.0	0.6045×10^{-8}	−18.9240	−8.2186	0.9968	1.0760
		$\frac{1}{a} = 2.5$			
0	1.0000	0	0	0	0
0.5	0.7867	−0.2399	−0.1042	0.658	0.2601
1.0	0.5486	−0.6005	−0.2608	0.780	0.3995
1.5	0.3658	−1.0058	−0.4368	0.839	0.4942
2.0	0.2379	−1.4357	−0.6235	0.878	0.5643
3.0	9.651×10^{-2}	−2.3381	−1.0154	0.922	0.6619
4.0	3.788×10^{-2}	−3.2735	−1.4217	0.947	0.7265
5.0	1.458×10^{-2}	−4.2280	−1.8362	0.9610	0.7720
6.0	0.5544×10^{-2}	−5.1949	−2.2561	0.9724	0.8051
7.0	0.2090×10^{-2}	−6.1704	2.6708	0.9787	0.8296
8.0	7.836×10^{-4}	−7.1516	−3.1059	0.9840	0.8484
9.0	2.924×10^{-4}	−8.1373	−3.5340	0.9878	0.8627
10.0	1.088×10^{-4}	−9.1263	−3.9635	0.9902	0.8737
12.0	0.1495×10^{-4}	−11.1107	−4.8253	0.9941	0.8893
14.0	2.043×10^{-6}	−13.1011	−5.6897	0.9962	0.8989
16.0	0.2782×10^{-6}	−15.0950	−6.5557	0.9977	0.9050
18.0	3.779×10^{-8}	−17.0912	−7.4226	0.9984	0.9088
20.0	0.5127×10^{-8}	−19.0887	−8.2901	0.9990	0.9113
		$\frac{1}{a} = 2.0$			
0	1.0000	0	0	0	0
0.5	0.7773	−0.2520	−0.1094	0.688	0.2480
1.0	0.5335	−0.6284	−0.2729	0.812	0.3716
1.5	0.3501	−1.0494	−0.4557	0.870	0.4506
2.0	0.2244	−1.4943	−0.6490	0.908	0.5057
3.0	8.859×10^{-2}	−2.4238	−1.0526	0.947	0.5762
4.0	3.397×10^{-2}	−3.3824	−1.4690	0.968	0.6176
5.0	1.282×10^{-2}	−4.3567	−1.8921	0.9794	0.6433
6.0	0.4795×10^{-2}	−5.3402	−2.3192	0.9876	0.6598
7.0	0.1783×10^{-2}	−6.3296	−2.7489	0.9911	0.6704
8.0	6.607×10^{-4}	−7.3222	−3.1800	0.9941	0.6778
9.0	2.442×10^{-4}	−8.3173	−3.6122	0.9963	0.6827
10.0	0.9014×10^{-4}	−9.3141	−4.0451	0.9974	0.6859
12.0	0.1224×10^{-4}	−11.3104	−4.9120	0.9988	0.6896
14.0	1.660×10^{-6}	−13.3086	−5.7799	0.9993	0.6914
16.0	2.249×10^{-6}	−15.3077	−6.6480	0.9998	0.6923
18.0	3.044×10^{-8}	−17.3074	−7.5165	0.9999	0.6926
20.0	0.4121×10^{-8}	−19.3073	−8.3851	1.0	0.6927

Table 10. (Continued.)

S	$F(S,a)$	$\ln F(S,a)$	$\log_{10} F(S,a)$	Slope	Disp.
		$\frac{1}{a} = 1.5$			
0	1.0000	0	0	0	0
0.5	0.7678	− 0.2642	− 0.1147	0.8543	0.2358
1.0	0.4960	− 0.7012	− 0.3045	0.8942	0.2988
1.5	0.3142	− 1.1577	− 0.5028	0.9320	0.3423
2.0	0.1953	− 1.6330	− 0.7092	0.9640	0.3670
3.0	7.357×10^{-2}	− 2.6095	− 1.1333	0.9866	0.3905
4.0	2.731×10^{-2}	− 3.6006	− 1.5637	0.9950	0.3994
5.0	1.008×10^{-2}	− 4.5971	− 1.9965	0.9977	0.4029
6.0	0.3714×10^{-2}	− 5.5956	− 2.4296	0.9990	0.4044
7.0	0.1367×10^{-2}	− 6.5952	− 2.8643	0.9996	0.4048
8.0	5.035×10^{-4}	− 7.5949	− 3.2984	0.9998	0.4051
9.0	1.851×10^{-4}	− 8.5946	− 3.7326	0.9999	0.4054
10.0	0.6810×10^{-4}	− 9.5946	− 4.1669	1.0000	0.4054
12.0	9.216×10^{-6}	− 11.595	− 5.0354	1.0000	0.405
14.0	1.247×10^{-6}	− 13.595	− 5.9042	1.0000	0.405
16.0	0.1688×10^{-6}	− 15.595	− 6.7728	1.0000	0.405
18.0	2.284×10^{-8}	− 17.595	− 7.6414	1.0000	0.405
20.0	0.3091×10^{-8}	− 19.595	− 8.5100	1.0000	0.405
		$\frac{1}{a} = 1.0$			
0	1.0	0	0	1.0	0
0.5	0.6065	− 0.5	− 0.2171		
1.0	0.3679	− 1.0	− 0.4343		
1.5	0.2231	− 1.5	− 0.6514		
2.0	0.1353	− 2.0	− 0.8686		
3.0	4.979×10^{-2}	− 3.0	− 1.3029		
4.0	1.832×10^{-2}	− 4.0	− 1.7372		
5.0	0.6738×10^{-2}	− 5.0	− 2.1715		
6.0	0.2479×10^{-2}	− 6.0	− 2.6058		
7.0	9.119×10^{-4}	− 7.0	− 3.0401		
8.0	3.355×10^{-4}	− 8.0	− 3.4744		
9.0	1.234×10^{-4}	− 9.0	− 3.9087		
10.0	0.4540×10^{-4}	− 10.0	− 4.3429		
12.0	6.144×10^{-6}	− 12.0	− 5.2115		
14.0	0.8315×10^{-6}	− 14.0	− 6.0801		
16.0	0.1125×10^{-6}	− 16.0	− 6.9487		
18.0	1.523×10^{-8}	− 18.0	− 7.8173		
20.0	0.2061×10^{-8}	− 20.0	− 8.6859		

Table 11. *The* FERMI *level and its temperature coefficient for selected donor concentration and energy level.* (Sect. 64.)

$n_D = 10^{18}$

V_T^{-1}	μ'	$E=-0.6$	$E=-0.8$	$E=-0.9$	$E=-1.0$	$E=-1.1$	$E=-1.2$	$E=-1.4$	$E=-1.6$
		μ							
8	2.512	− 2.425	− 2.425	− 2.425	− 2.425	− 2.425	− 2.425	− 2.425	− 2.425
10	1.976	− 1.907	− 1.907	− 1.907	− 1.907	− 1.907	− 1.907	− 1.907	− 1.911
12	1.624	− 1.566	− 1.566	− 1.566	− 1.566	− 1.566	− 1.567	− 1.576	− 1.616
14	1.375	− 1.326	− 1.326	− 1.326	− 1.327	− 1.329	− 1.336	− 1.384	− 1.468
16	1.191	− 1.148	− 1.148	− 1.149	− 1.153	− 1.166	− 1.194	− 1.278	− 1.375
18	1.049	− 1.010	− 1.012	− 1.017	− 1.034	− 1.067	− 1.105	− 1.205	− 1.305
20	0.936	− 0.902	− 0.907	− 0.925	− 0.960	− 0.998	− 1.051	− 1.151	− 1.251
22	0.844	− 0.813	− 0.831	− 0.865	− 0.907	− 0.956	− 1.006	− 1.106	− 1.206
24	0.769	− 0.741	− 0.780	− 0.820	− 0.870	− 0.920	− 0.970	− 1.070	− 1.170
26	0.705	− 0.682	− 0.743	− 0.789	− 0.839	− 0.889	− 0.939	− 1.039	− 1.139

Table 11. (Continued.)

$n_D = 10^{18}$ (Continued)

V_T^{-1}	$\frac{d\mu'}{dV_T}$	$E=-0.6$	$E=-0.8$	$E=-0.9$	$E=-1.0$	$E=-1.1$	$E=-1.2$	$E=-1.4$	$E=-1.6$
		$\frac{d\mu}{dV_T}$							
8	21.596	−20.902	−20.902	−20.902	−20.902	−20.902	−20.902	−20.894	−20.885
10	21.261	−20.598	−20.568	−20.568	−20.567	−20.564	−20.557	−20.478	−19.896
12	20.987	−20.294	−20.293	−20.290	−20.280	−20.244	−20.117	−18.621	−14.456
14	20.756	−20.063	−20.056	−20.030	−19.916	−19.468	−18.099	−13.335	−10.980
16	20.556	−19.861	−19.813	−19.595	−18.654	−16.252	−13.489	−10.790	−10.126
18	20.379	−19.680	−19.370	−18.062	−15.058	−12.384	−10.891	−10.045	−9.883
20	20.221	−19.498	−17.972	−14.661	−11.921	−10.508	−10.085	−9.818	−9.772
22	20.078	−19.262	−15.012	−11.891	−10.444	−9.966	−9.791	−9.706	−9.694
24	19.948	−18.785	−12.309	−10.472	−9.908	−9.720	−9.658	−9.631	−9.628
26	19.828	−17.623	−10.809	−9.916	−9.672	−9.598	−9.576	−9.568	−9.565

$n_D = 3\times 10^{18}$

V_T^{-1}	μ'	μ							
8	2.375	−2.288	−2.288	−2.288	−2.288	−2.288	−2.288	−2.288	−2.288
10	1.866	−1.797	−1.797	−1.797	−1.797	−1.797	−1.797	−1.799	−1.809
12	1.532	−1.475	−1.475	−1.475	−1.475	−1.476	−1.478	−1.497	−1.557
14	1.297	−1.247	−1.248	−1.248	−1.250	−1.255	−1.270	−1.336	−1.427
16	1.122	−1.079	−1.080	−1.082	−1.092	−1.115	−1.151	−1.242	−1.340
18	0.988	−0.949	−0.953	−0.964	−0.992	−1.032	−1.0776	−1.175	−1.275
20	0.881	−0.847	−0.860	−0.888	−0.929	−0.975	−1.024	−1.123	−1.223
22	0.795	−0.764	−0.796	−0.836	−0.883	−0.932	−0.982	−1.082	−1.182
24	0.723	−0.698	−0.753	−0.799	−0.842	−0.897	−0.947	−1.047	−1.147
26	0.663	−0.646	−0.720	−0.769	−0.818	−0.868	−0.918	−1.018	−1.118

V_T^{-1}	$\frac{d\mu'}{dV_T}$	$\frac{d\mu}{dV_T}$							
8	20.497	−19.804	−19.804	−19.803	−19.803	−19.803	−19.802	−19.794	−19.750
10	20.162	−19.469	−19.469	−19.468	−19.466	−19.459	−19.438	−19.210	−17.596
12	19.889	−19.196	−19.193	−19.202	−19.154	−19.048	−18.700	−15.756	−12.206
14	19.658	−18.963	−18.942	−18.866	−18.551	−17.504	−15.365	−11.440	−10.031
16	19.457	−18.759	−18.616	−18.041	−16.216	−13.511	−11.502	−9.878	−9.495
18	19.281	−18.567	−17.748	−15.450	−12.550	−10.783	−9.950	−9.418	−9.317
20	19.123	−18.341	−15.393	−12.243	−10.473	−9.720	−9.415	−9.246	−9.220
22	18.980	−17.938	−12.487	−10.427	−9.613	−9.313	−9.204	−9.151	−9.144
24	18.849	−16.971	−10.654	−9.607	−9.137	−9.135	−9.097	−9.080	−9.078
26	18.729	−15.083	−9.735	−9.235	−9.083	−9.037	−9.024	−9.018	−9.018

$n_D = 10^{19}$

V_T^{-1}	μ'	μ							
8	2.224	−2.137	−2.137	−2.137	−2.137	−2.137	−2.138	−2.138	−2.152
10	1.746	−1.676	−1.676	−1.677	−1.677	−1.677	−1.677	−1.682	−1.706
12	1.432	−1.374	−1.374	−1.375	−1.375	−1.377	−1.383	−1.422	−1.498
14	1.211	−1.161	−1.162	−1.163	−1.168	−1.181	−1.207	−1.287	−1.382
16	1.047	−1.004	−1.006	−1.013	−1.033	−1.066	−1.108	−1.203	−1.302
18	0.921	−0.883	−0.892	−0.914	−0.951	−0.995	−1.043	−1.141	−1.241
20	0.821	−0.787	−0.814	−0.851	−0.896	−0.944	−0.994	−1.093	−1.193
22	0.740	−0.712	−0.762	−0.807	−0.855	−0.904	−0.954	−1.054	−1.154
24	0.673	−0.654	−0.725	−0.773	−0.822	−0.872	−0.922	−1.022	−1.122
26	0.616	−0.612	−0.696	−0.745	−0.795	−0.845	−0.895	−0.995	−1.095

Table 11. (Continued.)

$n_D = 10^{19}$ (Continued)

V_T^{-1}	$\frac{d\mu'}{dV_T}$	$E=-0.6$	$E=-0.8$	$E=-0.9$	$E=-1.0$	$E=-1.1$	$E=-1.2$	$E=-1.4$	$E=-1.6$
		$\frac{d\mu}{dV_T}$							
8	19.293	− 18.600	− 18.600	− 18.599	− 18.599	− 18.597	− 18.594	− 18.568	− 18.426
10	18.958	− 18.265	− 18.264	− 18.261	− 18.253	− 18.231	− 18.162	− 17.500	− 14.985
12	18.685	− 17.991	− 17.987	− 17.954	− 17.856	− 17.535	− 16.652	− 13.016	− 10.450
14	18.454	− 17.757	− 17.688	− 17.448	− 16.611	− 14.739	− 12.517	− 9.963	− 9.181
16	18.253	− 17.544	− 17.104	− 15.753	− 13.283	− 11.164	− 9.955	− 9.041	− 8.842
18	18.077	− 17.315	− 15.364	− 12.580	− 10.531	− 9.512	− 9.052	− 8.760	− 8.706
20	17.919	− 16.945	− 12.532	− 10.316	− 9.305	− 8.889	− 8.723	− 8.630	− 8.615
22	17.776	− 16.095	− 10.436	− 9.247	− 8.799	− 8.634	− 8.575	− 8.545	− 8.541
24	17.645	− 14.379	− 9.344	− 8.766	− 8.571	− 8.507	− 8.486	− 8.477	− 8.476
26	17.525	− 12.266	− 8.810	− 8.535	− 8.451	− 8.427	− 8.419	− 8.416	− 8.415

$n_D = 3 \times 10^{19}$

V_T^{-1}	μ'	μ							
8	2.087	− 2.000	− 2.000	− 2.000	− 2.000	− 2.000	− 2.000	− 2.001	− 2.005
10	1.636	− 1.567	− 1.567	− 1.567	− 1.567	− 1.568	− 1.569	− 1.582	− 1.624
12	1.340	− 1.283	− 1.283	− 1.284	− 1.285	− 1.291	− 1.304	− 1.362	− 1.448
14	1.132	− 1.083	− 1.084	− 1.088	− 1.099	− 1.122	− 1.157	− 1.245	− 1.342
16	0.978	− 0.935	− 0.941	− 0.956	− 0.986	− 1.026	− 1.071	− 1.168	− 1.268
18	0.860	− 0.822	− 0.842	− 0.874	− 0.916	− 0.963	− 1.012	− 1.111	− 1.211
20	0.766	− 0.735	− 0.778	− 0.820	− 0.867	− 0.916	− 0.966	− 1.066	− 1.166
22	0.690	− 0.668	− 0.734	− 0.781	− 0.830	− 0.879	− 0.929	− 1.029	− 1.129
24	0.627	− 0.619	− 0.701	− 0.750	− 0.799	− 0.849	− 0.899	− 0.999	− 1.099
26	0.574	− 0.583	− 0.674	− 0.724	− 0.774	− 0.824	− 0.874	− 0.974	− 1.074

V_T^{-1}	$\frac{d\mu'}{dV_T}$	$\frac{d\mu}{dV_T}$							
8	18.194	− 17.501	− 17.501	− 17.500	− 17.498	− 17.494	− 17.485	− 17.408	− 17.020
10	17.860	− 17.166	− 17.163	− 17.155	− 17.131	− 17.062	− 16.871	− 15.416	− 12.405
12	17.586	− 16.891	− 16.863	− 16.782	− 16.513	− 15.751	− 14.250	− 10.889	− 9.289
14	17.355	− 16.652	− 16.452	− 15.844	− 14.300	− 12.190	− 10.519	− 8.958	− 8.504
16	17.155	− 16.415	− 15.327	− 13.241	− 11.019	− 9.629	− 8.911	− 8.397	− 8.266
18	16.978	− 16.086	− 12.837	− 10.504	− 9.214	− 8.617	− 8.350	− 8.182	− 8.150
20	16.820	− 15.387	− 10.448	− 9.055	− 8.463	− 8.223	− 8.127	− 8.073	− 8.065
22	16.677	− 13.900	− 9.097	− 8.400	− 8.141	− 8.046	− 8.011	− 7.995	− 7.992
24	16.546	− 11.887	− 8.429	− 8.094	− 7.982	− 7.945	− 7.933	− 7.927	− 7.927
26	16.426	− 10.209	− 8.095	− 7.935	− 7.887	− 7.873	− 7.868	− 7.867	− 7.867

$n_D = 10^{20}$

V_T^{-1}	μ'	μ							
8	1.936	− 1.850	− 1.850	− 1.850	− 1.850	− 1.850	− 1.850	− 1.853	− 1.864
10	1.516	− 1.446	− 1.446	− 1.447	− 1.447	− 1.449	− 1.454	− 1.482	− 1.546
12	1.240	− 1.182	− 1.183	− 1.185	− 1.190	− 1.204	− 1.228	− 1.302	− 1.395
14	1.046	− 0.997	− 1.001	− 1.011	− 1.032	− 1.066	− 1.107	− 1.201	− 1.299
16	0.903	− 0.861	− 0.876	− 0.902	− 0.940	− 0.985	− 1.032	− 1.130	− 1.230
18	0.793	− 0.758	− 0.795	− 0.835	− 0.880	− 0.928	− 0.978	− 1.077	− 1.177
20	0.706	− 0.680	− 0.742	− 0.788	− 0.836	− 0.886	− 0.936	− 1.036	− 1.136
22	0.635	− 0.624	− 0.704	− 0.753	− 0.802	− 0.852	− 0.902	− 1.002	− 1.102
24	0.577	− 0.585	− 0.675	− 0.724	− 0.774	− 0.824	− 0.874	− 0.974	− 1.074
26	0.528	− 0.556	− 0.651	− 0.701	− 0.751	− 0.801	− 0.851	− 0.951	− 1.051

Table 11. (Continued.)

$n_D = 10^{20}$ (Continued)

V_T^{-1}	$\frac{d\mu'}{dV_T}$	$E=-0.6$	$E=-0.8$	$E=-0.9$	$E=-1.0$	$E=-1.1$	$E=-1.2$	$E=-1.4$	$E=-1.6$
		$\frac{d\mu}{dV_T}$							
8	16.990	−16.297	−16.295	−16.293	−16.288	−16.274	−16.242	−16.243	−15.018
10	16.656	−15.961	−15.949	−15.923	−15.846	−15.634	−15.118	−12.708	−10.187
12	16.382	−15.682	−15.590	−15.344	−14.645	−13.253	−11.543	− 9.208	− 8.308
14	16.151	−15.424	−14.837	−13.552	−11.608	− 9.966	− 8.946	− 8.073	− 7.824
16	15.951	−15.107	−12.857	−10.694	− 9.198	− 8.399	− 8.002	− 7.715	− 7.647
18	15.774	−14.493	−10.372	− 8.859	− 8.130	− 7.800	− 7.663	− 7.562	− 7.544
20	15.616	−13.172	− 8.794	− 8.006	− 7.681	− 7.549	− 7.496	− 7.467	− 7.462
22	15.473	−11.282	− 7.997	− 7.614	− 7.471	− 7.420	− 7.401	− 7.391	− 7.390
24	15.342	− 9.644	− 7.600	− 7.416	− 7.355	− 7.335	− 7.328	− 7.325	− 7.325
26	15.222	− 8.574	− 7.390	− 7.302	− 7.276	− 7.268	− 7.266	− 7.265	− 7.265

$n_D = 3\times 10^{20}$

V_T^{-1}	μ'	μ							
8	1.799	−1.712	−1.712	−1.712	−1.713	−1.713	−1.714	−1.722	−1.746
10	1.406	−1.336	−1.337	−1.338	−1.340	−1.344	−1.356	−1.404	−1.482
12	1.149	−1.091	−1.093	−1.098	−1.111	−1.134	−1.167	−1.252	−1.347
14	0.968	−0.919	−0.929	−0.948	−0.979	−1.019	−1.064	−1.160	−1.260
16	0.835	−0.794	−0.824	−0.858	−0.901	−0.948	−0.997	−1.096	−1.196
18	0.732	−0.702	−0.757	−0.801	−0.848	−0.897	−0.947	−1.047	−1.147
20	0.651	−0.636	−0.712	−0.760	−0.809	−0.858	−0.908	−1.008	−1.108
22	0.585	−0.590	−0.678	−0.727	−0.777	−0.827	−0.877	−0.977	−1.077
24	0.531	−0.557	−0.652	−0.701	−0.751	−0.801	−0.851	−0.951	−1.051
26	0.486	−0.532	−0.630	−0.680	−0.729	−0.779	−0.829	−0.929	−1.029
V_T^{-1}	$\frac{d\mu'}{dV_T}$	$\frac{d\mu}{dV_T}$							
8	15.892	−15.198	−15.194	−15.187	−15.170	−15.131	−15.039	−14.431	−12.729
10	15.557	−14.860	−14.825	−14.748	−14.536	−14.025	−13.052	−10.438	− 8.726
12	15.284	−14.569	−14.309	−13.718	−12.485	−10.897	− 9.551	− 8.087	− 7.563
14	15.052	−14.260	−12.946	−11.209	− 9.567	− 8.494	− 7.886	− 7.378	− 7.235
16	14.852	−13.745	−10.550	− 8.916	− 7.993	− 7.525	− 7.295	− 7.129	− 7.184
18	14.675	−12.638	− 8.678	− 7.756	− 7.332	− 7.141	− 7.057	− 7.004	− 6.993
20	14.517	−10.892	− 7.686	− 7.227	− 7.039	− 6.963	− 6.932	− 6.915	− 6.913
22	14.374	− 9.252	− 7.192	− 6.970	− 6.888	− 6.858	− 6.847	− 6.842	− 6.841
24	14.244	− 8.143	− 6.934	− 6.828	− 6.793	− 6.781	− 6.777	− 6.776	− 6.775
26	14.124	− 7.475	− 6.787	− 6.737	− 6.722	− 6.717	− 6.716	− 6.715	− 6.715

$n_D = 10^{21}$

V_T^{-1}	μ'	μ							
8	1.648	−1.562	−1.562	−1.562	−1.563	−1.565	−1.586	−1.587	−1.634
10	1.285	−1.216	−1.218	−1.220	−1.226	−1.238	−1.260	−1.328	−1.415
12	1.048	−0.991	−0.998	−1.010	−1.033	−1.067	−1.107	−1.199	−1.296
14	0.882	−0.835	−0.858	−0.888	−0.927	−0.972	−1.019	−1.117	−1.216
16	0.759	−0.724	−0.774	−0.815	−0.861	−0.909	−0.959	−1.058	−1.158
18	0.665	−0.646	−0.719	−0.766	−0.814	−0.864	−0.913	−1.013	−1.113
20	0.591	−0.594	−0.680	−0.729	−0.778	−0.828	−0.878	−0.978	−1.078
22	0.530	−0.557	−0.650	−0.700	−0.750	−0.800	−0.850	−0.949	−1.049
24	0.481	−0.530	−0.626	−0.676	−0.726	−0.776	−0.826	−0.926	−1.026
26	0.439	−0.508	−0.606	−0.656	−0.706	−0.756	−0.806	−0.906	−1.006

Table 11. (Continued.)

$n_D = 10^{21}$ (Continued)

V_T^{-1}	$\frac{d\mu'}{dV_T}$	$E=-0.6$	$E=-0.8$	$E=-0.9$	$E=-1.0$	$E=-1.1$	$E=-1.2$	$E=-1.4$	$E=-1.6$
		$\frac{d\mu}{dV_T}$							
8	14.688	− 13.992	− 13.979	− 13.956	− 13.903	− 13.777	− 13.518	− 12.232	− 10.220
10	14.353	− 13.646	− 13.534	− 13.304	− 12.766	− 11.797	− 10.563	− 8.542	− 7.543
12	14.080	− 13.318	− 12.605	− 11.485	− 10.033	− 8.794	− 7.955	− 7.128	− 6.840
14	13.848	− 12.849	− 10.546	− 9.011	− 7.918	− 7.302	− 6.965	− 6.686	− 6.608
16	13.648	− 11.887	− 8.498	− 7.498	− 6.979	− 6.722	− 6.596	− 6.505	− 6.484
18	13.471	− 10.285	− 7.324	− 6.809	− 6.576	− 6.471	− 6.425	− 6.396	− 6.390
20	13.313	− 8.696	− 6.735	− 6.482	− 6.379	− 6.338	− 6.321	− 6.312	− 6.311
22	13.171	− 7.596	− 6.431	− 6.309	− 6.264	− 6.248	− 6.242	− 6.239	− 6.239
24	13.040	− 6.928	− 6.260	− 6.202	− 6.183	− 6.176	− 6.174	− 6.174	− 6.173
26	12.920	− 6.531	− 6.153	− 6.125	− 6.117	− 6.114	− 6.114	− 6.113	− 6.113

$n_D = 3 \times 10^{21}$

V_T^{-1}	μ'	μ							
8	1.511	− 1.425	− 1.425	− 1.426	− 1.428	− 1.433	− 1.441	− 1.478	− 1.543
10	1.175	− 1.107	− 1.110	− 1.117	− 1.130	− 1.152	− 1.184	− 1.265	− 1.357
12	0.957	− 0.901	− 0.917	− 0.939	− 0.972	− 1.012	− 1.056	− 1.152	− 1.250
14	0.804	− 0.761	− 0.802	− 0.840	− 0.883	− 0.930	− 0.979	− 1.077	− 1.177
16	0.691	− 0.666	− 0.733	− 0.778	− 0.826	− 0.874	− 0.924	− 1.024	− 1.124
18	0.604	− 0.603	− 0.686	− 0.734	− 0.783	− 0.833	− 0.883	− 0.983	− 1.083
20	0.536	− 0.560	− 0.652	− 0.701	− 0.751	− 0.801	− 0.851	− 0.951	− 1.051
22	0.480	− 0.529	− 0.625	− 0.675	− 0.725	− 0.775	− 0.825	− 0.925	− 1.025
24	0.435	− 0.505	− 0.603	− 0.653	− 0.703	− 0.753	− 0.803	− 0.903	− 1.003
26	0.397	− 0.486	− 0.585	− 0.635	− 0.685	− 0.735	− 0.785	− 0.885	− 0.985

V_T^{-1}	$\frac{d\mu'}{dV_T}$	$\frac{d\mu}{dV_T}$							
8	13.589	− 12.889	− 12.850	− 12.785	− 12.638	− 12.333	− 11.784	− 10.041	− 8.413
10	13.254	− 12.521	− 12.215	− 11.693	− 10.776	− 9.640	− 8.603	− 7.281	− 6.693
12	12.981	− 12.092	− 10.682	− 9.360	− 8.190	− 7.381	− 6.877	− 6.395	− 6.228
14	12.750	− 11.298	− 8.546	− 7.455	− 6.807	− 6.446	− 6.251	− 6.090	− 6.029
16	12.550	− 9.877	− 7.117	− 6.520	− 6.218	− 6.069	− 5.996	− 5.943	− 5.932
18	12.373	− 8.316	− 6.389	− 6.082	− 5.947	− 5.887	− 5.860	− 5.844	− 5.840
20	12.215	− 7.180	− 6.006	− 5.860	− 5.801	− 5.762	− 5.768	− 5.762	− 5.761
22	12.072	− 6.479	− 5.800	− 5.730	− 5.704	− 5.695	− 5.691	− 5.690	− 5.689
24	11.941	− 6.061	− 5.674	− 5.641	− 5.630	− 5.626	− 5.625	− 5.624	− 5.624
26	11.821	− 5.806	− 5.587	− 5.571	− 5.566	− 5.565	− 5.564	− 5.564	− 5.564

$n_D = 10^{22}$

V_T^{-1}	μ'	μ							
8	1.361	− 1.275	− 1.277	− 1.280	− 1.286	− 1.297	− 1.316	− 1.374	− 1.454
10	1.055	− 0.988	− 0.999	− 1.014	− 1.038	− 1.071	− 1.110	− 1.199	− 1.295
12	0.856	− 0.805	− 0.839	− 0.872	− 0.912	− 0.956	− 1.003	− 1.100	− 1.200
14	0.718	− 0.687	− 0.748	− 0.791	− 0.838	− 0.886	− 0.935	− 1.034	− 1.134
16	0.615	− 0.610	− 0.691	− 0.738	− 0.787	− 0.836	− 0.886	− 0.986	− 1.086
18	0.537	− 0.560	− 0.651	− 0.700	− 0.750	− 0.799	− 0.849	− 0.949	− 1.049
20	0.476	− 0.526	− 0.621	− 0.671	− 0.720	− 0.770	− 0.820	− 0.920	− 1.020
22	0.426	− 0.500	− 0.597	− 0.647	− 0.697	− 0.747	− 0.797	− 0.897	− 0.997
24	0.385	− 0.479	− 0.578	− 0.628	− 0.678	− 0.728	− 0.778	− 0.878	− 0.978
26	0.351	− 0.462	− 0.562	− 0.612	− 0.662	− 0.712	− 0.762	− 0.862	− 0.962

Table 11. (Continued.)

$n_D = 10^{22}$ (Continued)

V_T^{-1}	$\frac{d\mu'}{dV_T}$	$E=-0.6$	$E=-0.8$	$E=-0.9$	$E=-1.0$	$E=-1.1$	$E=-1.2$	$E=-1.4$	$E=-1.6$
		$\frac{d\mu}{dV_T}$							
8	12.388	−11.668	−11.547	−11.359	−10.988	−10.376	−9.572	−7.980	−6.910
10	12.050	−11.229	−10.463	−9.583	−8.556	−7.656	−6.989	−6.229	−5.905
12	11.772	−10.534	−8.486	−7.426	−6.688	−6.225	−5.944	−5.680	−5.588
14	11.552	−9.267	−6.860	−6.216	−5.854	−5.656	−5.549	−5.461	−5.436
16	11.340	−7.776	−5.982	−5.651	−5.485	−5.403	−5.364	−5.335	−5.328
18	11.166	−6.648	−5.535	−5.371	−5.297	−5.264	−5.249	−5.240	−5.238
20	11.020	−5.944	−5.293	−5.213	−5.181	−5.167	−5.162	−5.159	−5.159
22	10.872	−5.521	−5.148	−5.130	−5.096	−5.090	−5.088	−5.087	−5.087
24	10.740	−5.261	−5.050	−5.031	−5.025	−5.023	−5.022	−5.022	−5.022
26	10.626	−5.094	−4.975	−4.966	−4.963	−4.962	−4.962	−4.962	−4.962

$n_D = 3\times 10^{22}$

V_T^{-1}	μ'	μ							
8	1.223	−1.138	−1.144	−1.152	−1.166	−1.187	−1.216	−1.290	−1.378
10	0.945	−0.882	−0.906	−0.931	−0.965	−1.004	−1.048	−1.142	−1.239
12	0.765	−0.724	−0.777	−0.817	−0.861	−0.908	−0.956	−1.054	−1.154
14	0.639	−0.627	−0.703	−0.749	−0.797	−0.846	−0.895	−0.995	−1.095
16	0.547	−0.566	−0.655	−0.703	−0.752	−0.802	−0.852	−0.952	−1.052
18	0.476	−0.525	−0.620	−0.669	−0.719	−0.769	−0.819	−0.919	−1.019
20	0.421	−0.496	−0.593	−0.643	−0.693	−0.743	−0.793	−0.893	−0.993
22	0.376	−0.474	−0.572	−0.622	−0.672	−0.722	−0.772	−0.872	−0.972
24	0.339	−0.456	−0.555	−0.605	−0.655	−0.705	−0.755	−0.855	−0.955
26	0.308	−0.441	−0.541	−0.591	−0.641	−0.691	−0.741	−0.841	−0.941

V_T^{-1}	$\frac{d\mu'}{dV_T}$	$\frac{d\mu}{dV_T}$							
8	11.284	−10.524	−10.210	−9.806	−9.184	−8.428	−7.684	−6.561	−5.934
10	10.950	−9.916	−8.610	−7.686	−6.888	−6.298	−5.892	−5.448	−5.260
12	10.680	−8.836	−6.803	−6.104	−5.659	−5.388	−5.225	−5.072	−5.019
14	10.446	−7.413	−5.714	−5.334	−5.124	−5.010	−4.948	−4.897	−4.882
16	10.252	−6.254	−5.156	−4.964	−4.869	−4.822	−4.798	−4.782	−4.778
18	10.068	−5.513	−4.860	−4.765	−4.723	−4.704	−4.695	−4.690	−4.689
20	9.920	−5.064	−4.687	−4.641	−4.622	−4.615	−4.612	−4.610	−4.610
22	9.772	−4.789	−4.573	−4.551	−4.543	−4.541	−4.539	−4.538	−4.538
24	9.636	−4.611	−4.489	−4.478	−4.475	−4.473	−4.473	−4.473	−4.473
26	9.508	−4.489	−4.420	−4.415	−4.413	−4.413	−4.413	−4.413	−4.413

Appendix 1.

Thermionic constants.

The following empirical equations may be used with the tabulated constants to calculate approximate current densities in amp/cm.² from the sources listed.

$$I = A_R T^2 \mathrm{e}^{-\frac{e\varphi_R}{kT}}, \qquad I = A_R T^2 \mathrm{e}^{-\frac{b}{T}}, \qquad I = A_R T^2 10^{-\frac{b'}{T}},$$

$$I = a\,\mathrm{e}^{-\frac{e\Phi}{kT}}, \qquad I = a\,\mathrm{e}^{-\frac{\beta}{T}}, \qquad I = a\,10^{-\frac{\beta'}{T}}.$$

Note 1: T_m and T_n are minimum and maximum temperatures.
Note 2: T_0 computed from T_m and T_n by Eq. (50.5)
Note 3: Φ computed from φ_R by Eq. (50.3).
Note 4: a computed from A_R by Eq. (50.6).

Source	T_m	T_n	T_0	A_R	Φ_R	b	b'	a	Φ	β	β'	Ref.
C	1300	2200	1520	30	4.34	50340	21870	70×10^7	4.64	53820	23390	a
	1300	2200	1520	15	4.38	50810	22080	35×10^7	4.68	54290	23590	b
βFe	1040	1180	1010	26	4.48	51970	22580	27×10^7	4.68	54290	23590	c
γFe	1180	1680	1240	1.5	4.21	48840	21220	2.3×10^7	4.46	51740	22490	c
Mo	1300	2100	1480	115	4.37	50690	22020	250×10^7	4.69	54400	23640	d
	1350	2000	1450	55	4.15	48140	20920	155×10^7	4.44	51500	22380	e
Ni	1300	1700	1300	30	4.61	53480	23230	50×10^7	4.86	56380	24490	c
	1150	1700	1240	50	5.24	60780	26410	80×10^7	5.49	63680	27670	f
Pt	1700	2100	1650	32	5.32	61710	26810	90×10^7	5.65	65540	28480	g
Ta	1200	2000	1390	52	4.19	48600	21120	100×10^7	4.47	51850	22530	h
W	1400	2400	1650	72	4.52	52430	22780	200×10^7	4.85	56260	24440	i
	1200	2000	1390	60	4.51	52320	22730	120×10^7	4.79	55560	24140	j
W+Th	1200	2000	1390	3	2.63	30510	13255	6×10^7	2.91	33760	14670	k
"L" (W+Ba)	1300	1700	1300	1	1.8	20880	9070	2×10^7	2.06	23900	10380	l
	1300	1700	1300	15	2.0	23200	10080	20×10^7	2.26	26220	11390	l
La+LaB_6	1100	1900	1300	29	2.66	30860	13410	50×10^7	2.92	33870	14720	m
BaSrO	600	1200	780	0.5	1.0	11600	5040	3×10^6	1.16	13460	5846	n

a) A. L. Reimann: Proc. Phys. Soc. Lond. **50**, 496 (1938).
b) A. Braun and G. Busch: Helv. phys. Acta **20**, 33 (1947).
c) H. B. Wahlin: Phys. Rev. **61**, 509 (1942).
d) R. W. Wright: Phys. Rev. **60**, 465 (1941).
e) L. A. DuBridge and W. W. Roehr: Phys. Rev. **42**, 56 (1932).
f) A. B. Cardwell: Phys. Rev. **76**, 125 (1949).
g) L. V. Whitney: Phys. Rev. **50**, 1154 (1936).
h) M. D. Fiske: Phys. Rev. **61**, 513 (1942).
i) A. L. Reimann: Phil. Mag. **25**, 834 (1938).
j) W. B. Nottingham: Phys. Rev. **47**, 806 (1935).
k) S. Dushman and J. Ewald: Phys. Rev. **29**, 857 (1927).
l) H. J. Lemmens, M. J. Janson and R. Loosjes: Philips Rech. Rev. **11**, 341 (1950).
m) J. M. Lafferty: J. Appl. Phys. **22**, 299 (1951).

n) Reliable thermionic constants for the oxides are particularly difficult to obtain. The ones proposed here depend on emission measurements made on selected diodes constructed by the Raytheon Manufacturing Company.

Appendix 2.

Some useful equations from statistical theory of free electrons.

Particle current $I(\varepsilon_x)$ in x-direction per unit energy range of ε_x (Fermi Statistics)

$$I(\varepsilon_x)\,d\varepsilon_x = \frac{4\pi m k T}{h^3} \ln\left(1 + e^{-\frac{(\varepsilon_x - \mu)}{kT}}\right) d\varepsilon_x .$$

Energy of Fermi *level*:

For high concentrations of electrons:

$$\mu = \frac{h^2}{2m}\left(\frac{3n}{8\pi}\right)^{\frac{2}{3}} \left\{1 - \frac{\pi^2}{12}\left[\frac{kT}{\frac{h^2}{2m}\left(\frac{3n}{8\pi}\right)^{\frac{2}{3}}}\right]^2 + \cdots\right\}.$$

For

$$T = 0, \qquad \mu = \frac{h^2}{2m}\left(\frac{3n}{8\pi}\right)^{\frac{2}{3}}.$$

For low concentrations of electrons:

$$\mu = -kT \ln\left[\frac{2}{nh^3}(2\pi m k T)^{\frac{3}{2}}\right].$$

SPRINGER-VERLAG / BERLIN · GÖTTINGEN · HEIDELBERG

Landolt-Börnstein

Zahlenwerte und Funktionen aus Physik, Chemie, Astronomie, Geophysik und Technik

Sechste Auflage. Unter vorbereitender Mitwirkung von J. D'Ans, A. Eucken†, G. Joos, W. A. Roth† herausgegeben von **J. Bartels, P. ten Bruggencate, K. H. Hellwege, Kl. Schäfer, E. Schmidt.** In vier Bänden. Jeder Band und Bandteil ist einzeln käuflich.

Erster Band: **Atom- und Molekularphysik.** In 5 Teilen.

1. Teil: **Atome und Ionen.**
Herausgegeben von **A. Eucken** † in Gemeinschaft mit K. H. Hellwege. Mit 248 Abbildungen. XII, 441 Seiten 4°. 1950. In Moleskin gebunden DM 126.—

2. Teil: **Molekeln I (Kerngerüst).**
Herausgegeben von **A. Eucken** † und **K. H. Hellwege.** Mit 460 Abbildungen. VIII, 571 Seiten 4°. 1951. In Moleskin gebunden DM 168.—

3. Teil: **Molekeln II (Elektronenhülle)** nebst einem Anhang zu den Teilbänden I/1, I/2, I/3.
Herausgegeben von **A. Eucken** † und **K. H. Hellwege.** Mit 364 Abbildungen. XI, 724 Seiten 4°. 1951. In Moleskin gebunden DM 218.—

4. Teil: **Kristalle.**
Herausgegeben von **K. H. Hellwege.** Mit 930 Abbildungen. XI, 1007 Seiten 4°. 1955. In Moleskin gebunden DM 318.—

5. Teil: **Atomkerne und Elementarteilchen.**
Herausgegeben von **K. H. Hellwege.** Mit 471 Abbildungen. VIII, 470 Seiten 4°. 1952. In Moleskin gebunden DM 148.—

Zweiter Band: **Eigenschaften der Materie in ihren Aggregatzuständen.** In 7 Teilen.

1. Teil: **Mechanisch-thermische Konstanten homogener Systeme. — Mechanisch-thermische Zustandsgrößen.** In Vorbereitung

2. Teil: **Gleichgewichte außer Schmelzgleichgewichten.** In Vorbereitung

3. Teil: **Schmelzgleichgewichte und Grenzflächenerscheinungen.**
Herausgegeben von **Klaus Schäfer** und **Ellen Lax.** Mit 998 Abbildungen. XI, 535 Seiten 4°. 1956. In Moleskin gebunden DM 198.—

4. Teil: **Kalorische Zustandsgrößen.** In Vorbereitung

5. Teil: **Physikalische und chemische Kinetik und Akustik.** In Vorbereitung

6. Teil: **Elektrische Eigenschaften; Optische Konstanten (1. Teil).** In Vorbereitung

7. Teil: **Optische Konstanten (2. Teil); Magnetische Eigenschaften.** In Vorbereitung

Dritter Band: **Astronomie und Geophysik.**
Herausgegeben von **J. Bartels** und **P. ten Bruggencate.**
Mit 331 Abbildungen und 8 Nomogrammen. XVIII, 795 Seiten 4°. 1952. In Moleskin gebunden DM 248.—

Vierter Band: **Technik.** In 4 Teilen.

1. Teil: **Stoffwerte und mechanisches Verhalten von Nichtmetallen.**
Herausgegeben von **Ernst Schmidt.** Mit 1104 Abbildungen. XVI, 881 Seiten 4°. 1955. In Moleskin gebunden DM 288.—

2. Teil: **Metallische Werkstoffe.** In Vorbereitung

3. Teil: **Elektrotechnik. Lichttechnik. Röntgentechnik.** In Vorbereitung

4. Teil: **Wärmetechnik.** In Vorbereitung

Druck der Universitätsdruckerei H. Stürtz AG., Würzburg